USP28 regulates Squamous cell oncogenesis and DNA repair via ΔNp63 deubiquitination

USP28 reguliert Plattenepithelzell-Onkogenese und DNA-Reparatur über ΔNp63-Deubiquitinierung

Doctoral thesis

for a doctoral degree
at the Graduate School of Life Sciences,
Julius-Maximilians-Universität Würzburg,
Section Biomedicine

submitted by

Cristian Prieto García

from Málaga (Spain)

Würzburg 2021

Members of the Thesis Committee

Chairperson: Prof. Dr. Alexander Buchberger

Primary Supervisor: Dr. Markus Elmar Diefenbacher
Second Supervisor: Prof. Dr. Martin Eilers
Third Supervisor: Prof. Dr. Ivan Dikic
Fourth Supervisor: Prof. Dr. Stefan Gaubatz

Submitted on:

Date of Public Defence:

Date of Receipt of Certificates:

Substantial part of this thesis was published in the following articles:

Prieto-Garcia, C., Hartmann, O., Reissland, M., Braun, F., Fischer, T., Walz, S., Schülein-Völk, C., Eilers, U., Ade, C. P., Calzado, M. A., Orian, A., Maric, H. M., Münch, C., Rosenfeldt, M., Eilers, M., & Diefenbacher, M. E. (2020). Maintaining protein stability of ΔNp63 via USP28 is required by squamous cancer cells. EMBO Molecular Medicine, 12(4).

Prieto-Garcia, C., Hartmann, O., Reissland, M., Fischer, T., Maier, C. R., Rosenfeldt, M., Schülein-Völk, C., Klann, K., Kalb, R., Dikic, I., Münch, C., & Diefenbacher, M. E. (2021). Inhibition of USP28 overcomes Cisplatin-Resistance of Squamous Tumors by Suppression of the Fanconi Anemia Pathway. *(Under review)*

Prieto-Garcia, C., Tomašković, I., Shah, V. J., Dikic, I., Diefenbacher, M. E. (2021). USP28: oncogene or tumor suppressor? A unifying paradigm for Squamous cell carcinoma. *(Manuscript in preparation)*

Table of contents

Summary

ΔNp63 is a master regulator of squamous cell identity and regulates several signaling pathways that crucially contribute to the development of squamous cell carcinoma (SCC) tumors. Its contribution to coordinating the expression of genes involved in oncogenesis, epithelial identity, DNA repair, and genome stability has been extensively studied and characterized. For SCC, the expression of ΔNp63 is an essential requirement to maintain the malignant phenotype. Additionally, ΔNp63 functionally contributes to the development of cancer resistance toward therapies inducing DNA damage.

SCC patients are currently treated with the same conventional Cisplatin therapy as they would have been treated 30 years ago. In contrast to patients with other tumor entities, the survival of SCC patients is limited, and the efficacy of the current therapies is rather low. Considering the rising incidences of these tumor entities, the development of novel SCC therapies is urgently required. Targeting ΔNp63, the transcription factor, is a potential alternative to improve the therapeutic response and clinical outcomes of SCC patients.

However, ΔNp63 is considered "undruggable." As is commonly observed in transcription factors, ΔNp63 does not provide any suitable domains for the binding of small molecule inhibitors. ΔNp63 regulates a plethora of different pathways and cellular processes, making it difficult to counteract its function by targeting downstream effectors. As ΔNp63 is strongly regulated by the ubiquitin–proteasome system (UPS), the development of deubiquitinating enzyme inhibitors has emerged as a promising therapeutic strategy to target ΔNp63 in SCC treatment.

This work involved identifying the first deubiquitinating enzyme that regulates ΔNp63 protein stability. State-of-the-art SCC models were used to prove that USP28 deubiquitinates ΔNp63, regulates its protein stability, and affects squamous transcriptional profiles *in vivo* and *ex vivo*. Accordingly, SCC depends on USP28 to maintain essential levels of ΔNp63 protein abundance in tumor formation and maintenance. For the first time, ΔNp63, the transcription factor, was targeted *in vivo* using a small molecule inhibitor targeting the activity of USP28. The pharmacological inhibition of USP28 was sufficient to hinder the growth of SCC tumors in preclinical mouse models.

Finally, this work demonstrated that the combination of Cisplatin with USP28 inhibitors as a novel therapeutic alternative could expand the limited available portfolio of SCC therapeutics. Collectively, the data presented within this dissertation demonstrates that the inhibition of USP28 in SCC decreases ΔNp63 protein abundance, thus downregulating the Fanconi anemia (FA) pathway and recombinational DNA repair. Accordingly, USP28 inhibition reduces the DNA damage response, thereby sensitizing SCC tumors to DNA damage therapies, such as Cisplatin.

Zusammenfassung

ΔNp63 ist ein Hauptregulator der Plattenepithelzellidentität und reguliert mehrere Signalwege, die entscheidend zur Entstehung von Plattenepithelkarzinomen (SCC) beitragen. Sein Beitrag zur Koordination der Expression von Genen, die an der Onkogenese, der epithelialen Identität, der DNA-Reparatur und der Genomstabilität beteiligt sind, wurde umfassend untersucht und charakterisiert. Für SCC ist die Expression von ΔNp63 eine wesentliche Voraussetzung, um den malignen Phänotyp zu erhalten. Darüber hinaus trägt ΔNp63 funktionell zur Entwicklung einer Krebsresistenz gegenüber Therapien bei, die DNA-Schäden induzieren.

SCC-Patienten werden derzeit mit der gleichen konventionellen Cisplatin-Therapie behandelt, wie sie vor 30 Jahren behandelt worden wären. Im Gegensatz zu Patienten mit anderen Tumorentitäten ist das Überleben von SCC-Patienten begrenzt und die Wirksamkeit der aktuellen Therapien eher gering. Angesichts der steigenden Inzidenz dieser Tumorentitäten ist die Entwicklung neuer Therapien für das Plattenepithelkarzinom dringend erforderlich. Das Targeting von ΔNp63, dem Transkriptionsfaktor, ist eine potenzielle Alternative zur Verbesserung des therapeutischen Ansprechens und der klinischen Ergebnisse von SCC-Patienten.

ΔNp63 gilt jedoch als „nicht medikamentös". Wie bei Transkriptionsfaktoren häufig beobachtet, bietet ΔNp63 keine geeigneten Domänen für die Bindung von niedermolekularen Inhibitoren. ΔNp63 reguliert eine Vielzahl von verschiedenen Signalwegen und zellulären Prozessen, was es schwierig macht, seiner Funktion entgegenzuwirken, indem es nachgeschaltete Effektoren angreift. Da ΔNp63 stark durch das Ubiquitin-Proteasom-System (UPS) reguliert wird, hat sich die Entwicklung von deubiquitinierenden Enzyminhibitoren als vielversprechende therapeutische Strategie erwiesen, um ΔNp63 bei der Behandlung von Plattenepithelkarzinomen zu bekämpfen.

Diese Arbeit beinhaltete die Identifizierung des ersten deubiquitinierenden Enzyms, das die Stabilität des ΔNp63-Proteins reguliert. Hochmoderne SCC-Modelle wurden verwendet, um zu beweisen, dass USP28 ΔNp63 deubiquitiniert, seine Proteinstabilität reguliert und Plattenepithel-Transkriptionsprofile in vivo und ex vivo beeinflusst. Dementsprechend hängt SCC von USP28 ab, um wesentliche Mengen des Np63-Proteinüberflusses bei der Tumorbildung und -erhaltung aufrechtzuerhalten. Zum ersten Mal wurde ΔNp63, der Transkriptionsfaktor, in vivo mit einem niedermolekularen Inhibitor gezielt, der auf die Aktivität von USP28 abzielt. Die pharmakologische Hemmung von USP28 war ausreichend, um das Wachstum von SCC-Tumoren in präklinischen Mausmodellen zu verhindern.

Schließlich zeigte diese Arbeit, dass die Kombination von Cisplatin mit USP28-Inhibitoren als neuartige therapeutische Alternative das begrenzt verfügbare Portfolio an SCC-Therapeutika erweitern könnte. Zusammengefasst zeigen die in dieser Dissertation präsentierten Daten, dass die Hemmung von USP28 in SCC die Np63-Proteinhäufigkeit verringert, wodurch der Fanconi-Anämie (FA)-Signalweg und die rekombinatorische DNA-Reparatur herunterreguliert werden. Dementsprechend reduziert die Hemmung von USP28 die Reaktion auf DNA-Schäden und sensibilisiert dadurch SCC-Tumoren für DNA-Schädigungstherapien wie Cisplatin.

1. Introduction

1.1 Hallmarks of cancer

Cancer is defined as a large group of diseases characterized by uncontrolled division of malignant cells. Cancer is the second most common cause of death after heart diseases (Zaorsky et al. 2017). Accordingly, new therapies are urgently required to improve patient survival rates. Tumors can be classified as benign, if cells proliferate slowly and patients have good prognosis, or malignant, if cells show an invasive phenotype and divide faster. Malignant tumors have poor survival rates and often metastasize to other tissues (Jang et al. 2011). Histologically, cancer can be classified as follows according to the cell of origin:

1. Carcinoma: Tumors arise from an epithelial tissue.
2. Sarcoma: Cancer begins in the connective tissues.
3. Leukemia: Cancer starts in the white blood cells.
4. Lymphoma and myeloma: Cancer begins in the cells of the immune system.
5. Brain and spinal cord cancers: Tumors arise from the central nervous system.

Oncogenesis is defined as the transformation of normal cells into cancer cells. Malignant cells could form owing to the accumulation of specific mutations in undifferentiated stem cells. Alternatively, genetic alterations can cause the acquisition of an oncogenic undifferentiated state in differentiated cells (Polyak & Weinberg 2009). Owing to their capability of self-renewal and infinite lifespan, the acquisition of malignant phenotypes is probably more in undifferentiated stem cells than in differentiated cells (White & Lowry 2015), but both processes may occur in parallel.

A tumor suppressor is a gene that regulates cell proliferation or promotes apoptosis suppressing the development of cancer. An oncogene encodes a protein that has the potential to transform cells and induce tumor formation. Deletion or loss-of-function mutations in tumor suppressor genes and/or the amplification or increased activity of proto-oncogenes allow the transformation of normal cells to malignant cells. In cancer, p53, RB, INK4, BRCA1/2, and PTEN are common tumor suppressor. Alternatively, RAS, EGFR, PI3KCA, c-MYC, and BRAF are proto-oncogenes frequently amplified or altered in tumors (Lee et al. 2010). Particularly prominent are the genetic alterations in p53, as the tumor suppressor is deleted or mutated in more than 50% of all tumors (Perri et al. 2016). The activity of tumor suppressors or proto-oncogenes is altered not only by direct genetic alterations or regulating the pathways that control their activation but also by regulating their abundance and stability via the ubiquitin–proteasome system (UPS) (Yeh et al. 2018).

As cellular oncogenic transformation is a complex multifactorial process, to simplify cancer complexity, Douglas Hanahan and Robert Weinberg (Hanahan & Weinberg 2000) have listed the hallmarks of cancerous properties that every tumor acquires during neoplastic formation (Figure 1.1A). The hallmarks of cancer are the following:

1. Sustaining proliferative signaling
2. Evading growth suppressors
3. Cell death resistance
4. Enabling replicative immortality

5. Angiogenesis induction
6. Invasion and metastasis

Additionally, two emerging hallmarks (Figure 1.1A) (Douglas Hanahan and Robert Weinberg 2011) have been added to the above list:

1. Metabolism reprogramming
2. Evading immune destruction

The authors also define the existence of the following enabling characteristics (Figure 1.1A) that foster the function of several hallmarks (Douglas Hanahan and Robert Weinberg 2011):

1. Genome instability
2. Inflammation

A

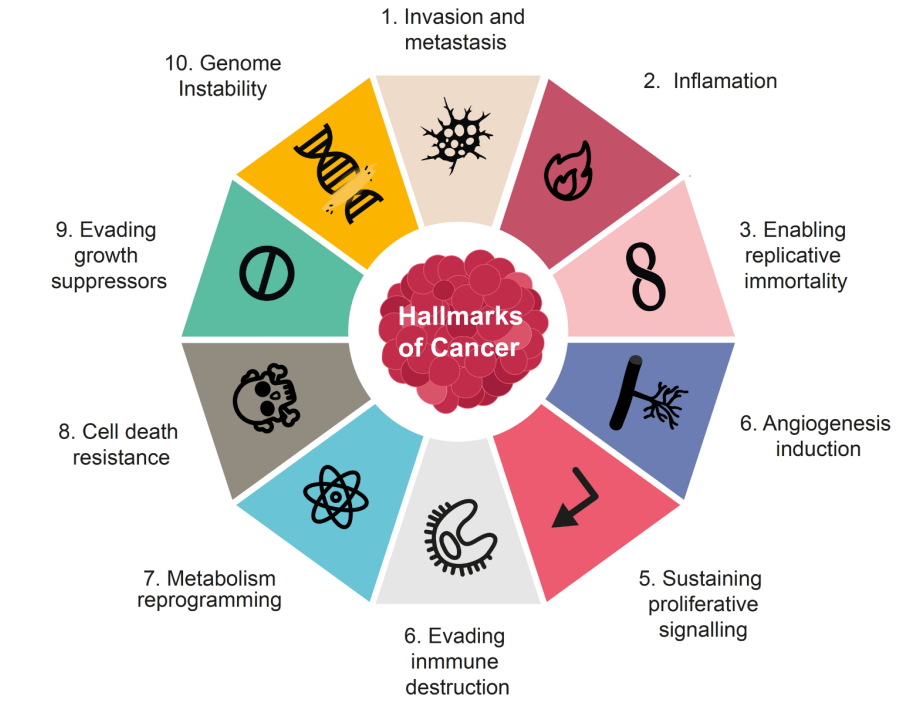

Figure 1.1: Hallmarks of cancer.

A) Hallmarks of cancer. Adapted from Douglas Hanahan and Robert Weinberg, 2011

1.2 Ubiquitin system

Ubiquitination is a posttranslational modification that regulates critical cellular processes, including protein degradation, cell cycle progression, autophagy, transcription, signal transduction, or DNA repair. Ubiquitin is a highly conserved protein of 76 amino acids encoded by four different genes, namely UBB, UBC, UBA52, and RPS27A. The ubiquitin molecule can covalently bind through its C-terminal carboxylate group to different residues of target proteins. Ubiquitin can bind to lysine residues via isopeptide bonds, cysteine residues via thioester bonds, serine and threonine residues via ester bonds, and N-terminal amine groups of a protein via peptide bonds. Canonical ubiquitination occurs on lysine residues, but nonlysine ubiquitination on serines, threonines, and cysteines has also been reported (McClellan et al. 2019). Furthermore, ubiquitin contains seven

different lysine residues (K6, K11, K27, K29, K33, K48, and K63) and N-terminal methionine (M1) groups that serve as secondary ubiquitination sites to induce polyubiquitination of substrates (Breitschopf et al. 1998; Ciechanover & Ben-Saadon 2004; Komander & Rape 2012).

Protein ubiquitination requires the action of three different enzymes: ubiquitin activating enzymes (E1), ubiquitin conjugating enzymes (E2), and ubiquitin ligases (E3) (Figure 1.2A). In humans, there are ~600 different E3-ligases, ~35 E2s, and only 2 E1s. (Hershko & Ciechanover 1998; Akutsu, Dikic & Bremm 2016). E1 catalyzes ATP activation of the ubiquitin and forms a thioester bond between the active cysteine and the C-terminal glycine of the ubiquitin. Then, ubiquitin is transferred from E1 to another catalytic cysteine, located on E2 (by transthiolation). Finally, E3 mediates substrate specificity and catalyzes, directly or indirectly, the binding between the ubiquitin molecule and the substrate protein. E3s determine substrate specificity acting as platforms to support the interaction between E2s and target proteins.

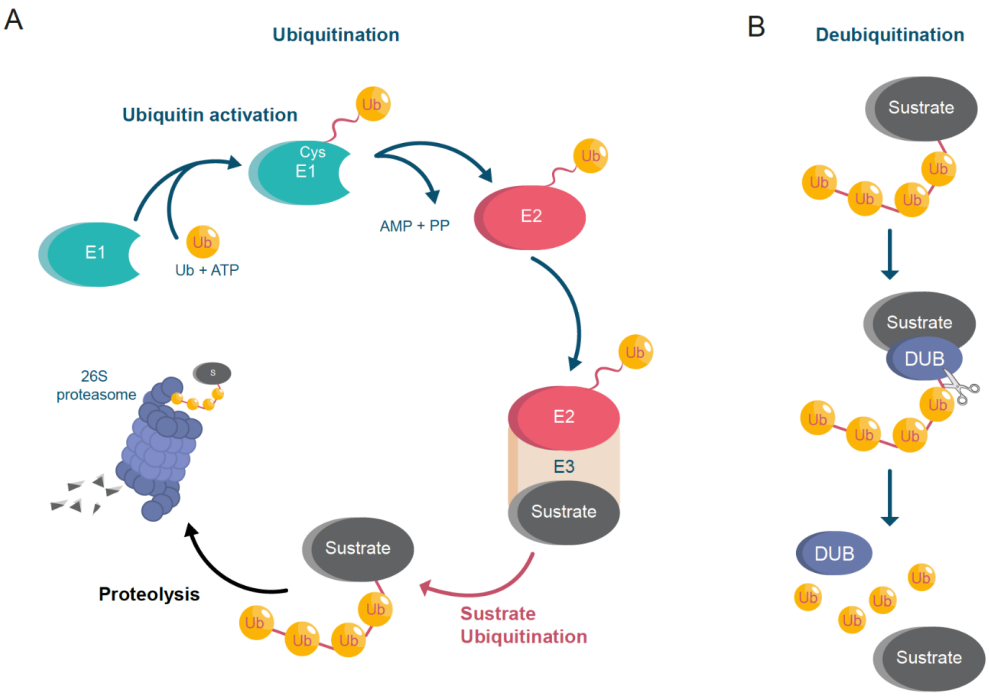

Figure 1.2: Ubiquitination and deubiquitination. **A)** The ubiquitin activating enzyme (E1) catalyzes ubiquitin ATP activation. The ubiquitin is transferred from E1 enzyme to the ubiquitin conjugating enzyme (E2 enzyme) by transthiolation. The ubiquitin ligase (E3 enzyme) mediates substrate specificity catalyzing the ubiquitination of the target protein (substrate). Ubiquitination regulates several processes such as proteosomal degradation, DNA repair or autophagy. Ub = ubiquitin. **B)** The deubiquitinating enzymes (DUBs) cleave the bond between ubiquitin and ubiquitinated target proteins (substrate). Ub = ubiquitin; DUB = deubiquitinase.

Protein substrates can be monoubiquitinated (only one ubiquitin protein is attached to a specific protein residue), multimonoubiquitinated (one ubiquitin protein is attached to several residues of the same protein), or polyubiquitinated (several ubiquitin molecules ligate to the first ubiquitin bound to the target protein) (Figure 1.3A). Under particular conditions, a ubiquitin chain assembly factor (E4) enhance the E3-ubiquitin transference inducing faster substrate polyubiquitination linked ubiquitin. There are eight different homotypic ubiquitin chains and several heterotypic chains reported (Figure 1.3B and C); the formation of these chains depends on the residues that serve as ubiquitination sites (Husnjak & Dikic 2012).

As indicated, the polyubiquitination sites are K6, K11, K27, K29, K33, K48, and K63 or M1 (Haakonsen & Rape 2019). The different polyubiquitin chains have topological differences that can determine the biological

consequences of protein ubiquitination. The K48-linked ubiquitin chain is the most studied; it mainly regulates proteolysis by signaling proteins for 20S proteasome-dependent degradation. The K48 degradation signal requires the attachment of four or more ubiquitin molecules. The K63-linked ubiquitin chains regulate processes such as endocytic trafficking and DNA repair; the K29-linked ubiquitin chains regulate lysosomal protein degradation, and the K11-linked chains are involved in mitosis and endoplasmic reticulum-associated degradation (Komander & Rape 2012).

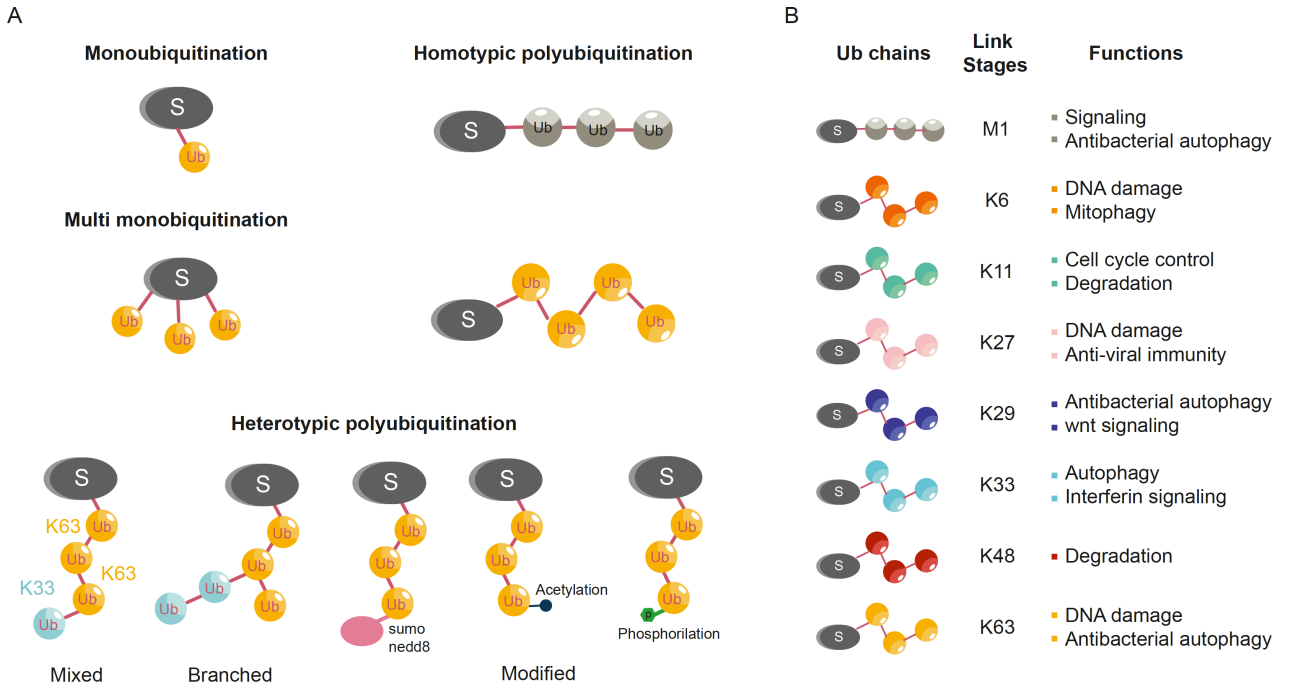

Figure 1.3: Ubiquitin chains.

A) Different Homotypic ubiquitin chains. S= substrate; ub= ubiquitin molecule; K = Lysine. **B)** Description of ubiquitin chains and their cellular function (van Wijk et al. 2019). S= substrate. **C)** Different Heterotypic ubiquitin chains. S= substrate; ub= ubiquitin molecule.

Ubiquitination is a reversible process occurring through the action of deubiquitinating enzymes (DUBs) that cleave the bond between ubiquitin and the target proteins (Figure 1.2B). In humans, there are approximately 100 DUBs, which can be divided into two main groups and eight different subgroups (Figure 1.4A). The two main groups are cysteine proteases and metalloproteases. The canonical catalytic sites of cysteine DUBs consist of Cys-His-Asp/Asn, whereas the catalytic sites of zinc metalloproteases contain Glu-X-[N]-His-X-His-X (10)-Asp. The classical subfamilies of cysteine DUBs are as follows: Ubiquitin-Specific Proteases (USPs), Ovarian Tumor (OTU), Machado–Josephin Domain (MJD), Ubiquitin–C-terminal Hydrolase (UCH), and MIU-containing novel DUB family (MINDY) proteases. Additionally, two new potential subfamilies of cysteine DUBs have been recently identified: Monocyte Chemotactic Protein-Induced Protein (MCPIP) and Zn-finger- UFSP domain protein (ZUFSP) (Lai et al. 2020) proteases. Additionally, JAB1/MPN/Mov34 (JAMM) is the only subfamily of the metalloproteases. (Hanpude et al. 2015)

The USPs are the largest DUB subfamily, with approximately ~60 different USPs. Although some USPs, such as USP7 and USP1, have been extensively studied, the majority of this subfamily remains highly unexplored, and further studies are required to analyze them. For most USPs, the substrate specificity, functional redundancies, and linkage selectivity are not yet fully elucidated.

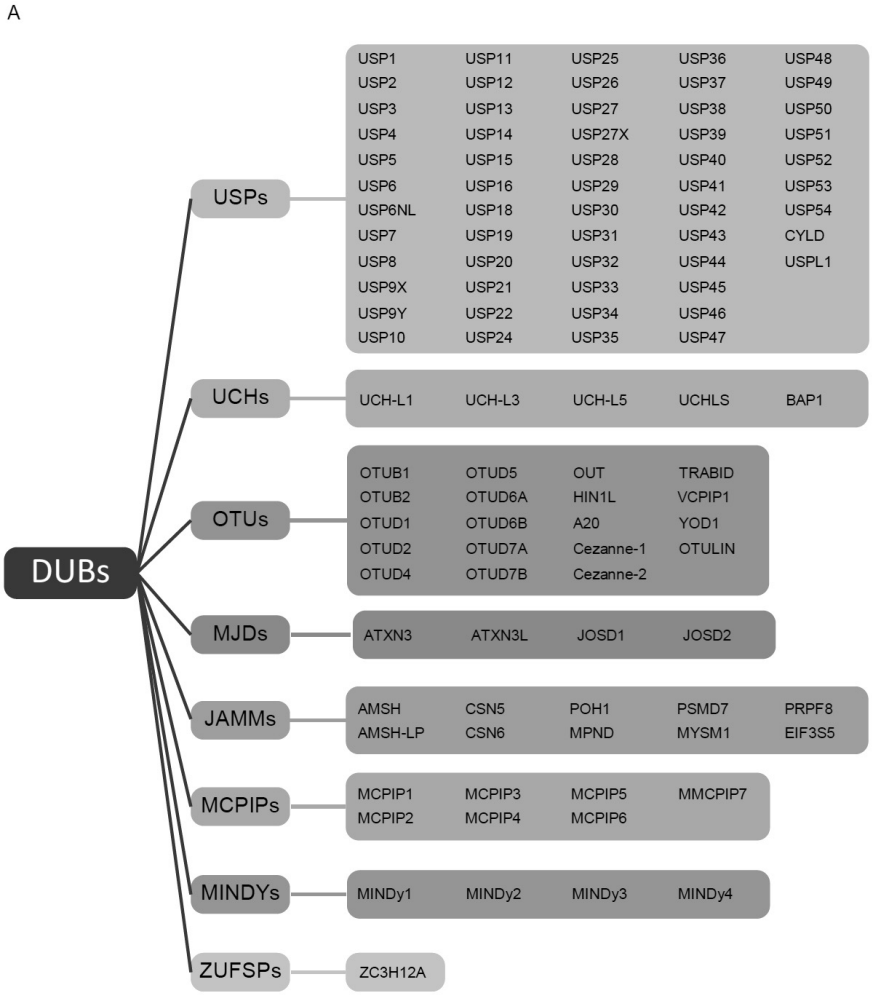

Figure 1.4: Classification of DUBs.

A) The cysteine DUBs are divided in Ubiquitin Specific Proteases (USPs), Ovarian Tumor (OTU) sub-family, Machado Josephin Domain (MJD), Ubiquitin C-terminal Hydrolase (UCH), MINDY proteases, Monocyte Chemotactic Protein-Induced Protein (MCPIP) and Zn-finger- UFSP domain protein (ZUFSP). Alternatively, JAMM is the only sub-family of the Metalloproteases.

1.3 Ubiquitin–proteasome system as a regulator of cancer homeostasis

The UPS is a strongly regulated system for maintaining protein homeostasis by intracellular protein degradation. Through the activities of enzymes E1, E2, and E3, proteins can be ubiquitinated and marked for proteasomal degradation. Alternatively, DUBs can increase the protein stability of their targets by deubiquitination, thereby avoiding proteasomal degradation.

Deregulated protein stability and UPS alterations are the common features of cancer cells (Fulda, Rajalingam & Dikic 2012). Increased proliferation levels, high tumor mutational burdens, and genomic alterations cause elevated proteotoxic stress levels. The fact that deregulation of the UPS could alter the stability of the key factors in oncogenesis was confirmed when it was noticed that several proto-oncogenes and tumor suppressor

genes were subjected to ubiquitination. Since then, many mutations and alterations in oncogenes and tumor suppressors have been shown to affect their ubiquitination and degradation.

In tumors, E3s are commonly altered, such as Von Hippel–Lindau (VHL) in renal cancer (Pause et al. 1997), *adenomatous polyposis coli* (APC), and F-Box and WD Repeat Domain Containing 7 (FBXW7) in colorectal cancer (Zhang & Shay 2017; Diefenbacher et al. 2014); and breast cancer 1 (BRCA1) and breast cancer 2 (BRCA2) genes in breast cancer (Walsh et al. 2006). For DUBs, USP4 is usually overexpressed in hepatocellular carcinoma (Li et al. 2018), USP28 in colorectal cancer (Diefenbacher et al. 2014), and USP10 in breast cancer and glioblastoma (Poondla et al. 2019). Alternatively, mutations in ubiquitin substrates can alter their stability by masking or losing the E3 / DUB interaction motif. For example, in-frame deletions between exon 2 and exon 7 within the EGFR coding sequence results in a truncated and constitutively active protein, which cannot be ubiquitinated (Schmidt et al. 2003).

Accordingly, the UPS is important to regulate protein homeostasis in cancer cells. Impairing the UPS systems induces a complex proteotoxic crisis, which ultimately leads to tumor death. Examples of proteostasis drugs are proteasome inhibitors such as Bortezomib and Carfilzomib, which target the proteolytic activity of the 20S proteasomal subunit. Unfortunately, tumor resistance development or low efficacy limits their usage, thus highlighting the importance of targeting additional regulators of protein stability, such as E3 and/or DUBs. The DUB USP28 is an interesting candidate, as it is amplified in several tumor entities and regulates the abundance of important oncoproteins, such as c-MYC, c-JUN, NOTCH1, and CCNE1 (Diefenbacher et al. 2015).

1.4 Oncogenesis regulation by deubiquitinase USP28

USP28 is a catalytically active DUB that regulates the ubiquitination status of several targets involved in proliferation, DNA repair, and oncogenesis. USP25 and USP28 have similar topological structures, comprising USP domains, ubiquitin-binding domains (UBDs), ubiquitin- associated domains (UBAs), and two ubiquitin-interacting motifs (UIMs) at the N-terminal region (Komander, Clague & Urbé 2009). However, USP25 and USP28 are not functionally redundant, and the protein localization of both the DUBs differs. USP25 is located in the cytosol, whereas USP28 is a nuclear protein. Additionally, USP28 can form functionally active dimers, but only USP25 can form inactive tetramers with two dimers (Sauer et al. 2019; Gersch et al. 2019). USP25 and USP28 can generate different tissue-specific isoforms by alternative splicing (Valero et al. 2001). Furthermore, USP28 was identified as the first DUB capable of antagonizing FBXW7, thus regulating c-MYC stability (Figure 1.5A) (Popov et al. 2007).

FBXW7 is an essential E3 ubiquitin ligase that regulates the stability of important oncogenic transcription factors, such as c-MYC, c-JUN, NOTCH1, and ΔNp63 (Cremona et al. 2015; Galli et al. 2010). FBXW7 is a member of the F-box family of E3-ligases. FBXW7 is part of the Skp1-Cdc53/Cullin-F-box (SCF) protein complex and mediates the binding and potential ubiquitination of substrates. FBXW7 contains seven tandem WD40 repeats, which can form a β-propeller structure, allowing the binding of FBXW7 to the cysteine protease domain (CPD) region of a phosphorylated target protein. Missense mutations within the WD40 domain of FBXW7 or in the CPD domain of a substrate disrupt the FBXW7-mediated ubiquitination of the target proteins

(Sailo et al. 2019; Yeh et al. 2018). FBXW7 is frequently mutated or deleted in malignant human tumors (Spruck et al. 2002).

Using genetically engineered mouse models (GEMMs), previous studies have demonstrated that the loss of FBXW7 significantly accelerated the progression of $APC^{min/+}$ colorectal tumors by accumulation of oncoproteins c-JUN, c-MYC, CCNE1, and NOTCH1. Alternatively, the deletion of USP28 counteracted the loss of FBXW7, thereby decreasing the oncoprotein stability of the ligase substrates and increasing the life expectancy of the animals from 70 days to 122 days. Accordingly, FBXW7 mutant tumors require USP28 activity to support and maintain the malignant transformation during colorectal oncogenesis (Diefenbacher et al. 2015; Diefenbacher et al. 2014). This example highlighted that oncogenic alterations in the UPS system require remodeling of the ubiquitin system, creating new oncogenic dependencies that can be therapeutically targeted.

USP28 not only stabilizes the substrates of FBXW7, but also deubiquitinates FBXW7 itself upon autocatalytic ubiquitination (Figure 1.5A and B) (Schülein-Völk et al. 2014). This dual regulation of USP28 and FBXW7 allows controlling the protein abundance of common substrates, such as c-MYC and NOTCH1. In addition to the substrates previously mentioned, USP28 stabilizes other targets involved in carcinogenesis, such as HIF-1α, LSD1, and CCNE (Wang et al. 2018). Furthermore, recent studies have demonstrated that USP28 deubiquitinates and stabilizes important tumor suppressors, such as TP53 and CHK2 (Müller et al. 2020; Meitinger et al. 2016, Bohgaki et al. 2013).

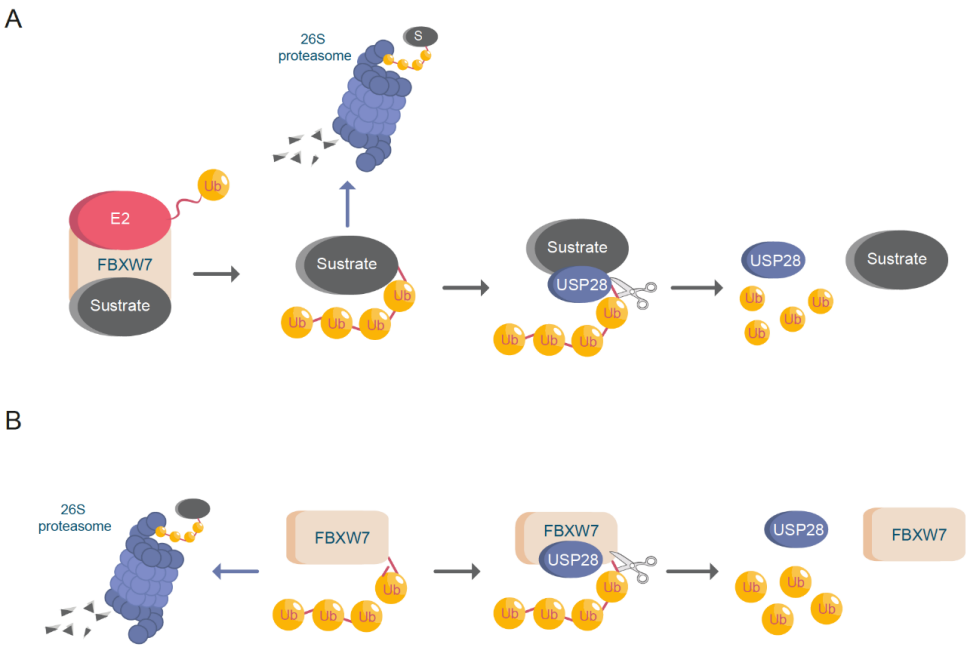

Figure 1.5: USP28 and FBXW7.
A) FBXW7 induces protein (substrate) ubiquitination enhancing proteasomal degradation. USP28 deubiquitinates FBXW7 substrates avoiding protein degradation. Ub = ubiquitin; E2 = ubiquitin conjugating enzyme. **B)** USP28 increases FBXW7 protein stability via deubiquitination. Ub= ubiquitin.

USP28 was originally identified as a protein involved in DNA damage response (DDR), interacting with the double-strand break repair protein 53BP1. This interaction results in the phosphorylation of USP28 upon exposure to ionizing radiation in an ATM-dependent manner (Knobel et al. 2014; Zhang et al. 2006). Furthermore, USP28 is involved in the stabilization of several other proteins related to DDR pathways, namely CLASPIN and CHK2 (Ito et al. 2018; Wang et al. 2018).

FBXW7 is commonly mutated or lost in SCCs, such as in the lungs (Ruiz et al. 2019), esophagus (Yokobori et al. 2012), head, and neck (Arita et al. 2017). Additionally, the reduced expression of FBXW7 correlates with aggressive tumors and resistance to therapy (Ruiz et al. 2019; Arita et al. 2017).
Considering the strong functional interconnection between DUB USP28 and E3 ligase FBXW7, this dissertation aims to clarify the functional relevance of USP28 in SCC tumors.

1.5 Complexity of squamous tumors

The epithelium is a basic tissue composed of three different types of cells classified by shape and function:

1. Cuboidal cells: These are cube-shaped cells with large, spherical central nuclei (Figure 1.6A). Cuboidal cells provide protection and mechanical support. Notably, they can differentiate and form secretory glands. Kidney or salivary glands are recovered by cuboidal cells upon tissue damage.
2. Squamous cells: The squamous epithelium is a selective permeable layer formed by a delicate line of thin and flat cells (Figure 1.6B). The esophagus or oral cavity is covered by squamous epithelial cells.
3. Columnar cells: These cells are taller than squamous or cuboidal cells and present an oval nucleus (Figure 1.6C). Columnar cells facilitate movement across the epithelial barrier, and some tissues with the columnar epithelium have cells with cilia. Intestine or uterus is covered by columnar cells.

The epithelium is considered simple, if contains one layer of cells (Figure 1.6A, B, and C) and stratified when it contains two or more layers of cells (Figure 1.6D). The higher the number of layers, the more protective is the epithelial tissue. One clear example of stratified epithelial tissue is the skin, where the squamous epithelial tissue of the skin is arranged in many layers to act as a barrier offering strong mechanical protection. Tumors arising from epithelial tissues are called carcinomas (Berman et al. 2004). Stratified epitheliums can comprise different types of epithelial cells assembling complex tissues (Xiong et al. 2014). The epithelial carcinoma is considered the most common type of cancer, and it can be subdivided in:

1. Squamous cell carcinoma (SCC): This is also called epidermoid carcinoma and it is composed of squamous cells. As mentioned earlier, squamous cells are flat cells that can be present in many different organs of the body. Accordingly, squamous tumors can be developed in several different tissues such as in the lung, esophagus, skin, pancreas, cervix, and thyroid. The precise “cell of origin” for SCC has not yet been identified, and various cellular pools have been suggested for the same (Kamate et al. 2017; Sánchez-Danés & Blanpain 2018).
2. Adenocarcinoma (ADC): ADC tumors arise from epithelial cells with secretory properties or glandular cells. ADC can be formed in different organs such as the lungs, breasts, esophagus, colon, stomach, and prostate (Zhang et al. 2015). Carcinomas can be considered adenosquamous (ADSCC) when the tumor is presenting the expression of markers and histopathological features of SCC and ADC, such as ΔNP63, CK5/6, or Napsin. Each type of cell must constitute at least 10% of the tumor bulk to be diagnosed as ADSCC (Li & Lu 2018).
3. Transitional cell carcinomas: These carcinomas arise from the transitional epithelium, which is a type of stratified epithelium tissue composed of multiple layers of epithelial cells with different

morphologies. Transitional carcinomas can be contracted or expanded to adapt themselves to the degree of distension needed by the tissue. Hence, this tumor type usually occurs in organs that form part of the urinary system such as the bladder (Al-Husseini et al. 2019)

4. Basal cell carcinomas: These tumors originate in the cells of the basal layer, located at the lower part of the epidermis. Basal cell carcinoma is the most common type of skin cancer (Clark et al. 2014).

SCCs comprise one of the largest groups of cancer types. They are histologically characterized by the presence of intercellular bridges, keratinization, and squamous pearls composed of keratins. ΔNP63 is the main histopathological marker used for classifying SCC (Conde et al. 2010, Kim et al. 2013). The common relevant secondary SCC markers are Keratin 5/6 (KRT5/6), Podoplanin, and Keratin 14 (KRT14) (Khayyata et al. 2009; Mostafa et al. 2004; Shimada et al. 2009).

Lung cancer, one of the primary causes of cancer-related deaths in the world, is a suitable model to study the differential epithelial-derived tumor types; this is because ADCs and SCCs arise in epithelial tissues, and suitable preclinical models, such as mouse non-small cell lung carcinoma (NSCLC models), are readily available (Hartmann et al. 2021). Based on the histology of the malignant cells, lung cancers are categorized into two large subgroups: NSCLC and small cell lung carcinoma (SCLC). NSCLC is the most common type of lung cancer and represents 85% of all lung cancer cases. NSCLC includes three large subtypes: ADC (40%), SCC (30%), and large cell carcinoma (15%). SCLC represents the remaining 15% of the lung cancer cases (Molina et al. 2008; American Cancer Society). Considering the high rates of epithelial carcinoma tumors arising from the respiratory system, lung cancer can be considered an exceptional model to study the main pathophysiological mechanism of SCC compared to other epithelial tumors, such as ADC.

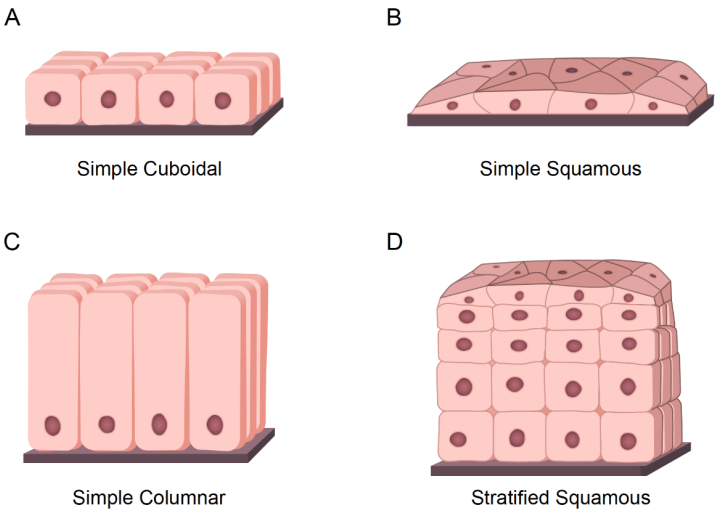

Figure 1.6: Epithelial tissue.
A) Representative model of simple cuboidal epithelium. **B)** Representative model of simple squamous epithelium. **C)** Representative model of simple columnar epithelium. **D)** Representative model of stratified epithelium; As example, the model represents the stratified squamous epithelium.

The work published by the Cancer Genome Atlas Research Network in 2012 focused on a detailed analysis of the mutational landscape of SCC tumors (Cancer Genome Atlas Research Network 2012). This extensive analysis comprises DNA copy number alterations, mutations, mRNA expression, and promoter methylation of SCC patient biopsies. These unprecedented novel insights into this disease increased our understanding of the mutational complexity of SCC tumors. SCCs present one of the genetically most complex tumors, as they vary dramatically between patients in terms of the occurrence of tumor drivers (Sos & Thomas 2012).

Predominantly recurring genetic alterations are found in Tp53; these are more frequent compared to other tumor entities (Smardova et al. 2015; Lahin et al. 2019). Copy number alterations of SOX2, PDGFRA, or FGFR1 along with deletions of tumor suppressor CDKN2A are frequently reported for SCC. In addition, recurrent mutations in RB1, KEAP1, NFE2L2, BAI3, FBXW7, GRM8, MUC16, RUNX1T1, LKB1, and ERBB4 have also been identified (Cancer Genome Atlas Research Network 2012). Common oncogenic drivers found in SCCs are FGFR1, KRAS, EGFR, DDR2, PIK3CA, and BRAF (Bass et al. 2009; Kan et al. 2010; Weiss et al. 2010). Another key player in human SCC oncogenesis is the proto-oncogene Tp63. The N-terminal-truncated variant of the Tp63 gene, ΔNP63, is commonly overexpressed or genetically amplified in most SCCs, including those in the lungs, skin, esophagus, prostate, pancreas, cervix, vulva, thyroid, head and neck, penis, or bladder (Rocco et al 2006).

SCCs are therapeutically challenging tumor entities. These tumors are frequently aggressive and highly metastatic. Low response rates to radiotherapy and chemotherapy are commonly observed in SCC patients, and accordingly, the mortality rate is relatively high compared to that observed for other tumor entities owing to lack of efficient personalized therapies. The mortality rate is particularly high in lung SCC patients, and ~400,000 patients die owing to lung SCC every year. Nevertheless, considerable progress has been achieved owing to the development of spiral low-dose computed tomography (LDCT) screening for early diagnosis of lung cancer, which could reduce the mortality of lung cancer patients by 20% (Reduced Lung-Cancer Mortality with Low-Dose Computed Tomographic Screening 2011).

1.6 Function of Tp63 in squamous cancer cells

Based on its structure, Tp63 is a member of the Tp53 superfamily of transcription factors. Previous phylogenetic analyses showed that Tp63 is the founding member of this family. The p63 gene is significantly conserved between species, and invertebrate organisms, such as *Caenorhabditis elegans* or *Drosophila melanogaster,* express a similar protein. Tp53, Tp63, and Tp73 contain N-terminal transactivation domains (TADs), DNA-binding domain (DBDs), and oligomerization domains (OD). Additionally, the C-terminus region of p63 contains a sterile alpha motif (SAM) and a transactivation inhibitory domain (TID) (Figure 1.7A). Tp53, Tp63, and Tp73 execute their transcriptional functions as homotetramers (four molecules of Tp53, Tp63, or Tp73) or heterotetramers (tetramers comprising heterogeneous combinations of Tp53, Tp63, or Tp73 proteins) through their ODs. Tp63 exhibits high preference for forming heterotetramers with Tp73 rather than Tp53. Members of the TP53 superfamily can interact with and regulate the functions of each other via multiple mechanisms. For example, the DBD domains from mutant and wild-type (WT) Tp53 can bind to Tp63 and Tp73, thereby regulating their transcriptional activity (Moses et al. 2019; Melino et al. 2003; Dötsch et al. 2010).

There are two predominant variants of the Tp63 protein, generated using two alternative promoters, TAp63 and ΔNp63 (Figure 1.7B). The TAp63 protein contains a consensus transactivation domain at its N-terminal region. This N-terminal consensus transactivation domain located in TAp63, TAp73, and Tp53 regulates proapoptotic signaling (Moses et al. 2019). In contrast, ΔNp63 variant lacks this domain, thereby acting as a dominant negative regulator (similar to mutant p53) toward TAp63, TAp73, and Tp53. Overall, 10 different

isoforms arise via alternative splicing at the C-terminal region. These are p63α, β, γ, δ, and ε for TAp63 and ΔNp63 proteins (Vanbokhoven et al. 2011).

Tp53 is expressed ubiquitously, whereas p63 and p73 are tissue-specific isoforms. The main isoform expressed in adult squamous tissues and SCC is ΔNp63α, containing a truncated p53 TAD at the N-terminal region, along with a second transactivation domain encoded mainly by exon 11 (Figure 1.7A and B) (Vanbokhoven et al. 2011).

ΔNp63α can regulate its target gene expression by directly binding to the promoters of its target genes, resulting in "canonical" target gene activation or repression. Alternatively, ΔNp63α can interact with other transcription factors, regulating their function or affinity toward consensus binding sites. ΔNp63α can act as a dominant negative regulator of TAp53, TAp63, and TAp73 (Rocco et al. 2006). Furthermore, ΔNp63α can modify chromatin accessibility upon its attachment to enhancer sites and binding to chromatin remodeling factors (Li et al. 2019) as well as regulate the processing and formation of microRNAs (Lin et al. 2015). ΔNp63α globally regulates gene expression and signaling networks through multiple processes and mechanisms.

One of the most recurrent and common genomic alterations observed in SCCs of different entities is the amplification of chromosome 3 in the region located between 3q26 and 3q28, which includes the Tp63 gene (Kang et al. 2009). Recent studies have extensively elucidated the function of ΔNp63 in SCC pathogenesis. These studies report that the increased expression of ΔNp63α regulates a large number of signaling pathways and genetic rearrangements that crucially contribute to SCC oncogenesis (Moses et al. 2019). ΔNp63α induces a specific genetic transcriptional profile that completely transforms genetic homeostasis and molecular processes. ΔNp63α regulates key factors in tumor development, such as EGFR, MAPK, and T-cell receptor signaling pathways; chromatin remodeler pathways; and WNT, BMP, TGF-B, and NOTCH, thereby significantly contributing to oncogenic transformation and tumor onset. Additionally, ΔNp63 is involved in tumor induction and maintenance functions, such as cell adhesion, proliferation, apoptosis, DNA repair, epithelial mesenchymal transition (EMT), glutathione metabolism, and cellular redox processes or senescence (Gatti et al. 2019).

Furthermore, the oncogenic potential of ΔNp63α collaborates with the RAS pathway to induce tumorigenesis (Keyes et al. 2011). Additional studies have observed that ΔNp63α is an indispensable transcription factor for the induction of oral SCC *in vivo* (Ramsey et al. 2013). Recently, in pancreatic cancer, ΔNp63α was identified to induce the transdifferentiation of PDAC to the squamous subtype by enhancer reprogramming (Somerville et al. 2018). Hence, SCCs, are addicted to ΔNp63 expression, and its depletion or loss triggers a proapoptotic program and suppresses SCC proliferation. Targeting ΔNp63 in SCCs based on its expression or stability, is a promising and highly specific therapeutic strategy to interfere with SCC proliferation.

The protein ΔNp63α is strongly regulated by the ubiquitin system. Several E3-ligases are involved in the regulation of its stability, localization, and activity. Thus far, the E3-ligases FBXW7, ITCH1, WWP1, PIRH2, and NEDD4 are reported to ubiquitinate ΔNp63α, resulting in its proteasome degradation (Vanbokhoven et al. 2011). Additionally, MDM2 monoubiquitinates ΔNp63α, which impacts its transcriptional activity by

affecting protein localization. Following MDM2 ubiquitination, ΔNp63α translocates from the nucleus to the cytosol (Galli et al. 2010).

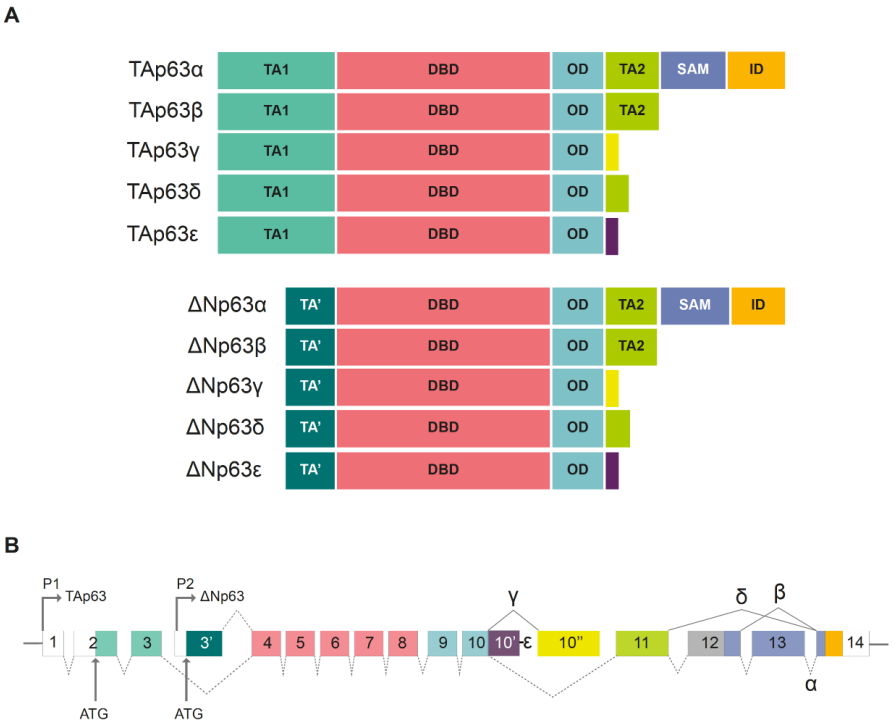

Figure 1.7: Tp63.
A) TAp63 and ΔNp63 with α, β, γ, δ, ε splice variant isoforms. TA: transactivation domain; TA′: N-terminally truncated transactivation domain; DBD: DNA binding domain; OD: oligomerization domain; TA2: second transactivation domain; SAM: sterile alpha motif; ID: inhibitory domain. **B)** Schematic representation of the P63 gene exon organization. Alternative promoters induce the synthesis of TAp63 (P1 promoter) or ΔNp63 (P2 promoter). α, β, γ, δ, ε splice variant isoforms are generated upon alternative splicing in C-terminal region. Alternatively, spliced forms for exon 10 are indicated as 10′ and 10′′. Exon numbering is indicated. The exon color code corresponds to protein domains. Adapted version from: Vanbokhoven, Melino et al. 2011.

The E3-ligase-dependent regulation of ΔNp63 in SCCs has clinical implications, as FBXW7 is commonly mutated or deleted in SCCs, leading to increased ΔNp63 protein abundance and stability (Ruiz et al. 2019; Galli et al. 2010). Although studies have investigated the posttranslational modification of ΔNp63 by E3 ligases, there are currently no known deubiquitylating enzymes reported for regulating of the stability or activity of ΔNp63.

1.7 DNA damagre response in oncogenesis and cancer therapy

DNA damage and replication stress have emerged as major hallmarks of cancer. In terminally differentiated cells, DNA is constantly damaged by either exogenous agents, such as ultraviolet (UV) or ionizing radiation (IR), or by endogenous agents, such as reactive oxygen (Broustas & Lieberman 2014). Cells can suffer different types of DNA damage, including but not limited to interstrand crosslinks (ICLs), single-strand breaks (SSBs), DNA protein crosslinks (DPCs), or double-strand breaks (DSBs). In addition to the DNA damage caused by exogenous and endogenous stressors, DNA damage constantly occurs during replication by collisions of the replication forks with DNA-binding proteins or the transcriptional machinery. DNA repair pathways are essential to maintain genome integrity, and deficiencies in DNA repair genes are a source of genetic alterations in oncogenes and tumor suppressors, which may serve as precursors inducing the development of malignant tumors (Basu 2018).

A mainstay in cancer therapy is the induction of DNA damage, thereby overwhelming the repair machinery of malignant cells. Frequently, owing to mutations in the genes controlling cell cycles, such as TP53, tumor cells accumulate DNA damage during therapy, whereas non-transformed somatic cells can halt their cell cycle to initiate the repair of damaged DNA segments. Hence, the efficacy of cancer therapies is highly influenced by the activity of the DNA repair machinery in cancer cells. Research has shown that exposure to DNA repair inhibitors is synergistic with DNA-damage-inducing therapies in preclinical models. Given the pervasive impact and clinical utility of the DNA repair system in cancer, it is important to develop novel strategies to elucidate the role of DNA repair pathways in cancer development and treatment (Torgovnick et al. 2015).

SSBs can be induced by various biological processes, such as deamination of bases, errors during replication, or the formation of bulky adducts. These breaks are commonly repaired by the base excision repair (BER), nucleotide excision repair (NER), or mismatch repair (MMR) machinery (Figure 1.8A). NER replaces damaged nucleotides, whereas BER repairs significant DNA alterations (as bulky adducts), and MMR substitutes mismatched base pairs during DNA synthesis. In contrast, DSBs are one of the most deleterious types of DNA damage and are predominantly repaired via non-homologous end joining (NHEJ) and homologous recombination repair (HRR) (Figure 1.8A). DNA repair via NHEJ is prone to introducing sequence errors, whereas HRR ensures error-free DNA repair (Minten & Yu 2019).

A

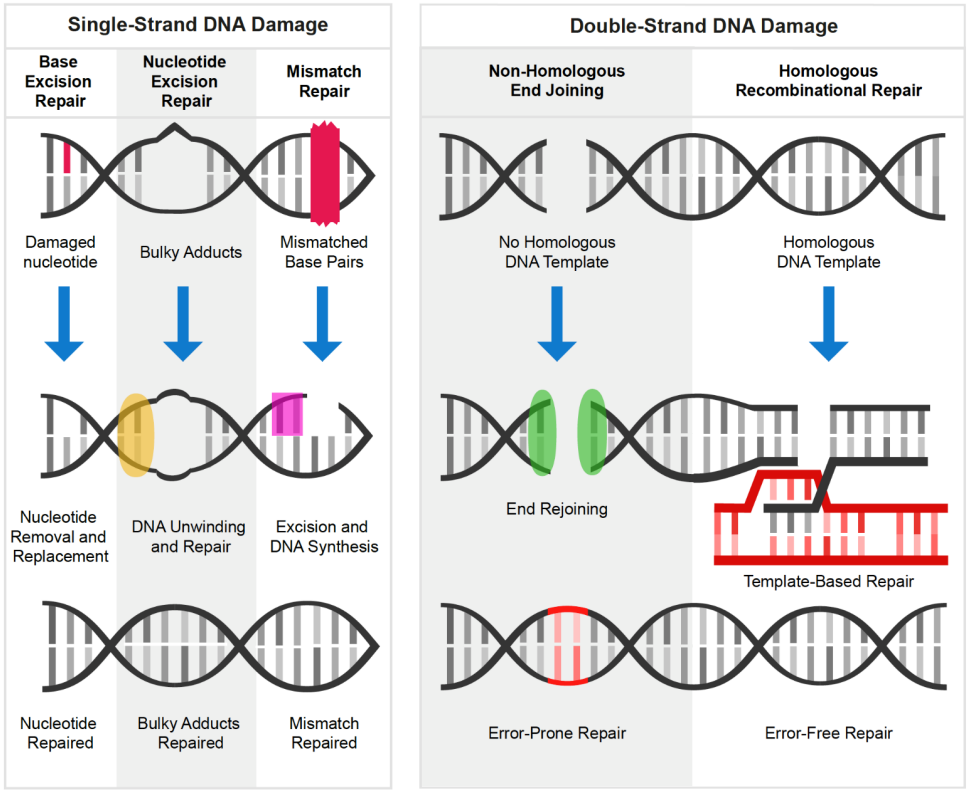

Figure 1.8: DNA repair pathways.

A) DNA repair pathways for DNA single-strand breaks: BER (base excision repair) repairs damage of nucleotides without altering significantly structure of the DNA. NER (Nucleotide excision repair) pathway repairs the DNA damage upon significant alterations of the DNA structure, as bulky adducts. MMR (Mismatch repair) repairs mismatched nucleotides caused during DNA synthesis. **DNA repair pathways for DNA double-strand breaks:** Non-homologous end joining (NHEJ) repairs DNA rejoining the broken DNA ends. NHEJ pathway does not require homologous DNA template but it is prone to introduce errors. and is prone to introducing errors.

Homologous recombination repair (HRR) requires the homologous DNA as a template. HRR pathway repairs without errors. Adapted version from: Minten & Yu 2019.

Classic DNA damage therapies, such as Cisplatin (CPPD) or radiotherapy, differ in the type of damage caused to DNA. CPPD is a mainstay in cancer therapy and is considered one of the most successful cancer therapies till date. CPPD causes DNA crosslinks leading to DNA damage, thereby resulting in replication inhibition and cell death. Its mode of action remains controversial, and the widely accepted action mechanism is that CPPD is intracellularly activated by the hydrolysis of chlorides and that the Pt, together with two different amines, interacts with DNA, forming Pt–DNA crosslinks. At the beginning, CPPD can only generate one covalent interaction with DNA, forming a monofunctional Pt–DNA adduct. Later, CPPD can react with another guanine, forming DNA crosslinks. If the interaction between Pt and DNA occurs on the same DNA strand, an intrastrand crosslink is formed; however, when two different DNA strands are linked, an ICL is formed. Upon CPPD treatment, the formation of intrastrand crosslinks is more frequent than the formation of ICLs. The formation of adducts and crosslinks trigger a multitude of different effects such as DNA unwinding, DNA bending, or replication stress, which induce the formation of DNA strand breaks. Ultimately, CPPD considerably increases the number of SSBs and DSBs (Rezaee et al. 2013).

1.8 DNA repair in squamous tumors: Fanconi anemia pathway

Low response rates to traditional cancer therapies, such as chemotherapy, are particularly common in SCC patients. Although initial responses to these treatments are observed, SCCs frequently acquire additional mutations, activating alternative signaling cascades that can restore tumor cell survival and proliferation (Ruiz et al. 2019). This effect is partially mediated by the SCC transcription factor ΔNp63. ΔNp63 enhances the transcription of DNA repair genes involved in recombinational repair (RR) and Fanconi anemia (FA) pathways (Bretz et al. 2016; Lin et al. 2009). RR is a DNA repair process based on a genetic exchange between a damaged DNA region and another homologous DNA region to repair broken DNA strands. RR included DNA repair processes such as recombinational ICLs or single and double-strand break HRR with SSBs and DSBs.
FA is a rare genetic disease that induces bone marrow failure, aging, chromosomal abnormality, and increased predisposition to leukemia, and the development of SCC. FA patients are particularly sensitive to DNA crosslinking agents (Walden et al. 2009). This anemic disease is induced by germline mutations in any member of the FA pathway (FANCA - FANCB - FANCC - FANCD1 - FANCD2 - FANCE - FANCF - FANCG - FANCI - FANCJ - FANCL - FANCM - FANCN - FANCO - FANCP - FANCQ - FANCR - FANCS - FANCT - FANCU - FANCV - FANCW). The FA pathway is strongly involved in the DDR and it mainly operates during the S-phase of the cell cycle. During Cisplatin-based chemotherapy, the FA pathway is particularly important for repair to resolve ICL lesions, promote replication fork stability, and control cytokinesis (Figure 1.9A) (Ceccaldi et al. 2016). ICL-induced genotoxic stress causes ATR-dependent phosphorylation of FANCM. which binds to the damaged DNA. FACNM serves as a recruitment platform for the assembly of the FA core complex. This complex is composed of FANCA, FANCB, FANCC, FANCE, FANCF, FANCG, FANCL, FANCM, FANCT, FAAP100, MHF1, MHF2, FAAP20, and FAAP24. The FA core complex is

required to initiate the phosphorylation and posterior monoubiquitination of FANCD2 and FANCI. This monoubiquitination is catalyzed by the E3-ligase FANCL and its corresponding E2 enzyme FANCT. The complex formed by FANCD2 and FANCI regulates several FA and non-FA proteins involved in DNA repair and genome stability, such as the HRR proteins BRCA1 and BRCA2 (Weidong Wang 2008).

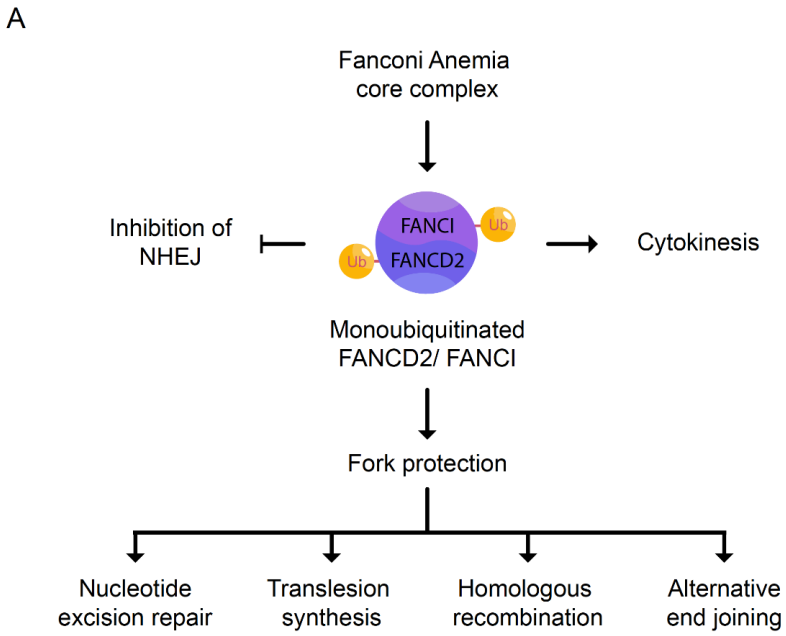

Figure 1.9: Fanconi Anemia pathway.
A) The Fanconi anemia core complex allows the phosphorylation and posterior monoubiquitination of FANCD2 and FANCI. The monoubiquitinated protein makes a complex which regulates cytokinesis and DNA fork protection via activation of the DNA repair pathways: Nucleotide excision repair, translesion synthesis, homologous recombination and alternative end joining. Furthermore, the FANCD2-FANCI complex also blocks the activation of the error prone repair pathway non-homologus end joining. Adapted version from: Ceccaldi, Sarangi & D'Andrea. 2016. Ub = Ubiquitin molecule.

There is an intimate relationship and a clear crosstalk between the FA pathway and additional repair processes. The FA pathway increases the activity of other DNA repair pathways, such as HRR, NER, translesion synthesis (TLS), and alternative end joining (Alt-EJ); at the same time, it inhibits NHEJ upon interaction between the FANCD2–FANCI complex and KU70/KU80 proteins (Figure 1.9A). In summary, there is an intricate network beyond the ICL–FA repair pathway that responds to diverse DNA insults (Nalepa & Clapp 2018; Niraj et al. 2019).

The depletion or mutation of any FA pathway member sensitizes cells to DNA crosslinking agents, such as CPPD (Kutler et al. 2016; Nepal et al. 2017). Considering that chemotherapy based on Pt compounds is commonly used for SCC patients (Ruiz et al. 2019), the FA pathway appears as a promising target to combine and potentiate DNA crosslinking agents. Previous studies have reported that depletion of ΔNp63 is sufficient to sensitize SCCs to DNA damage agents, such as CPPD, upon transcription inhibition of the FA pathway. (Matin et al., 2013). Hence, it is possible to hypothesize that reducing the abundance of the ΔNp63 protein will reduce the transcription FA repair proteins, thus decreasing the ability of SCC tumor cells to accurately repair DNA and accordingly sensitizing cancer cells to classical DNA damage therapies such as CPPD or radiotherapy.

1.9 Objectives and hypothesis of the thesis

The role of ΔNp63 in driving the transcription of the genes involved in SCC oncogenesis, DNA repair, and genome stability has been widely studied and characterized. ΔNp63 is strongly regulated at the protein level. Several E3-ligases are reported to ubiquitinate and regulate ΔNp63 protein stability, such as FBXW7. On the contrary, no DUB is reported for regulating ΔNp63 protein stability. Recent research has reported that the DUB USP28 is involved in malignant transformation and DNA repair. USP28 deubiquitinates key oncogenes, such as c-MYC and NOTCH1, thereby counteracting the E3-ligase FBXW7. USP28 also deubiquitinates Tp53, which is structurally highly similar to ΔNp63. Based on these observations, one can hypothesize that USP28 could stabilize ΔNp63 via deubiquitination, and its depletion or inhibition may be a promising strategy to treat SCC.

Therefore, the main objective of this thesis is to determine if USP28 regulates ΔNp63 stability directly and how relevant the expression of USP28 is to induce and maintain SCC tumors. To acquire a complementary view of the regulation of ΔNp63 by USP28, the focus was on elucidating the *in cellulo* and *in vivo* effects upon depletion of USP28, its inhibition or deletion effects on ΔNp63 protein stability, SCC cell identity, and DDR. Therefore, the SCC cancer cell line A-431, in combination with genetically engineered NSCLC mouse models, was used as the main experimental system for this thesis. A-431 is a well-established SCC mutant in the p53 cell line that expresses high levels of endogenous USP28 and ΔNp63. Lung cancer is a tumor entity that frequently develops into ADC and SCC tumors. Hence, it is suitable for studying the ΔNp63 biology and the role of USP28 in SCC tumors compared to other epithelial tumor entities such as ADC.

2. Materials

2.1 Antibodies

2.1.1 Primary antibodies

Antibodies	Company	Identifier	Application
Polyclonal rabbit anti-USP28	Sigma-Aldrich	HPA006778	WB (1/1000) IF (1/100) IHC (1/100) IP (2µg)
Polyclonal rabbit anti-USP28	Sigma-Aldrich	HPA006779	WB (1/1000) IF (1/100) IHC (1/100)
Rabbit monoclonal anti-p-ATM (ser1981)	Cell signalling	13050	WB (1/1000) IF (1/100) IHC (1/100) IP (5µg)
Monoclonal mouse anti p-ATM	Santa Cruz	sc-47739	WB (1/1000) IF (1/100) IHC (1/100) IP (5µg)
Monoclonal mouse anti-ACTIN/ B-ACTIN (C4)	Santa Cruz	sc-47778	WB (1/2000)
Polyclonal rabbit anti-ACTIN/ B-ACTIN	Santa Cruz	sc-1616	WB (1/2000)
Monoclonal mouse anti-VINCULIN (hVIN-1)	Sigma-Aldrich	V9131	WB (1/2000)
Monoclonal mouse anti-HA (16B12)	Abcam	ab130275	WB (1/1000) IF (1/100) IP (1µg)
Monoclonal mouse anti-FLAG (M2)	Sigma-Aldrich	F3165	WB (1/1000) IF (1/100) IP (1µg)

Monoclonal rabbit anti-KRT5 recombinant mAb	Bimake	A5439	WB (1/1000) IHC (1/100)
Polyclonal rabbit anti-KRT5	Santa Cruz	sc-66856	WB (1/1000) IHC (1/100)
Monoclonal rabbit anti-KRT14 recombinant mAb	Bimake	A5434	WB (1/1000) IHC (1/100)
Polyclonal rabbit anti-TTF1 (H-190)	Santa Cruz	sc-13040	WB (1/1000) IHC (1/100)
Polyclonal rabbit anti-p63	Thermo Scientific	PA5-36069	WB (1/1000) IF (1/100) IHC (1/100) IP (1µg)
Monoclonal mouse anti-GFP (B-2)	Santa Cruz	sc-9996	WB (1/1000) IHC (1/100)
Polyclonal rabbit anti-53BP1	Santa Cruz	sc-22760	WB (1/1000) IF (1/100) IHC (1/100)
Polyclonal rabbit anti p-ATR (ser428)	Cell signalling	2853	WB (1/1000) IF (1/100) IHC (1/100) IP (5µg)
Monoclonal rabbit anti-p-H2a.x (ser139)	Cell signalling	2577	WB (1/1000) IF (1/100) IHC (1/100) IP (2µg)
Monoclonal mouse anti-TUBULIN	Proteintech Europe	66031-1-lg	WB (1/2000)
Polyclonal rabbit anti-H3	Abcam	ab18521	WB (1/1000)
Polyclonal rabbit anti p-USP28 (ser67)	Thermo Scientific	PA5-64727	WB (1/500)

Polyclonal rabbit anti p-USP28 (ser714)	Thermo Scientific	PA5-64728	WB (1/500)
Polyclonal rabbit anti-P63	Biolegend	619001	WB (1/1000) IF (1/100) IHC (1/100) IP (2µg) ChIP (8µg)
Monoclonal rabbit anti-p63 recombinant	Bimake	A5182	WB (1/1000) IF (1/100) IHC (1/100)
Monoclonal rabbit anti-Notch1 recombinant	Bimake	A5176	WB (1/1000) IHC (1/100)
Polyclonal rabbit anti-cleaved caspase 3 (Asp175)	Cell signalling	9661	WB (1/1000) IF (1/100) IHC (1/100)
Monoclonal mouse anti c-JUN	Santa Cruz	sc-74543	WB (1/1000) IHC (1/100)
Polyclonal rabbit anti-c-MYC (N-262)	Santa Cruz	sc-764	WB (1/1000) IHC (1/100)
Monoclonal mouse anti FANCD2	Abcam	ab108928	WB (1/1000) IHC (1/100)
Polyclonal rabbit anti P53BP1	NOVUS	NB100-904	WB (1/1000) IF (1/100) IHC (1/100)
Polyclonal rabbit anti P-P53 (ser15)	Cell signalling	9284	WB (1/1000)
Monoclonal rabbit anti p-(Ser/Thr) ATM + ATR Substrate	Thermo Scientific	MA5-14872	WB (1/1000)
Monoclonal rabbit anti cleaved caspase 9	Bimake	A5074	WB (1/1000) IF (1/100) IHC (1/100)

Monoclonal mouse anti caspase 9	Santa cruz	sc-73548	WB (1/1000)
Monoclonal rabbit anti RAD51	Abcam	ab133534	WB (1/1000)
Monoclonal rabbit anti FANCI	Abcam	ab15344	WB (1/1000)

Table 2.1: Primary antibodies. Host, isotype, application and concentration used are indicated for all primary antibodies. IB= Immunoblot; IF= Immunofluorescence; IHC= Immunohistochemistry; ChIP= Chromatin immunoprecipitation; IP =Immunoprecipitation.

2.1.2 Secondary antibodies

Antibodies	Company	Identifier	Application
Donkey anti-Mouse IgG (H+L) Cross-Adsorbed Secondary Antibody, DyLight 680	Thermo Scientific	SA5-10170	WB (1/10000)
Donkey anti-Goat IgG (H+L) Cross-Adsorbed Secondary Antibody, DyLight 680	Thermo Scientific	SA5-10090	WB (1/10000)
Donkey anti-Rabbit IgG (H+L) Cross-Adsorbed Secondary Antibody, DyLight 680	Thermo Scientific	A32802	WB (1/10000)
Donkey anti-Rabbit IgG (H+L) Cross-Adsorbed Secondary Antibody, DyLight 800	Thermo Scientific	SA5-10044	WB (1/10000)
Donkey anti-Mouse IgG (H+L) Cross-Adsorbed Secondary Antibody, DyLight 800	Thermo Scientific	SA5-10172	WB (1/10000)
Donkey anti-Goat IgG (H+L) Cross-Adsorbed Secondary Antibody, DyLight 800	Thermo Scientific	SA5-10092	WB (1/10000)
Donkey anti-Rabbit IgG (H+L) Highly Cross-Adsorbed Secondary Antibody, Alexa Fluor 488	Thermo Scientific	A21206	IF (1/300)

Donkey anti-Mouse IgG (H+L) Highly Cross-Adsorbed Secondary Antibody, Alexa Fluor 488	Thermo Scientific	A21202	IF (1/300)
Donkey anti-Mouse IgG (H+L) Highly Cross-Adsorbed Secondary Antibody, Alexa Fluor 555	Thermo Scientific	A31570	IF (1/300)
Donkey anti-Rabbit IgG (H+L) Highly Cross-Adsorbed Secondary Antibody, Alexa Fluor 555	Thermo Scientific	A31572	IF (1/300)
Donkey anti-Rabbit IgG (H+L) Highly Cross-Adsorbed Secondary Antibody, Alexa Fluor 647	Thermo Scientific	A-31573	IF (1/300)

Table 2.2: Secondary antibodies. Host, isotype, application and concentration used are indicated for all primary antibodies. IB= Immunoblot; IF= Immunofluorescence.

2.2 Nucleotides

2.2.1 RT-Primers, shRNAs, gRNAs, gBlocks and repair templates

Oligonucleotides	Sequence	Company
RT-PCR hUsp28 FW	ACTCAGACTATTGAACAGATGTACTGC	Sigma
RT-PCR hUsp28 RV	CTGCATGCAAGCGATAAGG	Sigma
RT-PCR hKeratin10 FW	GCAAATTGAGAGCCTGACTG	Sigma
RT-PCR hKeratin10 RV	CAGTGGACACATTTCGAAGG	Sigma
RT-PCR hB-Actin FW	GCTACGAGCTGCCTGACG	Sigma
RT-PCR hB-Actin RV	GGCTGGAAGAGTGCCTCA	Sigma
RT-PCR hFANCI FW	TTTGCCATCAAATTGGACTATG	Sigma
RT-PCR hFANCI RV	TTGGAATCTCCTTGCTGTCC	Sigma
RT-PCR hFANCD2 FW	CCCAGAACTGATCAACTCTCCT	Sigma

RT-PCR hFANCD2 RV	CCATCATCACACGGAAGAAA	Sigma
RT-PCR hRAD51C FW	TGGATTTGGTGAGTTTCCCGC	Sigma
RT-PCR hRAD51C RV	TCTTTGCTAAGCTCGGAGGG	Sigma
RT-PCR hGpcr5A FW	AAGGTCTCCCCCAGCACT	Sigma
RT-PCR hGpcr5A RV	GGGACTGTTGTAGCCATTCTG	Sigma
RT-PCR hTp63 FW	GGAAAACAATGCCCAGACTC	Sigma
RT-PCR hTp63 RV	GTGGAATACGTCCAGGTGGC	Sigma
RT-PCR hTp63-2 FW	GAAAGCTGTTCCTTGGTCCTAGT	Sigma
RT-PCR hTP63-2 RV	GGTTTATTCAAACCCTCAGCA	Sigma
RT-PCR hKeratin5 FW	TCACCGTTCCTGGGTAACA	Sigma
RT-PCR hKeratin5 RV	GGAGGTGCTGGAGAGAACAG	Sigma
RT-PCR hKeratin14 FW	GGAAGTGAAGATCCGTGACTG	Sigma
RT-PCR hKeratin14 RV	GGACTGTAGTCTTTGATCTCAGCA	Sigma
RT-PCR hKeratin19 FW	TTGTCCTGCAGATCGACAAC	Sigma
RT-PCR hKeratin19 RV	GCCTGTTCCGTCTCAAACTT	Sigma
RT-PCR mSftpc5 FW	GGTCCTGATGGAGAGTCCAC	Sigma
RT-PCR mSftpc5 RV	GATGAGAAGGCGTTTGAGGT	Sigma
RT-PCR mkeratin5 FW	CAGAGCTGAGGAACATGCAG	Sigma
RT-PCR mKeratin5 RV	CATTCTCAGCCGTGGTACG	Sigma
RT-PCR mScgb1a1 FW	TTGTCACTGCCCTGTGTCTC	Sigma
RT-PCR mScgb1a1 RV	AAGAGGAAGGAGGGGTTGG	Sigma

RT-PCR mSox2 FW	GGCAGAGAAGAGAGTGTTTGC	Sigma
RT-PCR mSox2 RV	TCTTCTTTCTCCCAGCCCTA	Sigma
RT-PCR mUSP28 FW	ATGACAACTTGCCCCACTTC	Sigma
RT-PCR mUSP28 RV	AGTTCCACAGACAGGGCTTC	Sigma
RT-PCR mB-Actin FW	AGTGTGACGTTGACATCCGT	Sigma
RT-PCR mB-Actin RV	TGCTAGGAGCCAGAGCAGTA	Sigma
shRNA hΔNp63 #1 FW	TGAATGAACAGACGTCCAATTTCTCGAGAA ATTGGACGTCTGTTCATTCTTTTTC	Sigma
shRNA hΔNp63 #1 RV	TCGAGAAAAAGAATGAACAGACGTCCAATT TCTCGAGAAATTGGACGTCTGTTCATTCA	Sigma
shRNA hΔNp63 #2 FW	TCGAGTGGAATGATTTCAACTTCTCGAGAA GTTGAAATCATTCCACTCGTTTTTC	Sigma
shRNA hΔNp63 #2 RV	TCGAGAAAAACGAGTGGAATGATTTCAACT TCTCGAGAAGTTGAAATCATTCCACTCGA	Sigma
shRNA hUSP28 #1 FW	CCGGCAAGGAGCTTATTCGAAATCTCGAGA TTTCGAATAAGCTCCTTGTTTTTG	Sigma
shRNA hUSP28 #1 RV	AATTCAAAAACAAGGAGCTTATTCGAAATC TCGAGATTTCGAATAAGCTCCTTG	Sigma
shRNA hUSP28 #2 FW	CCGGGACTGAAGATCATCCATTACTCGAGT AATGGATGATCTTCAGTCTTTTTG	Sigma
shRNA hUSP28 #2 RV	AATTCAAAAAGACTGAAGATCATCCATTAC TCGAGTAATGGATGATCTTCAGTC	Sigma
shRNA mUSP28 #1 FW	TGCTGTTGACAGTGAGCGAGGATGTGAATT TGTATAAAAATAGTGAAGCCACAGATGTAT TTTTATACAAATTCACATCCCTGCCTACTGC CTCGGA	Sigma

shRNA mUSP28 #2 FW	TGCTGTTGACAGTGAGCGATCTGTTTATACTTTAGATAAATAGTGAAGCCACAGATGTATTTATCTAAAGTATAAACAGACTGCCTACTGCCTCGGA	Sigma
sgRNA mStk11/Lkb1 FW	CACCGCGAGACCTTATGCCGCAGGG	Sigma
sgRNA mStk11/Lkb1 RV	AAACCCCTGCGGCATAAGGTCTCGc	Sigma
sgRNA mUsp28 #1 FW	CACCGGGGAGCCTTCCGATCATCCG	Sigma
sgRNA mUsp28 #1 RV	AAACCGGATGATCGGAAGGCTCCCc	Sigma
sgRNA mUsp28 #2 FW	CACCGCGGATCGTTCCGTGAAGTAT	Sigma
sgRNA mUsp28 #2 RV	AAACATACTTCACGGAACGATCCGc	Sigma
sgRNA mKras #1 FW	CACCGACTGAGTATAAACTTGTGG	Sigma
sgRNA mKras #1 RV	AAACCCACAAGTTTATACTCAGTC	Sigma
sgRNA mTrp53 #1 FW	CACCGATGGTGGTATACTCAGAGC	Sigma
sgRNA mTrp53 #1 RV	AAACGCTCTGAGTATACCACCATC	Sigma
mKrasG12D repair template FW	TTTTGTGTAAGCTTTGGTAACTCCATGTATTTTTATTAAGTGTT	Sigma
mKrasG12D repair template RV	GAGCTTATCGATACCGTCGACACACCCAGTTTAAAGCCTTGGAA	Sigma
FLAG-hdeltaNp63alpha S383A Site-Directed mutagenesis FW	CAGCATGAACAAGCTGCCTGCCGTGAGCCAGCTTATCAACCCAC	Sigma
FLAG-hdeltaNp63alpha S383A Site-Directed mutagenesis RV	GTGGGTTGATAAGCTGGCTCACGGCAGGCAGCTTGTTCATGCTG	Sigma
Mutagenesis hUSP28 S67A FW	ATGAGAGAGTTAAGGAGCCCGCTCAAGACACTGTTGCTACAGA	Sigma

Mutagenesis hUSP28 S67A RV	TCTGTAGCAACAGTGTCTTGAGCGGGCTCCT TAACTCTCTCAT	Sigma
Mutagenesis hUSP28 S714A FW	AGTCCTCCACCAACTCCTCAGCACAGGACT ACTCTACATCACA	Sigma
Mutagenesis hUSP28 S714A RV	TGTGATGTAGAGTAGTCCTGTGCTGAGGAG TTGGTGGAGGACT	Sigma
hUSP28 S67A gblock BamHI	AAGCTTGGATCCTTACGTGCTTAGAATTGTG CCTG	Sigma
hUSP28 S714A gblock XBAI	AAGCTTTCTAGATCACATTCTAATGCCACAA TTC	Sigma
ChIP hFANCD2 FW	GCTGTCTGGCAAGTTAGG A TGG	Sigma
ChIP hFANCD2 RV	CAAGCTGTAAGGCATTTCC CCG	Sigma
ChIP hFANCI FW	GGCGGATCTTGTTGTTACGG	Sigma
ChIP hFANCI RV	CCTCCGCCACAAACTTCCAA	Sigma
ChIP hRAD51C FW	TTTGGGGAATCAAAACGGAATGG	Sigma
ChIP- hRAD51C RV	AGGCTCACCTGCTAACCCC	Sigma

Table 2.3. Oligonucleotides and gBlocks. List of RT-PCR primers, ChIP RT-PCR primers, shRNAs, gRNAs, gBlocks, and repair templates included. FW= Forward; RV= Reverse; h= Human; m= Mouse; ChIP= Chromatin immunoprecipitation

2.2.2 DNA Plasmids

DNA plasmids	Company/Source	Identifier
pLKO.DEST.EGFP	pLKO.DEST.EGFP was a gift from Ming-Sound Tsao (Addgene plasmid # 32684 ; http://n2t.net/addgene:32684 ; RRID:Addgene_32684)	Addgene plasmid # 32684

pLKO.1 puro	pLKO.1 puro was a gift from Bob Weinberg (Addgene plasmid # 8453 ; http://n2t.net/addgene:8453 ; RRID:Addgene_8453)	Addgene plasmid # 8453
pINDUCER20	pInducer20 was a gift from Stephen Elledge (Addgene plasmid # 44012 ; http://n2t.net/addgene:44012 ; RRID:Addgene_44012)	Addgene plasmid # 44012
deltaNp63alpha-FLAG	deltaNp63alpha-FLAG was a gift from David Sidransky (Addgene plasmid # 26979 ; http://n2t.net/addgene:26979 ; RRID:Addgene_26979)	Addgene plasmid # 26979
deltaNp63alpha S383A-FLAG	This thesis	N/A
pLKO-eGFP-shdeltaNp63-1 (GFP)	This thesis	N/A
pLKO-eGFP-shdeltaNp63-2 (GFP)	This thesis	N/A
pDZ Flag USP28	pDZ Flag USP28 (Addgene plasmid # 15665 ; http://n2t.net/addgene:15665 ; RRID:Addgene_15665)	Addgene plasmid # 15665
pINDUCER20 -mouse Usp28 WT (Neomycin)	This thesis	N/A
pLKO shUSP_28_1 (Puromycin)	This thesis	N/A
pLKO shUSP_28_2 (Puromycin)	This thesis	N/A
pcDNA3-HA-USP28	pcDNA3-HA-USP28 was a gift from Nikita Popov	N/A
pcDNA3-HA-USP28 C171A	pcDNA3-HA-USP28C171A was a gift from Nikita Popov	N/A
deltaNp63alphaS383A-FLAG	Site directed mutagenesis in deltaNp63alpha-FLAG. This thesis	N/A

pGEPIR 20-human-sh-Usp28	pINDUCER 20-human-shUsp28 was a gift from Carina Maier (Almut Schulze group)	N/A
pLKO USP28 S67A	This thesis	N/A
pLKO USP28 S714A	This thesis	N/A
pLKO USP28 S61A + S714A	This thesis	N/A
pcDNA3 His6-Ubi K48	pcDNA3 His6-Ubi K48 was a gift from Amir Orian	N/A
pcDNA3 His6-Ubi K63	pcDNA3 His6-Ubi K63 was a gift from Amir Orian	N/A
pcDNA3 His6-Ubi	pcDNA3 His6-Ubi was a gift from Amir Orian	N/A
psPAX2	psPAX2 was a gift from Didier Trono (Addgene plasmid # 12260 ; http://n2t.net/addgene:12260 ; RRID:Addgene_12260)	Addgene plasmid # 12260
pMD2G	pMD2.G was a gift from Didier Trono (Addgene plasmid # 12259 ; http://n2t.net/addgene:12259 ; RRID:Addgene_12259)	Addgene plasmid # 12259
pHelper	Cell Biolabs, INC.	VPK-400-DJ
pAAV2/8	AAV2/8 was a gift from James M. Wilson (Addgene plasmid # 112864 ; http://n2t.net/addgene:112864 ; RRID:Addgene_112864)	Addgene plasmid # 112864
pAAV-DJ Vector	Cell Biolabs, INC.	VPK-420-DJ
pLKO-eGFP-mshUSP_28_1 (GFP)	This thesis	N/A
pLKO--eGFP- mshUSP_28_2 (GFP)	This thesis	N/A
AAV:ITR- U6-sgRNA(p53)- pEFS-2A-mCherry-shortPA- ITR	This thesis	N/A

AAV:ITR-U6-sgRNA(Kras)-pEFS-2A-mCherry-shortPA-KrasG12D_HDRdonor-ITR	This thesis	N/A
AAV:ITR-U6-sgRNA(Kras)-U6-sgRNA(p53)-pEFS-2A-mCherry-shortPA-KrasG12D_HDRdonor-ITR	This thesis	N/A
AAV:ITR-U6-sgRNA(Kras)-U6-sgRNA(p53)-U6-sgRNA(Lkb1)-pEFS-2A-mCherry-shortPA-KrasG12D_HDRdonor-ITR	This thesis	N/A
AAV:ITR-U6-sgRNA(Kras)-U6-sgRNA(p53)-U6-sgRNA(Lkb1)-U6-sgRNA(Usp28^{1})-U6-sgRNA(Usp28^{2})-pEFS-2A-mCherry-shortPA-KrasG12D_HDRdonor-ITR	This thesis	N/A
AAV:ITR-U6-sgRNA(Kras)-U6-sgRNA(p53)-U6-sgRNA(Lkb1)-pEFS-Rluc-2A-Cre-shortPA-KrasG12D_HDRdonor-ITR (AAV-KPL)	AAV:ITR-U6-sgRNA(Kras)-U6-sgRNA(p53)-U6-sgRNA(Lkb1)-pEFS-Rluc-2A-Cre-shortPA-KrasG12D_HDRdonor-ITR (AAV-KPL) was a gift from Feng Zhang (Addgene plasmid # 60224 ; http://n2t.net/addgene:60224 ; RRID:Addgene_60224)	Addgene plasmid # 60224

Table 2.4. DNA plasmids. N/A= not applicable.

2.3 Experimental models

2.3.1 Cell lines

Cell lines	Company/Source	Identifier
Human: HEK 293T	ATCC	ATCC® CRL-11268™
Human: A-431	ATCC	ATCC® CRL-1555
Human: LUDLU-1	ECACC	92012463
Human: H1299	ATCC	ATCC® CRL-5803

Human: HELA	ATCC	ATCC® CCL-2
Human: SiHa	ATCC	ATCC® HTB-35
Human: Ca Ski	ATCC	ATCC® CRL-1550
Human: BEAS-2B	ATCC; It was a gift from Marco Antonio Calzado	ATCC® CRL-9609
Human: CALU1	ATCC	ATCC® HTB-54
Human: Detroit 562	ATCC	ATCC® CCL-138
Human: SK-MES1	ATCC	ATCC® HTB-58
Human: H23	ATCC	ATCC® CRL-5800
Human: PANC-1	ATCC	ATCC® CRL-1469
Human: BXPC-3	ATCC	ATCC® CRL-1687
Mouse: KP ADC	Primary tumor	N/A
Mouse: KP SCC	Primary tumor	N/A
Mouse: KPL SCC	Primary tumor	N/A

Table 2.5: Cell lines. N/A= not applicable

The human lung cancer cell line LUDLU-1 is maintained as a semi-attached. We subjected this cell line to a selection process, enriching for an adherent clone, which was further propagated and used for all experiments within this study. To highlight the difference towards the parental cell line, we decided to add the suffix adh. (adherent) naming the cell line LUDLU-1^{adh}. The selection process did not alter the expression of endogenous USP28, ΔNp63 and SCC markers. It is noteworthy that the overall short tandem repeat (STR) profile of the created subclone is similar, but not identical, to the parental cell line

2.3.2 Animal organisms

Animal organisms/ Strains.	Company	Identifier
B6(C)-Gt(ROSA)26Sor$^{em1.1(CAG-cas9*,-EGFP)Rsky}$/J	The Jackson laboratory	Stock No: 028555
C57BL/6J	The Jackson Laboratory	Stock No: 000664
B6.129-Kras^{tm4Tyj} Trp53^{tm1Brn}/J	The Jackson laboratory	Stock No: 032435

Table 2.6. Animal organisms/ strains.

2.4 Cell culture medium, consumables and supplements

Cell culture consumables were purchased from the companies Eppendorf, Greiner, Nunc, Sarstedt and VWR. Consumables included cell dishes, syringes, cryotubes, pipettes and in general, all disposable plastic items used in cell culture.

Cell culture medium and supplements	Company	Concentration
Gibco™ Dulbecco's Modified Eagle Medium (DMEM), high glucose	Thermo Scientific	N/A
Gibco™ RPMI 1640 Medium	Thermo Scientific	N/A
Gibco™ Trypsin-EDTA (0.5%), No Phenol Red	Thermo Scientific	N/A
Fetal Bovine Serum (FCS)	Sigma-Aldrich	10%
Penicillin-Streptomycin	Sigma-Aldrich	1%
Gibco™ GlutaMAX™ Supplement	Thermo Scientific	1%
Polybrene	Sigma-Aldrich	5 µg/ml
Polyethylenimine, Linear, MW 25000, Transfection Grade (PEI 25K)	Polysciences	N/A
Gibco™ Phosphate-buffered saline (PBS)	Thermo Scientific	N/A
Cycloheximide	Sigma-Aldrich	100 µg/ml
Doxycycline hyclate	Sigma-Aldrich	1 µg/ml
MG132	Millipore	20 µM
Puromycin	Invivogen	2.5 µg/ml
G418	Invivogen	250 µg/ml

Table 2.7. Commercial mediums and supplements used in cell culture. N/A= not applicable.

2.5 Bacterial strains, culture media and supplements

2.5.1 Bacterial strains

Bacterial strains	Description
DH5α	Escherichia coli, genotype F- Φ80lacZΔM15 Δ (lacZYAargF) U169 recA1 endA1 hsdR17 (rK-,mK+) phoA supE44 λ- thi-1 gyrA96 relA1
XL1 blue	Escherichia coli, genotype recA1 endA1 gyrA96 thi- 1hsdR17 supE44 relA1 lac [F′ proAB lacIqZΔM15 Tn10 (Tetr)]

Table 2.8. Bacterial strains.

2.5.2 Bacterial culture media

Culture media	Composition
LB medium	LB medium 10% (w/v) Bacto tryptone (Roth) 0.5% (w/v) yeast extract (Roth) 1% (w/v) NaCl (Roth)
LB agar	LB-medium with 1.2% (w/v) agar-agar (Roth)

Table 2.9. Composition of bacterial culture media.

2.5.3 Antibiotics for bacterial culture media

Antibiotics	Composition
Ampicilin (Roth)	100 µg/ml final concentration
Kanamycin (Roth)	100 µg/ml final concentration

Table 2.10. Antibiotics used in bacterial culture media.

2.6 Commercial kits

Commercial kits	Company
ReliaPrep™ RNA Cell Miniprep System Protocol	Promega
NEBNext® Ultra™RNA Library Prep Kit for Illumina	New England Biolabs (NEB)
NEBNext® Multiplex Oligos for Illumina (Dual Index Primers Set 1)	New England Biolabs (NEB)

NEBNext® Poly(A) mRNA Magnetic Isolation Module	New England Biolabs (NEB)
PureLink HiPure Plasmid Maxiprep Kit	Invitrogen
GeneJET Gel Extraction Kit	Thermo Scientific
MiniElute PCR Purification Kit	Qiagen
GeneEditor™ in vitro Site-Directed Mutagenesis System	Promega
One-Step TB Green® PrimeScript™ RT-PCR Kit	Takara
ReliaPrep™ FFPE Total RNA Miniprep System	Promega
Tandem Mass Tag (TMT) Systems labelling kits	Thermo Scientific
Pierce™ DAB Substrate Kit	Thermo Scientific
Actin Cytoskeleton / Focal Adhesion Staining Kit	Merck
Signal Stain DAB Substrate Kit	Cell Signaling
Chromatin Extraction Kit (ab117152)	Abcam

Table 2.10. Commercial kits.

2.7 Standards, chemicals and enzymes

Standards, chemicals and enzymes	Company
RNase A	Roth
RNase-free DNase	Qiagen
DNase	Applichem
Gene Ruler 1 kb Plus DNA ladder	Thermo Scientific
PageRuler Prestained Protein Ladder	Thermo Scientific
Protein HiMark Prestained High molecular weight Standard	Life Technologies
Phusion HF DNA polymerase	Thermo Scientific

10x Phusion High-Fidelity buffer	Thermo Scientific
Restriction endonucleases	Thermo Scientific and NEB
T4 DNA ligase	Thermo Scientific
Dimethyl sulfoxide (DMSO)	Sigma-Aldrich
Ethanol (Etoh)	Carl Roth
Nuclease-free water	Merck
Tandem ubiquitin binding entity (TUBE) GST-4× UIM-ubiquitlin fusion protein	It was a gift from Rune Busk Damgaard
Ub-VME, Ub-VS and Ub-PA suicide-probes	UbiQ
Propidium Iodide (PI)	Sigma-Aldrich
Protease Inhibitor Cocktail	Roche
Pierce™ Protein A/G Magnetic Beads	Thermo Scientific
Dynabeads. Protein A/G	Life Technologies
Agencourt AMPure XP Beads	Beckman Coulter
Nickel-NTA-agarose Beads	Qiagen
Glutathione Sepharose 4B beads	GE Healthcare
4′,6-diamidino-2-phenylindole (DAPI)	Thermo Scientific
Hoechst	Thermo Scientific
Coomassie Brilliant Blue R-250 Dye	Thermo Scientific
2-Propanol/ Isopropanol	Roth
Adenosintriphosphat (ATP)	Jena Bioscience
Agarose	Roth
Ampicillin (Amp)	Roth
Bovine serum albumine (BSA)	Merck Millipore

Mowiol® 40-88	Sigma-Aldrich
Cytoseal™ 60	Thermo Scientific
Dithiothreitol (DTT)	Sigma-Aldrich
Eosin	Sigma
Hematoxylin	Sigma
Differentiation Solution	Sigma
Polyvinylidene difluoride membranes (PVDF) Immobilon-FL	Merck
N,N,N',N'-tetramethylenethylendiamine (TEMED)	Roth
Natrium chloride (NaCl)	AppliChem
Neutrally buffered formalin (NBF)	Thermo Scientific
Tris-HCl	Roth
Triton X100	Roth
Xylene	Sigma
β-Mercaptoethanol	Roth
Methanol (MeOH)	Roth
peq GOLD Trifast	VWR (Peqlab brand)
M-MLV reverse transcriptase	Promega
M-MLV RT 5X Buffer	Promega
Deoxynucleotidetriphosphates (dNTPs) Mix	Promega
Random Hexamer Primer	Thermo Scientific
RiboLock RNase Inhibitor	Thermo Scientific
SYBR™ Green PCR Master Mix	Thermo Scientific

PrimeSTAR GXL polymerase	Takara
5x PrimeSTAR GXL buffer	Takara
N, N-Dimethylformamid (DMF)	Sigma
Trypsin	Promega
Collagenase 1	Thermo Scientific
Lys-C	Wako Chemicals
Sep-Pak tC18	Waters
Calf-Intestinal.Phosphatase (CIP)	New England Biolabs (NEB)
Whatman filter paper	A.Hartenstein
Pluronic F68	Gibco
Paraformaldehyde (PFA)	Sigma
Crystal Violet	Sigma
Ethidium bromide	Sigma
GlycoBlue	Fermentas
Protease inhibitor cocktail	Bimake
Hydrogen peroxide (H2O2)	Sigma

Table 2.11. Standards, chemicals and enzymes.

2.8 DNA damage drugs and inhibitors

Drug / Inhibitor	Company
Cisplatin	Selleckhem
5-Fluorouracil	Selleckhem
Oxaliplatin	Selleckhem

VE-821 (ATR inh.)	Selleckhem
KU-55933 (ATM inh.)	Selleckhem
PR-619 (pan-DUB inh.)	Selleckchem
AZ1 (USP28 inh.)	Probechem
AZ1 (USP28 inh.)	Selleckchem

Table 2.12. DNA damage drugs and inhibitors.

2.9 Buffers and solutions

All chemicals used in the preparation of buffers were purchased from AppliChem, Calbiochem, Invitrogen, Merck, Roth and Sigma, unless otherwise indicated. Homemade buffers were prepared using dd H2O, unless otherwise indicated.

Buffers and solutions	Recipe
20x TBS buffer	500 mM Tris base 2.8 M NaCl pH 7.4
1x TBS-T buffer	1 x TBS 0.2% Tween-20
TE buffer	10 mM Tris (pH 7.4) 1 mM EDTA (pH 8.0)
50x TAE buffer	2 M Tris (pH 8.0) 5.7% acetic acid 50 mM EDTA
10x Transfer buffer	250 mM Tris base 1.5 M glycine
1x Transfer buffer	1/10 Transfer buffer 10x dilution 20% (v/v) methanol

Blocking Buffer (Western Blot)	0.1% casein 0.2xPBS 0.1% Tween20
Primary antibody buffer (IF)	3% BSA in 1x PBS
Secondary antibody buffer (IF)	3% BSA in 1x PBS
FACS medium for in vivo cells	2% FCS in 1x PBS
6x SDS Loading Buffer/ lämmli buffer	1.2 g SDS pellet 6 mg bromphenol blue 4.7 ml 100% glycerol 1.2 ml 0.5 M Tris (pH 6.8) 2.1 ml ddH2O 0.93 g DTT
1x SDS Running Buffer	25 mM Tris base 250 mM glycine 0.1% (v/v) SDS
SDS stacking gel	4% (v/v) acrylamide/bisacrylamide 125 mM Tris HCl (pH 6.8) 0.1% (w/v) SDS 0.1% (w/v) APS 0.1% (v/v) TEMED
SDS separating gel	7.5-12.5% (v/v) acrylamide/bisacrylamide 375 mM Tris HCl (pH 8.8) 0.1% (w/v) SDS 0.1% (w/v) APS 0.1% (v/v) TEMED
Blocking Buffer (IF)	5% BSA in 1x PBS
Trypsin solution	0.25% trypsin 5 mM EDTA 22.3 mM Tris (pH 7.4) 125 mM NaCl

DNA preparation resuspension buffer	50 mM Tris HCl 10 mM EDTA 100 µg/ml RNAse
Primary antibody buffer (WB)	0.1% casein 0.2× PBS 0.1% Tween20
Secondary antibody buffer (WB)	0.1% casein 0.2× PBS 0.1% Tween20 0.01% SDS
DNA preparation lysis buffer	200 mM NaOH 1% (w/v) SDS
DNA preparation precipitation buffer	3.1 M potassium acetate (trihydrate) pH 5.4
RIPA Lysis Buffer	10mM TRIS HCl (pH 8.0) 1mM EDTA 0.5mM EGTA 1% Triton X100 0.1% Sodium Deoxycholate 0.1% SDS 140mM NaCl
Phenol-chloroform	25 ml phenol 24 ml chloroform 1 ml isoamyl alcohol
Crystal violet solution	0.5% (w/v) crystal violet 20% (v/v) Methanol
Propidium iodide-staining buffer	8 mM sodium citrate 54 µM propidium iodide 24 µg/ml RNase A
Ubiquitin-buffer 1	6 M guanidine-HCl 0.1 M Na2HPO4/NaH2PO4 10 mM imidazole

Ubiquitin-buffer 2	25 mM Tris-HCl (pH6.8) 20 mM imidazole
Bradford reagent	0.01% (w/v) Coomassie Brilliant Blue G250 8.5% phosphoric acid 4.75% ethanol
ChIP wash buffer 1	20 mM TRIS/HCl (pH8) 150 mM NaCl 2 mM EDTA 0.1% SDS 1% Triton X-100;
ChIP elution buffer	50 mM TRIS, pH 8.0 1 mM EDTA 1% SDS 50 mM NaHCO3
ChIP lysis buffer 1	5 mM PIPES (pH8) 85 mM KCl 0.5% NP-40
ChIP lysis buffer 2	50 mM HEPES pH 7.9 140 mM NaCl 1 mM EDTA 1% TritonX-100 0.1% deoxycholic acid sodium salt 0.1% SDS
ChIP wash buffer 2	20 mM TRIS HCl (pH8) 500 mM NaCl 2 mM EDTA 0.1% SDS 1% Triton X-100
ChIP wash buffer 3	10 mM TRIS HCl (H8) 250 mM LiCl 1 mM EDTA 1% NP-40 1% deoxycholic acid sodium salt

MS protein resuspension buffer	8 M Urea 10mM EPPS pH 8.2
MS protein digestion buffer	1 M Urea 10mM EPPS pH 8.2
DNA loading buffer 6x	10 mM EDTA (pH 8) 0.2% (w/v) Orange G 40% (w/v) sucrose
1X Phosphate-buffered saline (PBS)	137 mM NaCl 2.7 mM KCl 10.1 mM Na2HPO4
Warhead lysis buffer (HR lysis buffer)	50 mM TRIS HCl (pH 7.4) 5 mM MgCl2 250 mM sucrose 0.1% NP40 1 mM DTT 2 mM ATP
Ubiquitin pull-down lysis buffer	6M guanidine HCl 0.1 M Na2HPO4 0.1 M NaH2PO4 0.01 M Tris (pH 8.0) 10 mM β-mercaptoethanol
TMT resuspension buffer	10 mM ammonium bicarbonate (ABC) 5% acetonitrile (ACN)
HPLC solvent	0.1% Formic acid 80% ACN
Virus resuspension buffer	PBS (pH 7.4) 0.001% Pluronic F68
DAPI-staining buffer for FACS	20 µl DAPI (5 mg/ml) 0.5% Triton X 100 10 ml PBS

Warhead resuspension solution	50mM Sodium Acetate 5%DMSO pH 4.5
TUBE lysis buffer	50 mM Tris-HCl pH 7.4 1 % NP-40 0.5 % Deoxychylate 0.1 % SDS 150 mM NaCl 2 mM EDTA 5 mM MgCl2 1mM DTT
Citrate buffer	82 mM Sodium Citrate dehydrate 18 mM Citric Acid pH 6

Table 2.13. Buffers and solutions. MS= Mass spectrometry; ChIP= Chromatin immunoprecipitation; WB= Western blot. IF= Immunofluorescense TUBE= Tandem ubiquitin binding entity; TMT= Tandem Mass Tag.

2.10 Equipment and software

2.10.1 Equipment and instruments

Instrument	Company
Odyssey® CLx Imaging System	Licor
iBright™ FL1000 Imaging System	Invitrogen
BD FACSCanto II Cell Analyzer	BD Biosciences
StepOnePlus Real-Time PCR System	Thermo Scientific
Invitrogen Countess II FL Automated Cell Counter	Thermo Scientific
Pannoramic DESK scanner	3DHISTECH
FSX100 microscopy	Olympus Life Science
Operetta High-Content Imaging System	Perkin Elmer
Fragment Analyzer	Agilent formerly Advanced Analytical
Axiocam 503 mono	Zeiss
Branson Sonifier 250	Branson
250 mm long C18 column: X-Bridge, 4.6 mm ID, 3.5 µm particle size	Waters

EASY-nLC™ 1200 System	Thermo Scientific
Orbitrap Fusion Lumos mass spectrometer	Thermo Scientific
1.9 µm C18 particles	ReproSil-Pur, Dr. Maisch
Hyrax M55 Rotary Microtome	Leica
Mr. Frosty freezer container	Thermo Scientific
PCR cycler: SimpliAmp thermo cycler	Life technologies
Experion™ Automated Electrophoresis System	Bio-Rad
Cell culture incubator BBD 6220	Heraeus
Casy® cell counter	Innovatis
Centrifuge Avanti J-26 XP	Backman Coulter
Centrifuge Eppendorf 5417 R	Eppendorf
Centrifuge Eppendorf 5425	Eppendorf
Centrifuge Eppendorf 5430	Eppendorf
Centrifuge Galaxy MiniStar	VWR
Centrifuge Multifuge 1S-R	Heraeus
Deep-sequencer Genome Analyzer IIx	Illumina
Dry Bath System	Starlab
Thermomixer® comfort	Eppendorf
Incubator shaker Model G25	New Brunswick Scientific
Luminometer GloMax	Promega
Microscopes Axiovert 40CFL	Zeiss
PCR thermal cycler Mastercycler pro S	Eppendorf
Spectrofluorometer NanoDrop 1000	Thermo Scientific
UltrospecTM 3100 pro UV/Visible	Amersham Biosciences
SDS page system Minigel	Bio-Rad
SDS page system Tetra Cell	Bio-Rad
Maxi UV fluorescent table	Peqlab
Mixer Vortex-Genie 2	Scientific Industries
Julabo ED-5M water bath	Julabo
Memmert waterbath	Memmert

Immunoblot transfer system: Perfect Blue Tank Electro Blotter Web S	Peqlab
Power supply: Power Pac	Bio-Rad
Chemiluminescence imaging LAS-4000 mini Fujifim	Fujifim
Illumina GAIIx sequencer	Illumina
Sterile bench HeraSafe	Heraeus
Siemens linear accelerator for X-ray irradiation	Siemens
Pipetman Classic P2.5, P10, P20, P200 and P1000	Gilson
Dionex Ultimate 3000 analytical HPLC	Thermo Scientific
NextSeq 500 sequencer	Illumina
Leica VT 1200S	Leica
Microscope TCS SP5	Leica
BD FACS Aria III	BD Biosciences
Pipetboy acu 2	Integra
Consort EV243 electrophoresis power supply	Sigma
Ventana DP 200 slide scanner	Roche

Table 2.14. Equipment and instruments.

2.10.2 Software and online tools

Software	Company/Source
cBioportal	https://www.cbioportal.org
GEPIA and GEPIA2	http://gepia.cancer-pku.cn
KM-plotter	http://kmplot.com/analysis/
Operetta Imaging	Perkin Elmer
BoxPlotR	http://shiny.chemgrid.org/boxplotr/
Morpheus	https://software.broadinstitute.org/morpheus/
Excel	Microsoft
Affinity Desgner	h https://affinity.serif.com/es/designer/
Image Studio	Licor
Panther Classification system	http://pantherdb.org
AATBIO IC50 calculator	https://www.aatbio.com/tools/ic50-calculator

PRISM4	GraphPad Software, Inc.
Affinity Designer	Serif Europe
ImageJ	National Insistute of Health
Primerx	http://www.bioinformatics.org/primerx/cgi-bin/DNA_1.cgi
ROC Plotter	http://www.rocplot.org/
Pannoramic Case Viewer	3dHistech
R2: Genomics Analysis and Visualization Platform	http://r2.amc.nl
UCSC Xena	https://ucsc-xena.gitbook.io/project/
Proteome discoverer 2.2	Thermo Scientific
MaxQuant	https://www.maxquant.org/
Perseus 1.6.5.	https://maxquant.net/perseus/
Uniprot	https://www.uniprot.org/
GenerateFastq v1.1.0.64	http://emea.support.illumina.com/downloads/local-run-manager-generate-fastq-module.html
FastQC	http://www.bioinformatics.babraham.ac.uk/projects/fastqc/
Bowtie2 v2.3.4.1	http://bowtie-bio.sourceforge.net/index.shtml
TopHat v.2.1.1	https://ccb.jhu.edu/software/tophat/index.shtml
Samtools v1.3	http://samtools.sourceforge.net
R	https://www.r-project.org
EdgeR	https://bioconductor.org/packages/release/bioc/html/edgeR.html
GenomicAlignments	https://bioconductor.org/packages/release/bioc/html/GenomicAlignments.html
GSEA v2.2	http://software.broadinstitute.org/gsea/downloads.jsp
COMBENEFIT	https://www.cruk.cam.ac.uk/research-groups/jodrell-group/combenefit
Harmony Software	Perkin Elmer
EMBL	https://www.embl.de/
SPLASHRNA	http://splashrna.mskcc.org/
BD FACSDiva 6.1.2 BD	Biosciences
FlowJo 8.8.6	FlowJo, LLC

Illustrator TM,	Adobe Inc.
Photoshop TM,	Adobe Inc.
Acrobat TM	Adobe Inc.
Integrated Genome Browser	Nicol et al. 2009
Mac OS X	Apple Inc.
Office 2011 Mac	Microsoft Inc.
Qupath	https://qupath.github.io
UCSC Genome Bioinformatics	http://genome.ucsc.edu
ApE plasmid editor	By Wayne Davis
Venn diagrams	http://bioinformatics.psb.ugent.be/webtools/Venn/
Nemates	http://nemates.org
Online Web statistical calculator Astatsa	https://astatsa.com/
DOI citation formatter	https://citation.crosscite.org
Zhang lab gRNAs design resources	https://zlab.bio/guide-design-resources
CHOPCHOP	http://chopchop.cbu.uib.no/
RNAi Consortium	www.broadinstitute.org/rnai-consortium/rnai-consortium-shrna-library
Cancer Therapeutics Response Portal	https://portals.broadinstitute.org/ctrp.v2.1/
Genomics of Drug Sensitivity in Cancer	https://www.cancerrxgene.org/
Catalogue Of Somatic Mutations In Cancer (COSMIC)	https://cancer.sanger.ac.uk/cell_lines
Gene Expression and Mutations in Cancer Cell Lines (GEMiCCL)	https://www.kobic.kr/GEMICCL/

Table 2.15. Software and online tools.

3. Methods

3.1 Cell biology methods

3.1.1 Cultivation of eukaryotic cells

Mammalian cells were cultivated at 37°C, 5% CO2 and 95% relative humidity in a cell incubator for optimal growth conditions. Cell lines were originally obtained from American Type Culture Collection (ATCC) or European Collection of Authenticated Cell Cultures (ECACC). Primary murine cell lines were maintained in DMEM supplemented with 10% FCS and 1% Pen-Strep. A-431, BEAS-2B, SiHa, PANC-1 Ca SKI, DETROIT 562 and HEK-293T cells were cultured in DMEM supplemented with 10% FCS and 1% Pen-Strep. LUDLU-1^{adh}, NCI-H1299, CALU 1, BXPC-3, SK-MES1, and H23 cells were cultured in RPMI 1640 medium supplemented with 10% FCS/ 1% GlutaMAX and 1% Pen Strep. Cells were tested for mycoplasma infection by PCR and were found to be not infected. For the experiments, all cell lines were authenticated by STR profiling and tested for mycoplasma infection. Except when a different concentration was expressly indicated, the reagents were dissolved in Dimethyl sulfoxide (DMSO) or Dimethylformamide (DMF) and added to the cells in culture at the following concentrations: Cisplatin (CPPD; 5µM; dissolved in DMF), doxycycline (DOX; 1µg/ml), KU55933 (15 µM; dissolved in DMSO) and VE 821 (2.5 µM; dissolved in DMSO). AZ1 (15 µM; dissolved in DMSO).

3.1.1.1 Cell passaging

Mammalian cells were passaged every two to three days. After medium removal, adherent cells were washed twice with 1xPBS and then, trypsinized with 0,5% trypsin at 37 °C for 5 minutes in order to detach them from the plastic dish. To stop the enzymatic reaction, complete medium (medium with 10%FCS) was added to the trypsin in a 3:1 ratio. Suspended cells were collected in a 15ml Falcon tube and centrifuged at 1500rpm, room temperature (RT) for 5 min. After the supernatant solution was removed, the pellet was resuspended in appropriate complete medium and the desired fraction of cells is plated in a new cell culture dish. If specific number of cells are required, the number of cells in suspension were quantified using the CASY automated cell counter before plating in a cell culture dish.

3.1.1.2 Cell freezing

For freezing cells, wanted number of cells were collected by trypsinization as previously described. Upon centrifugation, cells were resuspended in appropriate volume of sterile freezing medium composed by 50% FCS, 40% DMEM or RPMI1640 and 10% DMSO. Cells were transferred to cryotubes and placed in a Mr. Frosty freezing container filled with isopropanol. Mr Frosty reduces the inner temperature 1°C per minute when stored at a -80°C. For long-term storage, cell lines were placed in a liquid nitrogen tank where they can be maintained for years.

3.1.1.3 Cell thawing

In order to thaw cells, cryoconserved tubes were rapidly located in a water bath at 37°C until for few minutes. Then, cells were rapidly transferred immediately into a falcon filled with 10 ml of the corresponding complete medium. In order to remove the toxic DMSO, cells were centrifuged at 1500rpm for 3 minutes. Upon resuspension in appropriate cell culture medium, cells were plated on plastic culture dishes and incubate at 37°C, 5% CO2 and 95% relative humidity.

3.1.2 Virus production

3.1.2.1 Production of Adeno-associated virus

Adeno-associated viruses (AAVs) were generated and packaged in HEK293-T cells seeded in 15-cm cell culture dishes. For AAV production, 60-70% confluence HEK293-T cells (70% confluence) were transfected with the plasmid of interest (10 µg), pHelper (15 µg) and pAAV-DJ or pAAV-2/8 (10 µg) using PEI in ratio 2:1 (70 µg). After 96 H, the cells and medium from 3 to 6 dishes were transferred to 5 ml chloroform in a 50ml Falcon tube. Before to add NaCl (1M), the Falcon tube was shaken at 37°C for 60 min. After NaCl is dissolved, the tubes were centrifuged at 20,000g at 4°C for 15 min and the chloroform layer was transferred to another Falcon tube containing 10% PEG8000. As soon as the PEG8000 is homogenized, the mixture was incubated at 4°C overnight. Next day, the mixture was centrifuged at 20,000g at 4°C for 15 min, the supernatant was discarded and the pellet was resuspended in a buffer composed by PBS with MgCl2 and 0.001% pluronic F68. Finally, viruses were purified using 1x chloroform and stored at -80°C. Viruses were quantified using Coomassie staining as described (Kohlbrenner et al. 2012).

3.1.2.2 Production of Lentivirus

For lentivirus production, HEK293-T cells (60-70% confluence) in complete medium were transfected with 15µg of the plasmid of interest, 10µg of the packaging vector pPAX and 10µg of the envelope vector pPMD2. As previously indicated, the transfection was performed using PEI in ratio 2:1 (70 µg of PEI). After 96h, the medium containing lentivirus was filtered (0.45µM) and stored at -80°C.

3.1.3 Transfection and infection of cells

3.1.3.1 Transfection of cells

DNA transfection was performed exposing 60% confluence cells plated in a 6-well cell culture dish to a mix of 2.5µg DNA, 200µl free medium (DMEM or RPMI1640 without FCS) and 5µl PEI (1:2 ratio). Upon 6h incubation at 37°C, 5% CO2 and 95% relative humidity, the medium was removed and substituted by complete supplemented medium. Cells express detectable levels of the transfected DNA after 48 hours.

3.1.3.2 Viral infection of cells

For viral infection, 10 MOI (multiplicity of infection) of adeno-associated virus (AAVs) or Lentiviruses (LVs) were added to normal medium of the cells in the presence of polybrene (5µg/ml). Cells exposed to the viruses

were incubated at 37°C, 5% CO2 and 95% relative humidity for 4 days. The infected cells were identified and collected by sorting the positive RFP or GFP cells or by exposing them to antibiotic. If required, High titer of viruses were obtained by concentrate them by ultra-centrifugation (25,000 rpm at 4 °C for 90 min). Supernatant was removed, the pellet was air-dried for 30min and then, resuspended in PBS and stored at -80 °C.

For infected cells expressing GFP and RFP, they were sorted from non-infected cells via fluorescence-activated cell sorting (FACS). To prepare the attached cultured cells for FACS sorting, they were trypsinized, re-suspended in 10ml DMEM and transferred to a 15ml Falcon. The falcon was centrifuged at 1000rpm for 3 min and the pellet resuspended in PBS with 2% FCS. Positively FACS sorted cells were reseeded on cell culture dishes.

For antibiotic selection, cells were treated with 2.5 µg/ml Puromycin for 4 days or 250µg/ml Neomycin for 2 weeks. Only infected cells survived the exposure of the indicated concentrations of Puromycin or Neomycin. As a negative control and in order to test the effectivity of the antibiotic, a non-infected control plate was treated with the same antibiotic concentration.

3.1.4 Cell viability assays and growth curves

3.1.4.1 Crystal violet staining

Cell density or number of colonies can be quantified using crystal violet staining. Increased density of cells or number of colonies indicate high rates of proliferation, low levels of cell death or resistance to therapies. Dead cells detach from the surface of the dish reducing the amount of crystal violet staining on the cell culture dish. For experimental purposes, the same number of cells were seeded in 24-well culture dishes and cultivated for a minimal of 48h to a maximal of 144h. Cells were fixed with 4% PFA for 5-10min, washed twice with PBS and stained with 0.5% crystal violet solution for 1h. The excess of purple dye was removed using several washes of desalted water and finally, the plates were dried at RT. Density of stained cells were quantified using ImageJ software (staining intensity is between 0 to 255) and normalized to a control sample. For ImageJ, the image was converted to black and white 8-bit resolution, the background threshold was adjusted in order to remove unspecified signal and the the cell density of the area selected was analyzed using the commands: "Analyse" → "Measure"

3.1.4.2 IC50, GI50 and Loewe synergy by Operetta system

Cells were seeded in 384-well dishes at equal density and treated with indicated drugs at different concentrations for 48h. Then, cells were fixed using 4% PFA for 10 min, permeabilized using 0.5% Triton X-100 in PBS for 5 min and the nucleus were stained using Hoechst. Number of cells was determined counting the number of nucleus with the Harmony software. purposes, unhealthy cells with altered nuclear morphology were excluded. For every condition, 30 fields from 2-3 independent wells were analysed. For quantification purposes, more than 5000 cells were quantified for every cell line and unhealthy cells with altered nuclear morphology were excluded from the analysis.

Upon different therapies, Loewe synergy, half cell growth inhibition (GI50) and half-maximal inhibitory concentration (IC50) were calculated using the Operetta High-Content Imaging System. IC50 is the maximal

concentration of drug to cause 50% inhibition of biological activity. GI50 is the concentration of drug to cause 50% maximal inhibition of cell proliferation. GI50 and IC50 were calculated and visualized using the online tool AATBIO. Loewe synergy was calculated using the Combenefit software (Di Veroli GY et al 2016). As described by Di Veroli and colleagues, the Combenefit software calculates the reference effect for the combination (a,b) by finding 2 doses a_u and b_u:

$$E_A(a_u) = E_B(b_u)$$

Then, the isobole equation is verified:

$$\frac{a}{a_U} + \frac{b}{b_U} = 1$$

Upon to solve both equations numerically, the solution is used to define the reference effect:

$$R_{AB\_Loewe}(a, b) = E(a_u) = E_B(b_u)$$

As monotonic dose response curves were considered, if a solution exists, it is unique. But, if the original isobole's equation of the Loewe model cannot be used due to differences in maximum effects, an extension was developed upon the assumption that high concentrations of A induce bigger effects than observed efficacy. If the concentration of a_u is really big, the ratio a/au become infinitely small and the isobole equation is the next:

$$\frac{b}{b_U} = 1$$

In consequence, for concentrations b which induces effects beyond A´s maximum effect, the Loewe model was extended in combenefit software by defining:

$$R_{AB\_Loewe}(a, b) = E(b_u) = E_B(b)$$

3.1.4.3 Growth curves, IC50 and GI50 by CASY cell counter

In order to determine if treated or genetically modified cells have altered proliferation capacities or responses to therapies using CASY automated cell counter. Cells were seeded in equal numbers (25000 to 75000 cells depending of the purpose of the experiment) in triplicates into 6-well-plate dishes and if required, exposed to different drugs or inhibitors after the cells were attached into the plastic dish (usually 24h after seeding). Cell density and morphology was checked every day using a microscope and the medium with supplements and drugs was replaced every 48h. If the cell confluence of a well reaches 90% but the experiment requires more time of culture, cells were trypsinized, counted, and replated at the same cell number than initially (25000-75000 cells per well).

Upon to determine the number of cells by CASY cell counter, GI50 and IC50 were calculated and visualized using the online tool AATBIO. For growth curves, The increase number of cells (R) was determined using the formula:

$$R = X / Z$$

X is the total number of viable cells and Z is the initial number of cells seeded per well (25000-75000 cells per well). The cumulative cell number (Y) of each passage (P) was calculated using the formula:

$$(Y_{(P)} = Y_{(P-1)} XR).$$

3.1.5 Cell cycle profile by fluorescence-activated cell sorting

For adjustments of FACS parameters, stained and and non-stained cells were used. Propidium iodide (PI) or DAPI was used to determine DNA-content and therefore, cell cycle profile of target cells. PI and DAPI are fluorescent dyes that determine the DNA content of the cells and in consequence the phase of the cell cycle. For adjustments of FACS parameters, stained and and non-stained cells were used.

For cell cycle profile the three classical phases are:

1. G1/ G0 phase: DNA content 2N
2. S phase: DNA content >2N and <4N
3. G2/ M phase: DNA content 4N

Additionally, it is possible to quantified apoptotic and polyploid cells:

1. Sub G1 phase: DNA content <2N. Indicated apoptotic cells and to quantified them, it is required to include the floating cells of the supernatant in the analysis.
2. Polyploid cells: DNA content > 4N, such as 6N or 8N.

3.1.5.1 Cell cycle profile by DAPI

Target cells were washed twice with PBS, trypsinized, centrifuged (1500rpm for 3-4 minutes) and resuspended in 200 µl cold PBS. The cells were fixed by adding 800 µl 100% cold EtOH while vortexing. Samples were fixed at -20°C overnight. Next day, cells were centrifuged at 4°C (1500 rpm for 10 min) and then, washed twice in cold PBS. After discarding the supernatant, pelleted cells were incubated in 500 µl DAPI staining solution at 4°C for 30 min protected from light. DAPI staining solution is composed by 20 µl DAPI (5mg/ml stock) in 10 ml PBS with 0.5% Triton X-100. Samples were transferred to FACS tubes and measured considering that DAPI bound to DNA has a maximum absorption at 358 nm and its emission maximum is at 461 nm. The cell cycle was analyzed using BD FACSDiva 6.1.2 and FlowJo 8.8.6 software.

3.1.5.2 Cell cycle profile by propidium iodide

Target cells were washed twice with PBS, trypsinized, centrifuged (1500rpm for 3-4 minutes) and resuspended in 200 µl cold PBS. The cells were fixed by adding 800 µl 100% cold EtOH while vortexing. Samples were fixed at -20°C overnight. Next day, cells were centrifuged at 4°C (1500 rpm for 10 min) and then, washed twice in cold PBS. After discarding the supernatant, pelleted cells were incubated in 400 µl PI staining solution at 4°C for 30 min protected from light. PI staining solution is composed by 38 mM sodium citrate containing 1 µl RNase A (10 mg/ml stock solution) and 15 µl propidium iodide (1 mg/ml stock solution). Samples were transferred to FACS tubes and measured considering that PI bound to DNA has an absorption maximum at the

wavelength of 536 nm and its emission maximum is at 617 nm. The cell cycle was analyzed using BD FACSDiva 6.1.2 and FlowJo 8.8.6 software.

3.1.6 Immunofluorescence

Cells were seeded in 384-well dishes for IF (for the Operetta system) or in Ibidi 8-well-chamber or 16-well-chamber slides (for classic fluorescence microscopes). The cell culture medium was discarded, and cells were washed twice with PBS. Then, cells were fixed with 4% PFA at RT for 5min. After 3 washes with PBS, cells were permeabilized in 0.5% Triton X-100 at RT for 5min. Cells were washed twice with PBS and then, blocked in 5% BSA in PBS at RT for 30 min. Next, cells were incubated with the primary ABs (1/100) diluted in 3% BSA overnight at 4°C. Next day, cells were washed three times with PBS and incubated for 45min with secondary ABs (1/300) and DAPI (1/1000 from 5mg/ml stock) at RT in the dark. Stained cells were washed three times with PBS and maintained at 4°C before imaging. For quantification of the IF staining intensity or counting the number of DNA damage foci per cell, the Harmony software from Operetta system or ImageJ were used.

3.2 Molecular biology methods

3.2.1 Polymerase chain reaction (PCR)

3.2.1.1 Traditional polymerase chain reaction (PCR)

In order to amplify DNA, polymerase chain reaction (PCR) was performed. Two different enzymes and protocols were used in this thesis. For PrimeSTAR GXL DNA Polymerase, the PCR reaction was composed by 10µl 5X PrimeSTAR GXL Buffer, 4 µl of 10 mM dNTPs (2.5 mM each), 1 µl 10 mM Forward primer, 1µl 10 mM Reverse primer, 2 µl of the DNA template (100-250 ng) and 1 µl of PrimeSTAR GXL DNA Polymerase and sterile distilled water to a total volume of 50 µl. The PCR cycling profile was the next:

1. Initial denaturation: 1x 98°C for 5 min
2. 30x: Denaturation: 98° for 10s
   Annealing: 60°C for 15s
   Extension: 68°C for 1 min
3. Final extension: 1x 68°C for 5 min

For Phusion HF DNA polymerase, the PCR reaction was composed by DNA (5-250 ng), 5 µl 10x Phusion High-Fidelity buffer, 1 µl 10 mM dNTPs, 1.25 µl 10 µM Forward primer, 1.25 µl 10 µM Reverse primer, 1.5 µl DMSO, 0.5 µl Phusion HF DNA polymerase and sterile distilled water to a total volume of 50 µl. The PCR cycling profile was the next:

1. Initial denaturation: 1x 98°C for 30s
2. 30x: Denaturation: 98° for 10s
   Annealing: 58°C for 30s
   Extension: 72°C for 15-30s per Kb
3. Final extension: 1x 68°C for 5 min

3.2.1.2 Quantitative real-time polymerase chain reaction (qPCR)

For gene expression analysis, quantitative real-time PCR (qPCR) was performed in order to determine mRNA abundance or enrichment of specified DNA regions after chromatin immunoprecipitation. For qPCR, a fluorescent dye intercalates into the newly synthesized double strand DNA during amplification. The fluorescent can be quantified. As fluorescent dye we used SYBR Green. The qPCR reaction is composed by 5-10 µl diluted complementary DNA (cDNA) or chromatin, 10 µl SYBR Green, 5 pmol Forward primer, 5 pmol Reverse primer and 20 µl nuclease-free water. The PCR cycling profile was the next:

1. Initial denaturation: 1x 95°C for 15 min
2. 40x: Denaturation: 95° for 15 s
   Annealing: 60°C for 20 s
   Extension: 72°C for 15 s
3. Final extension: 1x 72°C for 15 s

Exon-exon spanning primers were designed and product amplification was evaluated performing a melting curve upon qPCR as follow:

1. 1x 95°C for 1 min
2. 1x 60°C for 30s
3. 1x 95°C for 30s

For qPCR of the cDNA synthetized from mRNA, relative expression was generally calculated using ΔΔCt relative quantification method. Housekeeping
genes, as ACTIN, were used for normalization. During qPCR, the threshold cycle (Ct) was determined. The Ct indicates the PCR cycle which the fluorescence signal start to increase respect to the background fluorescence.

$$\Delta CT = Ct^{Housekeeping} - Ct^{Gene\ of\ interest}$$

Upon normalization using a housekeeping gene, the target samples were compared to a control sample in order to perform ΔΔCt quantification:

$$\Delta\Delta CT = \Delta Ct^{control} - \Delta Ct^{sample}$$

The relative expression of the target gene (X) is determined by:

$$X = 2^{-\Delta\Delta CT}$$

And the standard desviation (SD) was calculated using:

$$SD = \sqrt{\frac{\Sigma(X-\overline{X})^2}{(n-1)}}$$

For Chip-qPCR, fold enrichment method was used. In this method, ChIP signal is normalized respect to background signal (igG control without Ab). The method is based in the assumption that background signal is reproducible between different primer, samples, and replicate experiments. It is calculated comparing the raw Ct of the samples to the raw Ct of the control sample (igG control without Ab):

$$Y = Ct^{sample} - Ct^{IgG}$$

And then, the relative expression of the target gene is determined by: $X = 2^{-Y}$

3.2.2 DNA Electrophoresis

Solution of 1 to 3% agarose in 1X TAE was boiled and then, supplemented with 0.5 µl/ ml ethidium bromide before to pour into a gel chamber with combs. DNA Samples were mixed with DNA loading buffer and loaded into 1-2% agarose gel. DNA ladder was loaded in a well to determine DNA fragment size of the samples. Electrophoresis was run at 120 V for 45 min and DNA visualized using a UV transilluminator. DNA fragments can be visualized due to the ethidium bromide that can be intercalated into the DNA.

In order to purify DNA fragments from an agarose gel, the DNA was visualized using an UV transilluminator and then, cut out of the gel. The DNA was extracted and purify from the gel following the manufacturer's instructions of the GeneJET Gel Extraction Kit.

To cleave DNA at certain sites, restriction enzymes were applied. To conduct a restriction digest, 500 ng of the DNA template were combined with 10 % of 10x enzyme buffer and 0.5 µl of the enzyme and filled up to 50 µl with dH2O. The sample was mixed by pipetting it and incubated at 37°C for 1 hour (h). The enzyme might eventually be heat inactivated at corresponding settings.

3.2.3 Design of shRNAs, gRNAs and site-directed mutagenesis

sgRNAs were designed using the online tool available in Zhang lab: Zhang lab gRNAs design resources (https://zlab.bio/guide-design-resources) and CHOPCHOP software (http://chopchop.cbu.uib.no/). shRNA sequences were designed with the software SPLASH-algorithm (http://splashrna.mskcc.org/) or the RNAi Consortium / Broad Institute (www.broadinstitute.org/rnai-consortium/rnai-consortium-shrna-library). For site-directed mutagenesis, instructions from the kit GeneEditor™ in vitro Site-Directed Mutagenesis System (Promega) were followed for the design of the primers and the introduction of the mutation.

3.2.4 Restriction enzyme digestion of DNA

Sequence specific hydrolysis of DNA was performed using restriction enzymes. The endonucleases and buffers were used following manufacturer's instructions.

In order to conduct a restriction digest, 500-1000 ng of DNA were combined with 2 µl of 10x manufacturer enzyme buffer and 1 µl of the specific restriction enzyme and filled up to 20 µl with dH2O. The sample was mixed by pipetting it and incubated at manufacture recommended temperature (usually 37°C) for 60 min. To inactivate the enzymatic reaction, the mixture was incubated at 65°C for 15min or 10mM EDTA was added. If buffers and temperature are compatible, a DNA vector or fragment can be digested with different endonucleases at the same time.

3.2.5 DNA ligation

For the ligation of DNA samples, the T4 enzyme was used. The DNA backbone and the insert were mixed in 3x molar insert excess to the linearized vector. The DNA was combined to 1 µl T4 DNA ligase 1 µl T4 DNA ligase buffer and sterile water up to 10 µl. The mix was either incubated at 37°C for 1 h or at room temperature (RT) for at least 16 h. The ligated DNA can be transformed into competent bacteria.

3.2.6 Bacterial transformation

In order to amplify a DNA via bacterial transformation, 1 µg of DNA was added to chemically competent bacteria (XL-1 or DH5α) and the mixture was incubated for 30 min on ice. Afterwards, bacteria were heat shocked at 42°C for 1min and immediately put back on ice for 3-4 min. Then, 1 ml LB medium was added to the mixture and shaked at 37°C for 1h. The transformed bacteria were platted into LB agar plates with appropriate antibiotics and incubated overnight at 37 °C.

3.2.7 Isolation of DNA from bacteria

The DNA was amplified and isolated from chemically competent bacteria in two different scales depending of the DNA abundance extracted, low scale preparation or mini-DNA preparation (mini-prep) or large-scale preparation or maxi DNA Preparation (maxi-prep). For mini-prep, transformed bacteria was growing overnight in 5 ml LB medium supplemented with appropriate antibiotics. The medium with the competent bacteria was centrifuged at 3000 rpm, 4°C for 20 min. The supernatant was discarded and the bacterial pellet was dried. The pelett was resuspended in 300 µl DNA resuspension buffer. Next, 350 µl DNA lysis buffer was added and the mixture was incubated at RT 4-5 min. Then, 350 µl DNA precipitation buffer was added and the sample was incubated for 10 min on ice. Next, the samples were centrifuged at full speed, 4°C for 10 min and the supernatant was transferred to a new reaction tube and 600 µl Isopropanol was added. The mixture was vortexed and pelleted at full speed at 4°C for 10 min and the pellet was washed with 70% EtOH. Finally, the pellet was air dried and resuspended in 50 µl dH2O. For maxi-prep, 50 ml of LB medium with cultivated competent bacterial were centrifuged at 4000 rpm at RT for 10 min. Supernatant was discarded and the pellet was resuspended using 5 ml DNA resuspension buffer. Next, 5 ml DNA lysis buffer was added, tube was inverted and incubated at RT for 3-5 min and 5ml DNA precipitation buffer was added. The falcon tube was inverted and maintained on ice for 15 min. Afterwards, the lysate was centrifuged at 8000 rpm, 4°C for 30 min. The supernatant was filtered using a filter paper, 10 ml of isopropanol were added and then, the sample was centrifuged at 8000 rpm, 4°C for 30 min. Supernatant was discarded, pellet was washed with 70% EtOH. Upon centrifugation, the pellet was air dried and solubilized in 200 µl sterile water. of pellet. Finally, the purified plasmid DNA was adjusted to a concentration of 1 µg/µl.

3.2.8 Nucleic acid quantification

3.2.8.1 NanoDrop

NanoDrop 1000 was used in order to determine DNA and RNA concentration. To quantify the purity of DNA and RNA, the absorbance at 260 nm and the ratio absorbance 260 nm/ absorbance 280 nm (A260/280) were quantified. The ratio A260/280 for pure DNA is about 1.8 and for pure RNA is about 2.

3.2.8.2 Fragment Analyzer

Size, quantity and purity of DNA and RNA were determined by Fragment Analyzer (Advanced Analytical) according to manufacturer's protocols. For RNA-sequencing (RNA-seq.) purposes, the quality of the RNA was

determined measuring the RNA quality number (RQN). The RQN is based on a scale from 1 to 10, where 1 represents completely degraded RNA, and 10 represents intact RNA. A large RQN value indicates higher-quality RNA with minimal degradation in the sample.

3.2.9 RNA isolation

3.2.9.1 RNA isolation with TriFAST

Cells seeded in a 10cm dish were washed twice with PBS before RNA extraction. Cells were lysed directly on the plate with 1 ml Trifast and transferred into a 1.5 ml reaction tube. The mixture was incubated for 10 min at RT and then, 200 µl chloroform was added into the reaction tube. The mixture was heavily vortexed for 1-2 min and then, centrifuged at 4000rpm, 4 C° for 15min. Next, the upper phase was transferred to a new reaction tube and to precipitate the RNA, 500 µl isopropanol and 1 µl GlycoBlue (15 mg/ml stock) were added to the mixture. The samples were incubated on ice for 15 min followed by centrifugation at 14000 rpm, 4C° for 30 min. The supernatant was discarded and the pellet washed twice with 70% EtOH. Finally, the pellet was air-dried and then, solubilized in 50 µl sterile free water. The RNA isolated by triFAST was used for real-time qPCR.

3.2.9.1 RNA isolation with ReliaPrep™ RNA Cell Miniprep System

If RNA was used for RNA-Seq, the isolation was performed using the commercial kit ReliaPrep™ RNA Cell Miniprep System following the manufacturer's instructions. DNase I digestion was performed during RNA extraction.

3.2.10 cDNA synthesis

In order to quantify gene expression, the RNA extracted from cells was reverse transcribed into cDNA. First, 0.5-2 µg of isolated RNA was diluted in 20 µl sterile nuclease free water and 2 µl random hexanucleotide primers (2 µg/ml stock) were added to the diluted RNA (0.5-2 µg). For dissolving secondary structures, the RNA solution was incubated for 2m at 65°C. The samples were cooled down on ice and the cDNA synthesis mix composed by 10 µl 5x First strand reaction buffer, 5µl 10mM dNTPs, 2 µl random primers (2 µg/ml stock), 0.2 µl RiboLock RNase Inhibitor, 1 µl M-MLV enzyme and sterile water up to 50µl, was added. The samples were incubated for 10m at 25°C, 50m at 37°C and 70°C for 15m. The final cDNA was diluted in 200-300 µl sterile water and 5-10 µl of diluted cDNA was used per qPCR reaction.

3.3 Biochemical methods

3.3.1 Protein isolation

3.3.1.1 Protein isolation from cells

For whole cell protein extraction cells were washed twice with cold PBS and scraped directly from the cell culture dish upon addition of RIPA lysis buffer containing proteinase inhibitor (1/100). The suspended cells were transferred to a 1.5 ml reaction tube and snap-frozen in liquid nitrogen. The samples were thawed at

37°C, vortexed and centrifuged at 14000rpm ,4°C for 20 min in order to remove the cell debris. Upon centrifugation, the supernatant was transferred to a new reaction tube and protein concentration was determined by Bradford assay. For storage, samples were frozen at -20°C. To isolate protein from the chromatin fraction in cells, a commercial Chromatin Extraction Kit (ab117152; Abcam) was used. Chromatin fractionation was performed following the manufacturer's instructions and reagents of the commercial kit.

3.3.1.1 Protein isolation from tissue

For tissue protein extraction, the tissue was washed with cold PBS, transferred to a reaction tube and covered by RIPA lysis buffer containing proteinase inhibitor (1/100). The sample was sonicated using Branson Sonifier 250. The sample was processed with 10 sonication cycles with the duty cycle at 25 %, the output control set on level 2 and the time set to 30s cycles. The remaining mixture was snap-frozen in liquid nitrogen and then, thawed at 37°C, vortexed and centrifuged at 14000rpm ,4°C for 20 min in order to remove the tissue debris. Upon centrifugation, the supernatant was transferred to a new reaction tube and protein concentration was determined by Bradford assay. If the isolation of the chromatin proteins is required, 1% Triton X100 was added to the lysis buffer during protein extraction as previously described (Parisis Nikos; Labome; 2013). For storage, samples were frozen at -20°C.

3.3.2 Quantification of protein concentration

In order to quantify sample protein concentrations, colorimetric Bradford assay was performed (Bradford, 1976). 900 µL Bradford Reagent was mixed with 100 µl 150mM NaCl and 1 µL protein extract or lysis buffer in an optical cuvette and then, vortexed. Using a spectral photometer, the absorbance of the solution was measured at 595 nm. A blank sample with 1 lysis buffer without protein was used to set up the absorbance to 0. Protein abundance was interpolated from the measured sample absorbance compared to a precalculated standard curve using BSA.

3.3.3 Sodium Dodecyl Sulphate - Polyacrylamide gel electrophoresis (SDS-PAGE)

Electrophoresis in Sodium Dodecyl Sulphate- Polyacrylamide gel electrophoresis (SDS-Page) was performed to separate proteins according to their molecular weight. Upon Bradford quantification, the appropriate amount of 6x sample loading buffer or lämmli buffer was added to 50 µg of protein and then, boiled at 95°C for 5 min. Upon centrifugation of the samples at 14000 rpm, RT for 10 min, equal protein amounts were loaded on 7.5 to 12.5% SDS Tris-gels pockets and runned at 90V for 2.5h in 1x SDS Running Buffer. A protein ladder was loaded in the first well as a maker of protein molecular weight.

3.3.4 Immunoblot (IB)

After protein separation by SDS-page, proteins were transferred to a Polyvinylidene difluoride (PVDF) membrane in 1x Transfer Buffer upon incubation at 30V, 4°C overnight. Before protein transferring, the PVDF membrane was activated by exposure to methanol for 30s and then, equilibrated in 1x Transfer buffer. During

protein transferring, the immunoblot sandwich was composed by 2 sponges, 4 Whatman papers, a SDS-Page gel and a PVDF membrane. The distribution of the sandwich was: Black side of the cassette, 1 sponge, 2 Whatman filter papers, gel, PVDF membrane, 2 Whatman papers, 1 sponge and the red side of the cassette. The sandwich was placed into the tank following the next distribution: black side of the cassette with black side of the tank (negative charged) and red side of the cassette with red side of the tank (positive charged).
After transferring, the PVDF membrane was exposed to blocking buffer for 45 min at RT. Then, the membrane was incubated with the listed primary antibodies (Table 2.1) in primary antibody buffer for 6H at RT. The membrane was washed 3 times with 1x PBS and then, the membrane was incubated with diluted secondary antibodies (Table 2.2) in secondary antibody buffer for 1h at RT. Generally, membranes were recorded in Odyssey CLx Imaging System, and analysed using Image Studio software. For quantification of the normalized abundance of a target protein (N), the protein abundance of a housekeeping (Y), as ACTIN or VINCULIN, was used to normalized the measured target protein abundance (Z):

$$N= Z/Y$$

In order to obtain the relative protein abundance of a target protein (X) respect to a control sample, the normalized target protein abundance (N) was compared to a normalized control sample (C) using the next formula:

$$X= N/C$$

3.3.5 Protein stability assays

3.3.5.1 Cycloheximide assay

Cycloheximide (CHX) is a chemical compound that acts blocking protein synthesis by interfering eukaryotic translational elongation. CHX assay was performed to elucidate the half-life of a protein. In order to determine protein stability, cells were incubated with complete cell culture medium supplemented with 100 µg/ml CHX for different time points. Upon CHX exposure, cells were lysed and protein quantified by SDS-PAGE and immunoblot.

3.3.5.2 MG132 assay

MG132 is a reversible proteasome inhibitor that acts blocking protein degradation. MG132 assay was performed to study protein stability. For MG132 assay, cells were incubated with complete cell culture medium supplemented with 20 µM MG132 for 6h before protein isolation. Collected cells were lysed and protein abundance analyzed by SDS-PAGE and immunoblot. Protein abundance of MG132 treated cells were compared to non-treated cells in order to elucidate if protein stability is regulated via proteasome degradation.

3.3.6 Immunoprecipitation (IP)

To detect protein-protein interaction, co-Immunoprecipitations (Co-IP) were performed. For Co-IP, cells were lysed and protein isolated as previously described (3.3.1.1). Upon protein quantification using Bradford assay, 500 µg of protein abundance was immunoprecipitated using indicated antibody concentrations (Table 2.1). As

an input, a determine percentage (1-10%) of the 500 µg protein lysate was separate into a new reaction tube. The 500 µg protein lysate was incubated with a specific antibody on rotation at 4°C overnight. As a negative control sample, a different 500 µg protein lysate was incubated with IgG. Next day, 25 µl of protein A/G magnetic beads or 40µl of sepharose beads were washed twice with 1 ml of 5% BSA and then added to the protein lysates. The protein lysates with the beads were incubated in a rotating wheel at 4°C overnight and then, the supernatant was removed and the beads were washed six times with 1XPBS. Next, beads and inputs were resuspended in sample loading buffer or lämmli buffer and boiled at 95°C for 5 min. The samples and inputs were run in SDS-PAGE gels. Protein Immunoprecipitations and Co-immunoprecipitations were confirmed by immunoblot.

Transfected cells were lysed in 1 ml of buffer A (6M guanidine HCl, 0.1 M Na2HPO4, 0.1 M NaH2PO4, 0.01 M Tris (pH 8.0), 10 mM β-mercaptoethanol) per 100-mm dish 24 h after removal of the precipitate. The lysate was sonicated for 30 s to reduce viscosity and then mixed on a rotator with 50 µl (settled volume) of nickel-NTA-agarose (Qiagen, Chatsworth, CA) for 3 h at room temperature. The beads were washed three times with 1 ml of buffer A, twice with 1 ml of buffer A diluted in 25 mM with Tris-HCl (pH 6.8) / 20 mM imidazole 1:4 and twice with 1 ml of 25 mM Tris-HCl (pH 6.8) / 20 mM imidazole. Purified proteins were eluted by boiling the beads in 2× sample buffer supplemented with 200 mM imidazole and analysed by immunoblotting.

3.3.7 Ubiquitination assays

3.3.7.1 Nickel-NTA-agarose his-ubiquitin pull-down

His-Ubiquitin, His-ubiquitin K48 or His-ubquitin K63 transfected cells were lysed in ubiquitin pull-down lysis buffer and protein isolated as previously described (3.3.1.1). Upon protein quantification using Bradford assay, 2mg of protein abundance was immunoprecipitated using 50 µl of nickel-NTA-agarose beads for 3h at RT on rotation. The beads were washed three times with ubiquitin pull-down lysis buffer, twice with ubiquitin-buffer 1 and twice with ubiquitin-buffer 2. Purified proteins were eluted in sample loading buffer or lämmli buffer and boiled at 95°C for 5 min. In order to analyze the ubiquitination levels of the target protein, an immunoblot was performed using specific antibodies against the target protein upon immunoprecipitation.

3.3.7.2 Tandem ubiquitin binding entity (TUBE) pull-down

The Tandem ubiquitin binding entity reagent (Hjerpe et al. 2009) was expressed in Escherichia coli as previously described (Damgaard et al. 2019). Endogenous polyubiquitin conjugates were purified using TUBE affinity reagents as described previously (Fiil et al. 2013). Briefly, cells or tissue were lysed in TUBE lysis buffer supplemented with protease inhibitor cocktail (1/100) and 1mM DTT. To ensure protection of ubiquitin-chains, GST-Tandem-Ubiquitin-Binding-Entities (TUBEs) must be added immediately at a concentration of 50-100 µg/mL to lysates. Cells were mixed by pipetting five times and lysed on ice for 30 min. Lysate was cleared by centrifugation 14000 rpm, 4°C for 10 min and glutathione Sepharose 4B beads were added. The TUBE pulldown was performed incubating the lysate on rotation for 4-16 h at 4°C. The beads were then washed four times with ice-cold PBS, and bound material was eluted by mixing the beads in sample loading

buffer or lämmli buffer and boiled at 95°C for 5 min. In order to analyze the ubiquitination levels of the target protein, an immunoblot was performed using specific antibodies against the target protein upon immunoprecipitation.

3.3.7.3 Warhead-ubiquitin suicide probe assay

Warhead-ubiquitin suicide probes are molecules commonly used to quantify DUB activity. Warheads bind covalently to the active cysteine of a DUB trapping the enzyme and causing a shift in molecular weight (~8 kDa) that can be detected by SDS-PAGE - Immunoblot. Here, warhead assays were used to determine USP28 enzymatic activity and the specificity of the USP28 inhibitor, AZ1. Warhead probes were obtained from UbiQ and for the experiments, manufacturer instructions were followed. Cells were lysed in warhead lysis buffer (HR lysis buffer) supplemented with Protease-Inhibitor and protein was quantified using Bradford assay. To profile DUB activity, 25 µg of cell lysate were transferred to a new eppendorf tube and volume adjusted to 16 µL with HR-buffer. 3 µL of a 1:1:1 mixture of Ub-VME, Ub-VS and Ub-PA suicide-probes (in 50 mM NaOAc, 5 % DMSO) were added to the lysate and to adjust the pH, double the volume 50 mM NaOH compared to probes was added. Samples were mixed briefly and incubated for 1 hour at 37°C shaking. After addition of 6 µL of 5x lämmli buffer, samples were boiled for 5 min and applied to SDS-PAGE, followed by Western Blotting. Generally, membranes were recorded in Odyssey CLx Imaging System, and analysed using Image Studio software. For active DUBs, the resulting 8 kDa size-shift was observed.

3.3.8 Chromatin immunoprecipitation (ChIP)

Chromatin immunoprecipitation (ChIP) was perfomed to study protein-DNA interactions. Approximately $1x10^7$ cells were used for a single condition in a Chip-qPCR experiment. In summary, DNA and its associated proteins were crosslinked using formaldehyde. Next, chromatin was isolated and fragmented and the DNA bound to a target protein was precipitated by IP. Finally, DNA was purified and quantified by qPCR using primers specifically designed to elucidate if a protein interacts to a specific DNA sequence.

3.3.8.1 Formaldehyde fixation and chromatin isolation

Cells were fixed with 1% formaldehyde and incubated for 10min at RT with shaking. Then, 125mM glycine was added and cells were shaking for 5min at RT. Cells were washed twice with cold PBS and harvested in PBS containing protease inhibitor. Collected cells were centrifuged at 1200 rpm, 4°C for 5 min and pellet resuspended in 3 ml ChIP lysis buffer 1 supplemented with protease inhibitor. Before to centrifuge 200 rpm, 4°C for 5 min again, cells were incubated 20min on ice. The pellet of cells was resuspended in 2 ml ChIP lysis buffer II supplemented with protease inhibitor and incubated 10min on ice. Samples were then sonified in order to fragmentate the chromatin. Cells used in this study were sonicated for 60 min at 20% amplitude. Each sonification cycle takes 10s and is followed by 30s pause. Then, 25µl of chromatin were diluted in 475 µl of TE buffer. 160 mM NaCl and 20 µg/ml RNase were added to diluted chromatin before reverse-crosslinking. Then chromatin was incubated for 1h, 37°C and then samples were incubated at 65 °C overnight. Next, 5 mM EDTA and 200 µg/ml protease K were added to the samples and they were incubated for 2h at 45°C. Chromatin

was purified by phenol-chloroform extraction (section 3.3.8.6), and the DNA was resuspended in 45 °C in 25 µl TE buffer and the sample was run in 2% agarose gel (section 3.2.2) in order to determine proper fragmentation and chromatin size.

3.3.8.2 Immunoprecipitation for ChIP

30µl of protein A/G magnetic beads or 70µl protein of A/G agarose beads were used per immunoprecipitation. Beads were washed twice with of 5% BSA in 1x PBS and indicated concentration of antibodies (Table 2.1) were incubated with the beads overnight at 4 °C on rotation. Sonified chromatin was centrifuged at 13,000 rpm, 4°C for 15 min and the supernatant transferred to a new reaction tube. Beads were washed twice times with 5% BSA in 1x PBS and added to the chromatin samples. Upon NanoDrop quantification, 1% of the chromatin was transferred to a new reaction tube as an input control and stored at -80°C. Same amount of chromatin was incubated with beads overnight at 4 °C on a rotating wheel. Then, beads were washed twice 4 times with cold ChIP wash buffer 1, cold ChIP wash buffer 2, and cold ChIP wash buffer 3 and another wash with TE buffer was done before transferring the mixture to a new reaction tube.

3.3.8.3 Elution and decrosslinking

Beads were incubated with 200 µl ChIP elution buffer on rotation for 15min at 65°C. The supernatant was transferred to a new reaction tube. The beads were again incubated with 200 µl ChIP elution buffer and the supernatant was pooled to the same reaction tube where the first 200 µl ChIP elution buffer were transferred. 160 mM NaCl and 20 µg/ml RNase were added to the eluted and input samples and they were incubated by 1 h incubation at 37°C followed by t shaking at 65°C overnight. Next day, 5 mM EDTA and 200 µg/ml protease K were added to the samples and they were incubated at 45°C for 2 h.

3.3.8.4 DNA purification and qPCR

DNA was purified using phenol-chloroform extraction method. 300µl of phenol-chloroform-isoamyl alcohol mixture (25: 24: 1) was added to samples and vigorously vortexed for 45s. The mixture centrifugated at 14,000 rpm, RT for 5 min. The upper layer was transferred to a new reaction tube and 1ml ice-cold 100% ethanol, 50 µl, 3M sodium acetate (pH 5.2) and 1 µl glycogen blue was added to the mixture. Samples were incubated for 45 min at -20°C, DNA was pelleted by centrifugation at 13,000 rpm, 4°C for 30 min, DNA pellet was washed with 70% ethanol and resuspended in 500 µl sterile clean water. Purified DNA was uses for qPCR as previously described (section 2.2.1.2).

3.4 Animal models, human datasets and histological methods

3.4.1 Animal welfare and licenses

Licenses required for in vivo experiments were approved by the Regierung Unterfranken and the ethics committee under the license numbers 2532-2-362, 2532-2-367, 2532-2-374 and 2532-2-1003. The mouse strains used for this publication are listed (Table 2.6). All mice are housed in standard cages located in pathogen

free facilities on 12h light / dark cycles with ad libitum access to food and water. Veterinarians supervise the welfare of the animals every day. FELASA (Federation of European Laboratory Animal Science Associations) 2014 guidelines were followed for animal maintenance in order to assure animal safety and welfare. Sentinel animal screening was conducted every 3 months following the instructions found in FELASA 2014 guidelines. In presence of obvious indicators of pain, stress or suffering, mice were immediately euthanized by cervical dislocation upon Isoflurane anesthesia.

3.4.2 Mice euthanasia

The mouse was placed in a chamber with access to isoflurane and the vaporizer was set at 3%. When the animal was anaesthetized which was first indicated by the cessation of body movement, the mouse was euthanized by cervical dislocation applying pressure to the neck and dislocating the spinal column from the skull or brain. Death must be verified by loss of consciousness, loss of reflex muscle response, and loss of response to noxious stimuli.

3.4.3 Induction of primary lung tumors using CRISP/CAS9

Adult mice (around 8 weeks) were anaesthetized with isoflurane at 2% and endotracheally intubated with 50 µl AAVs (3×10^7 Plaque Formation Unit (PFU)). For endotracheal instillation, a gauge 24 catheter was introduced to the trachea and isolated viruses as previously described (Section 3.1.2.1) were pipetted to the top of the catheter and introduced into the proximal region of the trachea. During animal breathing, AAV viruses were distally expanded and delivered into the lungs. Animals were sacrified and tumors anlayzed as indicated time-points.

AAV viruses encoded CAS9 protein, two gRNAs against p53, two gRNAs against Kras and a repair template in order to introduce the mutation G12D in Kras gene. Optionally, the AAVs together with all the components previously described also express two gRNAs against Lkb1 or two gRNAs against Usp28 together with two gRNAs against Lkb1. In summary, mice developed primary tumors with the next genotypes:

1. KP: $Kras^{G12D;}$ $p53^{\Delta}$
2. KPL: $Kras^{G12D}$; $p53^{\Delta}$; $Lkb1^{\Delta}$
3. KPLU: $Kras^{G12D}$; $p53^{\Delta}$; $Lkb1^{\Delta}$; $USP28^{\Delta}$

3.4.4 Generation of primary murine lung cancer cell lines

Murine lung cancer cells from primary tumors were generated twelve weeks after AAV viruses were introduced into the animals as previously described (section 3.4.3). The lung lobes with KP or KPL tumors were excised and transferred to a petri dish. The lobes were washed in 1xPBS and macroscopically detectable tumor regions were excised and transferred to a tube containing PBS with collagenase I (100 U/ml). The tissue was digested for 30 min at 37°C, and the reaction was stopped by addition of 10% FCS. Upon centrifugation, the supernatant was removed, the tissue was resuspended in complete medium and plated in a 6-well cell culture dish. By selective trypsinization, cancer cells were selected and separated to fibroblasts. Finally, morphological homogenous colonies were expanded and these clones were subjected to further biochemical

analysis in order to characterize the cell line. The biochemical analysis included genotyping PCR, RNA sequencing and mass spectrometry. According to biochemical properties and the expression of specific markers, cells were classified as ADC or SCC.

3.4.5 Induction of lung tumors by orthotopic transplantation of cancer cells

Eight weeks adult mice were anaesthetized with isoflurane at 2% and endotracheally intubated with 200000 murine lung cancer cell lines (KP SCC, KP SCC^{shUSP28} or KPL SCC). For endotracheal instillation, a gauge 24 catheter was introduced to the trachea and counted cells were pipetted to the top of the catheter and introduced into the proximal region of the trachea. During animal breathing, cells were distally expanded and delivered into the lungs forming a lung tumor. Animals were sacrificed and tumors analyzed as indicated time-points.

3.4.6 USP28 inhibitor treatment in vivo

AZ1 inhibitor was dissolved in PBS / DMSO/ 0.1% Tween80 and injected intraperitoneally in vivo. Animals were treated with 6 doses of PBS / DMSO / 0.1% Tween 80 (as control), 125mg/kg or 375mg/kg AZ1. The 6 doses were administrated every 3 days starting on the day 28 upon re-transplantation of KPL cells as explained (section 3.4.5). At the indicated time points, animals were sacrificed by cervical dislocation and lungs were scanned for GFP+ tumors using the iBright™ FL1000 Imaging System scanner. Before fixation using 5% NBF, lung samples Samples were processed for histological analysis. Upon euthanasia, animal organs were examined macroscopically and the tissue structure of representative tissues as liver, spleen and intestine were histologically analyzed.

3.4.7 Organotypic lung tumor slice cultures ex vivo

Lung tumors developed upon endotracheal transplantation of KPL cells as previously explained (Section 3.4.5) or WT lung tissue from WT C57BL6/J-*Rosa26* Sor-CAGG-Cas9-IRES-eGFP animals were explanted and sectioned in slices using the vibratome. Ex vivo slices were relocated in cell culture dishes and maintained in standard cell culture medium (DMEM, 10% FCS) and conditions (37°C, 5% CO2 and 95% relative humidity). WT and SCC slices expressed GFP and in consequence, it was possible to assess the viability of the tumors quantifying the intensity of GFP upon exposure to drugs or inhibitors. At the indicated time-points, slices were analysed using a fluorescence microscope and the GFP intensity of the samples was quantified using ImageJ.

3.4.8 Histological processing of samples

Upon fixation of the tissue using 5% NBF, tissue samples were embedded in paraffin and sectioned at 6 µm using a microtome. Before staining, slides were deparaffinized and rehydrated using the next protocol:

- 2x5 min xylene
- 2x3 min 100% EtOH
- 2x3 min 95% EtOH
- 2x3 min 70% EtOH

- 1x3 min 50% EtOH
- 1x3 min water

Deparaffinized sllides were stained with hematoxylin and eosin (H&E) or were subjected to immunohistochemistry. For H&E the next protocol was followed:

- 1x10 min Haematoxylin
- 1x15 min rinse water
- 1x15 min differentiation solution
- 1x15 min rinse water
- 1x2 min Eosin
- 2x1 min tap water

For IHC, slides were subjected to epitope retrieval, blocking, antibody exposure and DAB staining before dehydration and mounting steps. For epitope retrieval, slides were placed into previously heated citrate buffer and then, they were subjected to the next epitope retrieval protocol:

- 1x5 min microwave (750W) in citrate buffer
- 1x5 min microwave (500W) in citrate buffer
- 1x5 min microwave (250W) in citrate buffer
- 1x1 min 1xPBS
- 1x5 min 0.2% Triton X 100
- 2x2 min 1xPBS
- 1x10 min 3% H2O2
- 2x2 min 1xPBS

Upon epitope retrieval, IHC slides were blocked in 3% BSA at RT for 1h. Antibody manufacturer instructions were followed for every antibody. But in general, primary antibodies (diluted in 1% BSA) were incubated ON at 4°C or for 3 h at 37°C, followed by three washes with 1xPBS and the subsequent incubation with the DAB secondary antibody for 1 hour at RT. Then, slides were washed twice with 1xPBS for 5 min and stained with the DAB staining solution in 1xPBS. Upon DAB staining, slides were counteracted with hematoxylin and washed three times with 1x PBS for 5 min.

For all types of staining, slides were dehydrated before mounting using the next protocol:

- 2x3 min 70% EtOH
- 2x3 min 95% EtOH
- 2x3 min 100% EtOH
- 2x3 Xylene

Slides subjected to H&E or IHC were mounted with 200 µl of Mowiol 40-88 or Cytoseal™60 and covered up by a glass coverslip. Slides were recorded using Pannoramic DESK scanner or using FSX100 microscopy system and analysed using Case Viewer software, ImageJ or QuPath. Staining intensity of murine sections were quantified using the QuPath software. In box plots generated upon quantification of staining intensity,

the centre line reflects the median, the cross represents the mean, and the upper and lower box limits indicate the first and third quartiles. Whiskers extend 1.5X the IQR, and outliers are marked as dots. The significance was calculated using two tailed T - test.

3.4.9 Human lung cancer samples

Lung cancer samples were obtained, stored and managed by Pathology Department Córdoba (Spain), Pathology Department University Hospital Würzburg (Germany) and U.S. Biomax (lung microarray slides; slide LC2083). Informed consent was obtained from all subjects, and conducted experiments conform to the principles set out in the WMA Declaration of Helsinki and the Department of Health and Human Services Belmont Report. Samples provided from the hospitals in Córdoba and Würzburg are approved under ethical approval license decret 439/2010 (Hospital Universitario Reina Sofía) and Ethics approval 17/01/2006 (University Hospital Würzburg). Human tissue samples were IHC stained against USP28 and ΔNP63 as previously described (section 3.4.7).

For quantification purposes, staining intensity was graded from 0 (no staining) up to 3 (staining intensity > 66%) by three independent pathologists. Box plots were generated using BoxPlotR online tool. In box plots, the centre line reflects the median, the cross represents the mean, and the upper and lower box limits indicate the first and third quartiles. Whiskers extend 1.5× the IQR, and outliers are marked as dots. The significance was calculated using two tailed T-test.

3.4.10 Analysis of human publicly available datasets

All publicly available data and software used for this publication are listed. In general, two tailed T-test statistical test was used to computation of the p-values, unless another statistical test was expressly indicated. All gene sets used in this thesis are publicly available. The generated gene list for this thesis, including the list of squamous cancer markers and the genes up-regulated or down-regulated in A-431 sh-USP28 or sh-ΔNP63 have been previously published and can be accessed in the Appendix section of the paper published by our research group (Prieto-Garcia et al. 2020). The DNA reapir gene list called: “Kaufmann_DNA_repair_genes” was previously published (Kaufmann et al. 2008).

Oncoprints were generated using cBioPortal (Cerami et al, 2012; Gao et al, 2013). Oncoprints generate graphical representations of genomic alterations, somatic mutations, copy number alterations and mRNA expression changes. The following studies were used for the different analysis: lung adenocarcinoma (“LUAD-TCGA, Provisional”), lung squamous cell carcinoma (“LUSC-TCGA, Provisional”), small-cell lung cancer (“U Cologne, Nature 2015”), lung normal samples (lung-GTEX), cervical cancer (“CESC-TCGA, Provisional”), oesophagus cancer (“ESCA-TCGA, Provisional”), head-and-neck tumors (“HNSC-TCGA, Provisional”) and pancreatic cancer (“PAAD-TCGA, Provisional”). Data was obtained using UCSC Xena (Goldman et al. 2020). Data was downloaded as log2(norm_count+1).

Box plots using TCGA and GTEx data was generated using the online tool BoxPlotR (Kampstra 2008) and GEPIA (Tang et al. 2017). For BoxPlotR, the data previously downloaded from UCSC Xena were used to generate the graphics, and P-values were calculated using two-tailed t-test. For box-plots, Tukey and Altman

whiskers where used depending of the number of samples. For GEPIA, the differential analysis was based on "TCGA tumors versus (TCGA normal + GTEx normal)", whereas the expression data was log2 (TPM+1) - transformed and the log2FC was defined as median (tumor) - median (normal). P-values were calculated with a one-way ANOVA comparing tumor with normal tissue. Tukey and Altman whiskers were used depending on the number of samples.

Correlation analysis was calculated using GEPIA software or Excel with the data obtained from UCSC Xena. The analysis was based on the expression of the following datasets: "TCGA tumors", "TCGA normal" and "GTEx normal". The expression of USP28 and TP63 and the gene set "Squamous Cancer Markers" [consensus list of upregulated genes for squamous tumors based on previous publications (Wilkerson et al. 2010; Mukhopadhyay et al. 2014; Xu et al. 2014; Ferone et al. 2016) were used for the calculation of Spearman's correlation coefficients and significance by GEPIA software.

The comparison of gene expression (using the dataset squamous cancer markers) across multiple tumor entities was done using GEPIA software based on the dataset "TCGA tumors". The colour code reflects the median expression of a gene in a tumor type, normalized with the maximum median expression across all different tumor types (row-wise Z-score). Genomic signature comparing primary human lung tumor was performed using UCSC Xena based on the dataset "TCGA tumors".

Kaplan-Meier curves were estimated with the KM plotter (Nagy et al. 2018), cBioPortal and R2: Genomics Analysis and Visualization Platform (http://r2.amc.nl). The KM plotter was used to analyse overall survival of lung cancer patients based on gene expression data from microarrays obtained from GEO, caBIG and TCGA. For R2 online tool, overall survival and gene expression data were obtained from TCGA. For the survival analysis of USP28-altered samples (mutation or deep deletion), cBioPortal was used to calculate disease-free survival using the dataset "Lung Squamous Cell Carcinoma (LUSC-TCGA, Provisional)". p-values were computed using a log-rank test. Heatmap Genomic signature expression comparing primary human lung tumor samples was performed using UCSC Xena based on the dataset "TCGA tumors". Compared Gene Expression across different cell lines was perfomed using the online tool R2.

3.5 Next-generation sequencing methods

3.5.1 RNA sequencing

RNA sequencing was performed with Illumina NextSeq 500 as described previously (Buchel et al. 2017). RNA was isolated using ReliaPrep™ RNA Cell Miniprep System Promega Kit, following the manufacturer's instruction manual. mRNA was purified with NEB Next Poly(A) mRNA Magnetic Isolation Module and the library was generated using the NEB Next Ultra RNA Library Prep Kit for Illumina, following the manufacturer's instructions. For the size selection of the libraries, Agencourt AMPure XP Beads were used. Library quantification and size determination were performed using the Fragment Analyzer.

Fastq files were generated using Illumina's base-calling software GenerateFASTQ v1.1.0.64, and overall sequencing quality was analysed using the FastQC script. Reads were aligned to the human genome (hg19) using TopHat v2.1.1 (Kim et al. 2013) and Bowtie 2 v2.3.2 (Langmead & Salzberg 2012) and samples were normalized to the number of mapped reads in the smallest sample. For differential gene expression analysis,

reads per gene (Ensembl gene database) were counted with the "summarizeOverlaps" function from the R package "GenomicAlignments" using the "union" mode and non-expressed or weakly expressed genes were removed (mean read count over all samples < 1). Differentially expressed genes were called using edgeR (Robinson et al. 2010), and resulting P-values were corrected for multiple testing by false discovery rate (FDR) calculations.

For gene set enrichment analyses (GSEA) (Mootha et al. 2003; Subramanian et al. 2005), five gene sets were generated: "Genes Down-regulated sh-USP28" ($q < 0.05$, $log2FC < -1.5$), "Gene Up-regulated sh-USP28" ($q < 0.05$, $log2FC > 1.5$), "Genes Down-regulated sh-ΔNP63" ($q < 0.05$, $log2FC < -3$), "Genes Up-regulated sh-ΔNP63" ($q < 0.05$, $log2FC > 3$) and "Squamous Cancer marker" (consensus list of upregulated genes for squamous tumors). Genes included in each gene set are reported in the Appendix section of the paper published by our research group (Prieto-Garcia et al. 2020).

Gene ontology analysis was performed with PANTHER (Mi et al. 2019) using the "Statistical overrepresentation test" tool with default settings. Three gene sets were generated based on the RNA-seq data and analysed: "Genes Down-regulated sh-USP28" ($q < 0.05$, $log2FC > 1.5$) and "Genes Down-regulated sh-ΔNP63" ($q < 0.05$, $log2FC < -1.5$).

Venn diagrams were visualized using the online tool: http://bioinformatics.psb.%c2%b5gent.be/webtools/Venn/. p-values were calculated with a hypergeometric test using the online tool at http://nemates.org. Pearson's correlation was used for RNA-seq data from A-431. P-values for Pearson's correlation were calculated using two-tailed Student's t-tests.

3.5.2 Proteomics

The sample preparation was performed as described previously (Klann et al. 2020). Lysates were precipitated by methanol/chloroform and proteins resuspended in 8M Urea/ 10mM EPPS at pH 8.2. Concentration of proteins was determined by Bradford assay and 100 µg of protein per samples was used for digestion. For digestion, the samples were diluted to 1M Urea with 10mM EPPS at pH 8.2 and incubated overnight with the endoproteinase LysC (1/50) and sequencing grade trypsin (1/100). Digests were acidified using TFA and tryptic peptides were purified by 50 mg tC18 SepPak. 125 µg peptides per sample were TMT labelled and the mixing was normalized after a single injection measurement by LC-MS/MS to equimolar ratios for each channel. 250 µg of pooled peptides were dried for offline High pH Reverse phase fractionation by HPLC.

Peptides were fractionated using a Dionex Ultimate 3000 analytical HPLC. 250 µg of pooled and purified TMT-labeled samples were resuspended in 10 mM ammonium-bicarbonate (ABC), 5% acetonitrile (ACN), and separated on a 250 mm long C18 column (X-Bridge, 4.6 mm ID, 3.5 µm particle size) using a multistep gradient from 100% Solvent A (5% ACN, 10 mM ABC in water) to 60% Solvent B (90% ACN, 10 mM ABC in water) over 70 min. Eluting peptides were collected every 45 s into a total of 96 fractions, which were cross-concatenated into 12 fractions and dried for further processing.

All mass spectrometry data was acquired in centroid mode on an Orbitrap Fusion Lumos mass spectrometer hyphenated to an easy-nLC 1200 nano HPLC system using a nanoFlex ion source applying a spray voltage of 2.6 kV with the transfer tube heated to 300°C and a funnel radio frequency (RF) of 30%. Internal mass

calibration was enabled (lock mass 445.12003 m/z). Peptides were separated on a self-made, 32 cm long, 75µm ID fused-silica column, packed in house with 1.9 µm C18 particles and heated to 50°C using an integrated column oven. HPLC solvents consisted of 0.1% Formic acid in water and 0.1% Formic acid, 80% ACN in water.

For proteome analysis, a synchronous precursor selection (SPS) multi-notch MS3 method was used in order to minimize ratio compression as previously described (McAlister et al. 2014). Individual peptide fractions were eluted by a non-linear gradient from 4 to 40% B over 210 minutes followed by a step-wise increase to 95% B in 6 minutes which was held for another 9 minutes. Full scan MS spectra (350-1400 m/z) were acquired with a resolution of 120000 at m/z 200, maximum injection time of 50 ms and AGC target value of 4 x 105. The most intense precursors with a charge state between 2 and 6 per full scan were selected for fragmentation within 3 s cycle time and isolated with a quadrupole isolation window of 0.4 Th. MS2 scans were performed in the Ion trap (Turbo) using a maximum injection time of 50ms, AGC target value of 1 x 104 and fragmented using CID with a normalized collision energy (NCE) of 35%. SPS-MS3 scans for quantification were performed on the 10 most intense MS2 fragment ions with an isolation window of 1.2 Th (MS) and 2 m/z (MS2). Ions were fragmented using HCD with an NCE of 65% and analyzed in the Orbitrap with a resolution of 50000 at m/z 200, scan range of 100-200 m/z, AGC target value of 1.5 x105 and a maximum injection time of 150ms. Repeated sequencing of already acquired precursors was limited by setting a dynamic exclusion of 60 seconds and 7 ppm and advanced peak determination was deactivated.

Proteomics raw files were processed using proteome discoverer 2.2. Spectra were recalibrated using the Homo sapiens SwissProt database (2018-11-21) and TMT as static modification at N-terminus and Lysines, together with Carbamidomethyl at cysteine residues. Spectra were searched against human database and common contaminants using Sequest HT with oxidation (M) as dynamic modification together with methionine-loss + acetylation and acetylation at the protein terminus. TMT6 (N-term, K) and carbamidomethyl were set as fixed modifications. Quantifications of spectra were rejected if average S/N values were below 5 across all channels and/or isolation interference exceeded 50%. Protein abundances were calculated by summing all peptide quantifications for each protein.

Reactome analysis were performed with PANTHER using the “Statistical overrepresentation test” tool with default settings. Proteins were considered significantly downregulated for reactome analysis when: FC<-0.5 and p-value<0.05. Heatmap visualization was performed using Morpheus from Broad Institute.

4. Results

4.1 USP28 regulates squamous cell identity and tumor formation via ΔNp63

USP28 has been extensively studied and characterized in several tumor entities, such as colorectal cancer (Diefenbacher et al. 2014; Diefenbacher et al. 2015). However, little is known regarding its expression and function in SCC tumors. This thesis studied the role of USP28 in regulating squamous cell identity by ΔNp63 deubiquitination in epithelial tumors. Malignant tumors with squamous identity require high levels of USP28 to maintain the malignant transcriptional profile of SCC induced by ΔNp63 overexpression.

4.1.1 USP28 and ΔNp63 are upregulated in lung squamous tumors

To determine the expression of USP28 in lung SCC tumors, publicly available TCGA datasets of human samples were analyzed (Figure 4.1A). USP28 was upregulated in human SCC samples compared to nontransformed tissue or ADC human samples (Figure 4.1A). As expected, the gene TP63 was heavily expressed in SCC tumors compared to normal tissue or human ADC samples. Additionally, the expression of USP28 significantly correlated with the TP63 expression in human SCC samples (Figure 4.1B). SCC samples with low TP63 expression also expressed low levels of USP28 (Figure 4.1C). The correlation between USP28 and TP63 in terms of the gene expression can be explained considering that ΔNp63 interacts with its own promotor, thus inducing its own transcription (Antonini et al. 2006). Consequently, if USP28 regulates the ΔNp63 stability at the protein level, the high abundance of the ΔNp63 protein will enhance the mRNA expression of TP63.

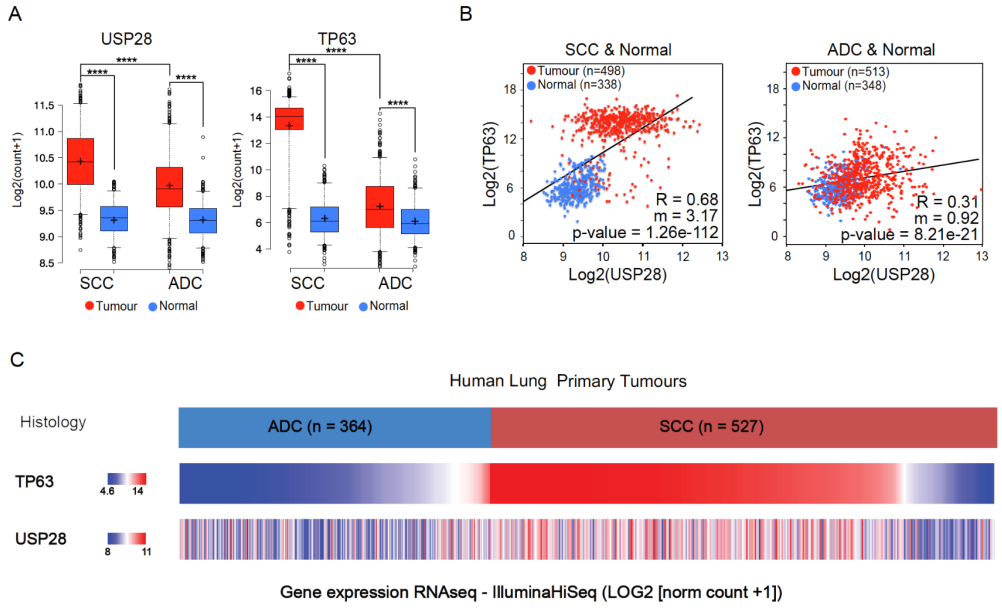

Figure 4.1: USP28 is up-regulated in human squamous tumors. **A)** Expression of USP28 (left) and TP63 (right) in lung human SCC tumors (n=498), ADC tumors (n=513) and normal (non-transformed tissue; SCCn=338; ADCn=348). https://xena.ucsc.edu. In box plots, the centre line reflects the median, the cross represents the mean and the upper and lower box limits indicates the first and third quartile. Whiskers extend 1.5x the IQR and outliers are marked as dots. . p-values were calculated using two-tailed t-test. Tumors=red ; Normal=blue. **** p-value < 0.001. **B)** Correlation of mRNA expression of USP28 and TP63 in lung SCC (left, n=498), ADC (right, n=513) and non-transformed tissue (nSCC=338, nADC=348). R: Spearmans correlation coefficient; m=Slope. https://xena.ucsc.edu. **C)** USP28 and TP63 gene expression heatmap in ADC (nADC=364) and SCC (nSCC=527) human lung cancer samples (www.xenabrowser.net).

Then, the protein abundances of USP28 in a total of 300 human-lung samples were quantified upon IHC (Figure 4.2A). Similar to mRNA expression, elevated levels of USP28 and ΔNp63 protein abundances were found in SCC tumors compared to those in ADC, SCLC, and nontransformed lung tissue. (Figure 4.2A). In summary, it is possible to conclude that USP28 and ΔNp63 are highly expressed in SCC tumors compared to normal tissue or other epithelial tumor entities.

4.1.2 USP28 correlates with poor prognosis in squamous lung cancer patients

To determine the relevance of USP28 and ΔNp63 in lung cancer patient survival, USP28 and ΔNp63 mRNA expression data were correlated to lung cancer survival using publicly available datasets. Patients with high levels of either ΔNp63 or USP28 presented bad prognosis and low survival compared to patients with low mRNA levels (Figure 4.3A). Importantly, USP28 gene expression correlated with poor prognosis and shortened lifespans even when only SCC patients were analyzed (Figure 4.3 B). Notably, most of the lung cancer patients did not present mutations or deletions in the USP28 gene (Figure 4.3C). However, 3% of the patients who presented genetically altered USP28 (deletion or mutation) showed better response to therapy and increased disease-free survival rates compared to SCC patients without USP28 alterations (Figure 4.3D). These data indicate that high levels of USP28 correlate with poor prognosis in SCC lung cancer patients.

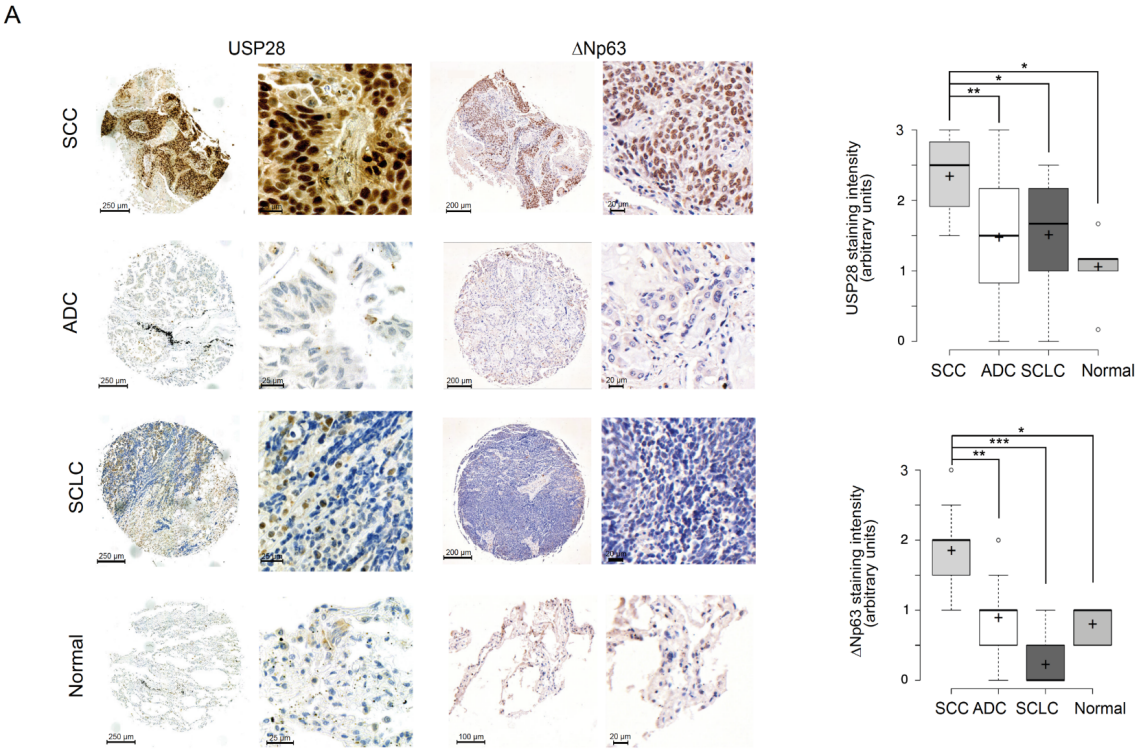

Figure 4.2: USP28 is highly abundant in lung squamous tumors.

A) IHC analysis of USP28 and ΔNp63 protein abundance in lung cancer and non-transformed human samples (n=300). The staining intensity was quantified i from 0 up to 3 arbitrary units by three independent pathologists. In box plots, the centre line reflects the median, the cross represents the mean and the upper and lower box limits indicates the first and third quartile. Whiskers extend 1.5x the IQR and outliers are marked as dots. p-values were calculated using two-tailed t-test. *p-value < 0.05; **p-value < 0.01; *** p-value < 0.001.

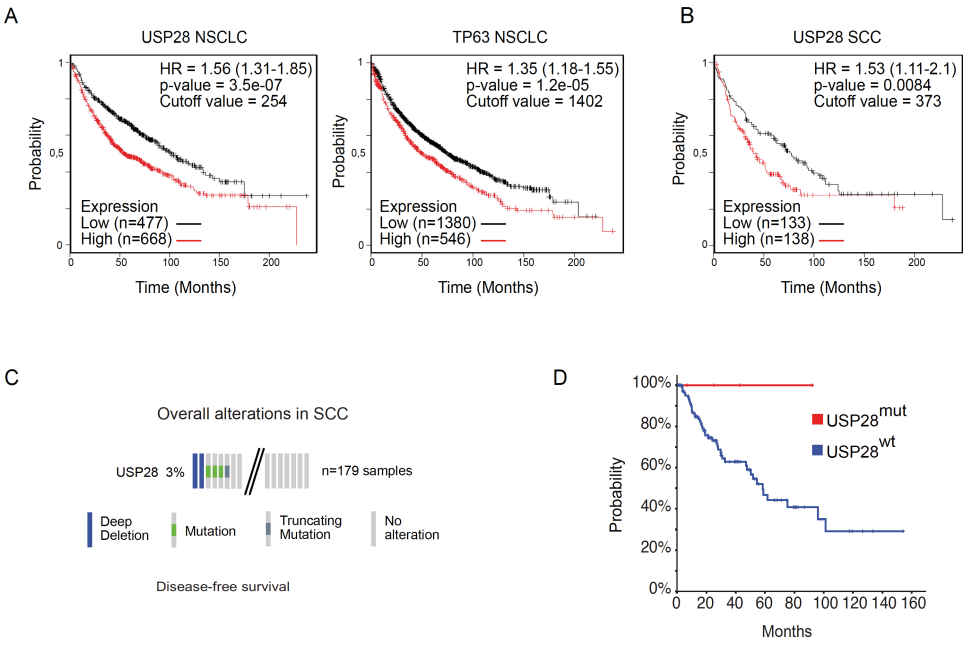

Figure 4.3: USP28 correlates with poor prognosis in SCC lung cancer patients.

A) Kaplan-Meier curve of NSCLC patients stratified by mRNA expression of USP28 (left, n=1145) or TP63 (right, n=1926) expression. p-values were calculated using log-rank test. HR: hazard ratio. https://kmplot.com**. B)** Kaplan-Meier curve of human lung SCC patients stratified by mRNA expression of USP28 (n=271). The p-value was calculated using a logrank test. HR: hazard ratio. https://kmplot.com. **C)** Genetic alterations of USP28 in human lung SCC. Each column represents a human tumor sample (n = 179). Data from TCGA were analyzed using cBioportal software **D)** Disease free survival of USP28 genetically altered (deletion or mutation) lung SCC tumors. Data from TCGA were analyzed using cBioportal software.

4.1.3 USP28 interacts with and stabilizes ΔNp63 by deubiquitinating K48-linked ubiquitin chains

To confirm if USP28 regulates ΔNp63 protein abundance and stability in cells, HA-USP28 and FLAG-ΔNp63 were transiently transfected in HEK293 cells. First, ectopic expressions of USP28 and ΔNp63 were tested in transfected HEK293 by IF staining (Figure 4.4A). Upon transient transfection, USP28 and ΔNp63 coexisted in the nucleus of the transfected HEK293 cells.

Coimmunoprecipitation assays were performed to determine if USP28 binds to ΔNp63. The assay results confirmed that ΔNp63 binds to USP28 in HEK293 cells (Figure 4.5A). To determine if USP28 deubiquitinates ΔNp63, a nickel-NTA ubiquitin pull-down assay was performed upon cotransfection of His-ubiquitin, HA-USP28, and FLAG-ΔNp63 in HEK293. The coexpression of USP28 and ΔNp63 resulted in decreased ubiquitination of ΔNp63 (Figure 4.5B).

Previous studies reported that FBXW7 ubiquitinates ΔNp63 in K48, thus regulating protein stability (Galli et al. 2010). To verify if USP28 deubiquitinates K48 on ΔNp63 upon ubiquitinating FBXW7, His-K48 ubiquitin and His-K63 ubiquitin chains were cotransfected with USP28 and ΔNp63. Immunoblotting revealed that K48 and K63 polyubiquitin chains were formed on ΔNp63 protein (Figure 4.5C). Moreover, the overexpression of USP28 mainly deubiquitinated the K48 polyubiquitin chains, whereas the K63 polyubiquitin chains were intact (Figure 4.5C).

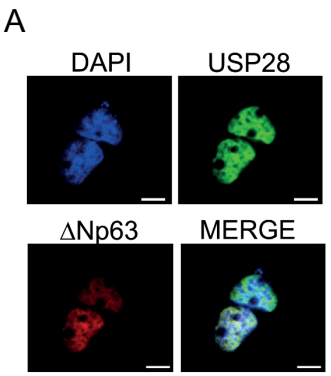

Figure 4.4: Immunofluorescence in HEK293 cells.

A) Immunofluorescence staining against overexpressed HA-USP28 and FLAG-ΔNp63 in HEK293 cells; Scale bar = 5µm; n=3.

Further, to determine if the catalytic activity of USP28 is required to bind and deubiquitinate ΔNp63, coimmunoprecipitation and Ni-NTA pull-down assays were performed upon co-transfection with the inactivated USP28 mutant (USP28 C171A) and ΔNp63 in HEK293 (Figure 4.5D and E). On immunoprecipitating ΔNp63, USP28 C171A could react with ΔNp63 (Figure 4.5D). However, overexpression of USP28C171A failed to deubiquitinate ΔNp63 (Figure 4.5E), demonstrating that cysteine 171 present in USP28 is required for deubiquitinating ΔNp63 (Figure 4.5E).

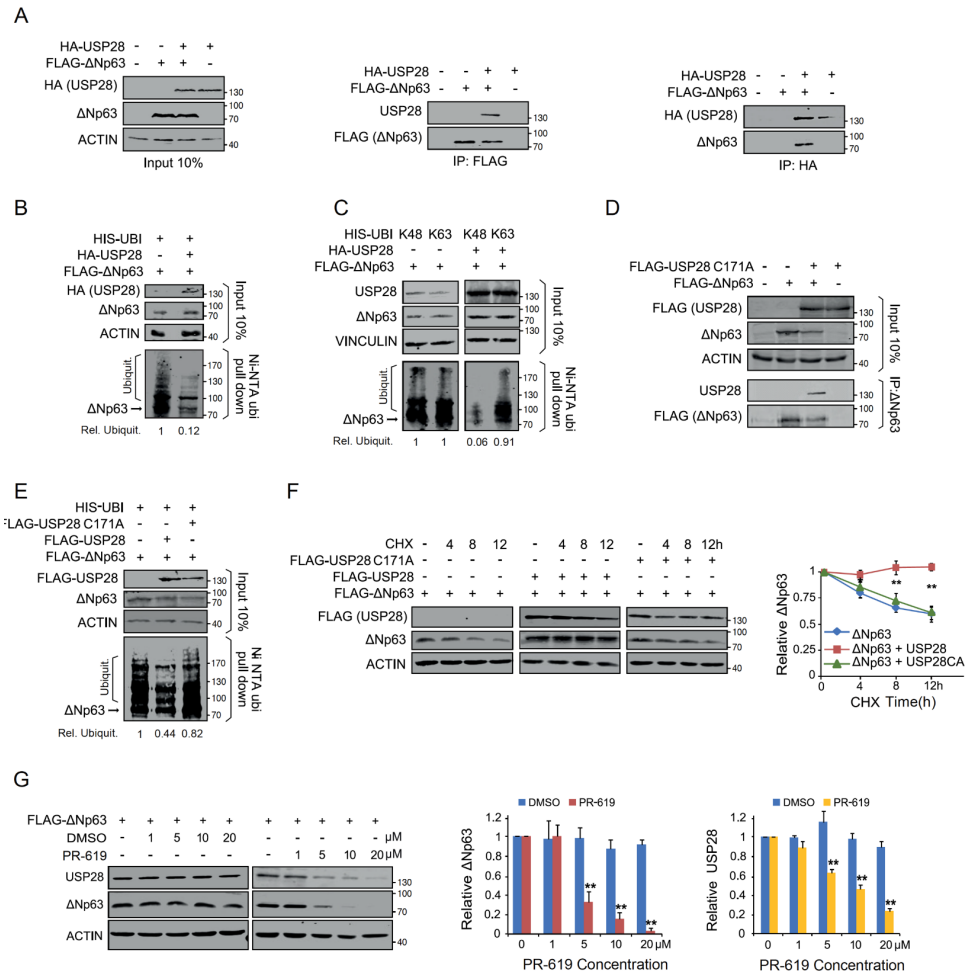

Figure 4.5: USP28 interacts and stabilizes ΔNp63 by deubiquitinating K48-linked ubiquitin chains.

A) HA-USP28 and FLAG-ΔNp63 Co-IP in HEK293 cells. HA or FLAG were precipitated and blotted against FLAG-ΔNp63 or HA-USP28. The input corresponds to 10% of the total protein amount (ACTIN as loading control). n=3. **B)** Ni-NTA His-ubiquitin pulldown in control or HA-USP28 transected HEK293 cells, followed by immunoblot against ΔNp63. The input corresponds to 10% of the total protein used for the pull down. Relative ubiquitination of the representative immunoblot was calculated using ACTIN for normalization. n=3. **C)** Ni-NTA His-ubiquitin pulldown K48 or K63 in control and HA-USP28 overexpressing HEK293 cells, followed by immunoblot against ΔNp63. The input corresponds to 10% of the total protein used for the pulldown. Relative ubiquitination of the representative immunoblot was calculated using ACTIN for normalization. n=3. **D)** Co-immunoprecipitation of FLAG-USP28 C171A and FLAG-ΔNp63 in HEK293 cells. ΔNp63 was precipitated and blotted against FLAG-USP28 or ΔNp63. The

input corresponds to 10% of the total protein used for the IP (ACTIN as loading control). n=3. **E)** Ni-NTA His-ubiquitin pulldown in control, FLAG-USP28 or FLAG-USP28 C171A transfected HEK293 cells, followed by immunoblot against exogenous ΔNp63. The input corresponds to 10% of the total protein used for the pulldown. Relative ubiquitination was calculated using ACTIN for normalization. n=3. **F)** CHX chase assay in control, FLAG-USP28 or FLAG-USP28 C171A transfected HEK293 cells for indicated time points. Representative immunoblot analysis of FLAG (USP28) and ΔNp63 as well quantification of relative protein abundance (ACTIN as loading control). p-values were calculated using two-tailed t-test statistical analysis; *p-value < 0.05; **p-value < 0.01. n=3. **G)** Immunoblot of USP28 and ΔNp63 in transfected HEK293 cells upon treatment with either DMSO or indicated concentrations of PR-619 for 24 hours. Relative protein abundance was calculated ACTIN as loading control. p-values were calculated using two-tailed t-test statistical analysis; *p-value < 0.05; **p-value < 0.01. n=3.

As USP28 deubiquitinates ΔNp63 in K48, the ability of USP28 to regulate ΔNp63 protein stability was investigated. In HEK293 cells, FLAG-USP28 and FLAG-USP28 C171A were overexpressed with ΔNp63. After transfection, cells were treated with cycloheximide (CHX) to block protein synthesis. The expression of USP28 rather than USP28 C171A significantly stabilized ΔNp63 protein stability upon CHX treatment (Figure 4.5F). To confirm if USP28 can be targeted by inhibiting its enzymatic catalytic activity, ΔNp63-transfected cells were treated with different concentrations of the pan-DUB inhibitor, PR-619, or DMSO (Figure 4.5G). Although ΔNp63 was strongly reduced upon treatment with PR-619, the cells exposed to DMSO showed ΔNp63 levels similar to those in the untreated cells (Figure 4.5G). Notably, exposure to the pan-DUB inhibitor also reduced USP28 protein abundance. These findings demonstrate that USP28 interacts with and stabilizes ΔNp63 by deubiquitinating K48-linked ubiquitin chains.

4.1.4 USP28 stabilizes ΔNp63 independently of the FBXW7 phospho-degron motif

The E3 ligase FBXW7 can ubiquitinate and regulate ΔNp63 protein stability (Galli et al. 2010). USP28 counteracts FBXW7, and they have several substrates in common, such as c-MYC, c-JUN and ΔNp63. However, FBXW7 is frequently mutated or lost in SCC tumors (Figure 4.6A) (Yokobori et al. 2012; Arita et al. 2017); consequently, it is important to know if USP28 can regulate ΔNp63 independently of FBXW7. As previously reported, the ΔNp63 phospho-degron (located on S383) is fully required to facilitate its binding to FBXW7(Galli et al. 2010).

By site-directed mutagenesis, a point mutation was introduced in the ΔNp63 phospho-degron, substituting the serine 383 for an alanine (S383A). ΔNp63 S383A cannot be phosphorylated by GSK3β and hence, the mutation eliminates the interaction of FBXW7 with ΔNp63 (Galli et al. 2010). To determine if USP28 can bind and stabilize ΔNp63 independently of FBXW7, USP28 and ΔNp63 S383A were cotransfected in HEK293 cells. The results showed that overexpressed USP28 binds to ΔNp63 and increases ΔNp63 S383A protein abundance (Figure 4.7A and B).

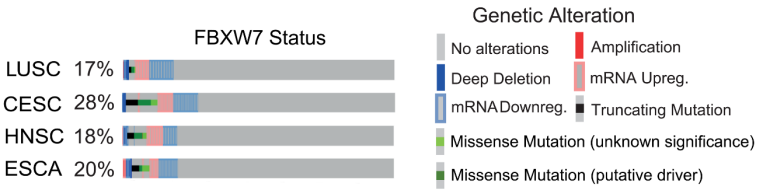

Figure 4.6: FBXW7 is frequently mutated or lost in SCC tumors.

A) Analysis of FBXW7 genetic alterations in SCC tumors. FBXW7 genetic alteration in lung (LUSC), cervical (CESC), head and neck (HNSC) and esophageal (ESCA) carcinoma tumors (Cbioportal).

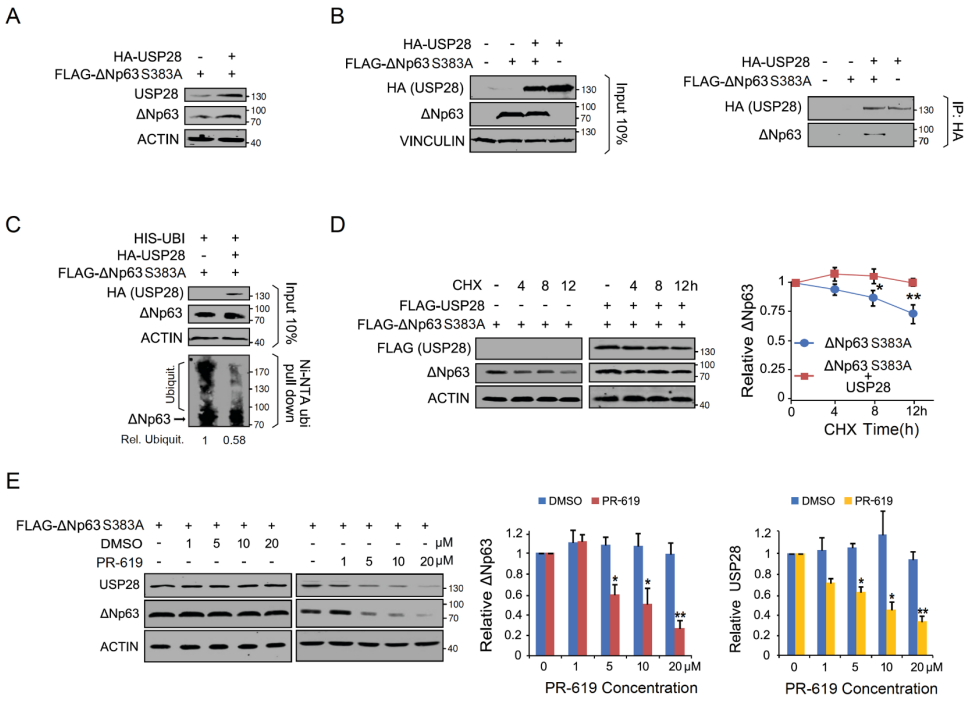

Figure 4.7: USP28 stabilizes ΔNp63 independently of FBXW7 phospho-degron motif.

A) Western blot of ΔNp63, USP28 and ACTIN in FLAG-ΔNp63 S383A or FLAG-ΔNp63 S383A + HA-USP28 HEK293-T transfected HEK293 cells. ACTIN as a loading control. n=3. **B)** Co-immunoprecipitation of exogenous HA-USP28 and FLAG-ΔNp63 S383A in HEK293 cells. HA was precipitated and western-blotted against ΔNp63 S383A or HA-USP28. VINCULIN served as loading control. n=3. **C)** Ni-NTA ubiquitin pulldown of FLAG-ΔNp63 S383A in control or HA-USP28 overexpressing HEK293 cells, followed by immunoblot against ΔNp63 protein. Relative Ubiquitination calculated using ACTIN for normalization. n=3. **D)** Western blot of HEK293 transfected with either FLAG-ΔNp63 S383A or FLAG-ΔNp63 S383A together with FLAG-USP28, followed by CHX chase for indicated timepoints. ACTIN served as loading control. Quantification of relative protein abundance of n=3. *p < 0.05, **p < 0.01. Two tailed t-test **E)** HEK293 cells transiently transfected with FLAG-ΔNp63S383A. 24 hours later cells were exposed to either DMSO or the pan-DUB inhibitor PR619 for 24 hours for indicated concentration, followed by western blot against endogenous USP28 and ΔNp63 S383A. ACTIN served as loading control. Quantification of relative protein abundance of n=3. *p < 0.05, **p < 0.01. Two tailed t-test

Furthermore, the expression of USP28 could decrease ΔNp63 S383A ubiquitination following the Ni-NTA ubiquitin pull-down assay (Figure 4.7C). To check if USP28 can post-translationally stabilize ΔNp63 S383A, a CHX chase assay was performed on the control and USP28-transfected HEK293 cells. Overexpression of USP28 increases the half-life of the ΔNp63 S383A protein (Figure 4.7D), demonstrating that USP28 can stabilize ΔNp63 S383A independently of FBXW7. Notably, ΔNp63 S383A (Figure 4.7D) showed a higher protein half-life compared to WT ΔNp63 (Figure 4.5F), confirming that FBXW7 regulates the stability of the ΔNp63 protein. Finally, it was demonstrated that exposure to the pan-DUB inhibitor PR-619 also reduced the ΔNp63 S383A protein abundance as is the case for WT ΔNp63.

4.1.5 USP28 deubiquitinates and stabilizes endogenous ΔNp63 in squamous cancer cells

To confirm whether USP28 regulates the ubiquitination and stability of endogenous ΔNp63, human A-431 SCC cells were used. A-431 cells have detectable abundance levels of endogenous USP28 and ΔNp63 (Figure 4.8A). Furthermore, A-431 cells are homozygous mutants (S462Y) for FBXW7 (Figure 4.8B) (Zieba et al. 2018). The S462Y mutant, located in one of the WD40 domains, prevents the recognition of FBXW7 substrates (Yeh et al. 2018).

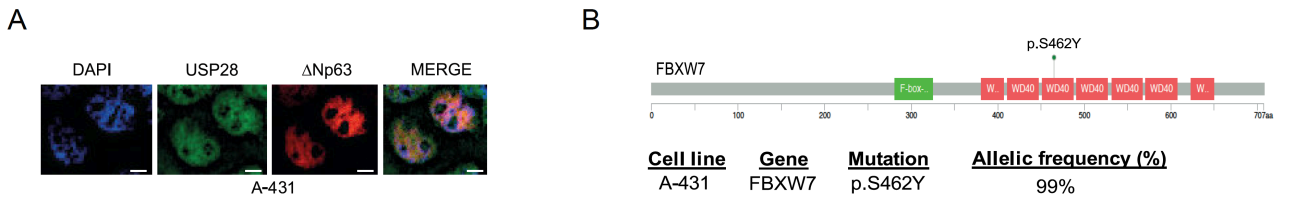

Figure 4.8: A-431 express ΔNp63 and USP28

A) Immunofluorescence staining against USP28 and ΔNp63 in A-431cells; Scale bar = 5µm; n=3. **B)** Mutational analyisis of FBXW7 in A-431 cell line (Cosmic sanger) (Zieba et al. 2018).

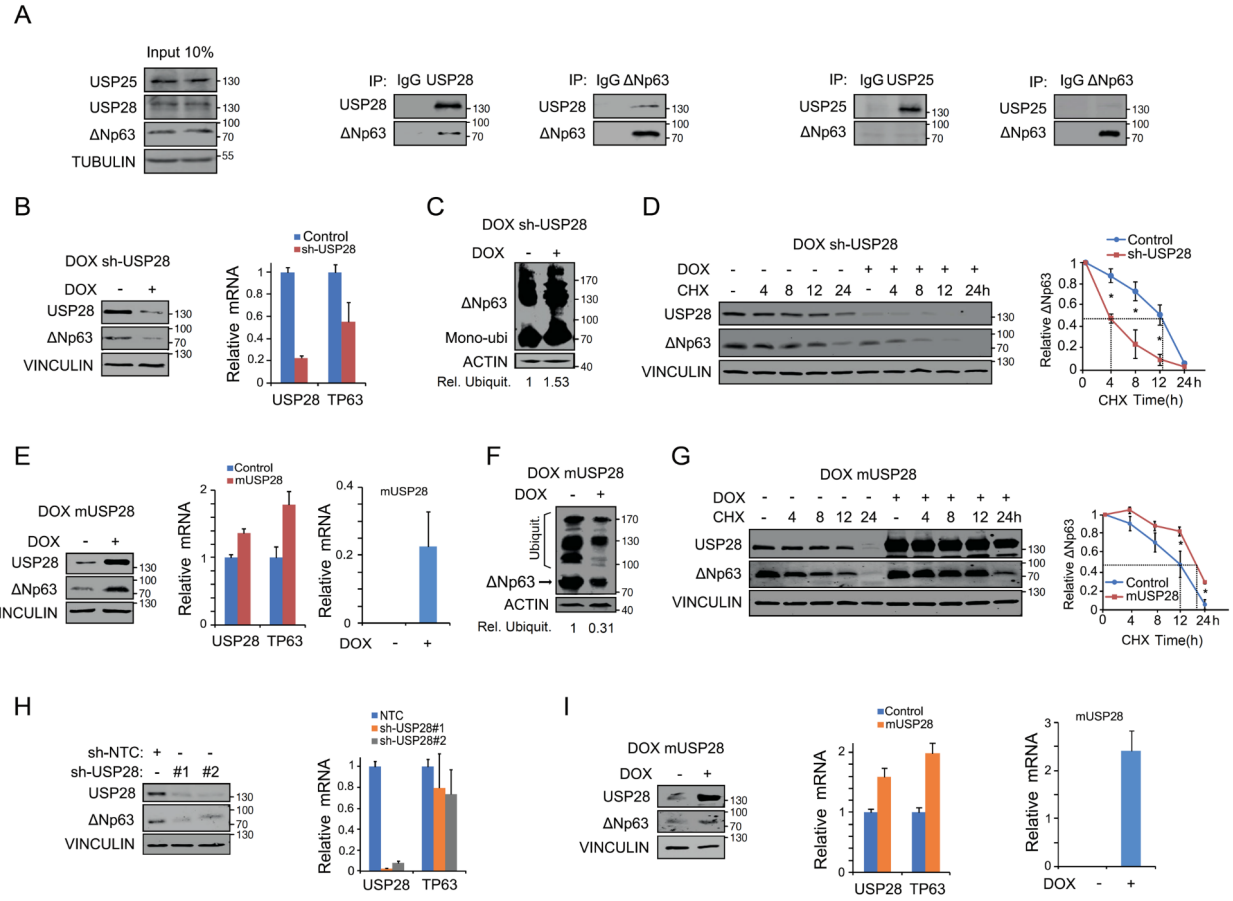

Figure 4.9: USP28 endogenously deubiquitinates and stabilizes ΔNp63 in A-431 cells.

A) Co-IP in A-431 cells. Western blot of USP25, USP28 and ΔNp63 IP and ΔNp63, USP25 or USP28 co-IP. The input corresponds to 10% of the total protein used for the IP. TUBULIN as loading control. n=3**. B)** Inducible depletion of USP28. Western blot (left) of A-431 cells upon DOX exposure. VINCULIN as loading control for western blot. qPCR analyzing mRNA levels of USP28 and ΔNp63 upon DOX exposure. Relative mRNA was calculated using ACTIN as housekeeping gene. Relative mRNA was calculated using ΔΔCt analysis. n=3**. C)** TUBE pulldown of endogenous ubiquitinated ΔNp63 in A-431 cells upon depletion of USP28. Relative ubiquitination was calculated using ACTIN for normalization. n=3**. D)** CHX chase assay of control or USP28 depleted A-431 cells for indicated time points. Representative immunoblot (left) using VINCULIN as loading control. Quantification of relative protein abundance (right) of n=3. p-values were calculated using two-tailed t-test statistical analysis; *p-value < 0.05. **E)** Inducible expression of murine USP28 upon DOX exposure. Western blot (left) of A-431 cells upon DOX exposure. VINCULIN as loading control for western blot. qPCR analyzing mRNA levels of USP28, mUSP28 and ΔNp63 upon DOX exposure. Relative mRNA was calculated using ACTIN as housekeeping gene. Relative mRNA was calculated using ΔΔCt analysis for human USP28 and ΔCt for mUSP28. n=3**. F)** TUBE pulldown of endogenous ubiquitinated ΔNp63 in A-431 cells upon over-expression of USP28. Relative ubiquitination was calculated using ACTIN for normalization. n=3**. G)** CHX chase assay of control or murine USP28 over-expressed A-431 cells for indicated time points. Representative immunoblot (left) using VINCULIN as loading control. Quantification of relative protein abundance (right) of

n=3. p-values were calculated using two-tailed t-test statistical analysis; *p-value < 0.05. **H)** Control (sh-NTC) and two independent constitutive shRNA targeting USP28 (sh-USP28#1 and #2) in LUDLU-1 $^{adh.}$ cells. Western blot (left) for ΔNp63 and USP28 protein abundance. VINCULIN as loading control. qPCR analysis of USP28 and ΔNp63 expression using ACTIN as housekeeping gene. n=3**. I)** Inducible expression of murine USP28 upon DOX exposure. Western blot (left) of A-431 cells upon DOX exposure. VINCULIN as loading control for western blot. qPCR analyzing mRNA levels of USP28, mUSP28 and ΔNp63 upon DOX exposure. Relative mRNA was calculated using ACTIN as housekeeping gene. Relative mRNA was calculated using ΔΔCt analysis for human USP28 and ΔCt for mUSP28. n=3

Further, to verify if USP28 regulates the stability of the endogenous ΔNp63 protein, A-431 cells were infected with a DOX-inducible shRNA system to acutely deplete USP28 (Figure 4.9B). Upon DOX exposure, the USP28 and ΔNp63 protein abundances were reduced compared to those in the untreated cells (Figure 4.9B). Analyzing the mRNA levels upon DOX exposure confirmed that the shRNA worked as expected (Figure 4.9B), reducing the mRNA levels of the targeted genes. As observed in previous studies (Antonini et al. 2006), ΔNp63 regulates its own transcription, and ΔNp63 mRNA levels are reduced in USP28-depleted cells compared to those in the control cells (Figure 4.9B). To determine if USP28 regulates ΔNp63 protein stability via deubiquitination, a TUBE pull-down assay was performed on the control and USP28-depleted cells. ΔNp63 was clearly more ubiquitinated in sh-USP28 cells than in the control cells (Figure 4.9C). Finally, the half-life of the ΔNp63 protein was determined upon depletion of USP28 by CHX exposure (Figure 4.9D). Depletion of USP28 strongly reduces the half-life of the ΔNp63 protein in the A-431 cells (Figure 4.9D).

The data demonstrated that depletion of USP28 decreases the stability of the ΔNp63 protein. Therefore, to confirm if USP28 overexpression deubiquitinates ΔNp63 by increasing its protein stability, an inducible A-431 cell line system was used that overexpresses murine USP28 upon DOX exposure. The structure of murine USP28 is highly similar to that of human USP28 (Figure 4.10A).

A

BLAST: USP28 human sequence

Protein	Organism	Identity	Similar
USP28	Human	100%	100%
USP28	Rat	91.3%	97.2%
USP28	Chicken	65.1%	82.4%
USP25	Human	49.7%	74.7%
USP25	Mouse	49.9%	74.4%
USP28	Mouse	87.5%	93.9%
USP48	Human	29.8%	59.9%

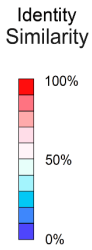

Figure 4.10: Identity and similarity of USP28 and USP25.
A) Identity and similarity of USP28 and USP25 in different organisms (European Bioinformatics Institute; EMBL-EBI).

Upon expression of murine USP28, increased abundance levels of the ΔNp63 protein and mRNA levels were found (Figure 4.9E). Additionally, the overexpression of murine USP28 decreases the ubiquitination of ΔNp63 (Figure 4.9F) and extends its protein half-life to 20 hours upon CHX treatment (Figure 4.9G). Alternatively, the overexpression of the catalytically inactive mutant of USP28 (C171A) did not increase the ΔNp63 protein abundance (Figure 4.11A) and did not decrease the ubiquitination of ΔNp63 (Figure 4.11B). Lastly, the results were confirmed using another FBXW7 WT SCC cell line (LUDLU-1^{adh}). Upon constitutive depletion of USP28 in the lung SCC cell line LUDLU-1^{adh}, the ΔNp63 protein abundance and mRNA levels were reduced (Figure 4.9 H). Alternately, the expression of murine USP28 increases the ΔNp63 protein abundance and

mRNA levels (Figure 4.9I). These data clearly demonstrate that USP28 enzymatically deubiquitinates ΔNp63, increasing its protein stability in SCC cells with WT or mutated FBXW7.

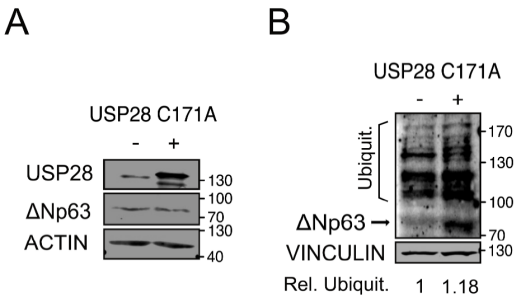

Figure 4.11. USP28 C171A cannot deubiqutinate ΔNp63 in A-431 cells.
A) Transfection of USP28 C171A upon DOX exposure. USP28 and ΔNp63 Western blot upon transfection. ACTIN as loading control. n=3.**B)** TUBE pulldown of endogenous ubiquitinated ΔNp63 in A-431 cells upon over-expression of USP28 C171A. Relative ubiquitination was calculated using VINCULIN for normalization. n=3.

4.1.6 USP28 regulates the ΔNp63 transcriptional profile in squamous cancer cells

ΔNp63 is a potent transcription factor that regulates SCC cell identities. As a transcription factor, ΔNp63 was considered "undruggable" (Bushweller 2019). However, considering the deterioration of the ΔNp63 stability observed following the depletion of USP28, it is possible to hypothesize that USP28 could be a suitable target to regulate the transcriptional activity of ΔNp63, thus making it "druggable."

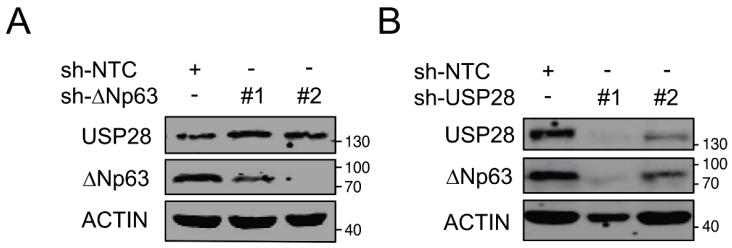

Figure 4.12. Constitutive depletion of USP28 and ΔNp63 in A-431 cells.
A) Western blot of ΔNp63, USP28 and ACTIN in A-431 upon depletion of ΔNp63 with two independent shRNAs. ACTIN as a loading control. n=3. sh-NTC= shRNA non-targeting control. **B)** Western blot of ΔNp63, USP28 and ACTIN in A-431 upon depletion of USP28 with two independent shRNAs. ACTIN as a loading control. n=3. sh-NTC= shRNA non-targeting control.

To investigate if USP28 regulates the characteristic gene expression profile of ΔNp63, RNA-sequencing analysis of A-431 cells was performed upon depletion of USP28 or ΔNp63. First, the constitutive depletions of USP28 and ΔNp63 were analyzed by immunoblotting (Figure 4.12A and B). For RNA-sequencing, sh-ΔNp63#2 and sh-USP28#1 cells were used. Global gene expression analysis confirmed a strong similarity between the sh-USP28 and sh-ΔNp63 cells, according to an important Pearson correlation coefficient comparing global changes in gene expression upon depletion of USP28 and ΔNp63 (Figure 4.13A). Even if USP28 regulates important oncogenes such as c-MYC, c-JUN, or NOTCH1, the analysis clearly indicates that the depletion of ΔNp63 causes stronger changes in gene expression than the depletion of USP28 for SCC cells (Figure 4.13B and C). The depletion of ΔNp63 significantly upregulated 972 genes and downregulated 1219 genes (Figure 4.13B and C). Alternatively, USP28 depletion significantly upregulated 132 genes and downregulated 418 genes (Figure 4.13B and C). The significant change in global gene expression upon ΔNp63 depletion confirmed the function of ΔNp63 as a master regulator of transcription in SCC cells. Furthermore, most of the genes altered by the depletion of USP28 (66 of the upregulated genes and 266 of the downregulated ones) were commonly altered by the depletion of ΔNp63 (Figure 4.13B and C). Gene set enrichment analysis

(GSEA) using the set of genes downregulated in response to the depletion of USP28 or ΔNp63 confirmed the strong similarity in the changes related to gene expression caused by the depletion of either USP28 or ΔNp63 (Figure 4.13D and E).

Finally, gene ontology (GO) analysis of the downregulated biological processes was performed in either the sh-USP28 or sh-ΔNp63 cells (Figure 4.13F and G). Notably, the most enriched biological processes for both conditions were processes involved in epithelial cell identification, squamous differentiation, and keratin expression (Figure 4.13F and G). The downregulated biological processes related to squamous identities were strongly enriched in the sh-ΔNp63 cells compared to the USP28-depleted cells (Figure 4.13F and G), suggesting that USP28 regulates SCC cell identities via its ability to regulate the ΔNp63 protein abundance.

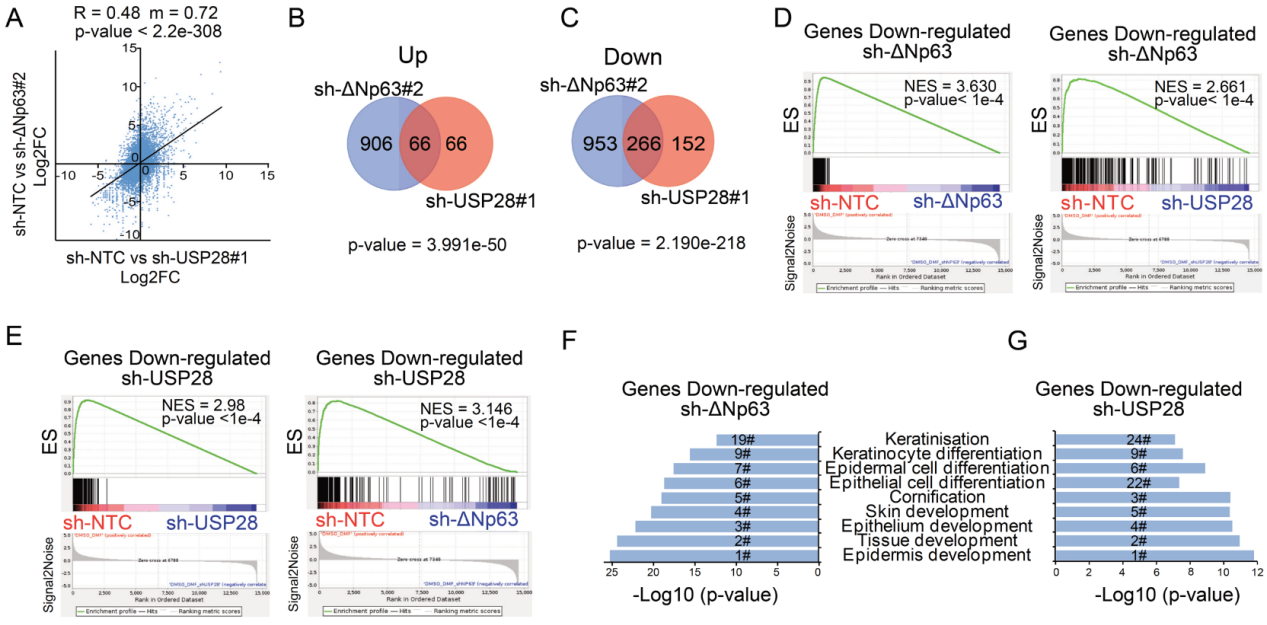

Figure 4.13. USP28 regulates ΔNp63 transcriptional profile in Squamous cancer cells.

A) Correlation of gene expression changes upon depletion of USP28 (sh-USP28#1) or ΔNp63 (sh-ΔNp63#2) relative to control A-431 cells (sh-NTC). The diagonal line reflects a regression build on a linear model. R: Pearsons correlation coefficient, m: slope of the linear regression model. sh-NTC= shRNA non-targeting control. **B)** Venn diagram of differentially up-regulated genes (log2FC>1.5 and q-value<0.05) between sh-ΔNp63#2 and sh-USP28#1 relative to control A-431 cells (sh-NTC). p-values was calculated using a hypergeometric test. **C)** Venn diagram of differentially down-regulated genes (log2FC<-1.5 and q-value<0.05) between sh-ΔNp63#2 and sh-USP28#1 relative to control A-431 cells (sh-NTC). p-values was calculated using a hypergeometric test. **D)** Gene set enrichment analysis (GSEA) of significantly down-regulated genes in sh-ΔNp63#2 A-431 cells. The gene set was analysed in sh-ΔNp63#2 (left) and sh-USP28#1-depleted (right) compared to control A-431 cells. (N)ES: (normalised) enrichment score. sh-NTC= shRNA non-targeting control. **E)** Gene set enrichment analysis (GSEA) of a gene set of significantly down-regulated genes in sh-USP28#1 transfected A-431 cells. The gene set was analysed in shUSP28#1 (left) and sh-ΔNp63#-depleted (right) compared to A-431 cells. (N)ES: (normalised) enrichment score. sh-NTC= shRNA non-targeting control. **F)** GO term analysis of biological processes enriched in sh-ΔNp63#2 A-431 relative to control cells. Numbers indicate the ranking position of all analysed GO terms based on the significance. **G)** GO term analysis of biological processes enriched in sh-USP28#1 A-431 relative to control cells. Numbers indicate the ranking position of all analysed GO terms based on the significance.

4.1.7 USP28 maintains squamous cell identity and proliferation via ΔNp63

The previously described results demonstrated that USP28 can adjust the transcriptional activity of ΔNp63 by regulating the squamous epithelial cell identity. This section of the thesis aims to elucidate how relevant USP28 is and its regulation of ΔNp63 to maintain the malignant identity and oncogenic phenotype of SCCs. A gene list (called squamous cancer markers) was generated with the most commonly upregulated genes in human SCC tumors (Fig 4.14A) (Prieto-Garcia et al. 2020). Analyzing publicly available datasets confirmed that the genes composing the SCC gene list are definitely more expressed in human SCC tumors than in other tumor entities (Fig 4.14A).

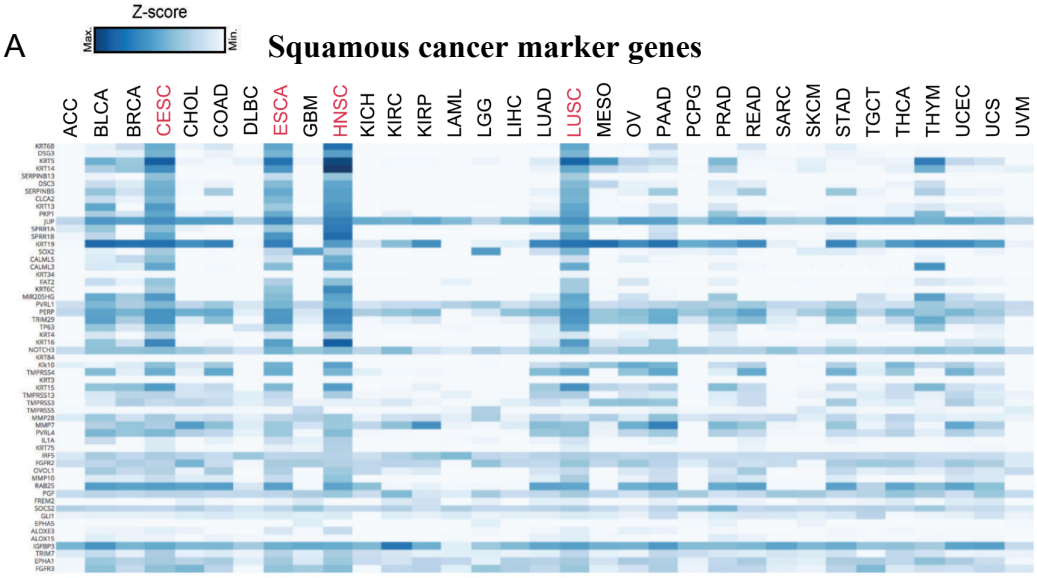

Figure 4.14. Common up-regulated genes in SCC human tumors
A) Relative gene expression of Squamous cancer markers in human samples. Z-Score calculated by www.gepia.cancer-pku.cn. Red = SCC tumors.

To verify if the depletion of USP28 or ΔNp63 reduces the expression of squamous cancer markers, GSEA was performed using the previously generated gene list of squamous cancer markers and comparing the control cells to the sh-USP28 or sh-ΔNp63 cells (Figure 4.15A and B).

Moreover, to confirm if USP28 can regulate the genetic profile of malignant SCCs in human samples, previously sequenced human-lung SCC tumors were analyzed (Figure 4.15C and D). An important correlation was observed between USP28 and the list of SCC markers (Figure 4.15D). The correlation was significantly stronger for ΔNp63 (Figure 4.15C), again suggesting that USP28 regulates SCC identity via ΔNp63.

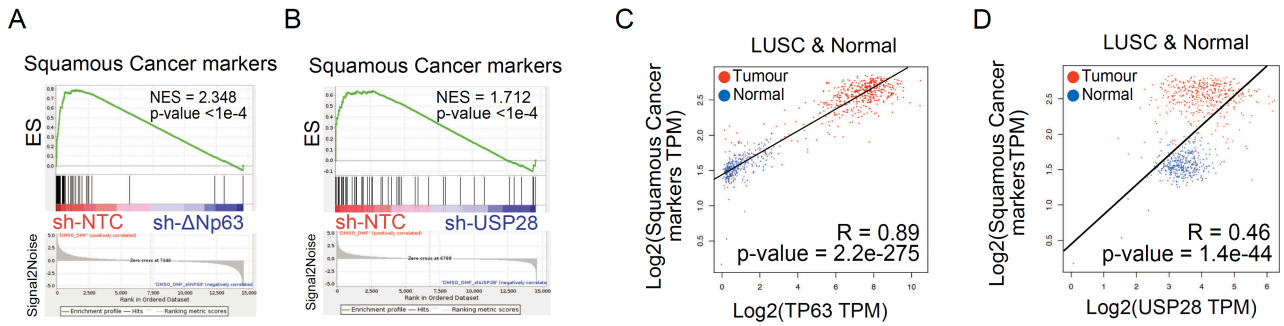

Figure 4.15. USP28-ΔNp63 axis regulates Squamous cancer marker genes.
A) Gene set enrichment analysis (GSEA) of squamous cancer marker genes in control compared to sh-ΔNp63#2 A-431 cells. (N)ES: (normalised) enrichment score. sh-NTC= shRNA non-targeting control. **B)** Gene set enrichment analysis (GSEA) of squamous cancer

marker genes in control compared to sh-USP28#1 A-431 cells. (N)ES: (normalised) enrichment score. sh-NTC= shRNA non-targeting control. **C)** Gene expression Spearman correlation of Squamous cancer marker genes and TP63 in lung SCC and normal human samples (Normal). R: Spearmans correlation coefficient. n=836. http://gepia.cancer-pku.cn. **D)** Gene expression Spearman correlation of Squamous cancer marker genes and USP28 in lung SCC and normal human samples (Normal). R: Spearmans correlation coefficient. n=836. http://gepia.cancer-pku.cn.

Some of the samples in the set of the sequenced human-lung SCC samples had low levels of USP28 expression (Figure 4.16A). Remarkably, the samples with low levels of USP28 also had low levels of ΔNp63, SCC markers (KRT5, KRT14, KRT19, and DSG3), and proliferative markers (MKI67 and PCNA) (Figure 4.16A). Furthermore, the tumor suppressor GPRC5A, regulated directly by ΔNp63 (Saladi et al. 2017), was highly expressed in the samples with low USP28 levels (Figure 4.16A).

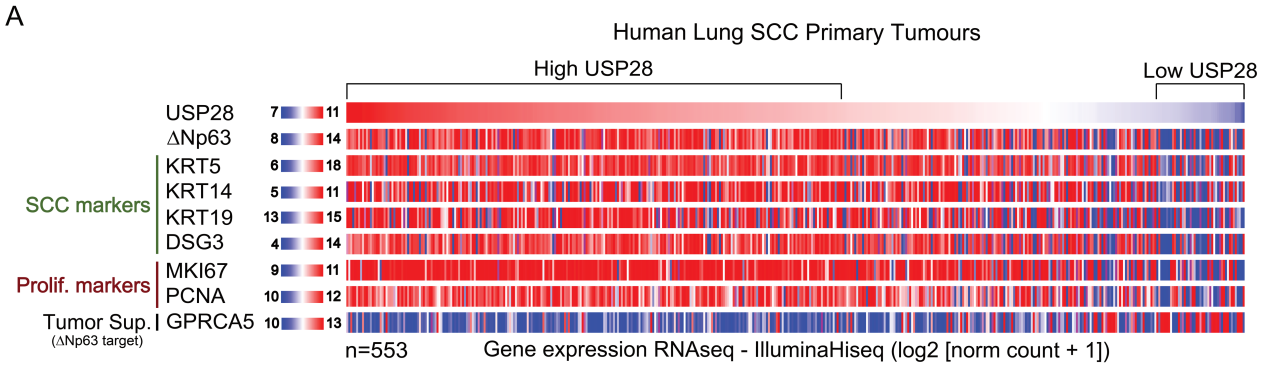

Figure 4.16. USP28-ΔNp63 axis regulates Squamous cancer marker genes.

A) Gene expression of human lung SCC samples for USP28, ΔNp63, KRT5, KRT14, KRT19, DSG3, MKI67, PCNA and GPRC5A. Samples were sorted using relative USP28 expression (high to low). Red= high gene expression; Blue= low gene expression. n=553. https://xena.ucsc.edu.

USP28 stabilizes important cell cycle regulators such as c-MYC, c-JUN, NOTCH1, and ΔNp63; additionally, the samples with reduced USP28 expression showed low levels of the proliferative markers MKI67 and PCNA (Figure 4.16A). To investigate the role of the USP28-ΔNp63 axis in SCC proliferation and cell cycle regulation, the growth rate of A-431 cells was quantified upon depletion of USP28 or ΔNp63. The effectiveness of the shRNAs used was previously confirmed by immunoblotting (Figure 4.12A and B). The control, sh-USP28, and sh-ΔNp63 cells were seeded at equal cell densities and quantified at specific time points (Figure 4.17A and B). The control cells proliferate significantly faster than the USP28- or ΔNp63-depleted cells (Figure 4.17A and B). Cell cycle analyses proved that the USP28- and ΔNp63-depleted cells show higher accumulation in the synthesis phase (S phase) than the control cells (Figure 4.17C and D).

As previously mentioned, USP28 deubiquitinates key oncogenes in cancer cells such as c-MYC or c-JUN. To demonstrate that USP28 regulates SCC cell identity and proliferation via ΔNp63, ΔNp63 was overexpressed in USP28 knockdown cells; then, the cell growth and expression of the SCC markers were analyzed (Figure 4.18A, B and C). First, it was observed that the transfection of ΔNp63 recovered the loss of the ΔNp63 protein abundance upon depletion of USP28 (Figure 4.18A). The protein abundance and gene expression of the SCC marker KRT14 were also partially restored

(Figure 4.18A). Regarding the expression of the other SCC markers, it was observed that the transfection of ΔNp63 recovered the mRNA levels in KRT5 and KRT19 (Figure 4.18C). Finally, the re-expression of ΔNp63 partially restored the proliferative rates of the USP28 knockdown cells (Figure 4.18B). These findings highlight the critical role of the USP28-ΔNp63 axis in regulating the malignant identity of SCCs.

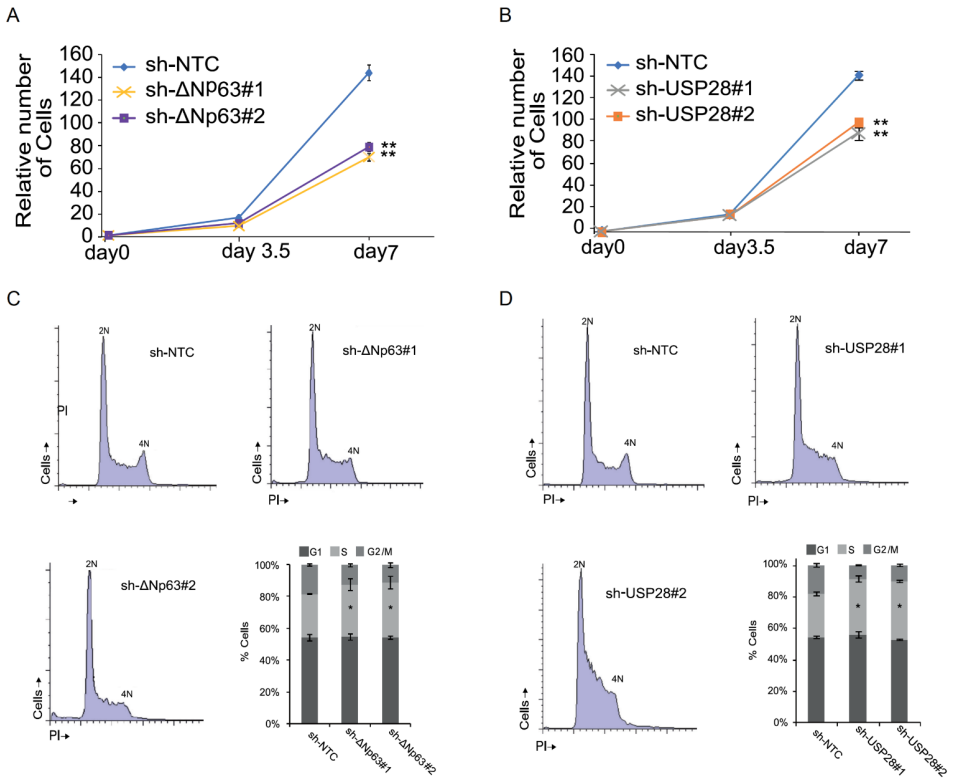

Figure 4.17. USP28 and ΔNp63 control cell cycle progression and proliferation in SCC cells.

A) Cell growth of control and ΔNp63 depleted cells. stably transduced with shRNA-non-targeting control (NTC) and two shRNA against ΔNp63. n=3 *p < 0.05, **p < 0.01; Two tailed t-test. sh-NTC= shRNA non-targeting control. **B)** Cell growth of control and USP28 depleted cells. stably transduced with shRNA-non-targeting control (NTC) and two shRNA against ΔNp63. n=3 *p < 0.05, **p < 0.01; Two tailed t-test. sh-NTC= shRNA non-targeting control. **C)** Cell cycle analysis by propidium iodide staining of control A-431 and ΔNp63 knock down A-431 cells. n=3; *p < 0.05 Two tailed t-test. sh-NTC= shRNA non-targeting control. **D)** Cell cycle analysis by propidium iodide staining of control A-431 and USP28 depleted A-431 cells. n=3; *p < 0.05 Two tailed t-test. sh-NTC= shRNA non-targeting control.

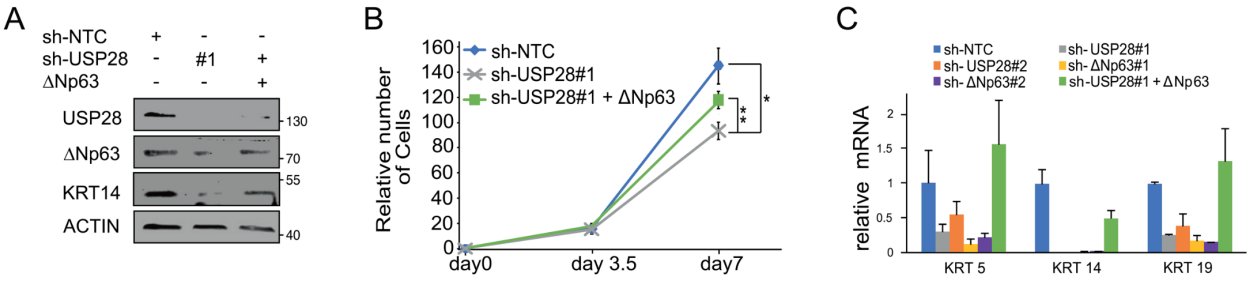

Figure 4.18. USP28 regulates proliferation and SCC identity via ΔNp63.

A) Western blot of ΔNp63, USP28 and KRT14 in control, sh-USP28 and ΔNp63 transfected sh-USP28. ACTIN as loading control. n=3. sh-NTC= shRNA non-targeting control. **B)** Cell growth of ΔNp63, USP28 and KRT14 in control, sh-USP28 and ΔNp63 transfected sh-USP28. n=3 p-values were calculated using two-tailed t-test statistical analysis. *p-value < 0.05, **p-value < 0.01. Sh-NTC= shRNA non-targeting control. **C)** q-PCR of ΔNp63, USP28 and KRT14 in control, sh-USP28 and ΔNp63 transfected sh-USP28. Normalised to ACTIN. n=3. Sh-NTC= shRNA non-targeting control.

4.1.8 ΔNp63-driven squamous cancer cells are vulnerable to USP28 depletion irrespective of the "tissue of origin"

To analyze the therapeutic potential of targeting USP28 in different SCC tissues, a set of ADC cell lines were compared to different SCCs from the same "tissue of origin." Pancreatic, (PANC-1 as the ADC cell line and BXPC-3 as the SCC line), cervical (HeLa as the ADC line, and SiHa and Ca-Ski as the SCC cell lines), and lung cancer cell lines (H1299 as the ADC cell line and LUDLU-1^{adh} as the SCC cell line) were used. Additionally, another SCC cell line from head and neck tumors (Detroit 562) were used, considering that 90% of the head and neck tumors are SCCs (Vigneswaran & Williams 2014). USP28 was expressed in all the cell lines during immunoblotting (Figure 4.19A), whereas ΔNp63 was only expressed in the Ca-Ski, BXPC3, and Detroit 562 SCC cell lines. Furthermore, ΔNp63 was not detected in the SiHa SCC line (Figure 4.19A). It was previously observed that the LUDLU-1$^{adh.}$ SCC cell line expressed detectable levels of endogenous USP28 and ΔNp63 (Figure 4.9H and I).

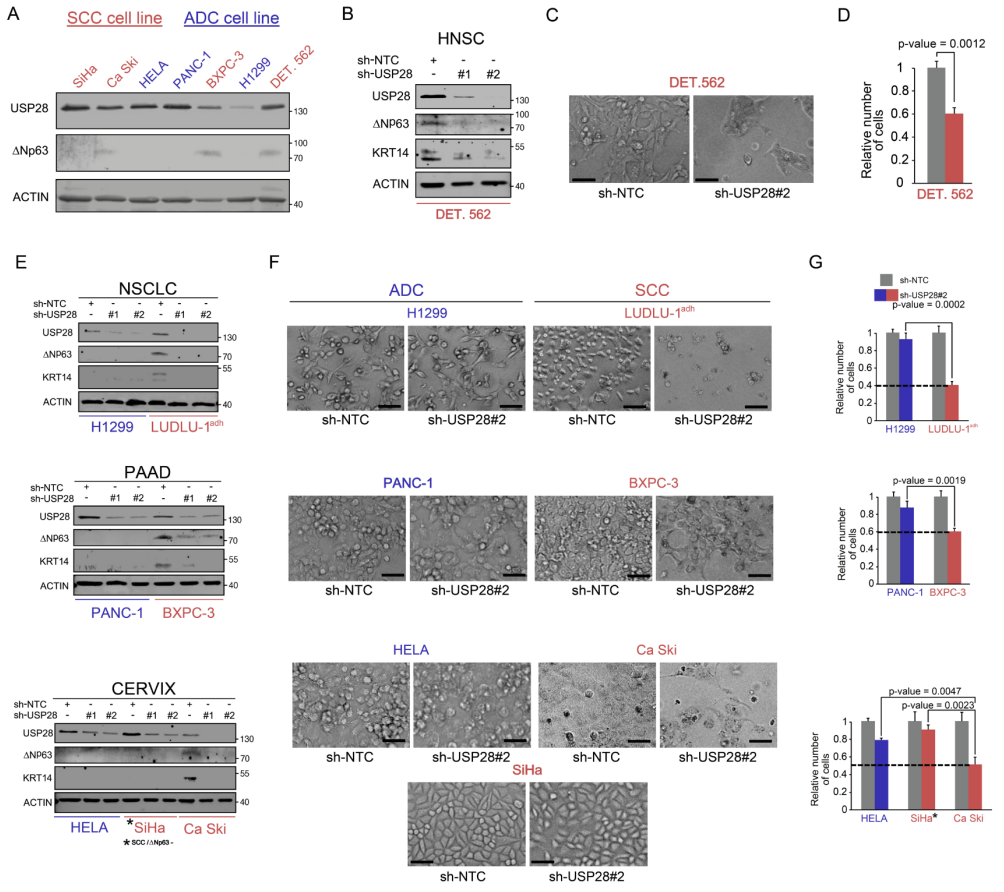

Figure 4.19. ΔNp63-driven SCC cells are vulnerable to USP28 depletion irrespective of 'tissue of origin'. **A)** Western blot against USP28 and ΔNp63 in ADC and SCC cell lines. ACTIN served as loading control. Red=SCC. Blue=ADC. Notably, the SCC cell line SiHa did not express ΔNp63. n=3. **B)** Immunoblot of USP28, ΔNp63 and KRT14 in control, sh-USP28#1 and sh-USP28#2 Detroit 562. ACTIN served as loading control. n=3. sh-NTC= shRNA non-targeting control. **C)** Brigthfield images of control and sh-USP28#2 Detroit 562 cells. Cells were seeded at equal cell density and the images were taken after five days. n=3. sh-NTC= shRNA non-targeting control. **D)** Relative number of USP28 knock down cells compared to sh-NTC Detroit 562 cells. Cells were seeded at equal cell density and the cells were quantified after five days p-values were calculated using two-tailed t-test statistical analysis. n=3. sh-NTC= shRNA non-targeting control. **E)** Immunoblot of USP28, ΔNp63 and KRT14 in control, sh-USP28#1 and sh-USP28#2 H1299, LUDLU-1 $^{adh.}$, HELA, SiHa, Ca Ski, PANC-1 and BXPC-3 cells. ACTIN served as loading control. n=3. sh-NTC= shRNA non-targeting control. * = SiHa does not express ΔNp63. **F)** Brigthfield images of control and sh-USP28#2 H1299, LUDLU-1 $^{adh.}$, HELA, SiHa, Ca Ski, PANC-1 and BXPC-3 cells. Cells were seeded at equal cell density and the images were taken after five days. n=3. sh-NTC= shRNA non-targeting control. * = SiHa does not express ΔNp63. **G)** Relative number of USP28 knock down cells compared to sh-NTC H1299, LUDLU-1 $^{adh.}$, HELA, SiHa, Ca Ski, PANC-1 and BXPC-3 cells. Cells were seeded at equal cell density and the cells were

quantified after five days p-values were calculated using two-tailed t-test statistical analysis. * = SiHa does not express ΔNp63. n=3. sh-NTC= shRNA non-targeting control.

Both USP28 shRNAs induced a significant decrease in the USP28 protein levels for all cell lines (Figure 4.19B and E). Upon depletion of USP28 in the SCC lines expressing detectable ΔNp63 levels, the protein abundances of KRT14 and ΔNp63 were reduced (Figure 4.19B and E). The SiHa and ADC cell lines did not express detectable levels of KRT14 or ΔNp63; consequently, the depletion of USP28 did not affect their protein abundance (Figure 4.19A and E).

SCCs are strongly dependent on ΔNp63 expression to maintain their identity and malignant phenotype (Ramsey et al. 2013; Moses et al. 2019). Assuming that USP28 modulates the ΔNp63 protein stability in SCCs, the influence of USP28 depletion on the proliferation of the SCC cell lines compared to the ADC cells was examined. Cell quantification showed that the proliferation of the ADC cells (HeLa, PANC-1 and H1299) was slightly reduced compared to that observed for the SCC cell lines (Detroit 562, LUDLU-1$^{adh.}$, Ca-Ski, and BXPC3) (Figure 4.9C, D, F and G). SiHa, which does not express endogenous ΔNp63, showed a similar mild reduction in proliferation as observed for the ADC cells (Figure 4.9F and G), demonstrating that USP28 partially regulates SCC proliferation via ΔNp63.

4.1.9 Squamous tumors depend on the USP28-ΔNp63 axis for tumor development *in vivo*

The previous experiments conducted using SCC cells confirmed that the main function of USP28 involved regulating ΔNp63 and SCC identity. Next, state-of-art genetically engineered mouse-lung SCC models were used to identify the role of USP28 in the induction of SCC tumors. The CRISPR/CAS9 system was used to genetically modify murine lung cells in vivo and develop SCC tumors.

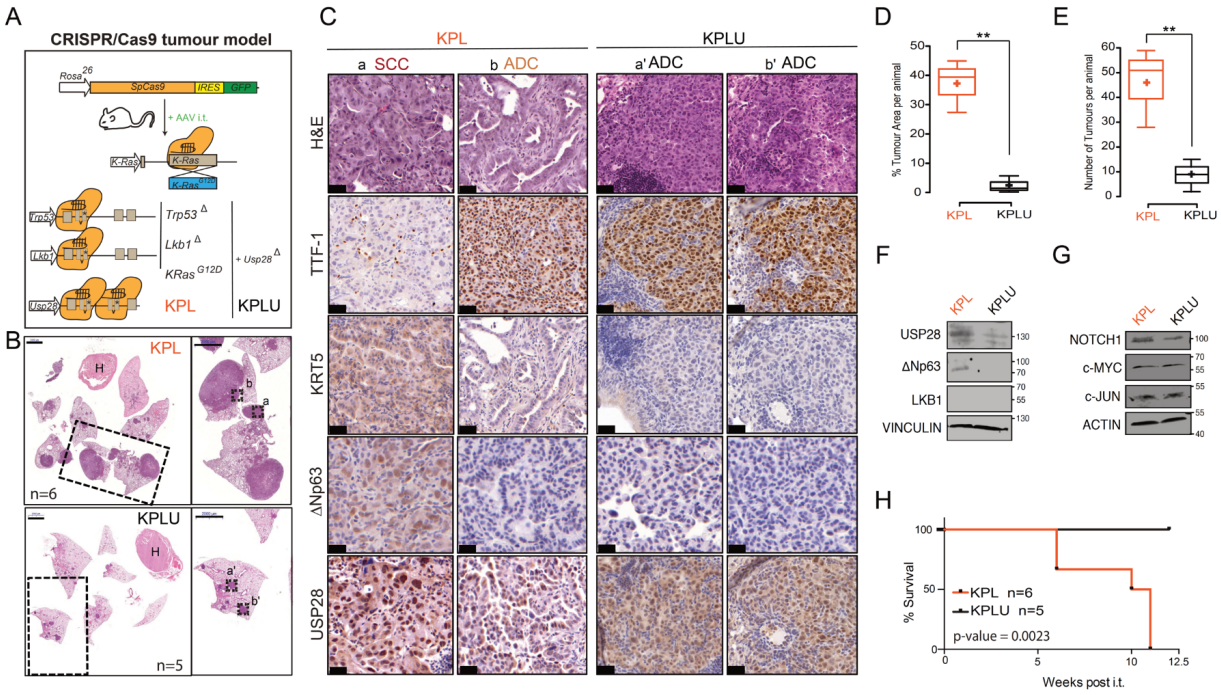

Figure 4.20. The axis USP28-ΔNp63 is required during Squamous tumor development.

A) Schematic diagram of CRISPR/Cas9 mediated tumor formation in Rosa26Sor-CAGG-Cas9-IRES-GFP animals; Lkb1^{Δ}; p53^{Δ}; KRas^{G12D} =KPL. Usp28^{Δ}; p53^{Δ}; Lkb1^{Δ}, KRas^{G12D}=KPLU. **B)** Hematoxylin and eosin (H&E) staining of lung tissue after 12 weeks

post-AAV infection. Boxes indicate highlighted tumor areas. Scale bar = 2000µm; nKPL= 6 and nKPLU = 5. **C)** Immunohistochemistry staining for Ttf1, Krt5, ΔNp63 and USP28 in KPL (n=6) and KPLU (n=5) tumors. H&E as a control. Scale bar: 20µm. **D)** Percentage of tumor area (normalized to total lung) in KPL (n=6) and KPLU (n=5) mice. In box plots, the centre line reflects the median, the cross represents the mean and the upper and lower box limits indicates the first and third quartile. Whiskers extend 1.5x the IQR. p-values using two-tailed t-test. **p-value < 0.01. **E)** Number tumors in KPL (n=6) and KPLU (n=6) animals. In box plots, the centre line reflects the median, the cross represents the mean and the upper and lower box limits indicates the first and third quartile. Whiskers extend 1.5x the IQR. p-values using two-tailed t-test. **p-value < 0.01. **F)** Western blot against Lkb1, Usp28 and ΔNp63 in KPL and KPLU tumors. (VINCULIN as loading control). n=3. **G)** Western blot against c-Myc, C-Jun and Notch1 in KPL and KPLU tumors. (Actin as loading control). n=3. **H)** Survival curves comparing KPL (n=6) and KPLU (n=5) mice after AAV infection. The p-value was calculated using a log-rank test.

To develop lung SCC tumors in *Rosa26^{Sor}-CAGG-Cas9-IRES-GFP* transgenic mice, adeno-associated virus (AAV)–containing sgRNAs were endotracheally instillated to delete p53 (p53$^{\Delta}$), Lkb1 (Lkb1$^{\Delta}$), and USP28 (USP28$^{\Delta}$). Additionally, a Kras G12D repair template and another sgRNA were introduced against the Kras locus to induce mutation of the oncogenic Kras (Figure 4.20A). The expression of the oncogenic Kras G12D together with the deletion of Lkb1 and p53 in murine lung cells resulted in the development of ADC (TTF1+ / ΔNp63- / KRT5-) and SCC (TTF1- / ΔNp63+ / KRT5+) tumors (Figure 4.20B and C). To analyze the role of USP28 during tumor initiation, KPL (Kras^{G12D}; P53$^{\Delta}$; Lkb1$^{\Delta}$) and KPLU (Kras^{G12D}; P53$^{\Delta}$; Lkb1$^{\Delta}$; USP28$^{\Delta}$) lung tumors were generated in mice (Figure 4.20B). First, it was confirmed that KPLU tumors express reduced levels of USP28 compared to KPL tumors (Figure 4.20C). However, there was no complete deletion, and detectable basal levels of USP28 expression were found in KPLU tumors, suggesting that the formation of these tumors requires the expression of USP28 (Figure 4.20C). According to the previous results obtained using SCC cells, a significant reduction in the tumor area and number of tumors occurred upon targeting USP28 (Figure 4.20D and E).

Importantly, KPLU mice developed only ADC (Ttf1+ / ΔNp63- / Krt5-) tumors, whereas KPL mice could develop ADC (Ttf1+ / ΔNp63- / Krt5-) and SCC (Ttf1- / ΔNp63+ / Krt5+) tumors (Figure 4.20C), indicating that high levels of USP28 are required to induce the development of SCC tumors. Immunohistochemistry and immunoblotting analyses of tumor samples showed reduced levels of ΔNp63 in KPLU tumors compared to those in KPL tumors (Figure 4.20C and F). Additionally, reduced protein abundance was observed for Notch1 in KPLU tumors compared to KPL tumors, but similar levels of c-Myc and c-Jun were observed in both the tumors (Figure 4.20G). Considering that c-Myc and c-Jun are bona fide USP28 substrates, it can be assumed that KPLU tumors required high levels of both oncogenes to be fully developed, and they found a mechanism to compensate the loss of USP28. Finally, it was observed that KPLU mice survived for a significantly longer time than KPL mice following AAV infection and lung tumor formation (Figure 4.20H). These data confirm that the USP28-ΔNp63 axis occurs in vivo, and high levels of USP28 expression are fully required to develop SCC tumors.

4.1.10 USP28 is essential for engraftment of squamous tumors in vivo

After confirming that USP28 is required for the formation of SCC tumors, the potential role of USP28 in tumor engraftment was investigated. The Cre-conditional p53 (*p53$^{flox/flox}$*) Kras G12D mouse model (LSL-Kras

G12D) (Figure 4.21A) was used. Upon Cre exposure, the animal lost p53 and expressed Kras G12D, allowing the development of lung tumors. AAV viruses encoding the Cre recombinase were intratracheally instillated. The viruses were previously generated using capsid 2/8, and notably, capsid 2/8 exhibits a tropism toward alveolar and tracheal lung cells (Winters et al. 2017). Twelve weeks after AAV administration, the mice developed ADC (Ttf1+ / ΔNp63- /Krt5-) and SCC (Ttf1- / ΔNp63+ /Krt5+) lung tumors (Figure 4.21B and C)

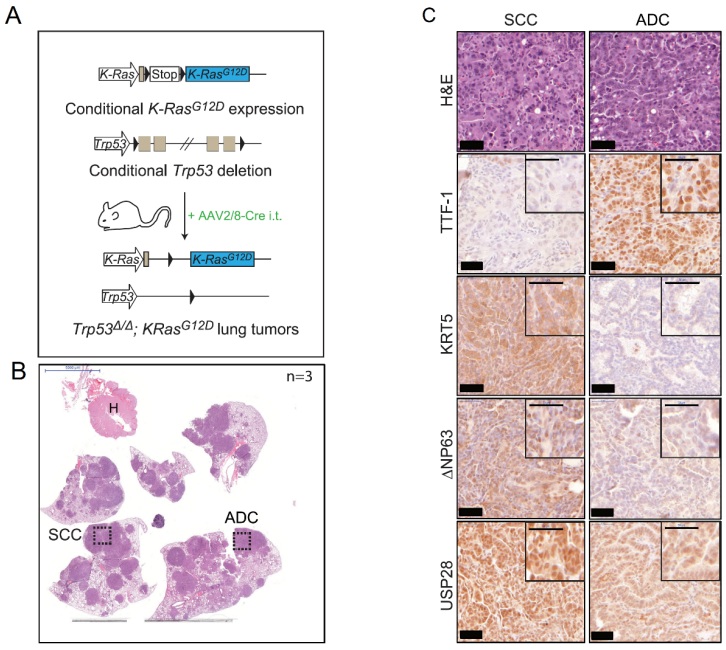

Figure 4.21. The Cre-conditional KP (p53$^{flox/flox}$; LSL - Kras G12D) mouse model.

A) Schematic diagram of the KP conditional mouse model. **B)** Hematoxylin and eosin (H&E) staining of lung tissue after 12 weeks post-AAV infection. Scale bar = 5000µm; n=3. **C)** Immunohistochemistry staining for Ttf1, Krt5, ΔNp63 and Usp28 in KPL (n=3) and KPLU (n=3) tumors. H&E as a control. Scale bar: 50µm.

Next, stable cell lines were generated using tumors from the mice (Figure 4.22A). By qPCR, the mRNA levels of the SCC markers, Sox2 and Krt5, and the ADC marker, Sftpc, were quantified to determine if the cells proceeded from the ADC or SCC tumor regions (Figure 4.22B). In one of the generated murine SCC cell lines, USP28 was depleted, and the efficiency of the shRNAs was assessed by immunoblotting (Figure 4.22C).

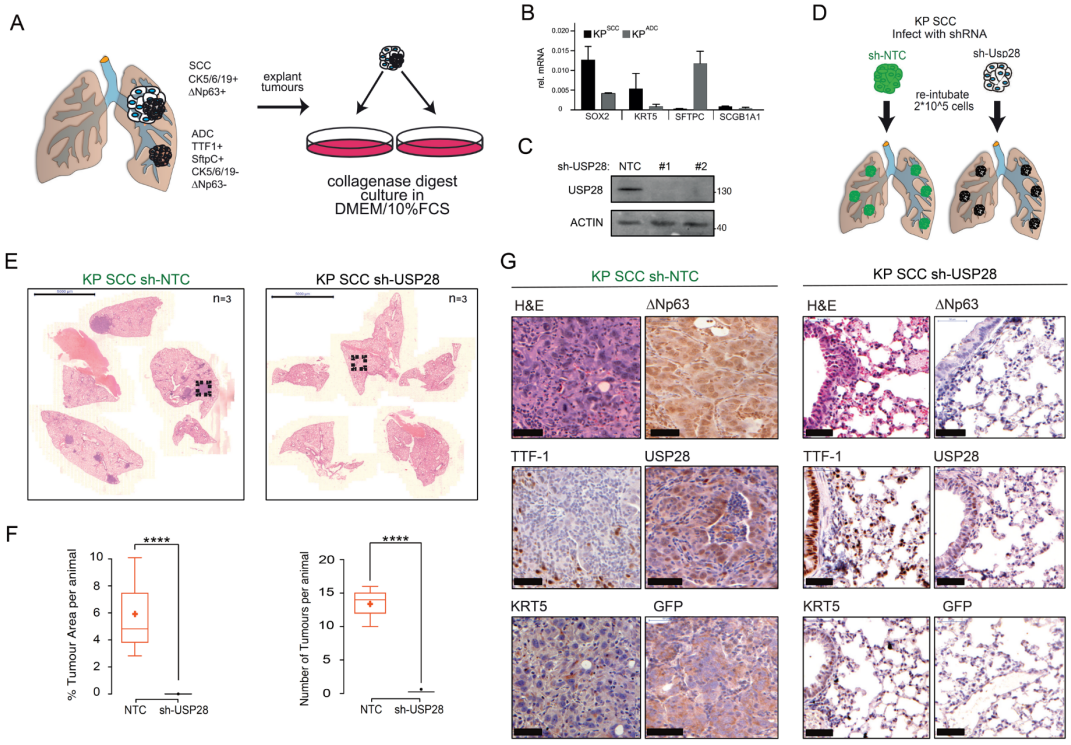

Figure 4.22. USP28 is essential for engraftment of Squamous tumors.

A) Establishment of murine cell lines. Schematic diagram. **B)** qPCR of SCC and ADC markers of two independent KP lung tumor clones, resulting in KP ADC and KP SCC; (Actin as control to calculate relative

mRNA). n=3. **C)** Western blot against Usp28 in control, sh-Usp28#1 and sh-Usp28#2, KP SCC cells. Actin served as loading control. n=3. **D)** Orthotopic re-transplantation of 200000 cells KP SCC cell lines into the lung of C57BL/6J mice. Schematic diagram. **E)** H&E staining of lung tissue after 8 weeks post-AAV infection. Scale bar = 5000µm; n= 3. **F)** Percentage of tumor area (normalized to total lung) in control (n=6) and sh-USP28#1 (n=6) SCC tumors. In box plots, the centre line reflects the median, the cross represents the mean and the upper and lower box limits indicates the first and third quartile. Whiskers extend 1.5x the IQR. p-values using two-tailed t-test. ****p-value < 0.0001. **G)** Immunohistochemistry staining for Ttf1, Krt5, ΔNp63 and Usp28 in KP SCC(n=3) and KP SCC sh-Usp28#1 (n=3) tumors. H&E as a control. Scale bar: 50µm.

Control and sh-Usp28 SCC cells were orthotopically transplanted into the lungs of WT mice by endotracheal intubation (Figure 4.22D). After eight weeks, the mice were sacrificed, and the lungs were histologically analyzed. The mice transplanted with the control cells formed SCC (Ttf1- / ΔNp63+ /Krt5+) tumors, whereas the mice transplanted with sh-Usp28 cells presented healthy lungs without malignant tissue (Figure 4.22E, F and G). These findings demonstrate that USP28 is essential for lung engraftment of SCC cells.

4.2 Pharmacological inhibition of USP28 as a therapy for squamous tumors

Considering that a specific inhibitor of USP28 has been developed (Gavory et al. 2017), regulation of the ΔNp63 protein abundance in vitro and in vivo was examined by pharmacological inhibition of USP28. Here, the efficacy and specificity of the USP28 inhibitor, AZ1, were studied in SCC cell lines and GEMMs. The obtained data strongly support the inhibition of USP28 as a strategy to regulate the ΔNp63 protein stability in vivo. The use of USP28 inhibitors is a promising alternative to treat SCC patients.

4.2.1 Inhibition of USP28 regulates ΔNp63 stability via deubiquitination in squamous cancer cells

First, the specificificity of the USP28 inhibitor was tested using ubiquitin suicide probes. The A-431 cells exposed to the AZ1 inhibitor showed decreased USP28 activity compared to that in the cells exposed to DMSO (Figure 4.23A). Next, the A-431 cells were exposed to different concentrations of AZ1 to observe if the inhibition of the DUB reduces the ΔNp63 protein abundance. Exposure to 10 µM AZ1 induced a strong reduction in the ΔNp63 protein abundance, as well as the abundance of USP28 and KRT14, the ΔNp63 transcriptional target (Figure 4.23B). The decreased USP28 protein abundance upon its inhibition is in line with previous reports stating that the catalytic activity of a DUB is required to regulate its own protein stability (De Bie & Ciechanover 2011; Wang et al. 2017). The USP28 protein abundance was reduced after treatment with AZ1 (Figure 4.23B).

Next, to confirm if AZ1 inhibits the enzymatic activity of USP28 when decreasing the ΔNp63 protein abundance, the ubiquitination levels of ΔNp63 after USP28 inhibition were analyzed. In the A-431 cells, exposure to AZ1 increased the ΔNp63 ubiquitination in a concentration-dependent manner (Figure 4.23C). During an MG132 assay on the A-431 cells, treating USP28 with the inhibitor reduced the ΔNp63 protein abundance, but coexposure to AZ1 and MG132 restored ΔNp63 protein levels confirming that the inhibition of USP28 regulates ΔNp63 via proteasome degradation (Figure 4.23D). Finally, it was observed that exposure

to the AZ1 inhibitor reduced cell growth in the A-431 cells (Figure 4.23E) owing to the genetic depletion of ΔNp63 or USP28 (Figure 4.17). Therefore, AZ1 effectively inhibits USP28, inducing the degradation of ΔNp63 in the A-431 cells.

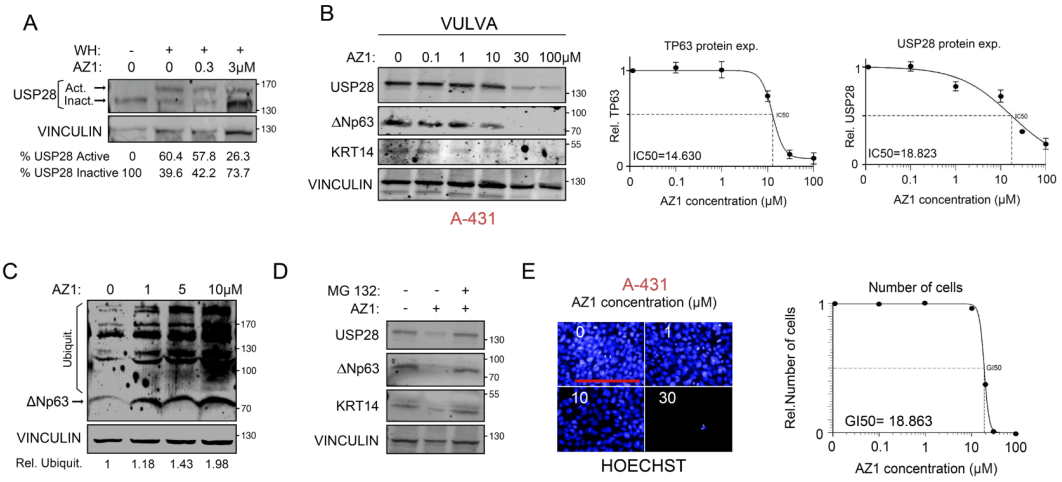

Figure 4.23. Inhibition of USP28 regulates ΔNp63 stability via deubiquitination in A-431 cells. **A)** USP28 Immunoblot upon treatment with warhead ubiquitin suicide probes (WH) and AZ1 at indicated concentrations for 24 hours in A-431 cells. USP28 Upper band → Active USP28; USP28 lower band →Inactive USP28. VINCULIN as loading control. n=3. **B)** Immunoblot of USP28, ΔNp63 and KRT14 in A-431 cells treated with indicated concentrations of AZ1 for 24 hours. VINCULIN served as loading control. ΔNp63 and USP28 half maximal inhibitory protein abundance (IC50) was calculated. n=3. **C)** ΔNp63 Immunoblot upon treatment with Tube ubiquitin pull down and AZ1 at indicated concentrations for 24 hours. VINCULIN served as loading control for calculation of relative Ubiquitination. n=3 **D)** Immunoblot of USP28, ΔNp63 and KRT14 in A-431 cells treated for 18 hours with 15μM AZ1 followed by 6 hours of exposure to the proteasome inhibitor MG-132 (20μM). VINCULIN served as loading control. n=3. **E)** A-431 cells were seeded at equal cell density and treated with DMSO or different concentrations of AZ1 (1μM, 10μM or 30μM) for 48h. Cells were quantified using Hoechst staining in Operetta imaging system. 50% growth inhibition (GI50) was calculated. Scale bar = 250μm. n= 30 fields.

4.2.2 USP28 inhibition shows a selective antiproliferative effect on ΔNp63-driven squamous cells irrespective of the "tissue of origin"

As previously indicated, USP28 stabilizes several oncogenes involved in cancer proliferation, such as c-MYC, NOTCH1, and CCNE. However, ΔNp63-driven SCC cells are strongly dependent on the USP28-ΔNp63 axis, irrespective of the other oncogenes stabilized by USP28 (Figure 4.8). Thus, to analyze if USP28 inhibition can mimic the phenotype previously observed upon the genetic depletion of USP28 (Figure 4.19), ADC, ΔNp63-driven SCC, and Si Ha (SCC cell line without detectable levels of ΔNp63 expression) cells were exposed to the AZ1 inhibitor. First, two independent SCC cell lines were exposed to AZ1, and it was observed that Detroit 562 (HNSC cells) and BXPC3 (Pancreatic SCC) decreased the USP28, KRT14, and ΔNp63 protein abundances depending on the concentration of AZ1 (Figure 4.24A). As expected, proliferation was strongly reduced in both the cell lines upon exposure to AZ1 (Figure 4.24B and C).

Next, the SCC and ADC cells were exposed to AZ1 to determine if the ΔNp63-driven SCC cells were more sensitive to the pharmacological inhibition of USP28. The ΔNp63-driven SCC cells LUDLU-1$^{adh.}$ (lung SCC), and Ca-Ski (Cervix SCC) reduced the ΔNp63 and KRT14 protein abundances upon AZ1 treatment (Figure 4.24D). Furthermore, LUDLU-1$^{adh.}$ and Ca-Ski strongly decreased the number of cells compared to the SiHa (cervical SCC but negative for ΔNp63 expression), ADC cell lines (H1299, LUAD), and Hela (cervical ADC)

upon AZ1 exposure (Figure 4.24E and F). These data demonstrate that the inhibition of USP28 by AZ1 particularly sensitizes ΔNp63-driven SCC cells irrespective of their "tissue of origin.".

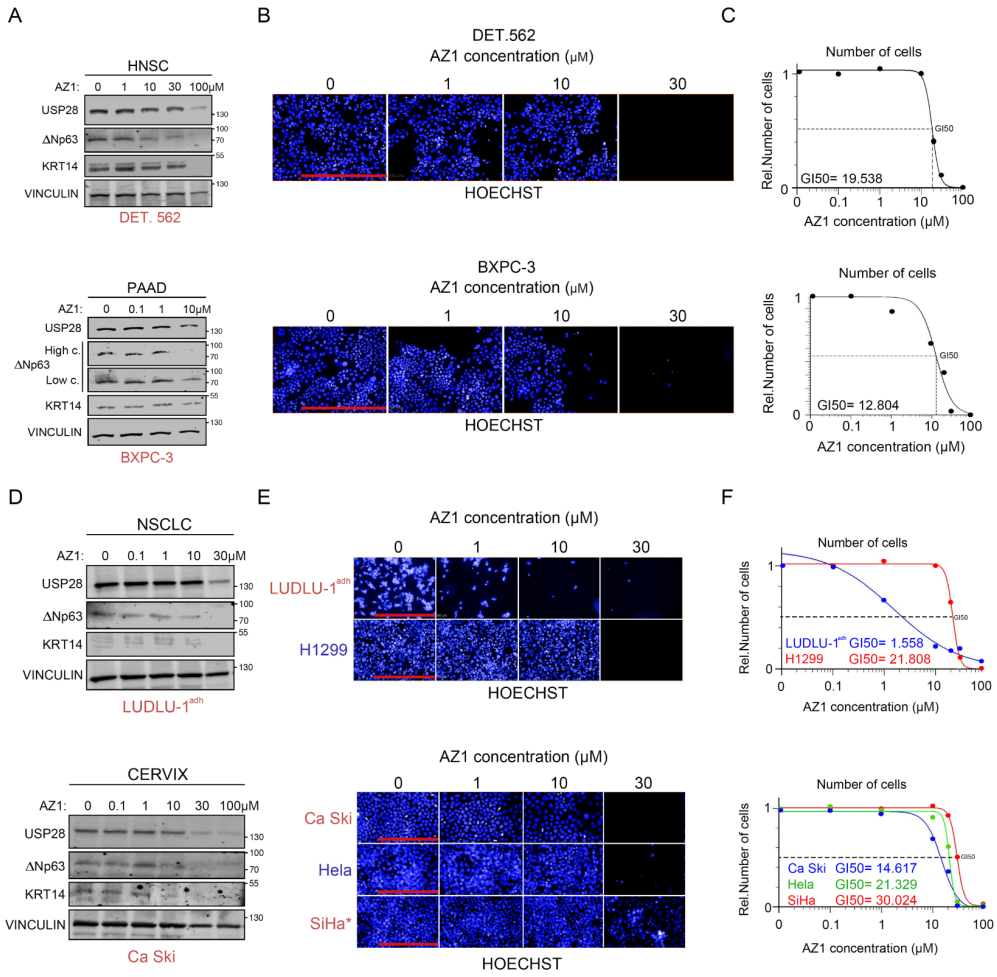

Figure 4.24. Inhibition of USP28 shows a stronger selective anti-proliferative effect in ΔNp63-driven SCC compared to ADC cells. **A)** Immunoblot of USP28, ΔNp63 and KRT14 in DETROIT 562 and BXPC3 SCC cells treated with indicated concentrations of AZ1 for 24 hours. VINCULIN served as loading control. n=3. **B)** DETROIT 562 and BXPC3 SCC cells were seeded at equal cell density and treated with DMSO or different concentrations of AZ1 (1μM, 10μM or 30μM) for 48h. Scale bar = 250μm. n= 30 fields. **C)** DETROIT 562 and BXPC3 SCC cells from B) were quantified using Hoechst staining in Operetta imaging system. 50% growth inhibition (GI50) was calculated. n= 30 fields. **D)** Immunoblot of USP28, ΔNp63 and KRT14 in LUDLU-1 $^{Adh.}$ and Ca Ski SCC cells treated with indicated concentrations of AZ1 for 24 hours. VINCULIN served as loading control. n=3. **E)** LUDLU-1 $^{Adh.}$, H1299, Ca Ski, SiHa and Hela cells were seeded at equal cell density and treated with DMSO or different concentrations of AZ1 (1μM, 10μM or 30μM) for 48h. . Scale bar for LUDLU-1 $^{Adh.}$ and H1299 = 500μm. Scale bar for Ca Ski, Hela and SiHa = 250μm n= 30 fields. **F)** Cells from E) were quantified using Hoechst staining in Operetta imaging system. 50% growth inhibition (GI50) was calculated. n= 30 fields.

4.2.3 Pharmacologic inhibition of USP28 reduces growth of lung squamous tumors in vivo

For determining whether the inhibition of USP28 is a suitable and safe therapeutical option to treat SCC tumors, lung orthotopic SCC tumors were generated by endotracheal retransplantation of KPL (Kras G12D; $p53^{\Delta}$; $LKB1^{\Delta}$) cells into WT mice. In contrast to the murine ADC (KP: Kras G12D; $p53^{\Delta}$) cells, the SCC cells expressed detectable levels of ΔNp63 (Figure 4.25A). To determine the importance of USP28 in maintaining SCC tumors in vivo, the animals were intraperitoneally treated with 6 doses of PBS/DMSO/Tween80 (as control), and 125 mg/kg or 375 mg/kg AZ1. The six doses were administrated every three days starting on day 28 following the retransplantation of the KPL cells (Figure 4.25B).

Importantly, the mice treated with AZ1 showed reduced SCC tumor areas compared to the control mice (Figure 4.26A and B). In particular, the tumor areas drastically decreased in the animals treated with 375 mg/kg AZI

compared to the tumor areas in the control mice or those treated with 125 mg/kg AZI. As observed in the previous results, the mice treated with the USP28 inhibitor expressed less ΔNp63 and USP28 than the control mice (Figure 4.26C and D). This result demonstrates that the inhibition of USP28 decreases the ΔNp63 protein abundance, thus reducing the SCC tumor burden in vivo.

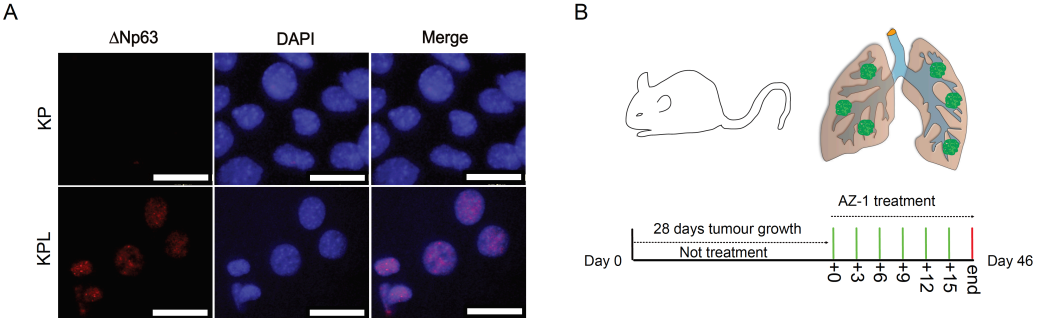

Figure 4.25. Generation of lung orthotopic SCC tumors.

A) Immunofluorescence staining against ΔNp63 in KP (Kras G12D; $p53^{\Delta}$) and KPL (Kras G12D; $p53^{\Delta}$; $LKB1^{\Delta}$) cells; Scale bar = 5µm; n=3. DAPI staining indicates nuclear localization. **B)** Model representing the administration regimen of AZ1 in mice. Animals were intraperitoneally treated with 6 doses of PBS/ DMSO/ Tween80 (as control), 125mg / kg or 375mg / kg AZ1

As it is a potential drug to treat cancer patients, the safety of AZ1 was tested in vivo. A histological analysis was performed on the mice after intraperitoneal administration of 125 mg/kg and or 375 mg/kg AZ1 (Figure 4.27A). Remarkably, the treated mice did not show any obvious toxic side effects or abnormalities in their tissue architecture (Figure 4.27A). Finally, the efficiency of AZ1 in vivo was confirmed by performing a warhead ubiquitin suicide probe assay of excised tissue (Figure 4.27B and 4.27C). The previous results suggest that inhibition of USP28 is a safe alternative to treat SCC tumors in vivo.

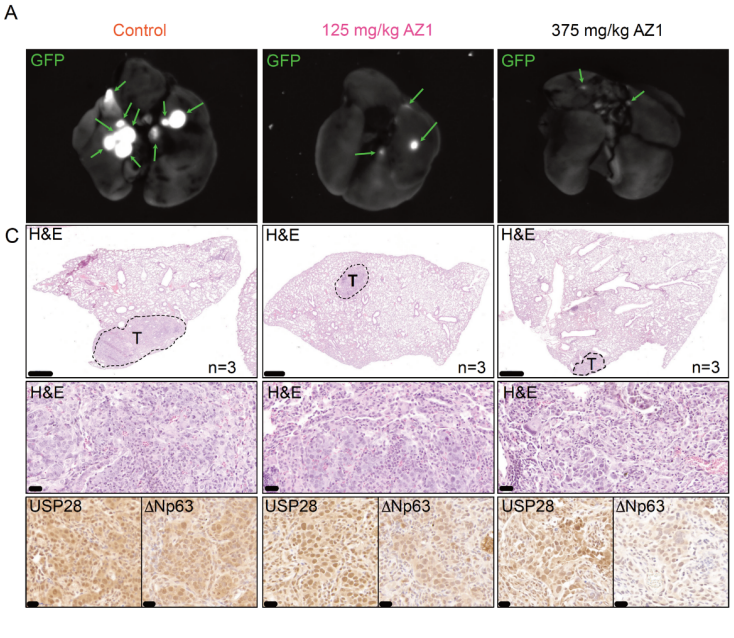

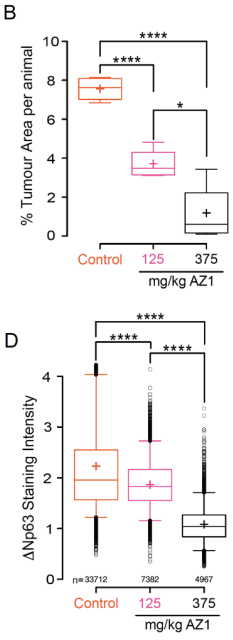

Figure 4.26. Pharmacologic inhibition of USP28 reduces tumor area of lung SCC tumors.

A) GFP images of animlas treated with AZ1. Tumor are GFP positive (green arrows). n=3. **B)** Tumor area in control and AZ1 treated mice (n=3). p-values calculated via two-tailed t-test. *p-value < 0.05; ****p-value < 0.0001. In box plots, the centre line reflects the median, the cross represents the mean and the upper and lower box limits indicates the first and third quartile. Whiskers extend 1.5x the IQR. **C)** SCC tumors H&E and IHC staining for Usp28 and ΔNp63 in control and AZ1 treated animals (n=3). Boxes indicated highlighted areas. First line Scale bars = 500µm; Lower scale bars = 20µm. **D)** ΔNp63 staining intensity of SCC tumors exposed to control or AZ1. (n=3). p-values calculated via two-tailed t-test. ****p-value <

0.0001. In box plots, the centre line reflects the median, the cross represents the mean and the upper and lower box limits indicates the first and third quartile. Whiskers extend 1.5x the IQR.

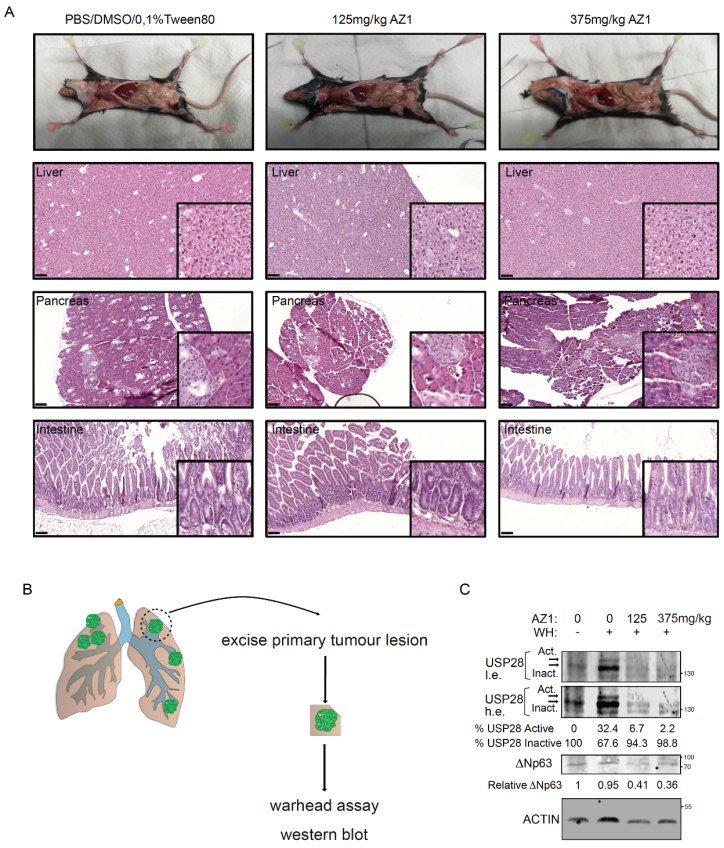

Figure 4.27. AZ1 inhibit USP28 in vivo without obvious toxicicity.

A) Macroscopic and histologic (H&E) analysis of liver, pancreas and intestine from mice treated with AZ1; (scale bars= 100µm). **B)** Schematic model for protein extraction from SCC tumors. **C)** Ubiquitin suicide probe (Warhead=WH) of endogenous USP28 in SCC tumors. Low exposure (l.e.); High exposure (h.e.). Representative immunoblot of endogenous USP28 and ΔNp63 from control or AZ1 treated mice. ACTIN served as loading control for quantification of active/inactive USP28 and relative protein abundance of ΔNp63 in SCC tumors in vivo.

4.3 The USP28-ΔNp63 axis regulates Fanconi anemia pathway and DNA repair in squamous tumors

Currently, SCC patients are treated with the same conventional Cisplatin therapy as they would have been treated 30 years ago (Pendleton & Grandis 2013; Gandara et al. 2015; Fennell et al. 2016; Isaka et al. 2017). Accordingly, the survival of SCC patients is limited and the efficacy of the current therapies is rather low. Owing to the rising incidences of SCC tumors, novel therapeutic strategies to treat SCC patients must be developed urgently. Here, the combination of Cisplatin and USP28 inhibition is proposed as a new alternative therapy to treat SCC patients. The data presented in this thesis demonstrate that the reduction of the ΔNp63 protein abundance, induced by USP28 inhibition, strongly downregulates DDR, by blocking the FA pathway and RR. Consequently, the inhibition of USP28 reduces DNA repair, thus sensitizing SCC cells to DNA damage therapies such as Cisplatin therapy.

4.3.1 USP28 is recruited to DNA repair complexes upon DNA damage induced by Cisplatin

Previous studies have demonstrated that USP28 takes part of the DNA repair complex upon DNA damage induced by IR (Knobel et al. 2014; N. Popov, Herold et al. 2007; Zhang et al. 2006). As Cisplatin (CPPD) is the most common therapy used in the treatment of SCC patients, it was examined if USP28 is recruited to

DNA repair complexes upon exposure to the DNA crosslinking agent. Following CPPD treatment of the A-431 SCC cells, USP28 formed damaged DNA nuclear foci comprising the following DNA damage markers: 53BP1, γ-H2AX, p-ATR, and p-ATM (Figure 4.28A). Furthermore, the quantity of USP28 bound to the chromatin at different time points during CPPD exposure was experimentally determined. After 3 hours of CPPD exposure, the USP28 protein abundance recruited to the chromatin was significantly higher compared to the untreated A-431 cells (Figure 4.28B). Accordingly, it is possible to conclude that USP28 is recruited to repair DNA complexes located on the chromatin upon DNA damage caused by CPPD exposure.

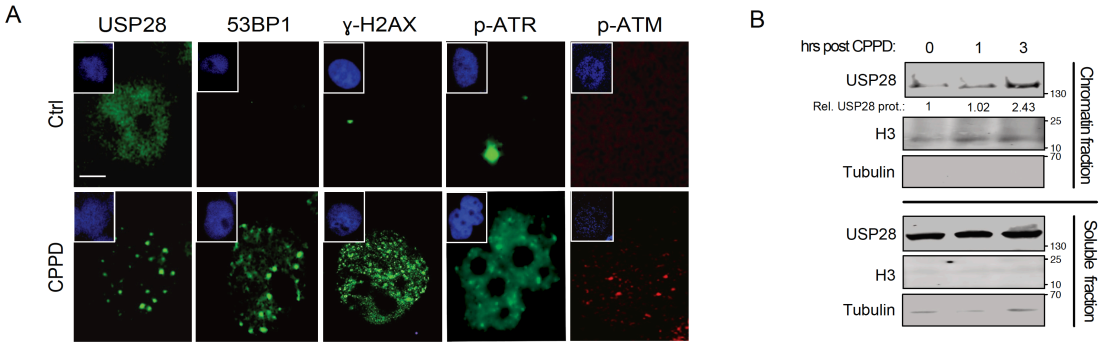

Figure 4.28. USP28 is recruited to DNA repair complexes upon DNA damage induced by Cisplatin.
A) Immunofluorescence staining against USP28, 53BP1, γ-H2AX, p-ATR and p-ATM in A-431 cells upon treatment with DMF or 5μM Cisplatin (CPPD) for 6 hours. Scale bar = 10μm. DAPI staining indicating nuclear localization. n=3**. B)** Chromatin and soluble fractionation, followed by western blot of endogenous USP28 in A-431 cells exposed to 5μM Cisplatin (CPPD) at indicated time points. Histone H3 and Tubulin serve as control. n=3

4.3.2 ATR regulates USP28 activity upon Cisplatin exposure in squamous cancer cells

The posttranslational modifications of proteins are important regulatory mechanisms of DNA repair signaling pathways. Generally, the phosphorylation of DNA repair factors was typically associated with a change in activity. (Summers et al. 2011). In response to DNA damage or replication stress, ATM and ATR phosphorylates hundreds of proteins orchestrating DNA repair pathways (Maréchal & Zou 2013). USP28 has previously been defined as an ATM substrate following IR (Zhang et al. 2006).

Analysis of the USP28 sequence revealed two consensus ATM/ATR S/TQ phosphorylation motifs (Figure 4.29A). Using specific phospho-USP28 antibodies showed that USP28 is phosphorylated in a dose-dependent manner upon CPPD exposure (Figure 4.29B). A warhead ubiquitin suicide probe assay demonstrated that the USP28 enzymatic activity increased after DNA damage caused by CPPD (Figure 4.29C). Consistent with previous experiments, CPPD exposure decreased protein ubiquitination levels of the USP28 substrates, c-MYC, and ΔNp63 (Figure 4.29D), suggesting that USP28 regulates the protein stability of c-MYC and ΔNp63 upon DNA damage induced by crosslinking agents.

To elucidate if USP28 is phosphorylated by ATM or ATR upon CPPD exposure, publicly available datasets were analyzed. It was found that ATR is more often amplified than ATM in lung SCC tumors (Figure 4.29E). Coimmunoprecipitation was performed after immunoprecipitation of p-ATM, p-ATR, and USP28, indicating that USP28 can interact with the phosphorylated forms of ATM and ATR upon CPPD exposure (Figure 4.29F). The binding was particularly strong with the activated form of ATR; almost all the completely

immunoprecipitated p-ATR could interact with USP28 upon CPPD treatment (Figure 4.29F). To determine if the phosphorylation of USP28 was induced by ATR or ATM, A-431 cells were cotreated with CPPD and DMSO, ATM or ATR inhibitors (Figure 4.29G). Immunoblotting using specific p-USP28 serine 67 and serine 714 antibodies showed that the phosphorylation of USP28 on serines 67 and 714 depends on ATR upon DNA damage caused by CPPD (Figure 4.29G).

As mentioned earlier, USP28 increases its enzymatic activity upon DNA damage. To observe if ATR regulates USP28 activity upon CPPD exposure, a USP28 warhead ubiquitin suicide probe assay was performed in SCC cells upon coexposure to CPPD and DMSO, and ATM or ATR inhibitors (Figure 4.29H). Exposure to the ATR inhibitor blocked the activity of USP28 in cells exposed to CPPD (Figure 4.29H). Notably, ATM inhibition did not affect USP28 activity upon CPPD exposure (Figure 4.29H). To demonstrate if USP28 increases the stability of its substrates in an ATR-dependent manner upon CPPD exposure, the protein abundances of c-MYC and ΔNp63 proteins were analyzed in the cells treated with CPPD and DMSO, and ATR or ATR inhibitors (Figure 4.29I). c-MYC and ΔNp63 were stabilized upon CPPD exposure in the control and ATM-inhibitor-treated cells, but not in the cells exposed to the ATR inhibitor (Figure 4.29I). These results demonstrate that ATR induces the phosphorylation of USP28, thus regulating its enzymatic activity upon CPPD exposure.

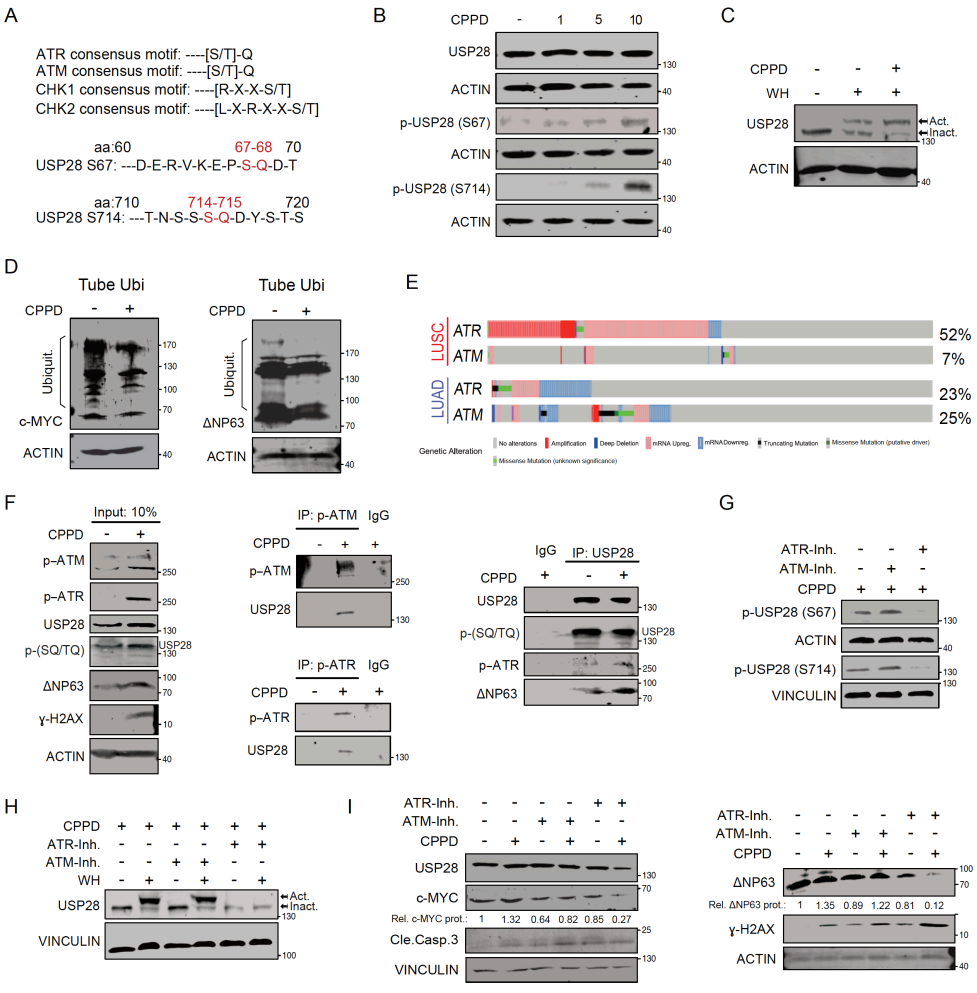

Figure 4.29. ATR regulates USP28 activity upon Cisplatin exposure.

A) USP28 consensus ATM/ATR S/TQ phosphorylation motif on serine 67 and 714. Scheme indicate ATM, ATR, CHK1 and CHK2 consensus motif. **B)** Western blot of total and phosphorylated USP28 on serine 67 and 714 in A-431 cells exposed to indicated concentrations of Cisplatin (CPPD) for 6 hours. n=3. ACTIN as control. n=3**. C)** Ubiquitin suicide probe (warhead) assay, followed by USP28 western blot in A-431 cells exposed to 5 μM CPPD for 6 hours. "Act." arrow indicates active USP28.' Inact.' arrow indicates inactive USP28. ACTIN serves as loading control. n=3. **D)** Tandem-ubiquitin binding entity (TUBE) pulldown of endogenous ubiquitin, followed by western blot for c-MYC and ΔNp63 in DMF or 5μM CPPD treated A-431 cells for 6 hours. ACTIN serves as loading control. n=3. **E)** Genetic alteration of ATR and ATM

in lung squamous (LUSC) and lung adenocarcinoma (LUAD) human tumors. Publicly available patient data obtained from CBIOPORTAL**. F)** Immunoprecipitation of rabbit IgG, endogenous phospho-ATM, phospho-ATR or USP28 of either control or 5µM CDD treated A-431 cells for 6hours, followed by western blot against ATM, ATR, USP28, ɣ-H2AX, ΔNp63 or ATM/ ATR SQ/TQ specific antibodies. ACTIN serves as loading control. n=3. **G)** Western blot of phosphorylated USP28 on serine 67 and 714 in A-431 cells treated with DMF or 5µM CPPD for 6 hours and co-treatment with either DMSO, 15µM ATM kinase inhibitor (KU55933) or 2.5 µM ATR kinase inhibitor (VE 821). VINCULIN as a loading control. n=3. **H)** Ubiquitin suicide probe (warhead) assay, followed by USP28 western blot in A-431 cells treated with DMF or 5µM CPPD for 6 hours and co-treatment with either DMSO, 15µM ATM kinase inhibitor (KU55933) or 2.5 µM ATR kinase inhibitor (VE 821). VINCULIN as a loading control. "Act." arrow indicates active USP28. "Inact." arrow indicates inactive USP28. n=3. **I)** Western blot of USP28, c-MYC, Cleaved Caspase 3, ΔNp63 and ɣ-H2AX in A-431 cells exposed to DMF or 5µM CPPD for 6 hours and co-treatment with either DMSO, 15µM ATM kinase inhibitor (KU55933) or 2.5 µM ATR kinase inhibitor (VE 821). VINCULIN and ACTIN as a loading control. n=3.

4.3.3 Phosphorylation of USP28 is required to repair DNA damage in squamous cancer cells

To examine the role of phosphorylated USP28 in DNA repair, A-431 phospho-mutant cell lines were generated by substituting serine 67, serine 714, or both (serine 67 and serine 714) for alanines (Figure 4.30A). First, basal levels of USP28 were tested in the mutant cell lines previously generated, and it was observed that USP28 was expressed at levels similar to those in the control cells (Figure 4.30B). Next, it was demonstrated that USP28 could not be phosphorylated upon CPPD exposure on the mutated residues of the CRISPR-mutant cell lines (Figure 4.30C). Notably, the mutation of one phospho-site, either serine 67 or serine 714, reduces the phosphorylation of the second phospho-site suggesting that the phosphorylation of one site facilitates the posttranslational modification at the second site (Figure 4.30C). Using warhead ubiquitin suicide probes, the USP28 activity was tested upon CPPD exposure. It was observed that the mutant cell lines, particularly the double mutant S67A/S714A, had reduced levels of USP28 enzymatic activity compared to the control cells (Figure 4.30D). Remarkably, the mutation of the phospho-site located on S714 seems to decrease the USP28 activity more than the mutation of the phospho-site located on S67 (Figure 4.30D).

Next, the protein abundances of USP28 substrates, such as c-MYC and ΔNp63, were analyzed in the control and CPPD-treated cells. It was noticed that the mutant cell lines expressed low levels of c-MYC and ΔNp63 compared to the control cells, even without CPPD exposure (Figure 4.30E left panel). During uncontrolled proliferation, oncogenic cells present certain levels of DNA damage and replication stress that require the activation of the ATR-USP28 axis, thereby explaining the reduced levels of c-MYC and ΔNp63 even without any DNA damage stress. Accordingly, increased protein abundance of the DNA damage marker ɣ-H2AX was found in the mutant cell lines compared to that in the control cells (Figure 4.30E left panel). It seems that mutant cell lines encounter problems in solving DNA repair conflicts even without exposure to CPPD or any other DNA damage agents.

Upon CPPD exposure, low levels of c-MYC and ΔNp63 were found in the mutant cell lines compared to the control cells (Figure 4.30E right panel). Notably, the protein reduction was particularly strong in cells with both serines mutated (S67A /S714A) (Figure 4.30E right panel). The cell line with the phospho-site on mutated S714 (S714A) also showed low abundance of c-MYC and ΔNp63 proteins than the cells with the phospho-site on mutated S67 (S67A) (Figure 4.30E right panel). In agreement with the results of the warhead ubiquitin suicide probe assay (Figure 4.30D), the above result suggests that the phospho-site located on S714 is more

relevant in regulating USP28 activity than the first phospho-site located on S67. Additionally, the mutant cell lines expressed more ɣ-H2AX than the control cells upon CPPD exposure (Figure 4.30E right panel).

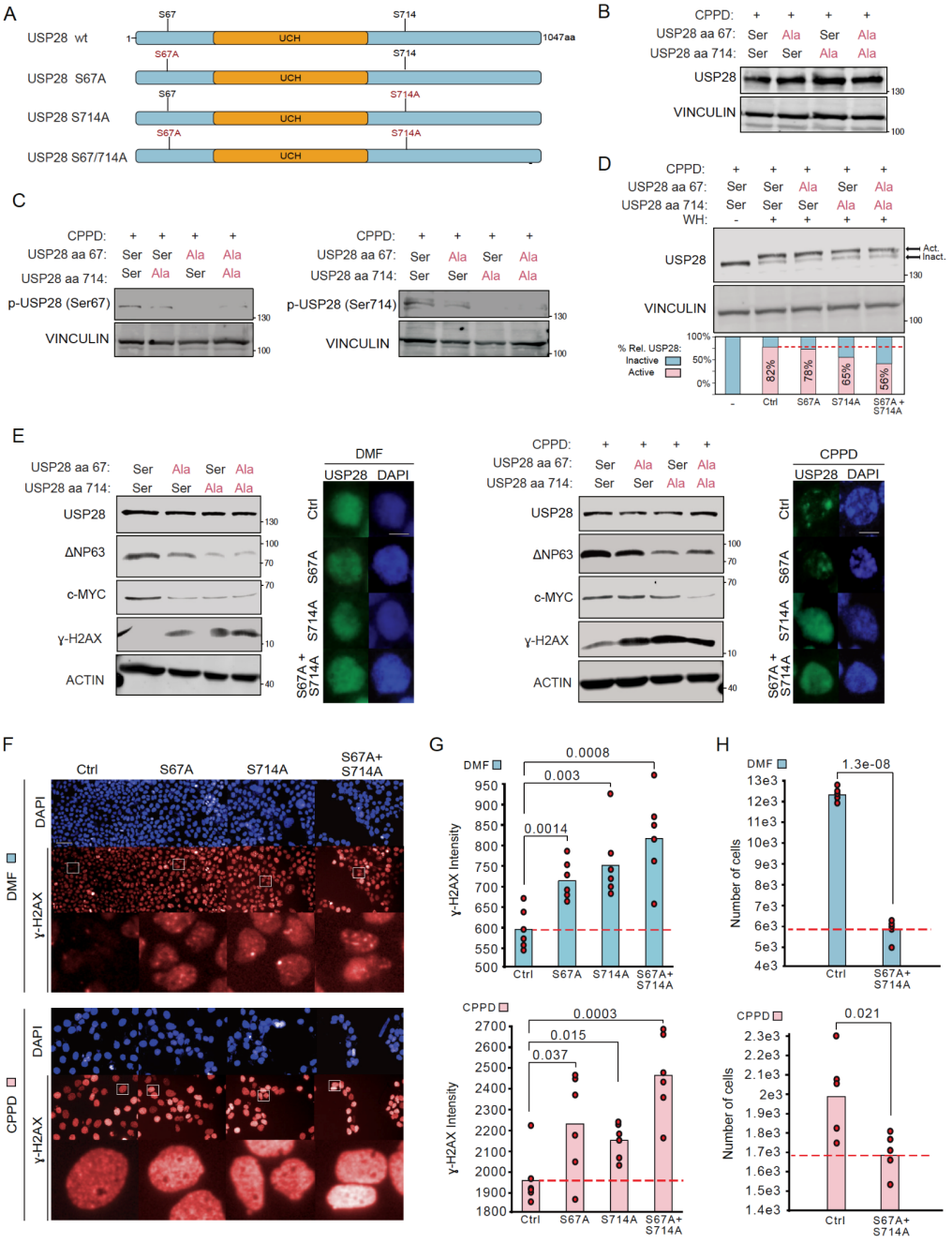

Figure 4.30. Phosphorylation of USP28 is required to repair DNA damage in Squamous cancer cells. A) Representation of the USP28 point mutations introduced into A-431 cells via Crispr-CAS9. Red=mutation; Black=WT. S=serine; A=Alanine. Aa=aminoacids. **B)** Western blot against endogenous USP28 in control, S67A, S714A and S67A+S714A mutant A-431 cells treated with 5µM CPPD for 6 hours. VINCULIN serves as loading control. n=3. **C)** Western blot of phosphorylated USP28 on serine 67 or serine 714 in control, S67A, S714A and S67A+S714A mutant A-431 cells treated with 5µM CPPD for 6 hours. VINCULIN serves as loading control. n=3. **D)** Warhead ubiquitin suicide probe assay, followed by immunoblotting against USP28 in control, S67A, S714A and S67A+S714A mutant A-431 cells exposed to 5 µM CPPD for 6 hours. 'Act.' arrow indicates active USP28.' Inact.' arrow indicates inactive USP28. VINCULIN serves as loading control. n=3. **E)** Immunoblotting of USP28, c-MYC, ΔNp63 and ɣ-H2AX in control, S67A, S714A and S67A+S714A mutant A-431 cells. ACTIN serves as loading control. n=3. Immunofluorescence against endogenous USP28 in control, S67A, S714A and S67A+S714A mutant A-431 cells. Scale bar= 10µm DAPI served as nuclear marker. n=3. Cells were either treated with DMF or 5 µM CPPD for 6 hours. **F)** Immunofluorescence against ɣ-H2AX in control, S67A, S714A and S67A+S714A mutant A-431 cells, treated with either DMF (blue) or 5µM CPPD (pink) for 48 hours. DAPI served as nuclear marker. n=6 wells (15 fields per well). Scale bar=100µm. DAPI as control. **G)** Quantification of F). DMF (blue) or 5µM CPPD (pink) for 48 hours. n=6 (15 fields per well). P-value using two-tailed T-test statistical analysis. **H)** Number of cells in control and S67A+S714A mutant A-431 cells, treated with either DMF (blue) or 5µM CPPD (pink) for 48 hours. n=5 wells (15 fields per well). P-value using two-tailed T-test statistical analysis.

It was shown that USP28 is recruited to the DNA repair machinery upon CPPD exposure (Figure 4.28). USP28 can be recruited to DNA repair foci in the control and S67A cell lines but not in the S714A and S67A/S714A cells (Figure 4.30E). The cells with the mutated phospho-site on S714 cannot form USP28 foci upon CPPD exposure, whereas the cell line with the mutation on S67 formed DNA damage foci (Figure 4.30E right panel), suggesting that S714 is required to bind USP28 to the chromatin upon CPPD exposure.

Immunofluorescence studies confirmed that the phospho-mutant cell lines expressed more ɣ-H2AX than the control cells with and without exposure to CPPD (Figure 4.30F and G). Notably, the cells with both serines mutated (S67A / S714A) had increased levels of ɣ-H2AX expression compared to the cells with only one phospho-site mutated (Figure 4.30 F and G). Accordingly, proliferation was strongly reduced in the cells with both phospho-sites mutated (S67A/S714A) compared to the control cells (Figure 4.30H). Upon CPPD exposure, the cells with both phospho-sites mutated (S67A/S714A) were more sensitive than the control A-431 cells (Figure 4.30H). These findings strongly suggest that phosphorylation of USP28 is required to maintain genome stability and activate DNA repair pathways in SCC cells.

4.3.4 USP28 positively regulates DNA repair pathways determining the response of squamous tumors to chemotherapy

Previous studies have demonstrated that high expression of DNA repair genes correlates with poor response to therapies causing DNA damage (Harris 1985; Rottenberg et al. 2020) and to the reduced overall patient survival rate (Figure 4.31A left panel). In particular, during chemotherapy, high expression of DNA repair genes indicates poor prognosis (Figure 4.31A right panel).

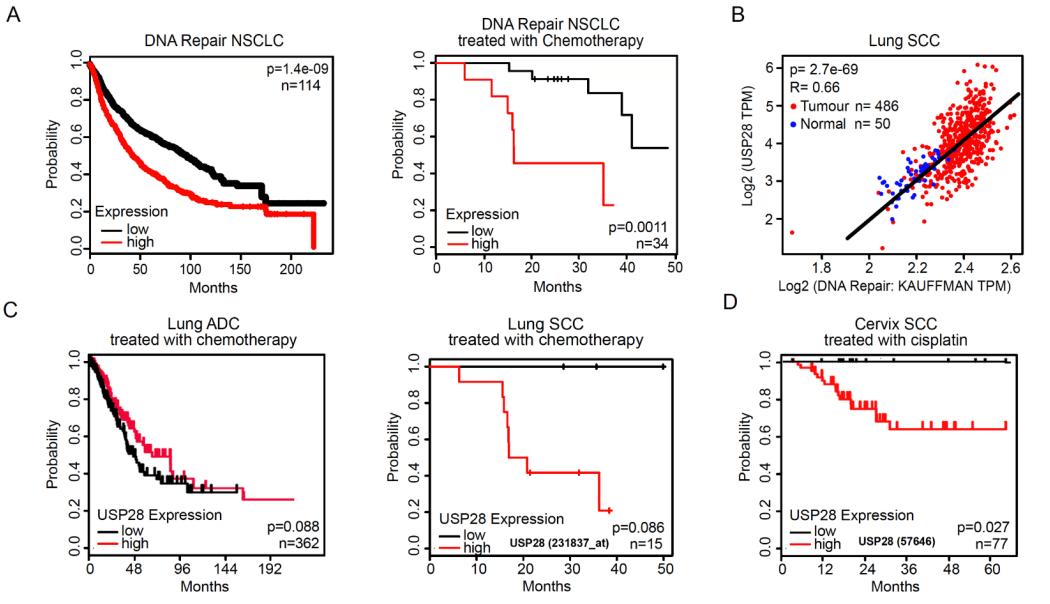

Figure 4.31. USP28 regulates the response to chemotherapy in SCC patients. **A)** Kaplan-Meier curves of NSCLC patients with low or high expression of DNA repair genes (DNA repair Kauffman signature gene set) Left panel= All NSCLC patients; Right panel= Only NSCLC treated with chemotherapy. www.kmplot.com. **B)** Correlation between USP28 gene expression and DNA repair Kauffmann signature in human SCC lung tumors and normal tissue. Spearman correlation R=0.66, p-value=2.7e-69. www.gepia2.cancer-pku.cn. **C)** Kaplan-Meier curves of chemotherapy treated lung ADC or SCC patients with low and high USP28 gene expression Left panel= ADC; Right panel= SCC. www.kmplot.com and www.r2.amc.nl **D)** Kaplan-Meier curves of chemotherapy treated cervix SCC patients with low and high USP28 gene expression. Left panel= ADC; Right panel= SCC. www.r2.amc.nl**.** The Kaufmann DNA repair gene list was previously published (Kaufmann et al. 2008).

Notably, SCC tumors exhibit poor response to therapy, thus leading to lower survival rates of patients compared to ADC or other tumor entities (Ruiz et al. 2019). USP28 is significantly upregulated in tumor entities with poor response to chemotherapy, such as SCC tumors (Figure 4.1 and 4.2) (Prieto-Garcia et al. 2020). To confirm if USP28 regulates the expression of DNA repair genes, publicly available datasets were analyzed, and it was observed that USP28 strongly correlates with the expression of DNA repair genes in SCC tumors (Figure 4.31B). Furthermore, USP28 acts as a potent prognostic factor for chemotherapy response in SCC tumors but not in ADC tumors (Figure 4.31C and D). Importantly, lung and cervical SCC patients with low levels of USP28 presented a 100% survival rate (50 months overall survival) after chemotherapy. The results clearly highlight the important role of USP28 in determining the response to chemotherapy in SCC patients.

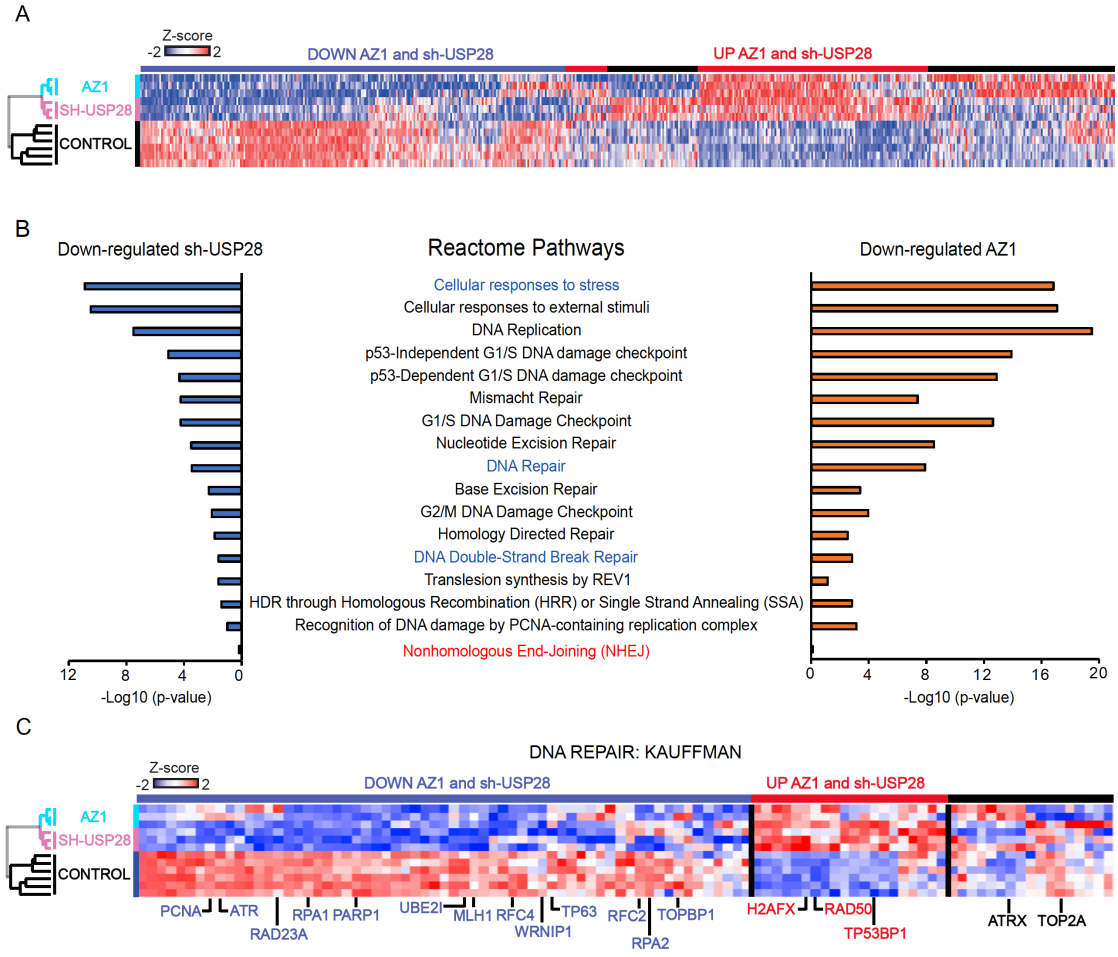

Figure 4.32. Proteome of A-431 cells upon USP28 depletion or inhibition.

A) Heatmap of the whole proteome in control, sh-USP28 and AZ1 treated A-431 cells. n=3. **B)** Reactome pathway analysis of proteomic data upon genetic depletion (sh-USP28) or pharmacological inhibition (AZ1) of USP28 in A-431 cells. n=3**. C)** Heatmap of the DNA repair Kauffman protein signature (Kauffmann et al. 2008) in control, sh-USP28 and AZ1 treated A-431 cells. n=3.

To analyze how USP28 determines chemotherapy response in SCC patients, a proteomic analysis was performed on the control, sh-USP28, and AZ1-treated A-431 cells (Figure 4.32A). The Sh-USP28 and AZ1-treated cells showed highly similar proteome profiles, thus confirming the specificity of the USP28 inhibitor, AZ1 (Figure 4.32A). The depletion or inhibition of USP28 significantly reduced the protein abundance of the

pathways associated with cell cycle progression, cellular responses to stress, DNA repair, or DNA replication (Figure 4.32B, 4.33A and B). Importantly, the loss of the USP28 activity caused the up-regulation of DNA damage sensors such as 53BP1 or RAD50 but downregulation of the effector proteins associated with DNA repair, such as RAD51 (4.32C). The main group of the DNA-repair-affected proteins after the loss of USP28 was the group of proteins involved in RR and homologous recombination (4.33A and B). In summary, the above analysis demonstrates that the depletion or inhibition of USP28 strongly reduces the expression of proteins involved in recombinational DNA repair determining the response to chemotherapy in SCC patients.

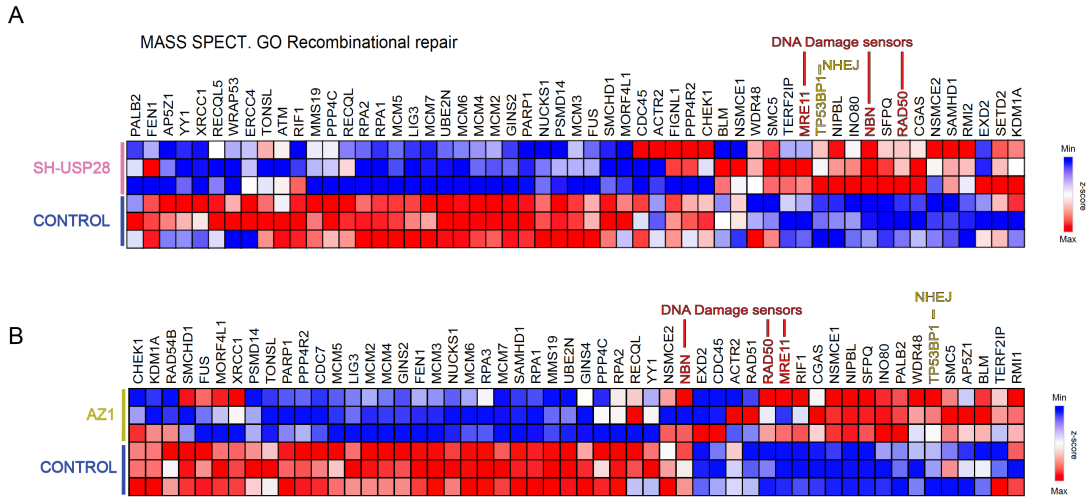

Figure 4.33. Recombinational repair proteome of A-431 cells upon USP28 depletion or inhibition.

A) Proteome heatmap of the GO recombinational repair protein signature in control and sh-USP28. n=3. **B)** Proteome heatmap of the GO recombinational repair protein signature in control and AZ1 treated cells. n=3.

4.3.5 USP28-ΔNp63 axis regulates resistance to Cisplatin in squamous cancer cells

It was previously shown that USP28 regulates the stability of ΔNp63, the central transcription factor of SCC tumors. Furthermore, ΔNp63 regulates the expression of DNA repair pathways and its depletion sensitizes chemotherapy (Bretz et al. 2016; Matin et al. 2013; Lin et al. 2009). Considering that USP28 regulates chemoresistance and RR in SCC cells, it is possible to hypothesize that USP28 regulates DDR via ΔNp63 in SCC cells.

To determine if the USP28-ΔNp63 axis is a promising target for sensitizing SCC cells to CPPD, USP28 and ΔNp63 were depleted in the A-431 cells. The USP28- and ΔNp63-depleted cells are more sensitive to CPPD and exhibit increased levels of the DNA damage markers ɣ-H2AX and p-p53 on serine 15 (Figure 4.34E, F and G). Notably, the depletion of USP28 or ΔNp63 leads to increased levels of ɣ-H2AX and p-p53 on serine 15 without CPPD exposure (Figure 4.34F and G). These results indicate that SCC cells require high expression of USP28 and ΔNp63 to maintain genome stability and consequently the viability of the oncogenic cells.

In cancer cells, CPPD exposure induces DNA damage and accumulation of cells in the G2/M phase of the cell cycle (Sandulache et al. 2017; Mueller et al. 2006; Zheng et al. 2018). Upon CPPD exposure, the USP28- or ΔNp63-depleted cell lines showed more cells in the G2/M phase compared to the control samples (Figure

4.34H). Previous reports demonstrated that the number of cells accumulated in the G2/M phase correlates with the toxicity of CPPD. Cancer cells are more resistant to CPPD during the G1-S phase than in G2/M phase (Mueller et al. 2006).

As USP28 depletion increases DNA damage in SCC cells, tests were conducted to confirm if the pharmacological inhibition of USP28 showed a similar effect. Upon treating SCC cells (A-431, DETROIT 562 and LUDLU-1) with AZ1, CPPD, or both, the ɣ-H2AX fluorescence signal increased in the AZ1+CPPD-treated cells compared to that in the control, AZ1- or CPPD-treated SCC cells (Figure 4.35A and B). Notably, the H1299 ADC cell line, treated with AZ1 and CPPD, had less ɣ-H2AX protein abundance than the CPPD-treated cells (Figure 4.35A and B). Hence, it is possible to conclude that the combination of AZ1 and CPPD increases DNA damage in SCC the cells but not in other epithelial tumor entities such as ADC cells.

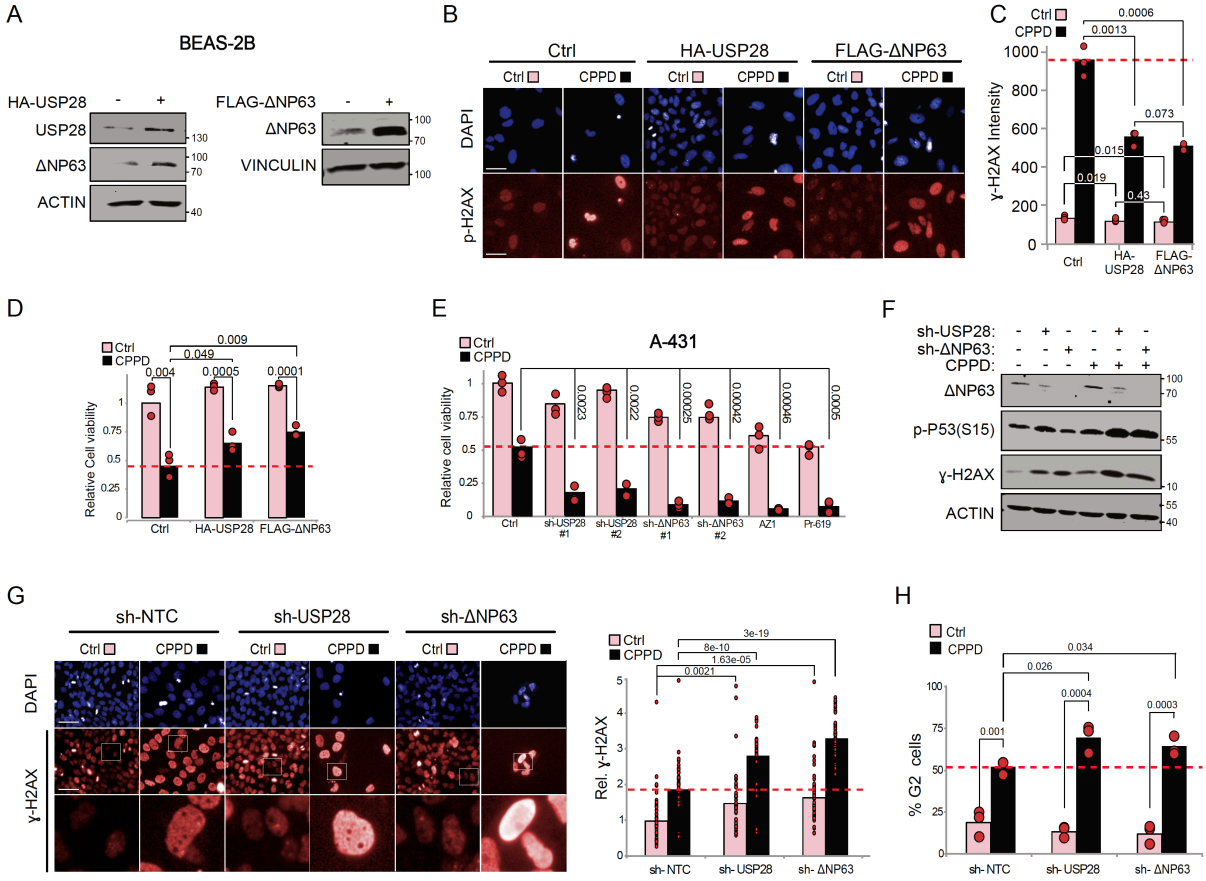

Figure 4.34. The USP28-ΔNp63 axis regulates chemo-resistance in Squamous cells.

A) Western blot of BEAS-2B cells transiently transfected with either USP28 or ΔNp63. ACTIN and VINCULIN as loading control. n=3. **B)** Immunofluorescence staining against the DNA damage marker ɣ-H2AX in BEAS-2B cells transiently transfected in A). Cels were exposed to DMF (Ctrl) or 2.5µM CPPD for 48 hours. DAPI indicates nucleus. n=3. Scale bar= 100µm. **C)** Quantification of relative ɣ-H2AX fluorescence intensity from B). We quantified 15 fields per well (n=3). P-value using two-tailed T-test statistical analysis. **D)** Quantification of relative cell survival from B). We quantified 15 fields per well (n=3). P-value using two-tailed T-test statistical analysis. **E)** Quantification of relative A-431 cell survival in control (Ctrl), sh-USP28#1, sh-USP28#2, sh-ΔNp63#1, sh-ΔNp63#2, AZ1 or PR-619 treated cells exposed to 5µM CPPD for 48 hours. n=3. P-value using two-tailed T-test statistical analysis. **F)** Western blot of ΔNp63, phospho-p53 (Serine15), ɣ-H2AX in control (Ctrl), sh-USP28#1 or sh-ΔNp63#1 cells exposed to 5µM CPPD for 24 hours. ACTIN served as loading control. n=3. **G)** Immunofluorescence staining against ɣ-H2AX in control (Ctrl), sh-USP28#1 or sh-ΔNp63#1 cells exposed to 5µM CPPD for 48 hours. DAPI as indicator of nuclear localization control. n=3 wells. Quantification of relative ɣ-H2AX fluorescence intensity in A-431 cells. n=50 cells. Scale bar= 200µm.

P-values were calculated using two-tailed T-test statistical analysis. **H)** FACS-based cell cycle analysis. We quantified the percentage of control (Ctrl), sh-USP28#1 or sh-ΔNp63#1 cell in G2 upon exposure to 5μM CPPD for 48 hours. n=3. P-values were calculated using two-tailed T-test statistical analysis.

Then, the CPPD survival curves of the control, sh-USP28, sh-ΔNp63, and AZ1 A-431 cells were plotted (Figure 4.36A). The depletion of USP28/ΔNp63 or USP28 inhibition strongly sensitized the cells to CPPD (Figure 4.36A). Upon CPPD treatment, the AZ1-treated cells show a GI50 of 2.4 μM compared to a GI50 of 5.5 μM GI50 shown by the control cells (Figure 4.36A).

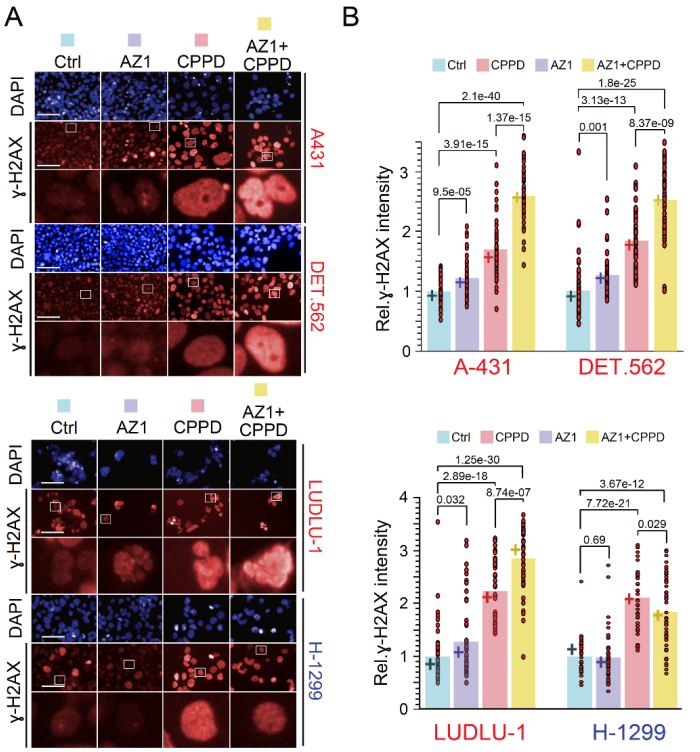

Figure 4.35. Inhibition of USP28 increases DNA damage induced by Cisplatin in squamous cancer cells.

A) Immunofluorescence staining against the DNA damage marker γ-H2AX in SCC (A-431, Detroit 562 and LUDLU-1) and ADC (H1299) cells exposed to 15μM AZ1, 5μM CPPD or 15μM AZ1 and 5μM CPPD for 48 hours. DAPI indicates nucleus. n=3 wells. Scale bar= 200μm. Red= SCC cell line; Blue= ADC cell line. **B)** Relative γ-H2AX quantification from A). n= 50 cells. Two tailed T-test was used to calculate p-values. Red= SCC cell line; Blue= ADC cell line.

In summary, the USP28-ΔNp63 axis regulates the resistance of SCC tumors to CPPD. The depletion or inhibition of USP28 reduces the ΔNp63 levels, thus resensitizing the SCC cells to CPPD. Moreover, as ΔNp63 is only expressed in the SCC cell lines, the inhibition of USP28 in the non-SCC cells, such as H1299, does not sensitize the cells to CPPD.

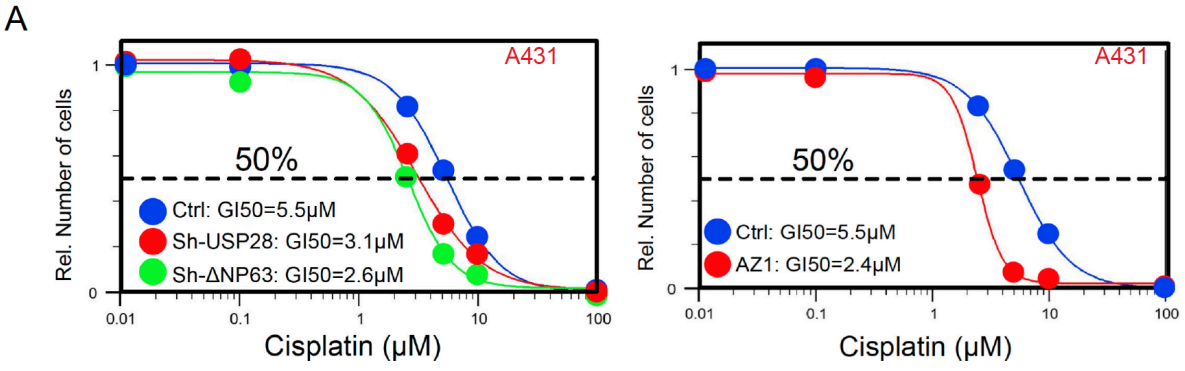

Figure 4.36. Depletion of USP28/ΔNp63 or USP28 inhibition sensitizes A-431 cells to Cisplatin.

A) Relative number of control (Ctrl), sh-USP28#1, sh-ΔNp63#1 or AZ1 treated A-431 cells upon exposure to different CPPD concentrations. Exact 50% growth inhibition (GI50) was calculated.

4.3.6 USP28-ΔNp63 axis facilitates DNA repair in squamous cells upon Cisplatin exposure

As the loss of USP28 (Figure 4.32 and 4.33) and ΔNp63 (Bretz et al. 2016; Lin et al. 2009) reduces the expression of DNA repair factors responsible for sensitizing the cells to CPPD (Figure 4.34 and 4.35), another main objective of this research was to determine how the loss of USP28 or ΔNp63 could affect the detection and repair of the damaged DNA. The reduction of ΔNp63 via depletion or inhibition of USP28 could reduce the expression of DNA repair pathways involved in RR. Accordingly, USP28-deficient SCC cells may require more time to assemble the complex involved in DNA repair and properly process the conflicts in DNA damage. To validate the above hypothesis, a CPPD pulse-chase experiment was performed on the control, sh-USP28, sh-ΔNp63, and AZ1-treated cells. The cells were collected at various time points upon CPPD exposure to analyze the expression of the DNA damage markers p-p53 (serine15) and ɣ-H2AX by immunoblotting (Figure 4.37A and B). The control cells exhibited reduced p-p53 and ɣ-H2AX levels after 9 hours of CPPD treatment than the knockdown or AZ1-treated cells (Figure 4.37A and B). This result demonstrates that USP28, potentially via ΔNp63, increases the CPPD resistance of the SCC cells, facilitating DNA repair upon CDDP treatment. The depletion or inhibition of USP28 reduces the abundance of DNA repair proteins and increases the required time to repair DNA in SCC cells effectively.

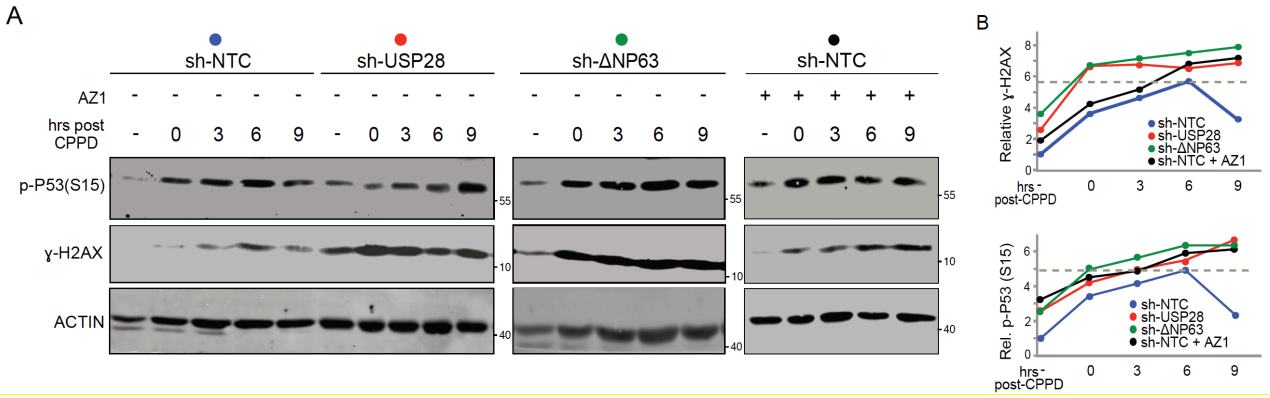

Figure 4.37. Depletion of USP28/ΔNp63 or USP28 inhibition dysregulate DNA damage response.

A) Western blot against endogenous p-p53 (serine15) and ɣ-H2AX in sh-control, sh-USP28#1, shΔNp63#1 or sh-control treated with AZ1. A-431 cells treated with 5µM CPPD for 1 hour and collected at indicated time points upon CPPD exposure. ACTIN as loading control (n=3). **B)** Quantification of p-p53 (serine15) and ɣ-H2AX relative protein abundance from the representative western blot presented in A). n=3

4.3.7 Inhibition of USP28 resensitizes squamous cells to DNA damage therapies other than Cisplatin

The inhibition of USP28 sensitizes SCC cells to CPPD. However, it is not known if AZ1 treatment sensitizes SCC cells to other DNA damage therapies such as Oxaliplatin, 5-Fluoracil, or IR. Oxaliplatin induces the formation of interstrand and intrastrand crosslinks, thus preventing DNA transcription and replication (Graham et al. 2004). Further, 5-Fluoracil principally acts as an inhibitor for thymidylate synthase formation, interrupting the synthesis of pyrimidine thymidylate required for DNA replication (Longley et al. 2003). Alternatively, radiotherapy induces mainly induces DSBs in DNA, considered the most lethal form of DNA damage (Baskar et al. 2012).

To confirm if the inhibition of USP28 sensitizes the SCC cells to Oxaliplatin, 5-Fluoracil, or IR, the SCC cells were treated with either DMSO or 15 µM AZ1 and exposed to 5 µM Oxaliplatin, 8 GY IR, or 20 µM 5-fluorouracil (Figure 4.38A and B). The results showed that the combination of AZ1 with 5 µM Oxaliplatin, 8 GY IR, or 20 µM 5-fluorouracil drastically reduced cell viability compared to that observed in individual treatments (Figure 4.38A and B). In conclusion, treatment with AZ1 sensitizes SCC cells to DNA damage therapies such as IR or Oxaliplatin.

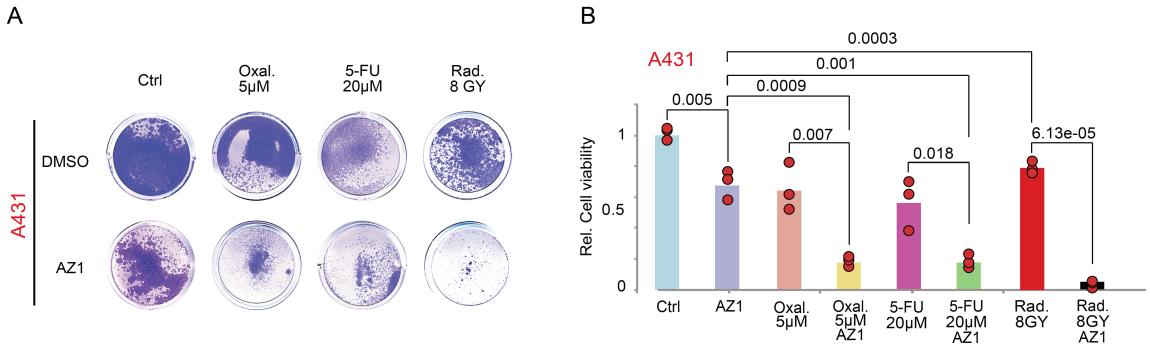

Figure 4.38. Pharmacological inhibition of USP28 sensitizes A-431 cells to Oxaliplatin, 5-Fluoracil and Ionizing radiation.
A) Crystal violet staining of A-431 cells upon treatment with either DMSO or 15µM AZ1 and 5µM Oxaliplatin (Oxal.), single dose 8GY of Ionizing radiation (Rad) or 20µM 5-fluorouracil (5-FU) for 48 hours. For radiotherapy, cells were treated with AZ1 before Ionizing radiation. n=3. **B)** Relative cell viability quantification of survival cells upon treatment with either DMSO or 15µM AZ1 and 5µM Oxaliplatin (Oxal.), single dose 8GY of Ionizing radiation (Rad) or 20µM 5-fluorouracil (5-FU) for 48 hours. For radiotherapy, cells were treated with AZ1 before Ionizing radiation. Quantification from A). n=3. Two tailed T-test was used to calculate p-values.

4.3.8 USP28 regulates Fanconi anemia DNA repair pathway via ΔNp63 in squamous cells

Previous research has demonstrated that ΔNp63 regulates the transcription of FA members, such as FANCD2 or RAD51 (Bretz et al. 2016; Lin et al. 2009). The FA pathway is an important regulator of DNA repair and strongly correlates with the resistance of SCC cells to DNA damage therapies (Bhattacharjee & Nandi 2017). The FA pathway is the central regulator of homologous recombination (Michl et al. 2016). The inhibition of the FA pathway by the development of small molecules regulating the activity of the pathway could play an important role in the development of new cancer treatments (Jo & Kim 2015). Here, it is proposed that the inhibition of USP28 modulates the activity of the FA pathway via ΔNp63 in SCC tumors.

First, human-lung SCC tumors express significantly higher levels of FA members, USP28, ATR, and TP63 than ADC lung tumors (Figure 4.39A). The increased expression of FA members could explain the resistance of SCC tumors to DNA damage therapies (Hutchinson et al. 2020). The expression of ΔNp63, facilitated by USP28, could be responsible for the expression of FA members in SCC tumors and in turn to their resistance to DNA damage therapies. Tumors with high levels of TP63 are more resistant to chemotherapy than the tumors with low levels of ΔNp63, leading to significantly shorter patient survival times (Figure 4.39B). Furthermore, USP28 and TP63 are strongly correlated to the expression of FA pathway members (Figure 4.39C and D).

To determine if USP28 regulates the FA pathway via ΔNp63, USP28 was overexpressed or depleted in A-431 cells. The expression of mUSP28 increased the protein abundance of the FA member FANCD2 (Figure 4.39E).

Alternatively, the depletion of USP28 reduced the FANCD2 protein abundance (Figure 4.39E). Thus, to determine if the USP28-ΔNp63 regulates the transcription of the FA members, an RT-PCR was performed to analyze the mRNA levels of FANCD2, FANCI, and RAD51C mRNA 50% the, sh-USP28, sh-ΔNp63, or ΔNp63-transfected sh-USP28 cells (Figure 4.39F).

The depletion of USP28 or ΔNp63 reduced the mRNA levels of the three FA members compared to that in the control cells (Figure 4.39F). Notably, the transfection of ΔNp63 in USP28 depleted the cells by partially recovering the mRNA levels of FANCD2, FANCI, and RAD51C (Figure 4.39F), thereby demonstrating that USP28 regulates the FA pathway, at least partially, via ΔNp63. TO confirm if USP28 regulates the quantity of ΔNp63 bound to the promoters of FANCD2, RAD51C, and FANCI, a ChIP-qPCR experiment was conducted upon immunoprecipitation of ΔNp63 (Figure 4.39G). The quantity of ΔNp63 bound to the FANCD2, RAD51C, and FANCI promoters was reduced in the USP28-depleted cells compared to that in the control cells (Figure 4.39G), indicating that ΔNp63 regulates the transcription of the three FA members directly by binding to their promoters.

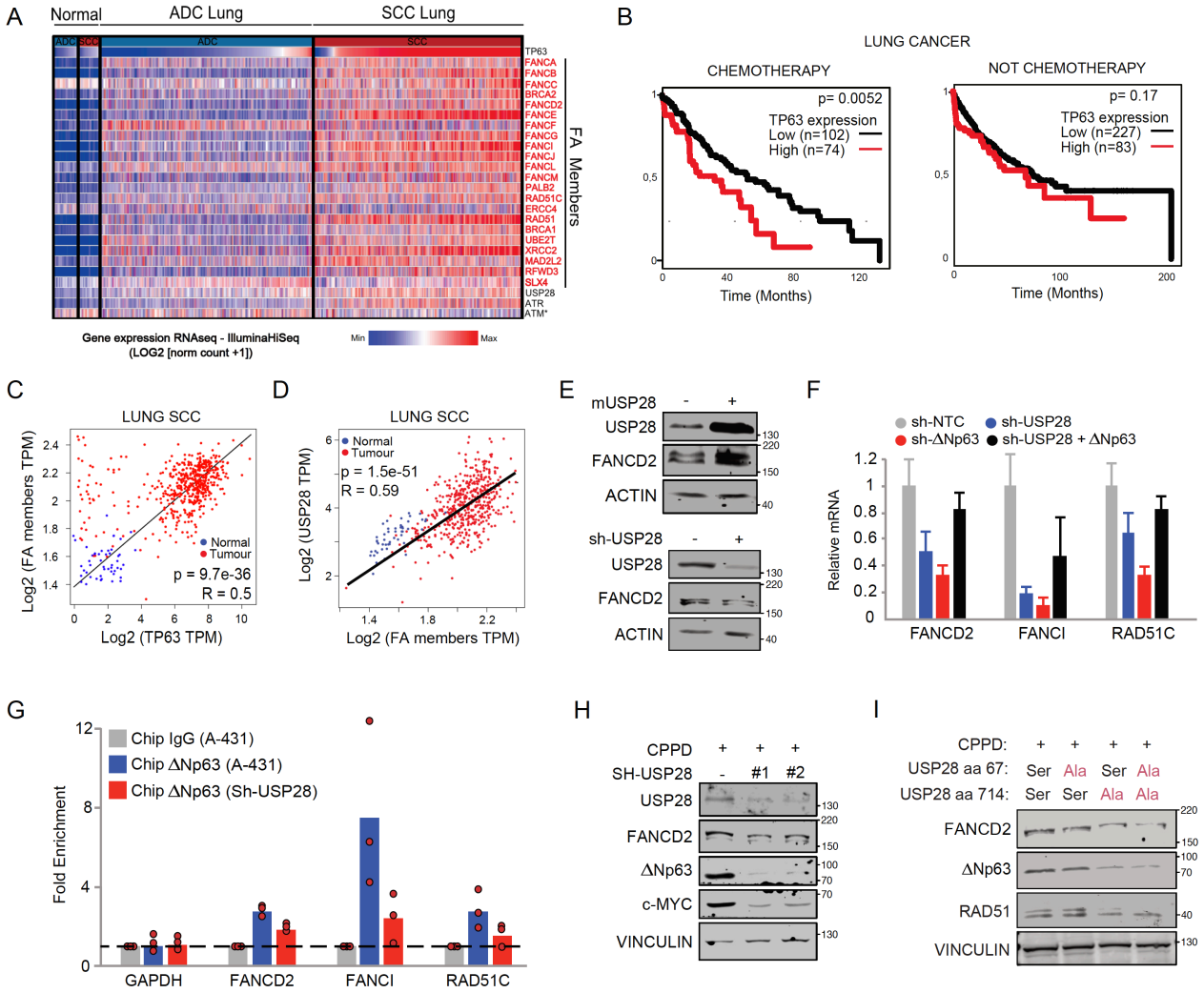

Figure 4.39. USP28 regulates Fanconi Anemia DNA repair pathway via ΔNp63 in Squamous cells.

A) Gene expression heatmap of TP63, Fanconi Anemia pathway genes, USP28, ATM and ATR in normal lung tissue, lung ADC and lung SCC TCGA human tumors. www.xena.ucsc.edu. FA members=Red. Each column is a different sample. **B)** Kaplan-Meier curves of NSCLC patients with low or high expression of TP63 Left panel= NSCLC patients treated with chemotherapy; Right panel= NSCLC

non treated with chemotherapy. www.kmplot.com. **C)** Gene expression Spearman correlation of FA member genes and TP63 in lung SCC and normal human samples (Normal). R: Spearmans correlation coefficient. n=836. http://gepia.cancer-pku.cn. The diagonal line reflects a regression build on a linear model. **D)** Gene expression Spearman correlation of FA member genes and USP28 in lung SCC and normal human samples (Normal). R: Spearmans correlation coefficient. n=836. http://gepia.cancer-pku.cn. The diagonal line reflects a regression build on a linear model. **E)** Western blot of USP28 and FANCD2 in A-431 cells virally transduced with inducible overexpression of murine Usp28 or doxycycline (DOX) inducible shRNA targeting USP28. Cells were exposed to 1µg/ml DOX for 96 hours prior to analysis. ACTIN serves as loading control. n=3. **F)** RT-PCR of FANCD2, FANCI and RAD51C in A-431 sh-NTC, sh-USP28#1, sh-ΔNp63#1 or sh-USP28#1 transfected with ΔNp63 cells normalized to ACTB. Quantitative graphic is represented as mean ± SD of three experiments. n=3. **G)** RT-PCR of GAPDH, FANCD2, FANCI and RAD51C promoter regions upon Chromatin immuno-precipitation (CHIP) of either IgG or ΔNp63 in sh-NTC, sh-USP28#1 and sh-ΔNp63#1 A-431 cell lines. Normalized to IgG. Quantitative graphic is represented as mean of three experiments. n=3. **H)** Immunoblot of endogenous USP28, FANCD2, ΔNP63 and c-MYC in control and sh-USP28#1 and sh-USP28#2 A-431 cells upon 5µM CPPD exposure for 6 hours. VINCULIN serves as loading control. n=3. **I)** Immunoblot of endogenous FANCD2, ΔNP63 and RAD51 in control, S67A, S714A and S67A+S714A mutant A-431 cells treated with 5µM CPPD for 6 hours. VINCULIN serves as loading control. n=3

Furthermore, USP28-depleted cells showed reduced levels of ΔNp63, c-MYC, and FANCD2 protein abundances compared to those in the control cells (Figure 4.39H). The experiment was repeated but using the mutant USP28 phospho-site cells previously described (Figure 4.30). The cells with mutation of the phospho-site located on S714 and the cells with double mutation, on S67 and S714, exhibited significantly reduced levels of FANCD2, RAD51, and ΔNp63 protein abundances compared to those in the control cells (Figure 4.39H). However, the cells with the mutation of the phospho-site on S67 showed only a slight reduction in the FANCD2 and ΔNp63 protein abundances (Figure 4.39H). This result again proves that the phospho-site located on S714 strongly regulates USP28 activity.

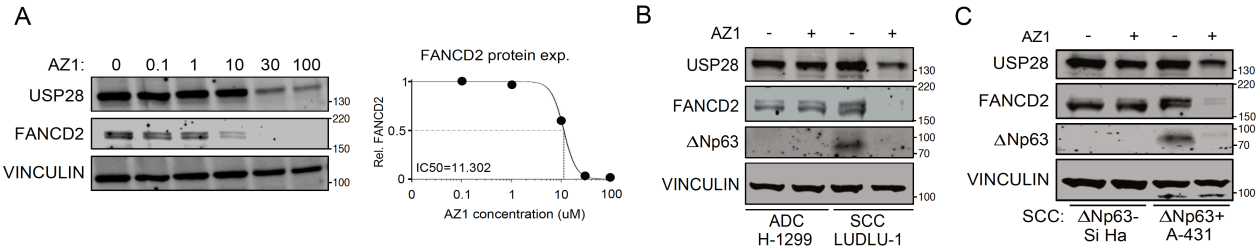

Figure 4.40 USP28 pharmacological inhibition reduces the expression of Fanconi Anemia genes in cancer cells that express ΔNp63.

A) Immunoblot of endogenous USP28 and FANCD2 in A-431 cells exposed to different concentrations of AZ1 for 24 hours. The exact AZ1 concentration required to reduce 50% FANCD2 protein abundance was calculated (IC50=11.302µM AZ1). VINCULIN serves as loading control. n=3. **B)** Immunoblot of endogenous FANCD2, ΔNP63 and USP28 in control and 15µM AZ1 treated H1299 (ADC) and LUDLU-1 (SCC) lung cells for 24 hours. VINCULIN serves as loading control. n=3. **C)** Immunoblot of endogenous FANCD2, ΔNP63 and USP28 in control and 15µM AZ1 treated Si Ha (ΔNP63-) and A-431 (ΔNP63+) SCC cells for 24 hours. VINCULIN serves as loading control. n=3.

Next, to determine if the pharmacological inhibition of USP28 reduces the protein abundance of the FA pathway members, the A-431 cells were treated with different concentrations of AZ1. The protein abundance of FANCD2 gradually decreased upon increasing the concentration of AZ1 (Figure 4.40A). Approximately

11.302 µM of AZ1 was required to reduce 50% combination tthe total FANCD2 protein abundance in the A-431 cells.

Furthermore, to prove that USP28 regulates the protein abundances of the FA members via ΔNp63, the H1299 ADC (ΔNp63-) and LUDLU-1 SCC (ΔNp63+) cells were exposed to AZ1. Only the SCC cell line had reduced levels of FANCD2 protein abundance following AZ1 exposure (Figure 4.40B). Then, the Si Ha (ΔNp63-) SCC cell line was exposed to AZ1. As Si Ha cells do not express detectable levels of ΔNp63, it was found that AZ1 exposure reduced the FANCD2 protein abundance in the A-431 cells but not in the Si Ha cells (Figure 4.40C), demonstrating that the expression of ΔNp63 is required for the regulation of FANCD2 by USP28.

In summary, the mutation, depletion, or pharmacological inhibition of USP28 strongly reduced the genetic expression of the FA members via ΔNp63. USP28 regulates the FA members in only ΔNp63+ tumors, suggesting that the regulation of the FA pathway by USP28 is restricted to SCC tumors. Inhibition of USP28 could be a suitable method to modulate the FA pathway for resensitizing ΔNp63+ tumors to DNA damage therapies, such as chemotherapy or radiotherapy.

4.3.9 USP28 regulates the Fanconi anemia pathway maintaining genome stability of squamous tumors in vivo

It was previously shown that USP28 regulates the FA pathway via ΔNp63 in SCC cells. To confirm that USP28 can regulate the FA pathway in vivo, the previously described KPL ($Kras^{G12D}$; $p53^{\Delta}$; $Lkb1^{\Delta}$) and KPLU ($Kras^{G12D}$; $p53^{\Delta}$; $Lkb1^{\Delta}$; $Usp28^{\Delta}$) animal models were used. Immunohistochemistry and immunoblotting experiments showed that the KPLU tumors showed significantly lower FANCD2, FANCI, USP28, and ΔNp63 protein abundances than those in the KPL tumors (Figure 4.41A and B). Alternatively, the KPLU tumors expressed increased levels of the DNA damage markers 53BP1 and ɣ-H2ax (Figure 4.41A and B), demonstrating that SCC tumors require the expression of USP28 to maintain genome stability by regulating the axial ΔNp63-FA pathway in vivo.

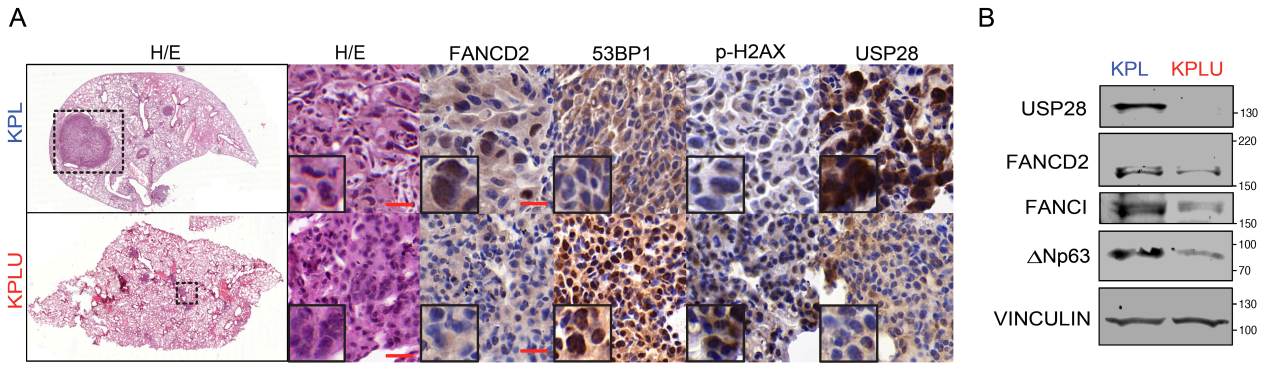

Figure 4.41 USP28 regulates genome stability and the axis ΔNp63-Fanconi anemia pathway in vivo.

A) Representative images of sections from KPL (KrasG12D; $p53^{\Delta}$; $Lkb1^{\Delta}$) and KPLU (KrasG12D; $p53^{\Delta}$; $Lkb1^{\Delta}$; $Usp28^{\Delta}$) mice stained with haematoxilin and eosin (H/E). Inlay shows higher magnification. Immunohistochemistry of Fancd2, 53bp1, ɣ-H2ax (p-H2ax) and Usp28 in primary KPL or KPLU tumors. Scale bar = 50µm. nKPL=6; nKPLU=5. **B)** Western blot against Usp28, Fancd2, Fanci and ΔNp63 in KPL and KPLU tumors. Vinculin serves as loading control. n=3

The above result confirms that USP28 regulates the FA pathway in vivo. To confirm if exposure to AZ1 regulates the FA and genomic stability in lung SCC tumors, the SCC (Kras G12D; $p53^{\Delta}$; $Lkb1^{\Delta}$) cells were endotracheally retransplanted into WT mice to develop in vivo tumors. Upon tumor formation, the mice were intraperitoneally exposed to 6 doses of PBS/ DMSO/Tween80 (control) or 375 mg/kg AZ1 (Figure 4.42A), as previously described (Figure 4.25B). The mice systemically treated with 375 mg/kg AZ1 expressed lower levels of FANCD2, USP28, and ΔNp63 compared to those expressed by the control mice (Figure 4.42B, C and D). Furthermore, the AZ1-treated tumors showed increased protein abundances of the DNA damage markers 53BP1 and ɣ-H2ax compared to those observed in the control mice (Figure 4.42B and C). Thus, it is possible to modulate the FA pathway using USP28 inhibitors in vivo. Accordingly, it could be possible to sensitize SCC tumors to chemotherapy or radiotherapy upon USP28 inhibition. The combination of AZ1 with DNA damage therapies appears as a promising method to treat resistant SCC tumors in vivo.

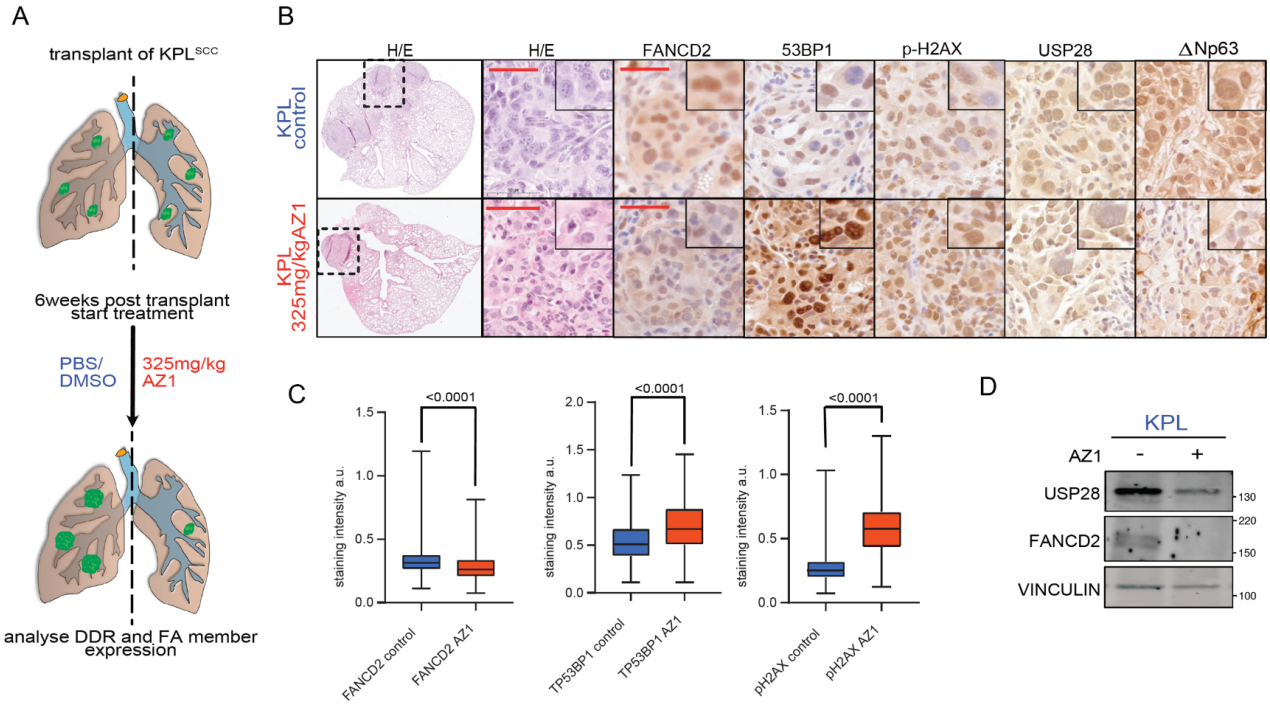

Figure 4.42 Inhibition of USP28 modulates Fanconi anemia pathway and DNA repair in murine SCC tumors.
A) Schematic model representing the administration of AZ1 in mice. Animals were intraperitoneally treated with 6 doses of PBS/ DMSO/ Tween80 (as control) or 375mg / kg AZ1. **B)** SCC tumors H&E and IHC staining for Usp28, ΔNp63, Fancd2, 53BP1 and ɣ-H2ax (p-H2ax) in control and AZ1 treated animals (n=3). Boxes indicated highlighted areas. Scale bars = 50µm. **C)** Fancd2, 53BP1 and ɣ-H2ax (pH2ax) staining intensity of SCC tumors exposed to control or AZ1. p-values calculated via two-tailed t-test. In box plots, the centre line reflects the median, the cross represents the mean and the upper and lower box limits indicates the first and third quartile. Whiskers extend 1.5x the IQR. The quantification was performed using QuPath (version0.2.8). Boxplots were generated using Graphpad Prism8. a.u.= Arbitrary units. nFancd2= 6200 cells control and 3616 cells AZ1; nɣ-H2ax =17075 cells control and 9140 cells AZ1; nP53BP1=18831cells control and 8586 cells AZ1. **D)** Western blot against Usp28 and Fancd2 in SCC tumors from control and AZ1 treated animals. Vinculin serves as loading control. n=3.

4.3.10 Inhibition of USP28 increases sensitivity to Cisplatin in ex vivo organotypic lung squamous tumor slice cultures

To investigate the potential of using USP28 inhibitors to treat aggressive SCC tumors in combination with DNA damage therapies, organotypic lung slice cultures were used to study the potential synergy between chemotherapy and AZ1. The SCC tumors developed upon endotracheal transplantation of the KPL (Kras G12D; $p53^{\Delta}$; $Lkb1^{\Delta}$) cells were explanted and sectioned into slices using a vibratome (Figure 4.43A). The ex vivo SCC tumor slices were maintained in a standard cell culture medium (DMEM, 10% FCS) and exposed to CPPD (5 µM) and/or different concentrations of AZ1 (0, 10, 30, and 100 µM) (Figure 4.43A). The KPL (Kras G12D; $p53^{\Delta}$; $Lkb1^{\Delta}$) SCC cells expressed GFP, thus enabling the assessment of the tumor viability by quantifying the intensity of GFP expression after the treatments (Figure 4.43A). To confirm if SCC tumors are more sensitive to the AZ1+CPPD treatment than the WT lung tissue, nontransformed lung slices from WT C57BL6/J-*Rosa26* Sor-CAGG-Cas9-IRES-eGFP mice expressing GFP were used (Figure 4.43A). Before exposing the lung slices to the AZ1+CPPD treatment for one day, the samples were treated with only AZ1 for three days to deregulate the FA pathway and resensitize the SCC tumors to DNA damage therapy (Figure 4.43A).

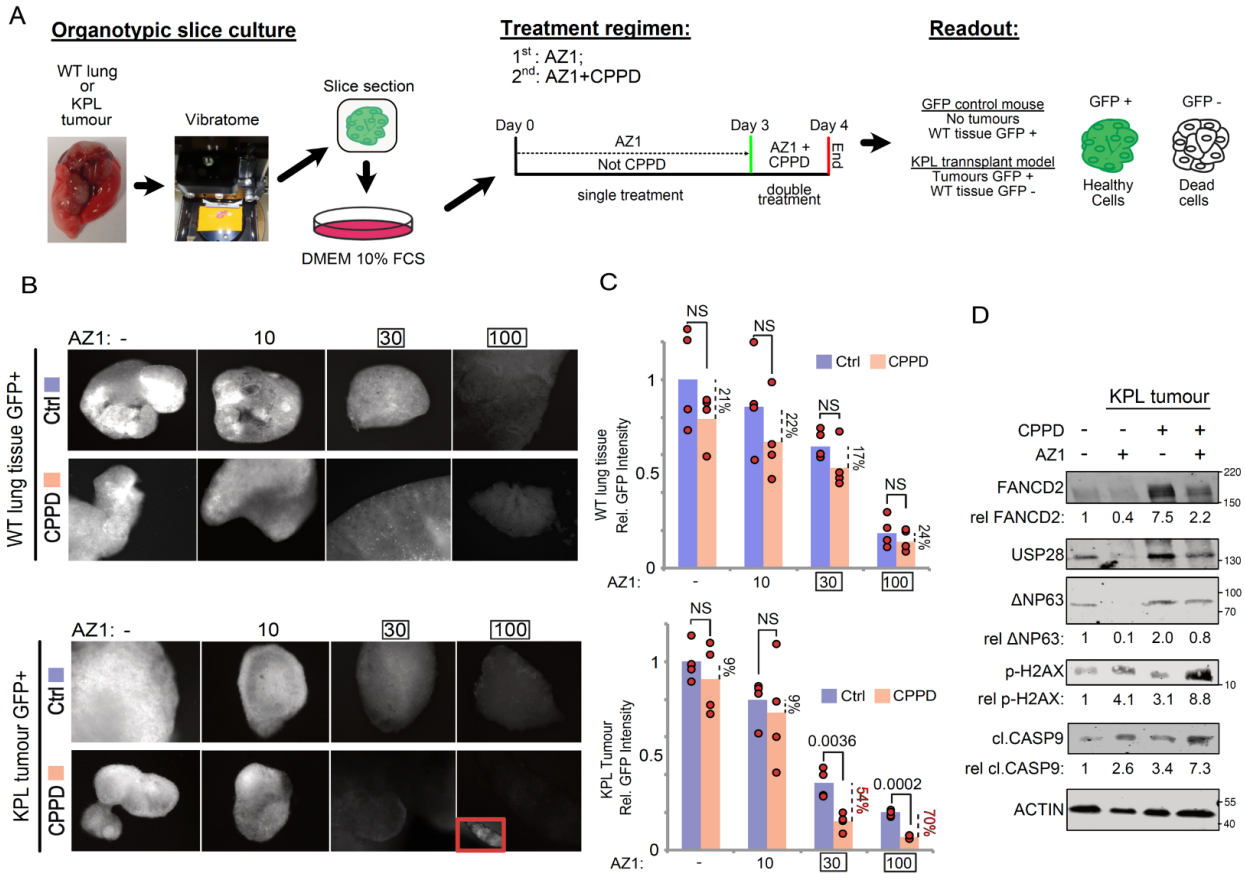

Figure 4.43 Inhibition of USP28 increases sensitivity to Cisplatin in ex vivo organotypic lung squamous tumor slice cultures. **A)** Schematic diagram of the ex-vivo organotypic lung slice culture experiment exposed in B), C) and D). **B)** Immunofluorescence of ex vivo WT GFP+ lung organotypic slice culture and ex vivo KPL ($p53^{\Delta}$; $Lkb1^{\Delta}$; KRasG12D) GFP+ SCC organotypic slice culture after 72 hours of indicated AZ1 concentrations and 24 hours of co-treatment with 5µM CPPD. n=4. **C)** Quantification of relative GFP+ signal intensity of ex vivo organotypic slice cultures from B). The different in GFP intensity between Ctrl and CPPD treated slices was indicated by percentage. n=4. P-values were calculated using two-tailed T-test statistical analysis. **D)** Immunoblot against Fancd2,

Usp28, cleaved Caspase9, ɣ-H2ax (p-H2ax) and ΔNp63 of ex vivo KPL ($p53^{\Delta}$; $Lkb1^{\Delta}$; KRasG12D) GFP+ SCC lung tumor organotypic slice culture after 72 hours of indicated AZ1 concentrations and 24 hours of co-treatment with 5μM CPPD. Actin as a loading control. Quantification of relative protein abundance using Actin for normalization. n=4.

Treating the SCC tumors with AZ1 alone strongly reduced the GFP intensity when compared to that in the nontransformed lung tissue (Figure 4.43B and C). Notably, the combination of AZ1 and CPPD significantly reduced the viability of SCC tumor cells compared to individual treatments (AZ1 or CPPD) or WT lung tissues treated with the same combination (Figure 4.43B and C). The SCC tumors treated with 30 μM AZ1 and 5 μM CPPD had a considerably low number of cells expressing GFP compared to that in the WT lung tissue (Figure 4.43B and C). The above result indicates that SCC tumors are more sensitive to the AZ1+CPPD treatment than normal cells; therefore, the AZ1+CPPD method can efficiently treat SCC tumor patients.

Upon immunoblotting, the slices treated with 30 μM AZ1 showed reduced levels of USP28, FANCD2, and ΔNp63 protein abundances compared to the untreated slices (Figure 4.43D). Furthermore, the SCC slices treated with 30 μM AZ1 and 5 μM CPPD presented reduced USP28, FANCD2 and ΔNp63 protein abundances than the slices treated with 5 μM CPPD (Figure 4.43D). Notably, the treatment with 30 μM AZ1 + 5 μM CPPD strongly increased the protein abundances of the DNA damage marker ɣ-H2ax and the apoptotic marker cleaved Caspase 9 compared to those in the SCC slices subjected to individual treatments (Figure 4.43D). Using ex vivo murine- lung SCC tumors, it was possible to confirm the potential of the AZ1 + CPPD treatment method. The combination of USP28 inhibitors with CPPD could improve the currently limited portfolio of therapies available to treat aggressive SCC tumors.

5. Discussion

5.1 ΔNp63 is essential for squamous tumors

High levels of ΔNp63 protein abundance are essential to induce and maintain SCC tumors (Figure 4.20, 4.22 and 4.26). ΔNp63 regulates several signaling pathways that crucially contribute to the development of SCC tumors. ΔNp63 is a crucial protein to maintain the malignant transcriptional profile and SCC identity of epithelial tumors. (Somerville et al. 2018; Hamdan & Johnsen 2018; Prieto-Garcia et al. 2020). However, ΔNp63 is also critical for maintaining genome stability, and its depletion strongly increases DNA damage in SCC tumors (Figure 4.34, 4.36 and 4.37).

Genomic instability has emerged as a major hallmark in oncogenesis. Deficiencies in DNA repair pathways lead to genetic alterations in oncogenes and tumor suppressor genes, which could induce the development of malignant tumors. Alternatively, in highly proliferative malignant cells, uncontrolled levels of DNA damage trigger the activation of intracellular death programs, such as apoptosis. Consequently, the transformation of somatic cells to malignant SCC cells requires maintaining the DNA damage levels below a certain threshold to avoid programmed cell death. This thesis proposes that ΔNp63 plays a critical role in maintaining a certain degree of genomic stability, thus allowing the malignant transformation of somatic cells to SCC cells. In SCC cells, the expression of genes involved in the FA pathway and RR is mainly regulated by ΔNp63 (Figure 4.39) (Bretz et al. 2016; Lin et al. 2009). Accordingly, ΔNp63 triggers the transcription of the genes involved in DNA repair, allowing oncogenic reprogramming and malignant proliferation without the activation of an intracellular death program (Figure 5.1A).

SCC tumors depend on ΔNp63 to regulate the typical SCC basal epithelial cell identity (Ratovitski 2014; Romano et al. 2012; Hackett et al. 2013; Yoh & Prywes 2015). Ectopic expression of ΔNp63 overrides the established lineage identities and induces transdifferentiation to the SCC epithelial signature, thus demonstrating the potency of ΔNp63 as a master regulator of SCC tumor formation (Hamdan & Johnsen 2018; Soares & Zhou 2018; Somerville et al. 2018). The depletion of ΔNp63 eliminates the squamous epithelial signature in SCC cell lines (Figure 4.13 and 4.15). Considering the results presented above, it may be hypothesized that the depletion of ΔNp63 can cause the transdifferentiation of SCC tumors to another malignant epithelial entity like ADC. However, our results demonstrated that the acute depletion of ΔNp63 in SCC triggered the activation of programmed cell death (Figure 4.43), thus reducing the tumor area (Figure 4.26). Hence, it is proposed that the depletion of ΔNp63 strongly increases genome instability, thereby exceeding the permitted DNA damage threshold for malignant proliferative cells.

ΔNp63 acts as a dominant negative regulator for the proapoptotic activities of TAp63, TAp73, and p53. Accordingly, one cannot eliminate the possibility that activation of the programmed cell death upon genetic depletion of ΔNp63 is mediated by direct interference with the activity of TAp63, TAp73, or p53 (Rocco et al. 2006). However, the results presented herein suggest that ΔNp63 regulates programmed cell death independently of TAp63, TAp73, and p53. Most of the experimental systems used for the research leading to this thesis exhibited genetically altered p53 states (deletion or mutations). Additionally, detectable levels of TAp63 were not found in the SCC tumors or cell lines indicating that ΔNp63 is the main Tp63 isoform

expressed in SCCs. Finally, no changes were observed in the expression of the reported TAp73 transcriptional pathway (Schaefer et al. 2009) upon genetic deletion of ΔNp63.

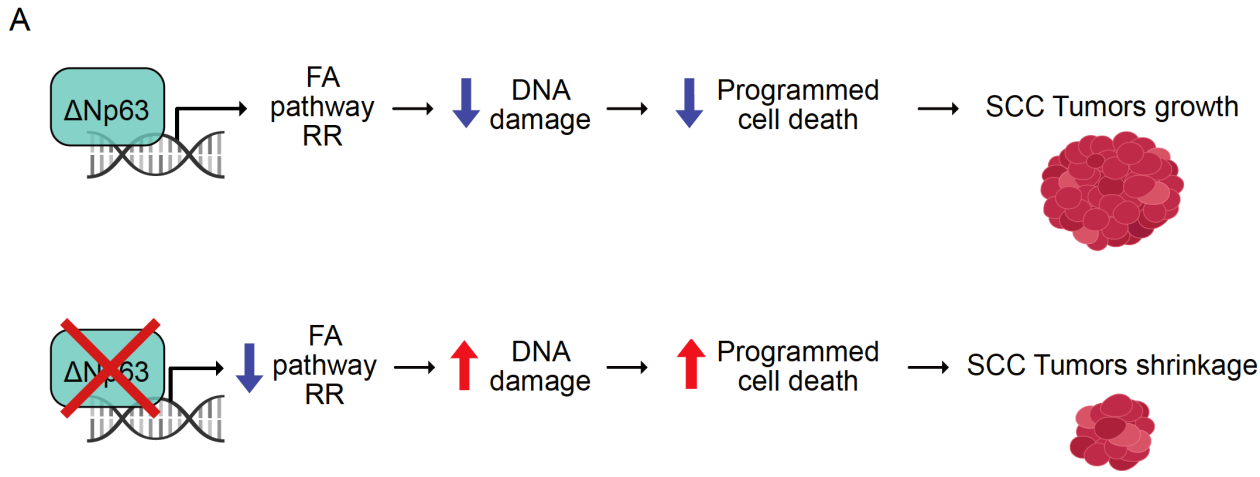

Figure 5.1 ΔNp63 is essential for Squamous tumors.

A) ΔNp63 triggers the transcription of genes involved in Fanconi anemia (FA) and recombinational repair (RR) pathway allowing basal levels of DNA damage caused by oncogenic proliferation without the induction of intracellular death programs. The depletion of ΔNp63 strongly increases DNA damage levels activating cell death programs.

Accordingly, previous studies have demonstrated that the loss of Tp53 or TAp73 does not counteract the cell death, and reduced proliferation caused by ΔNp63 depletion in SCC cells (Gallant-Behm & Espinosa 2013; Gallant-Behm et al. 2012). The data clearly indicate that ΔNp63 activity is fully required to develop SCC tumors, and it regulates programmed cell death independently of TAp63, TAp73, or Tp53.

In summary, the main function of ΔNp63 in SCC tumors is the regulation of the SCC cell identity and maintenance of acceptable DNA damage levels during cell division to avoid the activation of intracellular death programs.

5.2 Targeting the transcription factor ΔNp63

The essential functions of ΔNp63 in SCC tumors have been extensively explained. Considering the limited portfolio of effective therapies available to treat SCC tumors, ΔNp63 is considered a promising therapeutic target to increase the low survival rate of SCC patients. However, ΔNp63 is a transcription factor and as with most transcription factors, it is considered undruggable (Bushweller 2019). The structure of the transcription factors does not provide suitable domains for the binding of small molecule inhibitors. (Dang et al. 2017; Lambert et al. 2018).

As a master regulator of SCC tumors, ΔNp63 regulates several signaling pathways involved in a multitude of cellular processes such as proliferation, adhesion, metabolism, or differentiation. Furthermore, ΔNp63 also controls the epigenetic landscape of squamous cells by recruiting epigenetic modulators and chromatin remodeling factors (Fessing et al. 2011; Mardaryev et al. 2014; Yi et al. 2020; Abraham et al. 2018). The fact that ΔNp63 directly or indirectly regulates a massive subset of different genes and cellular processes makes it almost impossible to completely block the ΔNp63 SCC profile targeting downstream effectors.

DUB inhibitors that can regulate the intracellular protein degradation in specific cancer-associated targets have emerged as novel therapeutic options for cancer treatment (Liu et al. 2015; Wang et al. 2018; Harrigan et al. 2017). Considering that ΔNp63 is tightly regulated by the UPS (Armstrong et al. 2016). Herein, it is proposed that modulation of the ΔNp63 protein stability is a novel viable option to treat SCC tumors. For the first time, it was possible to target the transcription factor ΔNp63 in vivo using small molecule inhibitors (Prieto-Garcia et al. 2020). The stability of ΔNp63 was modulated by targeting the deubiquitinase USP28 using small molecule inhibitors in vivo.

This research showed that USP28 is a suitable therapeutic option to drug transcription factors considered undruggable to date and, therefore, the results presented herein serve as a proof of concept that it is indeed possible to target previously considered undruggable oncogenic transcription factors, such as c-MYC, ΔNp63, or c-JUN.

5.3 USP28: oncogene or tumor suppressor? The importance of genetics

USP28 is a deubiquitinase extensively characterized in several tumor entities, such as colorectal cancer (Diefenbacher et al. 2014; Diefenbacher et al. 2015). However, its function in SCC tumors was not studied. This research showed that USP28 acts as an oncogene for stabilizing ΔNp63 to induce squamous cell identity. Additionally, USP28 is an essential oncogene required to maintain the permitted DNA damage threshold for malignant proliferative cells and increases the resistance of SCC tumors to DNA damage therapies. The inhibition of USP28 reduces the growth of SCC tumors, increases cell death, and sensitizes SCC cells to DNA damage therapies, such as CPPD. Our data (Prieto-Garcia et al. 2020) were recently reproduced and published as a preprint, showing that the inhibition of USP28 using an inhibitor other than AZ1 can be effective for treating lung SCC tumors in vivo (Ruiz, Pinto-Fernandez et al. 2021).

In SCC tumors, USP28 can be considered a strong oncogene that stabilizes the SCC transcription factor ΔNp63 and other ubiquitous potent oncogenic proteins, such as c-MYC, c-JUN, or NOTCH1 (Figure 5.2A). Previous studies have shown that USP28 also acts as an oncogene counteracting FBXW7 in different tumor entities, such as colorectal cancer (Diefenbacher et al. 2014; Diefenbacher et al. 2015), breast cancer (Wu et al. 2013), glioblastoma (Wang et al. 2015), and lung ADC (Zhang et al. 2015).

Moreover, depending on context, USP28 can function as a tumor suppressor. Recent reports have demonstrated that USP28 stabilizes and regulates the activity of Tp53, acting as tumor suppressor (Müller et al. 2020; Meitinger et al. 2016). The regulation of Tp53 by USP28 was partially expected considering that the Tp53 isoforms share part of their structure with ΔNp63 (Dötsch et al. 2010). One cannot exclude the possibility that USP28 regulates other members of the Tp53 superfamily, such as Tp73 or TAp63. However, to date, no studies have demonstrated that USP28 stabilizes the tumor suppressors Tp73 or TAp63. Furthermore, previous research showed that USP28 stabilizes CHK2, hence, counteracting the E3 ligase PIRH2 (Bohgaki et al. 2013). Considering that CHK2 phosphorylates and stabilizes p53, inducing its apoptotic activity upon DNA damage, it can also be deduced that USP28 acts as a tumor suppressor when it increases the stability of CHK2.

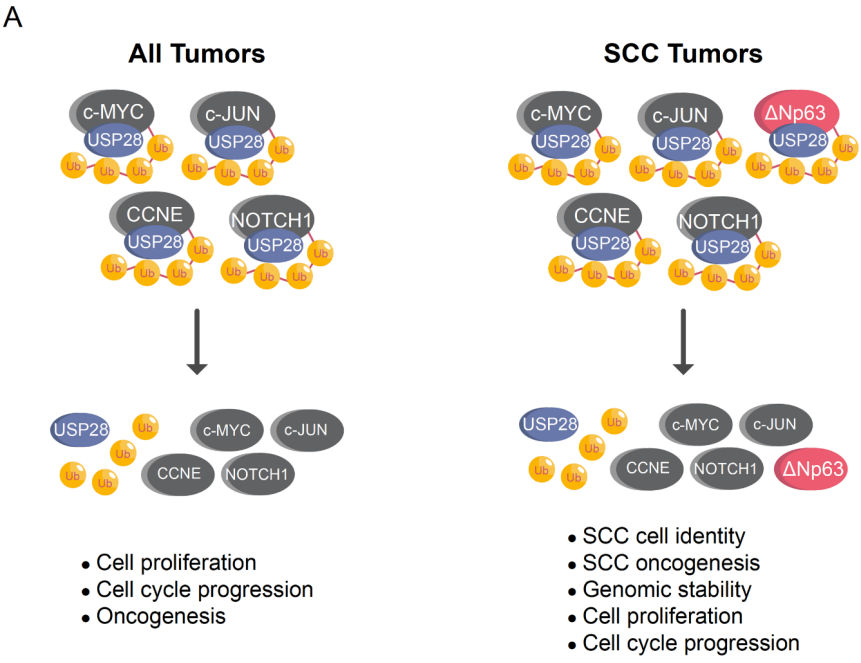

Figure 5.2 USP28 stabilizes ΔNp63 enhancing SCC cell identity, oncogenesis, proliferation, cell cycle progression and genomic stability. **A)** Ubiquitously, USP28 regulates the stability of several oncogenes involved in proliferation, cell cycle progression and oncogenesis, such as c-MYC, c-JUN, NOTCH1 or CCNE. In SCC tumors, USP28 regulates the same oncogenes but also ΔNp63. ΔNp63 strongly regulates SCC cell identity, oncogenesis, proliferation, cell cycle progression and genomic stability. Ub = ubiquitin.

In summary, USP28 stabilizes oncogenic transcription factors, such as c-MYC, C-JUN, or NOTCH1; it also regulates tumor suppressor proteins such as p53 or CHK2. Hence, is USP28 a tumor suppressor or an oncogene? To answer this question, we must consider the nature of the genetic alterations occurring in cancer. In particular, the state of p53 is highly important to elucidate the role of USP28 as an oncogene or tumor suppressor (Figure 5.3A).

In tumors with deleted p53, the proapoptotic function of CHK2 cannot be accomplished (Hirato et al. 2000) and the stabilization of CHK2 by USP28 may not have tumor suppression functional consequences. In tumors with functional mutations in p53, the stabilization of p53 by USP28 may even prove detrimental for cancer patients because mutant p53 is considered an oncogene. Mutant p53 acts as a negative regulator of the tumor suppressor p73 (Como et al. 1999) and positively regulates the frequency of metastasis and therapy resistance (Parrales & Iwakuma 2015). In p53 mutant tumors, similar to p53 null tumors, the proapoptotic function of CHK2 cannot be accomplished and the stabilization CHK2 by USP28 may not have functional consequences such as tumor suppression.

In SCC tumors, USP28 can clearly be considered an oncogene because most tumors harbor alterations impairing p53 function (Smardova et al. 2015 and Lahin et al. 2019). Furthermore, SCC tumors express high levels of the oncogenic transcription factors NOTCH1, c-JUN, c-MYC, and ΔNp63. In particular, ΔNp63 is extensively expressed in SCC tumors, as explained in this dissertation. Accordingly, SCC is the perfect example of a tumor entity where USP28 is an oncogene because most SCC tumors have genetically altered p53 pathways but high levels of oncogenic USP28 substrates (Figure 5.4A).

However, in differentiated cells, the expression of USP28 targets involved in stemness or malignant transformation is reduced and USP28 may act as a tumor suppressor stabilizing p53 and CHK2 (Figure 5.3A). Furthermore, the regulation of DNA damage by USP28 can be a double-edged sword, depending on the cell scenario. In somatic cells, USP28 stabilizes p53, allowing programmed cell death; it also maintains genome

stability, thus avoiding the accumulation of oncogenic mutations upon regulation of DNA damage substrates such as CHK2 or CLASPIN. Therefore, it is possible that USP28 helps maintain genome stability and facilitates apoptosis via p53, causing difficulties in the malignant transformation of somatic cells. Alternatively, in already transformed cancer cells and particularly in SCC cancer cells, USP28 acts as an oncogene facilitating cancer proliferation and DNA damage therapy resistance via stabilization of the ΔNp63-FA pathway axis and oncogenic substrates, such as c-MYC, c-JUN, NOTCH1, and CCNE (Figure 5.3A).

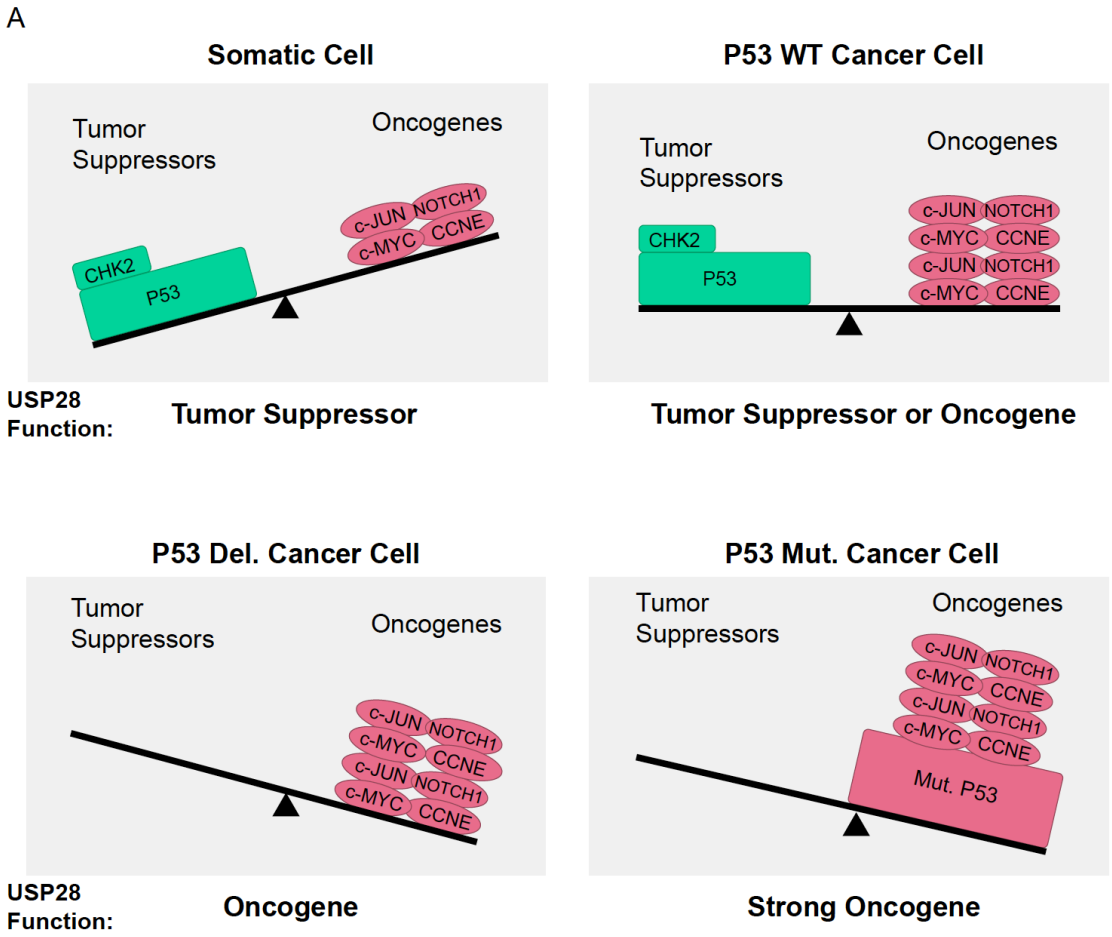

Figure 5.3 USP28 acts as an oncogene in tumors with p53 functional genetic alterations.

A) In somatic cells, the expression of oncogenic USP28 substrates is quite reduced and it is possible to consider USP28 a tumor suppressor gene. In p53 wildtype (WT) cancer cells, the role of USP28 is not clear and might be determined by the expression and the genetic status of USP28 substrates. In p53 deleted (Del.) or mutant (Mut.) cancer cells, the pro-apoptotic function of CHK2 cannot be accomplished and the stabilization CHK2 by USP28 will not have functional consequences as tumor suppressor. In consequence USP28 acts as an oncogene in p53 deleted (Del.) or mutant (Mut.) cells.

In summary, the balance between the expression and genetic status of USP28 substrates could determine the potential role of USP28 as an oncogene or tumor suppressor. In SCC, USP28 may be a clear oncogene, but one cannot exclude the possibility that USP28 could act as a tumor suppressor in other tumor entities with functional p53.

A

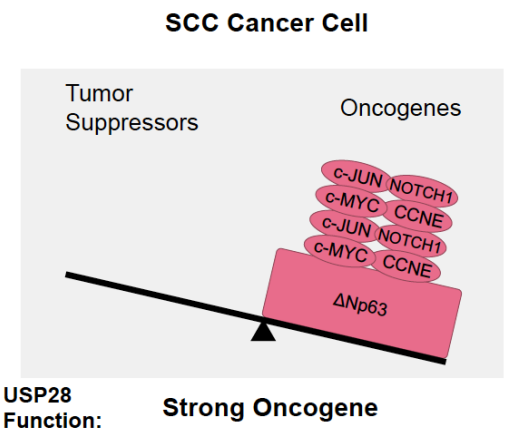

Figure 5.4 USP28 is an oncogene in Squamous tumors.
A) In SCC cancer cells, the expression of oncogenic USP28 substrates c-MYC, c-JUN, NOTCH1 and ΔNp63 is high and p53 is frequently deleted or mutated. In consequence, it is possible to consider USP28 a strong oncogene in SCC cancer cells.

5.4 Are USP28 substrates recruited via another E3-ligase in FBXW7- deficient cells?

Previous studies have proposed that USP28 substrates are recruited via FBXW7, and therefore, their interaction with USP28 is less efficient in FBXW7-deficient systems (Schülein-Völk et al. 2014; Popov et al. 2007). The so-called "piggyback" model suggests that FBXW7 is required for USP28 substrate recognition; consequently, USP28 would only be able to stabilize substrates in the presence of functional FBXW7 (Popov et al. 2007). The results of this research showed that USP28 stabilized ΔNp63 independently of the FBXW7 CPD phospho-degron (Figure 4.7). Additionally, USP28 strongly regulated ΔNp63 in a functionally inactivated FBXW7 (S462Y homozygous mutant) cell line system (A431, Figure 4.9). In line with this finding, previous reports indicated that USP28 can stabilize FBXW7 substrates, such as c-MYC, c-JUN, or NOTCH1, in FBXW7 knockout animals (Diefenbacher et al. 2015).

Considering the disparities among the results, three alternative models are proposed (Figure 5.5). In the first model, another E3-ligase would act as FBXW7 in the "piggyback" model and the hypothetical second E3-ligase would be required for USP28 substrate recognition (Figure 5.5A). USP28 counteracts PIRH2 in the regulation of CHK2 (Bohgaki et al. 2013). Similar to FBXW7, USP28 forms a complex with PIRH2 and CHK2, thus antagonizing the ubiquitination of CHK2 by PIRH2 (Bohgaki et al. 2013).

The protein PIRH2 (also called RCHY1) is a promising candidate for maintaining the previously demonstrated USP28 "piggyback" model. It is possible that PIRH2 is required for USP28 substrate recognition in FBXW7-deficient systems. Therefore, USP28 would only be able to stabilize substrates in the presence of functional FBXW7 or PIRH2. Additionally, several USP28 substrates, namely p53, CHK2, c-MYC, and ΔNp63, are polyubiquitinated by PIRH2 (Leng et al. 2003; Hakem et al. 2011; Jung et al. 2013). Similar to USP28, the role of PIRH2 has been a subject of controversy in cancer treatment (Halaby et al. 2013). As a regulator of p53 and CHK2, PIRH2 was considered a tumor suppressor gene (Leng et al. 2003). However, PIRH2 knockout animals exhibited increased levels of c-Myc and 25% of the animals developed spontaneous solid tumors (Hakem et al. 2011). Notably, 60% of PIRH2$^{-/-}$ and p53$^{-/-}$ compound germline knock out mice developed tumors and lived for a significantly shorter time than PIRH2$^{-/-}$ or p53$^{-/-}$ single knock out animals (Hakem et al.

2011). The above result reconfirms that the role of E3-ligases or DUBs as oncogenes or tumor suppressors depend on the context and cancer genetic.

It is not possible to exclude the possibility that E3-ligases other than FBXW7 or PIRH2 could form a complex with USP28, allowing USP28 substrate recognition. Another potential candidate is UBR5, an E3 ligase that interacts with several reported USP28 substrates such as CHK2, p53, and c-MYC (Henderson et al. 2006; Ling & Lin 2011; Schukur et al. 2020; Qiao et al. 2020). Similar to USP28, it is not clear if UBR5 functions as an oncogene or a tumor suppressor (Shearer et al. 2015).

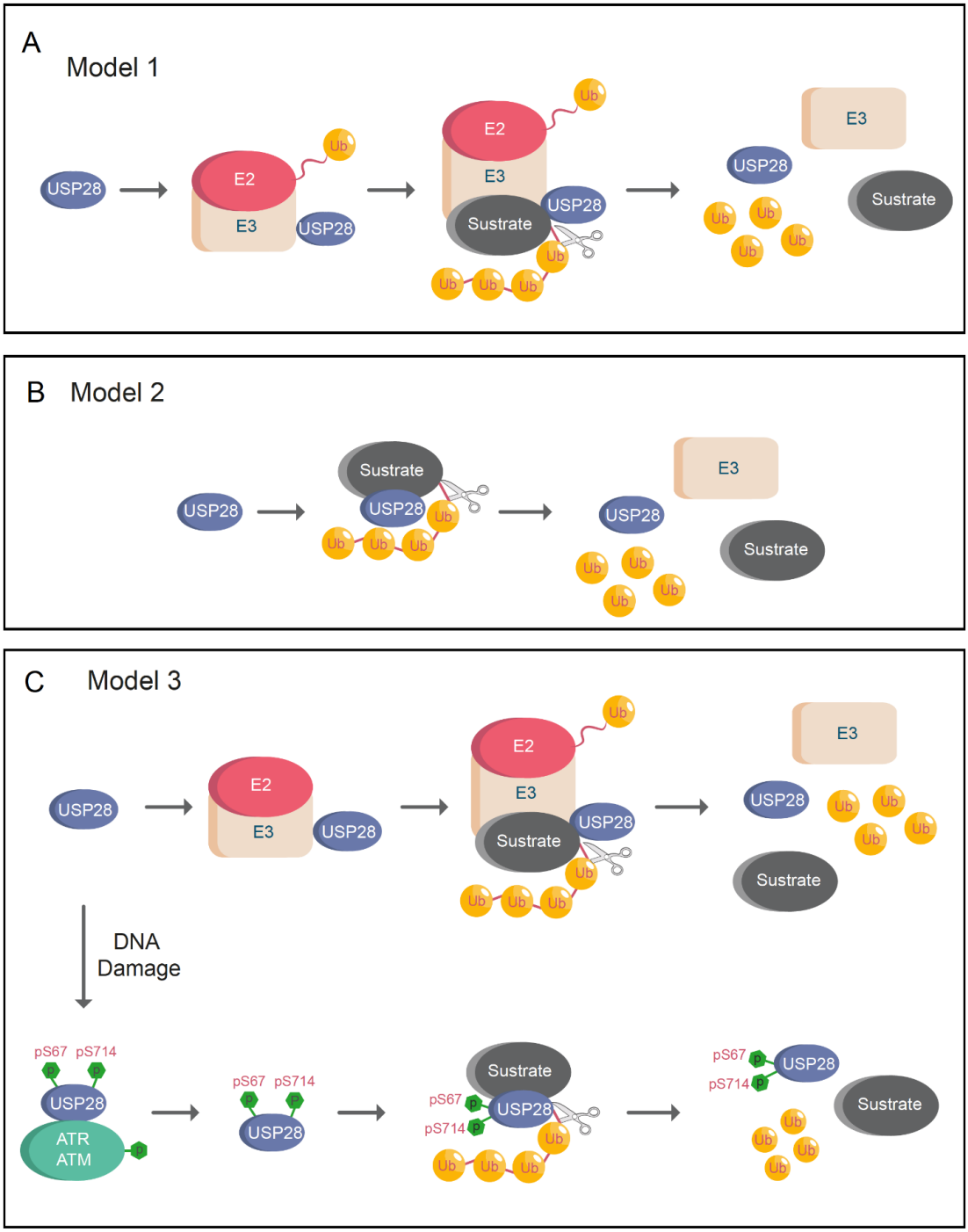

Figure 5.5. Models proposed for USP28 substrate recognition

A) Model 1: An E3-ligase is required for USP28 substrate recognition. USP28 only stabilizes proteins upon the formation of a complex with the E3-ligase. **B)** Model 2: USP28 deubiquitinates substrates independently of E3-ligases. **C)** Model3: Unphosphorylated USP28

acts as A) (model 1). Upon DNA damage or replication stress, the phosphorylated USP28 on serine 67 and serine 714 acts as B) (model 2). Ub = ubiquitin; p = phosphorylation; S = serine

The second alternative model proposed is a simpler one, wherein USP28 interacts with and deubiquitinates substrates independently of E3-ligases (Figure 5.5B). USP28 need not form a complex with another E3-ligase to interact with the target proteins. There are a multitude of DUBs that can interact with their substrates without forming a complex with E3-ligases, and it is possible that USP28 can deubiquitinate substrates independently of E3-ligases. Furthermore, it is possible that USP28 activity and substrate affinity are regulated in a tissue-specific manner and depending on the target tissue, USP28 may or may not require an interaction with another E3-ligase for substrate recognition.

This research has proved that phosphorylation of USP28 increases its enzymatic activity upon DNA damage (Figure 4.29 and 4.30). It could also be possible that posttranslational modifications regulate USP28 activity, thus enhancing substrate recognition and switching from the proposed first "piggyback" model to the second one (Figure 5.5C). Briefly, unphosphorylated USP28 requires complex formation with another E3-ligase, such as FBXW7, for substrate recognition, whereas phosphorylated USP28 can interact and deubiquitinate substrates independently of E3-ligases.

The last model based on posttranslational modifications reinforces the "piggyback" model because previously reported results demonstrate that USP28 can stabilize targets in FBXW7- deficient oncogenic models. Highly proliferative malignant cells frequently present increased levels of DNA damage and replication stress. The increased basal levels of DNA damage presented in cancer cells could induce phosphorylation of USP28, thereby allowing the stabilization of USP28 substrates independently of E3-ligases in cancer cells. Alternatively, in cells with low levels of DNA damage, such as nontransformed cells, USP28 remains non-phosphorylated, and E3-ligases are required for USP28 substrate recognition. It is possible that the applicability of the abovementioned models is tissue-specific, considering that some tissues have more propensity to accumulate DNA damage than others. Therefore, it is possible that posttranslational modifications other than phosphorylation can also regulate the substrate recognition and deubiquitinating activities of USP28. For example, SUMOylation of the N-terminal region of USP28 negatively regulates its enzymatic activity (Zhen et al. 2014; Du et al. 2019). Further studies are required to clarify the mechanism involved in USP28 substrate recognition and deubiquitinating activities.

5.5 ATR- and non-ATM-induced phosphorylation of USP28 upon Cisplatin exposure in squamous tumors

ATM and ATR are strong regulators of DDR and required to maintain genomic stability in cells (Awasthi et al. 2015). Herein, ATM and ATR kinases regulate different types of DNA damage. While ATM primarily processes DSBs in DNA (Paull 2015), ATR, in contrast, maintains the integrity of replicating chromosomes (Branzei & Foiani 2008) and is activated following single strand breaks (SSBs) in DNA (Zou & Elledge 2003). Apart from SSBs, the MRE11-RAD50-NBS1 complex increases the activity of ATR in response to double strand breaks (DSBs, Doksani et al. 2009).

As previously indicated, USP28 is a DUB strongly related to DDR. The data presented in this thesis shows that phosphorylation of USP28 increases its enzymatic activity upon DNA damage (Figure 4.29 and 4.30) (Prieto-Garcia et al. 2020). ATR- and non-ATM-induced phosphorylation of USP28 on serine 67 and serine 714 regulates its enzymatic activity in SCC cells upon CPPD exposure (Figure 5.6A). Alternatively, ATM phosphorylates USP28 on serine 67 and serine 714 under ionizing irradiation in large lung carcinoma cells (Zhang et al. 2006). These disparities can be explained considering that IR mainly induces DNA DSBs (Baskar et al. 2012), whereas CPPD causes replication stress and the formation of single- and DSBs, along with ICLs, (Rezaee et al. 2013).

Thus, it can be concluded that CPPD activates USP28 via ATR through replication stress and DNA ICLs, whereas IR induces the phosphorylation of USP28 by ATM via DNA DSBs. The presented research work highlighted that inhibition of USP28 sensitized cancer cells to CPPD (Figure 4.36) and IR (Figure 4.38), suggesting that USP28 is important to regulate DNA damage caused by replication stress, SSBs, and DSBs in SCC cells.

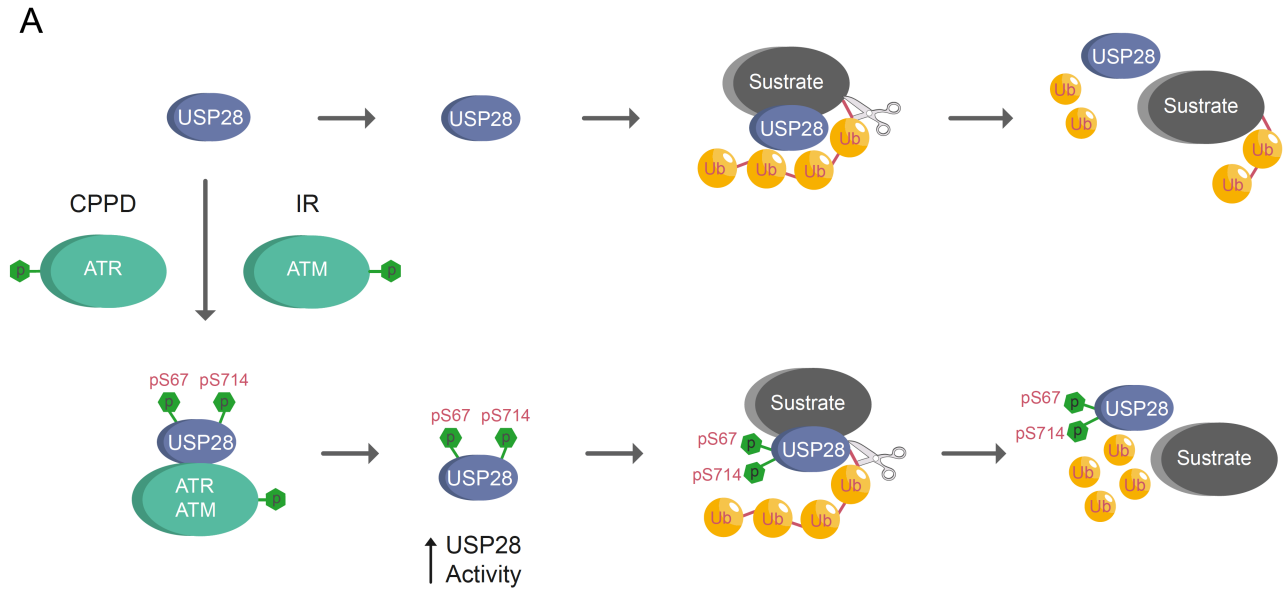

Figure 5.6. ATM or ATR phosphorylates USP28 regulating its enzymatic activity upon DNA damage.
A) Upon DNA damage induced by cisplatin (CPPD) exposure, ATR phosphorylates USP28 increasing its enzymatic activity. Upon DNA damage caused by Ionizing radiation (IR), ATR phosphorylates USP28 increasing its enzymatic activity upon DNA damage.

Although ATM and ATR are ubiquitously expressed, in cancer, ATR is frequently amplified in SCC tumors when compared to other tumor entities (Figure 4.29E). Considering that ATR is frequently highly expressed and the strong dependency of SCC cells on USP28 to repair damaged DNA, it is highly possible that SCC tumors rely more on the ATR-USP28 axis than on the ATM-USP28 axis to regulate DDR under genotoxic stress. The strong dependence of the SCC tumors on the ATR-USP28 axis is supported by the presented results in this thesis, indicating that ATR is the main regulator of USP28 in SCC cell lines (Figure 4.29).

Finally, kinases other than ATR or ATM could phosphorylate USP28 under DNA damage stress. The downstream ATM/ATR kinases CHK1 and CHK2 could be potential USP28 kinases following DNA damage. Additionally, USP28 interacts with CHK2 (Bohgaki et al. 2013). However, analyses of the USP28 sequence

did not reveal any CHK1 or CHK2 phosphorylation motif, suggesting that USP28 cannot be phosphorylated by CHK1 or CHK2 (Figure 4.29).

5.6 Inhibitors of USP28 for cancer therapy: Progress and perspective

USP28 is a targetable DUB enzyme that stabilizes crucial oncogenes in cancer, such as the transcription factor c-MYC (Popov et al. 2007). c-MYC is considered an essential oncogene and it is dysregulated in most tumors (Vita & Henriksson 2006; Adhikary & Eilers 2005). However, it is a transcription factor and considered "undruggable" (Bushweller 2019). Targeting "undruggable" transcription factors by dysregulating their protein stability via DUB inhibition could be a feasible alternative. Therefore, it is not surprising that different pharmaceutical companies and research groups have tried to develop efficient USP28 inhibitors as drugs to target cancer cells (Liu et al. 2019; Wrigley et al. 2017; Ruiz et al 2021; Wang et al. 2020; Bushman et al. 2020; Anthony C. Varca et a. 2021; Wang et al. 2018).

In this study, we used AZ1, which is the first established USP28 inhibitor (Wrigley et al. 2017). AZ1 is a dual USP25/USP28 inhibitor that directly interacts with the catalytic domain of the DUBs (Liu et al. 2019). Its efficiency has been proven by several studies that used AZ1 as a model compound to compare newly developed inhibitors against (Liu et al. 2019; Bushman et al. 2020). In the presented thesis, AZ1 was successfully applied *in vivo* for the first time, and showed little to no adverse effects on organismal level (Figure 4.26, 4.27 and Prieto-Garcia et al. 2020). Other studies have confirmed the safety and potential applicability of alternative USP25/USP28 inhibitors *in vivo* (Wang et al. 2020; Ruiz. et al 2021).

USP25 and USP28 are closely related DUBs; hence, USP28 shows a high structural homology to USP25 (Figure 4.10). However, USP25 is a cytosolic protein and shows low affinity to USP28 nuclear substrates, such as c-MYC or c-JUN. USP25 is not functionally related to USP28 and they interact with different targets. This study indicated that USP25 cannot interact with ΔNp63 *in vivo* (Figure 4.9). The phenotypes of ΔNp63-/USP28-depleted cells and AZ1- exposed SCC cells were highly similar, indicating that treatment with AZ1 inhibits the USP28-ΔNp63 axis. Considering that USP25 cannot bind to ΔNp63, the ΔNp63-deficient phenotype observed in SCC cells upon AZ1 exposure may have mainly resulted from USP28 inhibition occurring independently of USP25 inhibition. However, off-target effects or phenotypes resulting from the chemical structure of the inhibitor, or USP25 inhibition may indirectly influence the expression of ΔNp63 in SCC tumors.

All USP28 inhibitors developed till date also target USP25. It would be interesting to develop USP28-specific inhibitors that do not affect the activity of USP25. Due to their highly similar structures this task appears almost impossible. Interestingly, the two USP28 SQ/TQ motifs on serine 67 and serine 714 are not conserved in USP25 (Figure 5.7A). Considering that phosphorylation of USP28 on serine 67 and serine 714 regulates its enzymatic activity, it could be possible to develop drugs targeting the phospho-sites. The USP25 activity may not be affected upon exposure to an inhibitor blocking the phosphorylation of USP28 on serine 67 and serine 714. This study showed that the mutation of the phospho-sites by CRISPR/CAS9 reduced the enzymatic activity of USP28 and affected the protein abundances of c-MYC and ΔNp63 in SCC cells (Figure 4.30). Even

in the absence of DNA damage stressors, the mutations on serine 67 and/or serine 714 reduced the c-MYC and ΔNp63 protein abundances. Developing an inhibitor blocking the phosphorylation of USP28 on serine 67 and serine 714 could be a suitable method to target USP28 without affecting the USP25 activity.

The USP28 activity in SCC cells reduced with mutated USP28 on serine 67 and/or serine 714 without exposure to DNA damage compounds (Figure 4.30). It is possible that the basal levels of DNA damage induced by elevated rates of proliferation and replication caused the phosphorylation of USP28 in SCC cancer cells without exposure to any DNA damage stressor. This could be another therapeutic option to target the binding between ATM/ATR and USP28 and reduce the phosphorylation of USP28, thus decreasing its enzymatic activity.

This study demonstrated that mutation of the USP28 phospho-site on serine 714 reduces the enzymatic activity of USP28 more than the mutation on serine 67 (Figure 4.30). Furthermore, the serine 714 is more conserved than the ATM/ATR SQ-motif located on serine 67 (Figure 5.7A). Accordingly, the highly conserved serine 714 may be more important for USP28 activity than serine 67, and it could be worth developing specific inhibitors targeting the phosphorylation of USP28 on serine 714. Further studies are required to elucidate how posttranslational modifications regulate USP28 activity. In future, specific compounds targeting USP28 without altering the USP25 activity could be developed by targeting the posttranslational modifications of USP28 to regulate its activity.

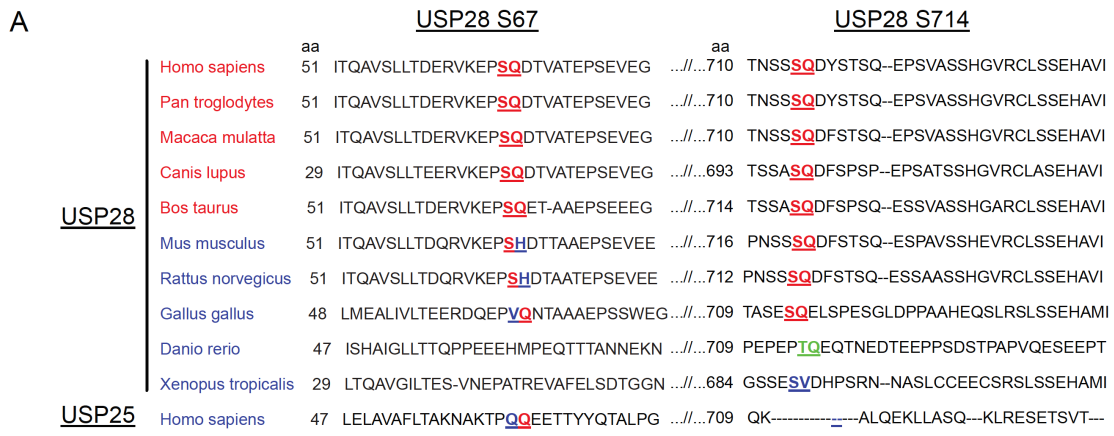

Figure 5.7. USP28 and USP25 protein sequence.

A) Protein sequence alignment for USP28 and USP25 on serine 67 and serine 714. USP28 sequence was analyzed for different species. Red=Conserved USP28 ATM/ATR phospho-motif respect to human; Blue=Non-conserved USP28 ATM/ATR phospho-motif respect to human; Green =SQ ATM/ATR phospho-motif was replaced for TQ ATM/ ATR phospho-motif.

5.7 Combination of USP28 inhibitor and Cisplatin as a therapy for squamous tumors

CPPD is one of the most effective anticancer drugs developed till date and is currently the most common therapy used for SCC patients (Fennell et al. 2016; Gandara et al. 2015; Isaka et al. 2017). CPPD damages genomic DNA by causing ICLs, triggering programmed cell death if the damage cannot be properly repaired.

Despite its notable efficiency in treating malignancies, most SCC tumors respond poorly to CPPD, and patients frequently develop cancer resistance and tumor recurrence. Accordingly, the median survival rate of SCC patients is low and the efficacy of Pt-based drugs is also rather low (Prieto-Garcia et al. 2020, Ruiz et al. 2019). The development of CPPD resistance in patients depends on multiple molecular processes and cellular alterations. Importantly, the enhanced expression of genes involved in DNA repair pathways is a vital factor in the development of CPPD resistance (Martin et al. 2008; O'Grady et al. 2014; Bouwman & Jonkers 2012). In mouse models, DNA repair inhibitors strongly increase the efficiency of anticancer DNA damage therapies, such as CPPD. Additionally, the hypersensitivity of testicular cancer can serve as a proof of concept that reduced expression of DNA repair pathways sensitizes cells to CPPD (Köberle et al. 1998). Testicular cancer represents an exceptional model of curable cancer and most testicular cancer patients, including those with advanced metastatic testicular cancer, have been completely cured using CPPD treatment (Rocha et al. 2018). Hence, one can conclude that the efficacy of CPPD therapy is highly influenced by the capacity of the cancer cells in repairing the damaged DNA (Lobo et al. 2020).

Even if the success of CPPD as cancer drug is unquestionable, there is an urgent need to improve current therapies for treating SCC tumors. SCC tumors are particularly resistant to DNA damage therapies because they express high levels of the oncogene ΔNp63. The transcription factor ΔNp63 regulates the transcription of Fanconi Anemia (FA) genes (Figure 4.39). Furthermore, the presented data suggest that the hyperactivation of USP28 caused by ATR upon DNA damage could serve as a mechanism for SCC tumors to develop therapy resistance and for cancer recurrence. Upon phosphorylation of USP28 induced by DNA damage, SCC tumors increase the stability of ΔNp63, thus enhancing the DNA repair efficiency via genetic expression of the FA and recombinatorial repair (RR) factors (Figure 4.33 and 4.39).

A

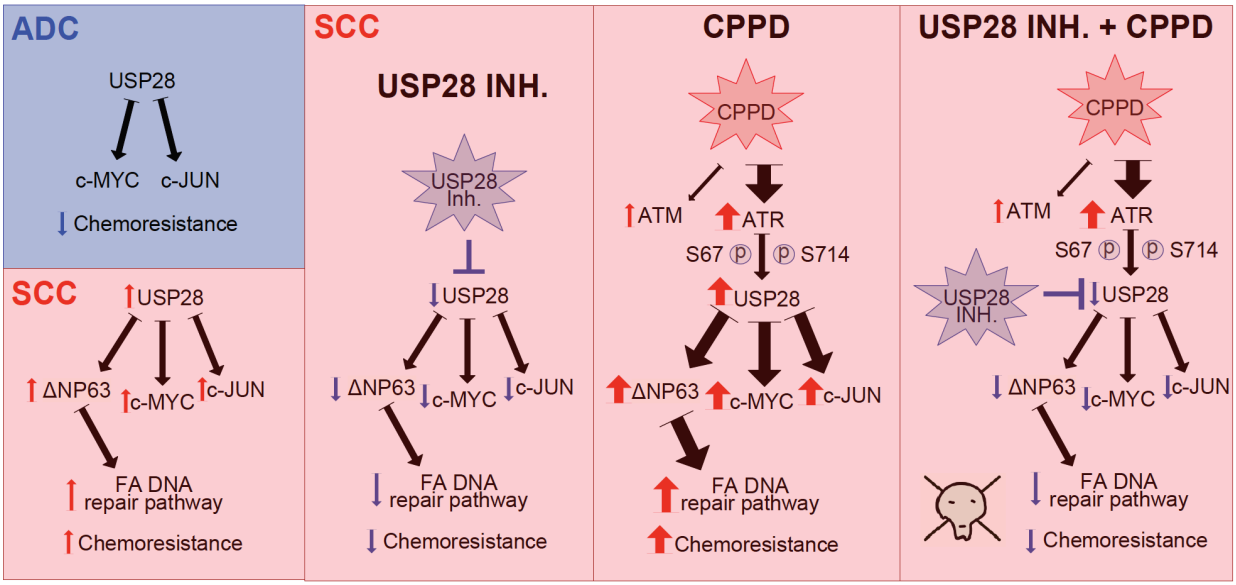

Figure 5.8. Proposed model for squamous cancer therapy: Combination of USP28 inhibitor and Cisplatin.

A) ADC tumors does not express ΔNp63. In ADC cells, USP28 regulates oncogenic substrates, such as c-MYC or c-JUN, but not ΔNp63. In **SCC tumors**, USP28 regulates its oncogenic substrates and also ΔNp63. ΔNp63 increases Fanconi anemia (FA) pathway enhancing chemoresistance to CPPD. In consequence, SCC tumors are more resistance to CPPD than ADC. Upon exposure to the

USP28 inhibitor, SCC cells reduce ΔNp63 protein abundance decreasing FA pathway and increasing chemosensitivity. **Upon CPPD**, ATR phosphorylates USP28 enhancing its enzymatic activity and increasing DNA damage repair pathways via the ΔNp63-FA axis. **Upon USP28 inhibitor-CPPD therapy**, CPPD cannot increase the expression of FA pathway via ΔNp63 and in consequence, SCC cells become more sensitive to DNA damage caused by CPPD.

This thesis proposes a new combined method to resensitize SCC cells to DNA damage therapies and avoid the development of therapy resistance or tumor relapse. The presented results demonstrate that combining AZ1 and CPPD is a promising therapeutic method to treat SCC patients. The exposure of SCC cells to the USP28 inhibitor reduced the stability of ΔNp63, thereby decreasing the expression of the FA members involved in DNA damage repair and, ultimately, sensitizing SCC tumors to chemotherapy (Figure 5.8A). Additionally, exposure to AZ1 may inactivate USP28 independently of its phosphorylation status and ATR. It is worth noting that human adenocarcinoma cell lines, which does not express ΔNp63, behaved differently. The inhibition of USP28 here led to a reduction of ɣ-H2AX, and co-treatment with cisplatin had no additive nor synergistic effect (Figure 4.35). This is in line with previous reports, where loss of USP28 in a NSCLC adenocarcinoma cell line H460 mediated resistance to ionising radiation (Zhang et al. 2006).

One major limitation of CPPD is its toxicity. Nephrotoxicity and ototoxicity remain important clinical limitations in using CPPD therapy (Ayed et al. 2020). Using USP28 inhibitors to resensitize SCC tumors to CPPD can reduce the CPPD dosage required for therapy, thereby ameliorating unwanted side effects. Additionally, this study showed that only SCC cells are sensitized to CPPD upon AZ1 exposure (Figure 4.35). ADC cells or ΔNp63-deficient cells failed to downregulate the FA pathway upon AZ1 exposure (Figure 4.40), suggesting that systemic exposure to USP28 inhibitors may only sensitize SCC cells to CPPD. In ΔNp63-deficient cells, expression of the FA proteins is regulated by the E2F protein family (Hoskins et al. 2008). Most somatic cells do not express ΔNp63, and accordingly, FA and DNA repairs pathways may not be negatively affected by exposure to USP28 inhibitors.

Considering that USP28 regulates other factors involved in DDR, such as CLASPIN or CHK2 (Ito et al. 2018; Bohgaki et al. 2013), USP28 inhibition could induce toxicity in somatic cells and affect DNA repair pathways other than FA. However, several studies analyzing the function of USP28 in non-SCC tissues reported that USP28 plays a minor role in DNA repair regulation (Knobel et al. 2014; Zhang et al. 2006). Additionally, the deletion of USP28 is well tolerated in mice (Knobel et al. 2014; Schülein-Völk et al. 2014; Diefenbacher et al. 2015; Diefenbacher et al. 2014; Prieto-Garcia et al. 2020). This thesis presents the first study explaining the important differences in DDR upon USP28 deletion. In line with the presented data, it is entirely possible to hypothesize that the role of USP28 in DNA repair could be restricted to the regulation of the ΔNp63-FA axis in SCC tissues.

To increase the efficiency, while decreasing the toxicity of the therapy using the CPPD–USP28 inhibitor (AZ1) combination, tumors were exposed to a particular two-step treatment regimen. First, the tumors were exposed to only the USP28 inhibitor for three days; then, the SCC cells were exposed to the CPPD–AZ1 combination for just one day (Figure 4.43). Exposure to only AZ1 for three days reduced the expression of the ΔNp63-FA pathway, thus potentially causing replication stress and sensitizing tumors to posterior DNA damage caused by CPPD exposure. The exposure regime enabled CPPD dose reduction, thus decreasing its toxic effects on

patients. *Ex vivo* SCC tumors were exposed to AZ1 for three days before CPPD considering the long half-life of ΔNp63 (Figure 4.9) and the FA proteins, such as FANCD2 (Howlett et al. 2009). Further studies using animal models are required to analyze the effectiveness of the combined therapy for SCC tumors in vivo.

This study proved that inhibition of USP28 by AZ1 sensitized cells to DNA damage therapies other than CPPD, such as Oxaliplatin, 5-Fluorouracil, and IR (Figure 4.38). Similar to CPPD, Oxaliplatin is a platinum (Pt) analog that induces the formation of DNA interstrand and intrastrand crosslinks, thereby preventing DNA replication and transcription, and if not resolved, culminating in cell death (Graham & Kirkpatrick 2004). In addition, 5-Fluorouracil is an inhibitor of the thymidylate synthase, blocking the synthesis of pyrimidine thymidylate required for DNA replication (Longley et al. 2003). IR releases sufficient energy to alter the molecular structures and bonds of the irradiated organic tissues. Furthermore, molecules broken by irradiation release highly reactive free radicals causing chemical damage. The most important type of DNA damage caused by IR is the formation of DSBs (Mahaney et al. 2009). The data presented herein indicate that USP28 inhibition can sensitize SCC cells to a diverse range of different DNA damage therapies. In summary, USP28 is a promising therapeutic target in combination with DNA-damaging therapies for treating SCC tumors.

5.8 Schematic summary of the study

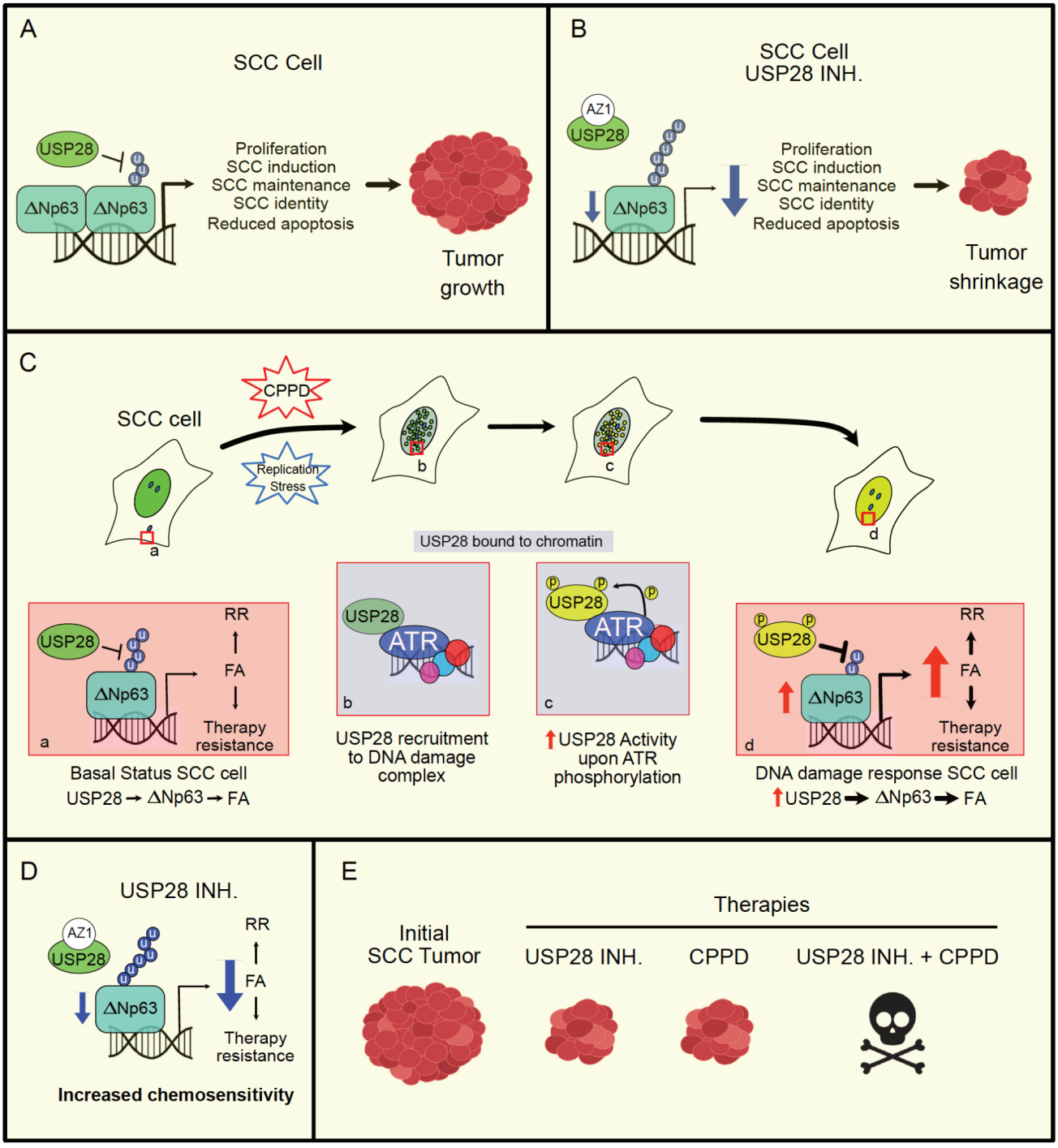

Figure 5.9. Schematic summary of the study.

A) In squamous (SCC) cells, USP28 stabilizes ΔNp63 via deubiquitination. ΔNp63 positively regulates proliferation, SCC tumor induction, identity and maintenance. Additionally, ΔNp63 also reduces apoptosis in SCC tumors. The USP28-ΔNp63 axis acts as an oncogene inducing tumor growth. u=ubiquitin molecule. **B)** Upon inhibition of USP28 (USP28 INH.) in SCC cells, ΔNp63 stability and transcriptional activity decreases. The reduction of ΔNp63 protein abundance increases programmed cell death and reduces proliferation, SCC identity, maintenance and induction. In consequence, SCC tumors shrinks upon USP28 inhibition. AZ1= USP28 Inhibitor; u=ubiquitin molecule. **C)** In SCC cells, USP28 stabilizes ΔNp63 allowing the transcription of Fanconi anemia genes (FA) which positively regulate DNA recombinational repair (RR) and DNA damage therapy resistance (a). Upon Cisplatin (CPPD) or replication stress, USP28 binds to chromatin allowing the interaction with ATR (b). ATR phosphorylates USP28 on serine 67 and serine 714 (c). Upon phosphorylation, USP28 increases its enzymatic activity enhancing ΔNp63 protein stability which increases the

transcription of FA genes enhancing therapy resistance (d). u=ubiquitin molecule. **D)** Upon exposure to USP28 inhibitor, SCC cells reduce ΔNp63 protein abundance decreasing FA and RR pathways. In consequence, USP28 inhibitor exposure increases chemosensitivity to DNA damage therapies. AZ1= USP28 Inhibitor; u=ubiquitin molecule. **E)** The double therapy USP28 inhibitor + CPPD is a promising alternative to treat SCC patients. The combination of CPPD with USP28 inhibitor is significantly more effective SCC therapy than the single therapy of CPPD or USP28 inhibitor.

6. Bibliography

1. Abraham, C. G., Ludwig, M. P., Andrysik, Z., Pandey, A., Joshi, M., Galbraith, M. D., Sullivan, K. D., & Espinosa, J. M. (2018). ΔNp63α Suppresses TGFB2 Expression and RHOA Activity to Drive Cell Proliferation in Squamous Cell Carcinomas. Cell Reports, 24(12), 3224–3236.
2. Adhikary, S., & Eilers, M. (2005). Transcriptional regulation and transformation by Myc proteins. Nature Reviews Molecular Cell Biology, 6(8), 635–645.
3. Akutsu, M., Dikic, I., & Bremm, A. (2016). Ubiquitin chain diversity at a glance. Journal of Cell Science, 129(5), 875–880.
4. Al-Husseini, M. J., Kunbaz, A., Saad, A. M., Santos, J. V., Salahia, S., Iqbal, M., & Alahdab, F. (2019). Trends in the incidence and mortality of transitional cell carcinoma of the bladder for the last four decades in the USA: a SEER-based analysis. BMC Cancer, 19(1).
5. American Cancer Society. Cancer Statistics Center. http://cancerstatisticscenter.cancer.org
6. Amlani, L., Bellile, E., Spector, M., Smith, J., Brenner, C., Rozek, L., Nguyen, A., Zarins, K., Thomas, D., McHugh, J., Taylor, J., & Wolf T, G. (2019). Expression of P53 and Prognosis in Patients with Head and Neck Squamous Cell Carcinoma (HNSCC). International Journal of Cancer and Clinical Research, 6(4).
7. Antonini, D., Rossi, B., Han, R., Minichiello, A., Di Palma, T., Corrado, M., Banfi, S., Zannini, M., Brissette, J. L., & Missero, C. (2006). An Autoregulatory Loop Directs the Tissue-Specific Expression of p63 through a Long-Range Evolutionarily Conserved Enhancer. Molecular and Cellular Biology, 26(8), 3308–3318.
8. Arita, H., Nagata, M., Yoshida, R., Matsuoka, Y., Hirosue, A., Kawahara, K., Sakata, J., Nakashima, H., Kojima, T., Toya, R., Murakami, R., Hiraki, A., Shinohara, M., & Nakayama, H. (2017). FBXW7 expression affects the response to chemoradiotherapy and overall survival among patients with oral squamous cell carcinoma: A single-center retrospective study. Tumor Biology, 39(10), 101042831773177.
9. Armstrong, S., Wu, H., Wang, B., Abuetabh, Y., Sergi, C., & Leng, R. (2016). The Regulation of Tumor Suppressor p63 by the Ubiquitin-Proteasome System. International Journal of Molecular Sciences, 17(12), 2041.
10. Awasthi, P., Foiani, M., & Kumar, A. (2016). ATM and ATR signaling at a glance. Journal of Cell Science, 129(6), 1285–1285.
11. Baskar, R., Lee, K. A., Yeo, R., & Yeoh, K.-W. (2012). Cancer and Radiation Therapy: Current Advances and Future Directions. International Journal of Medical Sciences, 9(3), 193–199.
12. Bass, A. J., Watanabe, H., Mermel, C. H., Yu, S., Perner, S., Verhaak, R. G., Kim, S. Y., Wardwell, L., Tamayo, P., Gat-Viks, I., Ramos, A. H., Woo, M. S., Weir, B. A., Getz, G., Beroukhim, R., O'Kelly, M., Dutt, A., Rozenblatt-Rosen, O., Dziunycz, P., … Meyerson, M. (2009). SOX2 is an amplified lineage-survival oncogene in lung and esophageal squamous cell carcinomas. Nature Genetics, 41(11), 1238–1242.
13. Basu, A. (2018). DNA Damage, Mutagenesis and Cancer. International Journal of Molecular Sciences, 19(4), 970.
14. Ben Ayed, W., Ben Said, A., Hamdi, A., Mokrani, A., Masmoudi, Y., Toukabri, I., Limayem, I., & Yahyaoui, Y. (2020). Toxicity, risk factors and management of cisplatin-induced toxicity: A prospective study. Journal of Oncology Pharmacy Practice, 26(7), 1621–1629.
15. Berman, J. J. (2004). Tumor taxonomy for the developmental lineage classification of neoplasms. BMC Cancer, 4(1).
16. Bhattacharjee, S., & Nandi, S. (2017). DNA damage response and cancer therapeutics through the lens of the Fanconi Anemia DNA repair pathway. Cell Communication and Signaling, 15(1).

17. Bohgaki, M., Hakem, A., Halaby, M. J., Bohgaki, T., Li, Q., Bissey, P. A., Shloush, J., Kislinger, T., Sanchez, O., Sheng, Y., & Hakem, R. (2013). The E3 ligase PIRH2 polyubiquitylates CHK2 and regulates its turnover. Cell Death & Differentiation, 20(6), 812–822.
18. Bouwman, P., & Jonkers, J. (2012). The effects of deregulated DNA damage signalling on cancer chemotherapy response and resistance. Nature Reviews Cancer, 12(9), 587–598.
19. Bradford, M. M. (1976). A rapid and sensitive method for the quantitation of microgram quantities of protein utilizing the principle of protein-dye binding. Analytical Biochemistry, 72(1–2), 248–254.
20. Branzei, D., & Foiani, M. (2008). Regulation of DNA repair throughout the cell cycle. Nature Reviews Molecular Cell Biology, 9(4), 297–308.
21. Breitschopf, K. (1998). A novel site for ubiquitination: the N-terminal residue, and not internal lysines of MyoD, is essential for conjugation and degradation of the protein. The EMBO Journal, 17(20), 5964–5973.
22. Bretz, A. C., Gittler, M. P., Charles, J. P., Gremke, N., Eckhardt, I., Mernberger, M., Mandic, R., Thomale, J., Nist, A., Wanzel, M., & Stiewe, T. (2016). ΔNp63 activates the Fanconi anemia DNA repair pathway and limits the efficacy of cisplatin treatment in squamous cell carcinoma. Nucleic Acids Research, 44(7), 3204–3218.
23. Broustas, C. G., & Lieberman, H. B. (2014). DNA Damage Response Genes and the Development of Cancer Metastasis. Radiation Research, 181(2), 111–130.
24. Büchel, G., Carstensen, A., Mak, K.Y., Roeschert, I., Leen, E., Sumara, O., Hofstetter, J., Herold, S., Kalb, J., Baluapuri, A., Poon, E., Kwok, C., Chesler, L., Maric, H. M., Rickman, D. S., Wolf, E., Bayliss, R., Walz, S., & Eilers, M. (2017). Association with Aurora-A Controls N-MYC-Dependent Promoter Escape and Pause Release of RNA Polymerase II during the Cell Cycle. Cell Reports, 21(12), 3483–3497.
25. Bushman, J. W., Donovan, K. A., Schauer, N. J., Liu, X., Hu, W., Varca, A. C., Buhrlage, S. J., & Fischer, E. S. (2020). Proteomics-Based Identification of DUB Substrates Using Selective Inhibitors. Cell Chemical Biology.
26. Bushweller, J. H. (2019). Targeting transcription factors in cancer — from undruggable to reality. Nature Reviews Cancer, 19(11), 611–624.
27. Cancer Genome Atlas Research Network, Comprehensive genomic characterization of squamous cell lung cancers. (2012) Nature 489, 519–525.
28. Ceccaldi, R., Sarangi, P., & D'Andrea, A. D. (2016). The Fanconi anaemia pathway: new players and new functions. Nature Reviews Molecular Cell Biology, 17(6), 337–349.
29. Cerami, E., Gao, J., Dogrusoz, U., Gross, B. E., Sumer, S. O., Aksoy, B. A., Jacobsen, A., Byrne, C. J., Heuer, M. L., Larsson, E., Antipin, Y., Reva, B., Goldberg, A. P., Sander, C., & Schultz, N. (2012). The cBio Cancer Genomics Portal: An Open Platform for Exploring Multidimensional Cancer Genomics Data. Cancer Discovery, 2(5), 401–404.
30. Ciechanover, A., & Ben-Saadon, R. (2004). N-terminal ubiquitination: more protein substrates join in. Trends in Cell Biology, 14(3), 103–106.
31. Clark, C. M., Furniss, M., & Mackay-Wiggan, J. M. (2014). Basal Cell Carcinoma: An Evidence-Based Treatment Update. American Journal of Clinical Dermatology, 15(3), 197–216.
32. Conde, E., Angulo, B., Redondo, P., Toldos, O., García-García, E., Suárez-Gauthier, A., Rubio-Viqueira, B., Marrón, C., García-Luján, R., Sánchez-Céspedes, M., López-Encuentra, A., Paz-Ares, L., & López-Ríos, F. (2010). The Use of P63 Immunohistochemistry for the Identification of Squamous Cell Carcinoma of the Lung. PLoS ONE, 5(8), e12209.
33. Cremona, C. A., Sancho, R., Diefenbacher, M. E., & Behrens, A. (2016). Fbw7 and its counteracting forces in stem cells and cancer: Oncoproteins in the balance. Seminars in Cancer Biology, 36, 52–61.

34. Damgaard, R. B., Elliott, P. R., Swatek, K. N., Maher, E. R., Stepensky, P., Elpeleg, O., Komander, D., & Berkun, Y. (2019). OTULIN deficiency in ORAS causes cell type-specific LUBAC degradation, dysregulated TNF signalling and cell death. EMBO Molecular Medicine, 11(3).
35. Dang, C. V., Reddy, E. P., Shokat, K. M., & Soucek, L. (2017). Drugging the "undruggable" cancer targets. Nature Reviews Cancer, 17(8), 502–508.
36. De Bie, P., & Ciechanover, A. (2011). Ubiquitination of E3 ligases: self-regulation of the ubiquitin system via proteolytic and non-proteolytic mechanisms. Cell Death & Differentiation, 18(9), 1393–1402.
37. Di Como, C. J., Gaiddon, C., & Prives, C. (1999). p73 Function Is Inhibited by Tumor-Derived p53 Mutants in Mammalian Cells. Molecular and Cellular Biology, 19(2), 1438–1449.
38. Di Veroli, G. Y., Fornari, C., Wang, D., Mollard, S., Bramhall, J. L., Richards, F. M., & Jodrell, D. I. (2016). Combenefit: an interactive platform for the analysis and visualization of drug combinations. Bioinformatics, 32(18), 2866–2868.
39. Diefenbacher, M. E., Chakraborty, A., Blake, S. M., Mitter, R., Popov, N., Eilers, M., & Behrens, A. (2015). Usp28 Counteracts Fbw7 in Intestinal Homeostasis and Cancer. Cancer Research, 75(7), 1181–1186.
40. Diefenbacher, M. E., Popov, N., Blake, S. M., Schülein-Völk, C., Nye, E., Spencer-Dene, B., Jaenicke, L. A., Eilers, M., & Behrens, A. (2014). The deubiquitinase USP28 controls intestinal homeostasis and promotes colorectal cancer. Journal of Clinical Investigation, 124(8), 3407–3418.
41. Doksani, Y., Bermejo, R., Fiorani, S., Haber, J. E., & Foiani, M. (2009). Replicon Dynamics, Dormant Origin Firing, and Terminal Fork Integrity after Double-Strand Break Formation. Cell, 137(2), 247–258.
42. Dötsch, V., Bernassola, F., Coutandin, D., Candi, E., & Melino, G. (2010). p63 and p73, the Ancestors of p53. Cold Spring Harbor Perspectives in Biology, 2(9), a004887–a004887.
43. Du, S., Zhu, L., Wang, Y., Liu, J., Zhang, D., Chen, Y., Peng, Q., Liu, W., & Liu, B. (2019). SENP1-mediated deSUMOylation of USP28 regulated HIF-1α accumulation and activation during hypoxia response. Cancer Cell International, 19(1).
44. FELASA. The Federation of European Laboratory Animal Science Associations. (2014).
45. Fennell, D. A., Summers, Y., Cadranel, J., Benepal, T., Christoph, D. C., Lal, R., Das, M., Maxwell, F., Visseren-Grul, C., & Ferry, D. (2016). Cisplatin in the modern era: The backbone of first-line chemotherapy for non-small cell lung cancer. Cancer Treatment Reviews, 44, 42–50.
46. Ferone, G., Song, J.-Y., Sutherland, K. D., Bhaskaran, R., Monkhorst, K., Lambooij, J.-P., Proost, N., Gargiulo, G., & Berns, A. (2016). SOX2 Is the Determining Oncogenic Switch in Promoting Lung Squamous Cell Carcinoma from Different Cells of Origin. Cancer Cell, 30(4), 519–532.
47. Fessing, M. Y., Mardaryev, A. N., Gdula, M. R., Sharov, A. A., Sharova, T. Y., Rapisarda, V., Gordon, K. B., Smorodchenko, A. D., Poterlowicz, K., Ferone, G., Kohwi, Y., Missero, C., Kohwi-Shigematsu, T., & Botchkarev, V. A. (2011). p63 regulates Satb1 to control tissue-specific chromatin remodeling during development of the epidermis. Journal of Cell Biology, 194(6), 825–839.
48. Fiil, B. K., Damgaard, R. B., Wagner, S. A., Keusekotten, K., Fritsch, M., Bekker-Jensen, S., Mailand, N., Choudhary, C., Komander, D., & Gyrd-Hansen, M. (2013). OTULIN Restricts Met1-Linked Ubiquitination to Control Innate Immune Signaling. Molecular Cell, 50(6), 818–830.
49. Fulda, S., Rajalingam, K., & Dikic, I. (2012). Ubiquitylation in immune disorders and cancer: from molecular mechanisms to therapeutic implications. EMBO Molecular Medicine, 4(7), 545–556.
50. Gallant-Behm, C. L., & Espinosa, J. M. (2013). How does ΔNp63α drive cancer? Epigenomics, 5(1), 5–7.

51. Gallant-Behm, C. L., Ramsey, M. R., Bensard, C. L., Nojek, I., Tran, J., Liu, M., Ellisen, L. W., & Espinosa, J. M. (2012). Np63 represses anti-proliferative genes via H2A.Z deposition. Genes & Development, 26(20), 2325–2336.
52. Galli, F., Rossi, M., D'Alessandra, Y., De Simone, M., Lopardo, T., Haupt, Y., Alsheich-Bartok, O., Anzi, S., Shaulian, E., Calabro, V., La Mantia, G., & Guerrini, L. (2010). MDM2 and Fbw7 cooperate to induce p63 protein degradation following DNA damage and cell differentiation. Journal of Cell Science, 123(14), 2423–2433.
53. Gandara, D. R., Hammerman, P. S., Sos, M. L., Lara, P. N., Jr, & Hirsch, F. R. (2015). Squamous Cell Lung Cancer: From Tumor Genomics to Cancer Therapeutics. Clinical Cancer Research, 21(10), 2236–2243.
54. Gao, J., Aksoy, B. A., Dogrusoz, U., Dresdner, G., Gross, B., Sumer, S. O., Sun, Y., Jacobsen, A., Sinha, R., Larsson, E., Cerami, E., Sander, C., & Schultz, N. (2013). Integrative Analysis of Complex Cancer Genomics and Clinical Profiles Using the cBioPortal. Science Signaling, 6(269), pl1–pl1.
55. Gatti, V., Bongiorno-Borbone, L., Fierro, C., Annicchiarico-Petruzzelli, M., Melino, G., & Peschiaroli, A. (2019). p63 at the Crossroads between Stemness and Metastasis in Breast Cancer. International Journal of Molecular Sciences, 20(11), 2683.
56. Gavory, G., O'Dowd, C. R., Helm, M. D., Flasz, J., Arkoudis, E., Dossang, A., Hughes, C., Cassidy, E., McClelland, K., Odrzywol, E., Page, N., Barker, O., Miel, H., & Harrison, T. (2017). Discovery and characterization of highly potent and selective allosteric USP7 inhibitors. Nature Chemical Biology, 14(2), 118–125.
57. Gersch, M., Wagstaff, J. L., Toms, A. V., Graves, B., Freund, S. M. V., & Komander, D. (2019). Distinct USP25 and USP28 Oligomerization States Regulate Deubiquitinating Activity. Molecular Cell, 74(3), 436-451.e7.
58. Goldman, M. J., Craft, B., Hastie, M., Repečka, K., McDade, F., Kamath, A., Banerjee, A., Luo, Y., Rogers, D., Brooks, A. N., Zhu, J., & Haussler, D. (2020). Visualizing and interpreting cancer genomics data via the Xena platform. Nature Biotechnology, 38(6), 675–678.
59. Graham, J., Muhsin, M., & Kirkpatrick, P. (2004). Oxaliplatin. Nature Reviews Drug Discovery, 3(1), 11–12.
60. Haakonsen, D. L., & Rape, M. (2019). Branching Out: Improved Signaling by Heterotypic Ubiquitin Chains. Trends in Cell Biology, 29(9), 704–716.
61. Hakem, A., Bohgaki, M., Lemmers, B., Tai, E., Salmena, L., Matysiak-Zablocki, E., Jung, Y.-S., Karaskova, J., Kaustov, L., Duan, S., Madore, J., Boutros, P., Sheng, Y., Chesi, M., Bergsagel, P. L., Perez-Ordonez, B., Mes-Masson, A.-M., Penn, L., Squire, J., … Hakem, R. (2011). Role of Pirh2 in Mediating the Regulation of p53 and c-Myc. PLoS Genetics, 7(11), e1002360.
62. Halaby, M., Hakem, R., & Hakem, A. (2013). Pirh2. Cell Cycle, 12(17), 2733–2737.
63. Hamdan, F. H., & Johnsen, S. A. (2018). DeltaNp63-dependent super enhancers define molecular identity in pancreatic cancer by an interconnected transcription factor network. Proceedings of the National Academy of Sciences, 115(52), E12343–E12352.
64. Hanahan, D., & Weinberg, R. A. (2000). The Hallmarks of Cancer. Cell, 100(1), 57–70.
65. Hanahan, D., & Weinberg, R. A. (2011). Hallmarks of Cancer: The Next Generation. Cell, 144(5), 646–674.
66. Hanpude, P., Bhattacharya, S., Dey, A. K., & Maiti, T. K. (2015). Deubiquitinating enzymes in cellular signaling and disease regulation. IUBMB Life, 67(7), 544–555.
67. Hartmann, O., Reissland, M., Maier, C. R., Fischer, T., Prieto-Garcia, C., Baluapuri, A., Schwarz, J., Schmitz, W., Garrido-Rodriguez, M., Pahor, N., Davies, C. C., Bassermann, F., Orian, A., Wolf, E., Schulze, A., Calzado, M. A., Rosenfeldt, M. T., & Diefenbacher, M. E. (2021). Implementation of CRISPR/Cas9 Genome Editing to

Generate Murine Lung Cancer Models That Depict the Mutational Landscape of Human Disease. Frontiers in Cell and Developmental Biology, 9.

68. Harrigan, J. A., Jacq, X., Martin, N. M., & Jackson, S. P. (2017). Deubiquitylating enzymes and drug discovery: emerging opportunities. Nature Reviews Drug Discovery, 17(1), 57–78.
69. Harris, A. L. (1985). DNA repair and resistance to chemotherapy. Cancer Surv. 4, 601–624.
70. Henderson, M. J., Munoz, M. A., Saunders, D. N., Clancy, J. L., Russell, A. J., Williams, B., Pappin, D., Khanna, K. K., Jackson, S. P., Sutherland, R. L., & Watts, C. K. W. (2006). EDD Mediates DNA Damage-induced Activation of CHK2. Journal of Biological Chemistry, 281(52), 39990–40000.
71. Hershko, A., & Ciechanover, A. (1998). THE UBIQUITIN SYSTEM. Annual Review of Biochemistry, 67(1), 425–479.
72. Hirao A, Kong YY, Matsuoka S, Wakeham A, Ruland J, Yoshida H, Liu D, Elledge SJ, Mak TW. (2000). DNA damage-induced activation of p53 by the checkpoint kinase Chk2. Science, 287(5459):1824-7.
73. Hjerpe, R., Aillet, F., Lopitz-Otsoa, F., Lang, V., England, P., Rodriguez, MS. (2009) Efficient protection and isolation of ubiquitylated proteins using tandem ubiquitin-binding entities. EMBO Rep 10: 1250–1258
74. Hoskins, E. E., Gunawardena, R. W., Habash, K. B., Wise-Draper, T. M., Jansen, M., Knudsen, E. S., & Wells, S. I. (2008). Coordinate regulation of Fanconi anemia gene expression occurs through the Rb/E2F pathway. Oncogene, 27(35), 4798–4808.
75. Howlett, N. G., Harney, J. A., Rego, M. A., Kolling, F. W., IV, & Glover, T. W. (2009). Functional Interaction between the Fanconi Anemia D2 Protein and Proliferating Cell Nuclear Antigen (PCNA) via a Conserved Putative PCNA Interaction Motif. Journal of Biological Chemistry, 284(42), 28935–28942.
76. Husnjak, K., & Dikic, I. (2012). Ubiquitin-Binding Proteins: Decoders of Ubiquitin-Mediated Cellular Functions. Annual Review of Biochemistry, 81(1), 291–322.
77. Hutchinson, M.-K. N. D., Mierzwa, M., & D'Silva, N. J. (2020). Radiation resistance in head and neck squamous cell carcinoma: dire need for an appropriate sensitizer. Oncogene, 39(18), 3638–3649.
78. Isaka, T., Nakayama, H., Yokose, T., Ito, H., Katayama, K., Yamada, K., & Masuda, M. (2017). Platinum-Based Adjuvant Chemotherapy for Stage II and Stage III Squamous Cell Carcinoma of the Lung. Annals of Thoracic and Cardiovascular Surgery, 23(1), 19–25.
79. Ito, F., Yoshimoto, C., Yamada, Y., Sudo, T., & Kobayashi, H. (2018). The HNF-1β—USP28—Claspin pathway upregulates DNA damage-induced Chk1 activation in ovarian clear cell carcinoma. Oncotarget, 9(25), 17512–17522.
80. Jang, S. J., Gardner, J. M., & Ro, J. Y. (2011). Diagnostic Approach and Prognostic Factors of Cancers. Advances in Anatomic Pathology, 18(2), 165–172.
81. Jo, U., & Kim, H. (2015). Exploiting the Fanconi Anemia Pathway for Targeted Anti-Cancer Therapy. Molecules and Cells, 38(8), 669–676.
82. Jung, Y.-S., Qian, Y., Yan, W., & Chen, X. (2013). Pirh2 E3 Ubiquitin Ligase Modulates Keratinocyte Differentiation through p63. Journal of Investigative Dermatology, 133(5), 1178–1187.
83. Kamate, W., Baad, R., Vibhute, N., Belgaumi, U., Kadashetti, V., & Gugwad, S. (2017). Trending Speculations of Tumor-Initiating Cells in Squamous Cell Cancers of Head and Neck. International Journal of Stem Cells, 10(1), 21–27.
84. Kampstra, P. (2008). Beanplot: A Boxplot Alternative for Visual Comparison of Distributions. Journal of Statistical Software, Code Snippets 28(1). 1-9.

85. Kan, Z., Jaiswal, B. S., Stinson, J., Janakiraman, V., Bhatt, D., Stern, H. M., Yue, P., Haverty, P. M., Bourgon, R., Zheng, J., Moorhead, M., Chaudhuri, S., Tomsho, L. P., Peters, B. A., Pujara, K., Cordes, S., Davis, D. P., Carlton, V. E. H., Yuan, W., … Seshagiri, S. (2010). Diverse somatic mutation patterns and pathway alterations in human cancers. Nature, 466(7308), 869–873.
86. Kang, J. U., Koo, S. H., Kwon, K. C., Park, J. W., & Kim, J. M. (2009). Identification of novel candidate target genes, including EPHB3, MASP1 and SSTat 3q26.2–q29 in squamous cell carcinoma of the lung. BMC Cancer, 9(1).
87. Keyes, W. M., Pecoraro, M., Aranda, V., Vernersson-Lindahl, E., Li, W., Vogel, H., Guo, X., Garcia, E. L., Michurina, T. V., Enikolopov, G., Muthuswamy, S. K., & Mills, A. A. (2011). ΔNp63α Is an Oncogene that Targets Chromatin Remodeler Lsh to Drive Skin Stem Cell Proliferation and Tumorigenesis. Cell Stem Cell, 8(2), 164–176.
88. Khayyata, S., Yun, S., Pasha, T., Jian, B., McGrath, C., Yu, G., Gupta, P., & Baloch, Z. (2009). Value of P63 and CK5/6 in distinguishing squamous cell carcinoma from adenocarcinoma in lung fine-needle aspiration specimens. Diagnostic Cytopathology, 37(3), 178–183.
89. Kim, D., Pertea, G., Trapnell, C. et al. (2013). TopHat2: accurate alignment of transcriptomes in the presence of insertions, deletions and gene fusions. Genome Biol 14, R36.
90. Kim, M. J., Shin, H. C., Shin, K. C., & Ro, J. Y. (2013). Best immunohistochemical panel in distinguishing adenocarcinoma from squamous cell carcinoma of lung: tissue microarray assay in resected lung cancer specimens. Annals of Diagnostic Pathology, 17(1), 85–90.
91. Klann, K., Tascher, G., & Münch, C. (2020). Functional Translatome Proteomics Reveal Converging and Dose-Dependent Regulation by mTORC1 and eIF2α. Molecular Cell, 77(4), 913-925.e4.
92. Knobel, P. A., Belotserkovskaya, R., Galanty, Y., Schmidt, C. K., Jackson, S. P., & Stracker, T. H. (2014). USP28 Is Recruited to Sites of DNA Damage by the Tandem BRCT Domains of 53BP1 but Plays a Minor Role in Double-Strand Break Metabolism. Molecular and Cellular Biology, 34(11), 2062–2074.
93. Köberle, B., Grimaldi, K. A., Sunters, A., Hartley, J. A., Kelland, L. R., & Masters, J. R. W. (1997). DNA Repair capacity and cisplatin sensitivity of human testis tumour cells. International Journal of Cancer, 70(5), 551–555.
94. Kohlbrenner, E., Henckaerts, E., Rapti, K., Gordon, R. E., Linden, R. M., Hajjar, R. J., & Weber, T. (2012). Quantification of AAV Particle Titers by Infrared Fluorescence Scanning of Coomassie-Stained Sodium Dodecyl Sulfate–Polyacrylamide Gels. Human Gene Therapy Methods, 23(3), 198–203.
95. Komander, D., & Rape, M. (2012). The Ubiquitin Code. Annual Review of Biochemistry, 81(1), 203–229.
96. Komander, D., Clague, M. J., & Urbé, S. (2009). Breaking the chains: structure and function of the deubiquitinases. Nature Reviews Molecular Cell Biology, 10(8), 550–563.
97. Kutler, D. I., Patel, K. R., Auerbach, A. D., Kennedy, J., Lach, F. P., Sanborn, E., Cohen, M. A., Kuhel, W. I., & Smogorzewska, A. (2015). Natural history and management of Fanconi anemia patients with head and neck cancer: A 10-year follow-up. The Laryngoscope, 126(4), 870–879.
98. Lai, K. P., Chen, J., & Tse, W. K. F. (2020). Role of Deubiquitinases in Human Cancers: Potential Targeted Therapy. International Journal of Molecular Sciences, 21(7), 2548
99. Lambert, M., Jambon, S., Depauw, S., & David-Cordonnier, M.-H. (2018). Targeting Transcription Factors for Cancer Treatment. Molecules, 23(6), 1479.
100. Langmead, B., & Salzberg, S. L. (2012). Fast gapped-read alignment with Bowtie 2. Nature Methods, 9(4), 357–359.

101. Lee, E. Y. H. P., & Muller, W. J. (2010). Oncogenes and Tumor Suppressor Genes. Cold Spring Harbor Perspectives in Biology, 2(10), a003236–a003236.

102. Leng, R. P., Lin, Y., Ma, W., Wu, H., Lemmers, B., Chung, S., Parant, J. M., Lozano, G., Hakem, R., & Benchimol, S. (2003). Pirh2, a p53-Induced Ubiquitin-Protein Ligase, Promotes p53 Degradation. Cell, 112(6), 779–791.

103. Li, C., & Lu, H. (2018). Adenosquamous carcinoma of the lung. OncoTargets and Therapy, Volume 11, 4829–4835.

104. Li, L., Wang, Y., Torkelson, J. L., Shankar, G., Pattison, J. M., Zhen, H. H., Fang, F., Duren, Z., Xin, J., Gaddam, S., Melo, S. P., Piekos, S. N., Li, J., Liaw, E. J., Chen, L., Li, R., Wernig, M., Wong, W. H., Chang, H. Y., & Oro, A. E. (2019). TFAP2C- and p63-Dependent Networks Sequentially Rearrange Chromatin Landscapes to Drive Human Epidermal Lineage Commitment. Cell Stem Cell, 24(2), 271-284.e8.

105. Li, T., Yan, B., Ma, Y., Weng, J., Yang, S., Zhao, N., Wang, X., & Sun, X. (2018). Ubiquitin-specific protease 4 promotes hepatocellular carcinoma progression via cyclophilin A stabilization and deubiquitination. Cell Death & Disease, 9(2).

106. Lin, C., Li, X., Zhang, Y., Guo, Y., Zhou, J., Gao, K., Dai, J., Hu, G., Lv, L., Du, J., & Zhang, Y. (2015). The microRNA feedback regulation of p63 in cancer progression. Oncotarget, 6(11), 8434–8453.

107. Lin, Y.L., Sengupta, S., Gurdziel, K., Bell, G. W., Jacks, T., & Flores, E. R. (2009). p63 and p73 Transcriptionally Regulate Genes Involved in DNA Repair. PLoS Genetics, 5(10), e1000680.

108. Ling, S., & Lin, W.C. (2011). EDD Inhibits ATM-mediated Phosphorylation of p53. Journal of Biological Chemistry, 286(17), 14972–14982.

109. Liu, J., Shaik, S., Dai, X., Wu, Q., Zhou, X., Wang, Z., & Wei, W. (2015). Targeting the ubiquitin pathway for cancer treatment. Biochimica et Biophysica Acta (BBA) - Reviews on Cancer, 1855(1), 50–60.

110. Liu, Z., Zhao, T., Li, Z., Sun, K., Fu, Y., Cheng, T., Guo, J., Yu, B., Shi, X., & Liu, H. (2020). Discovery of [1,2,3]triazolo[4,5-d]pyrimidine derivatives as highly potent, selective, and cellularly active USP28 inhibitors. Acta Pharmaceutica Sinica B, 10(8), 1476–1491.

111. Lobo, J., Jerónimo, C., & Henrique, R. (2020). Cisplatin Resistance in Testicular Germ Cell Tumors: Current Challenges from Various Perspectives. Cancers, 12(6), 1601.

112. Longley, D. B., Harkin, D. P., & Johnston, P. G. (2003). 5-Fluorouracil: mechanisms of action and clinical strategies. Nature Reviews Cancer, 3(5), 330–338.

113. Mahaney, B. L., Meek, K., & Lees-Miller, S. P. (2009). Repair of ionizing radiation-induced DNA double-strand breaks by non-homologous end-joining. Biochemical Journal, 417(3), 639–650.

114. Mardaryev, A. N., Gdula, M. R., Yarker, J. L., Emelianov, V. N., Poterlowicz, K., Sharov, A. A., Sharova, T. Y., Scarpa, J. A., Chambon, P., Botchkarev, V. A., & Fessing, M. Y. (2013). p63 and Brg1 control developmentally regulated higher-order chromatin remodelling at the epidermal differentiation complex locus in epidermal progenitor cells. Development, 141(1), 101–111.

115. Marechal, A., & Zou, L. (2013). DNA Damage Sensing by the ATM and ATR Kinases. Cold Spring Harbor Perspectives in Biology, 5(9), a012716–a012716.

116. Martin, L. P., Hamilton, T. C., & Schilder, R. J. (2008). Platinum Resistance: The Role of DNA Repair Pathways. Clinical Cancer Research, 14(5), 1291–1295.

117. Matin, R. N., Chikh, A., Law Pak Chong, S., Mesher, D., Graf, M., Sanza', P., Senatore, V., Scatolini, M., Moretti, F., Leigh, I. M., Proby, C. M., Costanzo, A., Chiorino, G., Cerio, R., Harwood, C. A., & Bergamaschi,

D. (2013). p63 is an alternative p53 repressor in melanoma that confers chemoresistance and a poor prognosis. Journal of Experimental Medicine, 210(3), 581–603.

118. McAlister, G. C., Nusinow, D. P., Jedrychowski, M. P., Wühr, M., Huttlin, E. L., Erickson, B. K., Rad, R., Haas, W., & Gygi, S. P. (2014). MultiNotch MS3 Enables Accurate, Sensitive, and Multiplexed Detection of Differential Expression across Cancer Cell Line Proteomes. Analytical Chemistry, 86(14), 7150–7158.
119. McClellan, A. J., Laugesen, S. H., & Ellgaard, L. (2019). Cellular functions and molecular mechanisms of non-lysine ubiquitination. Open Biology, 9(9), 190147.
120. Meitinger, F., Anzola, J. V., Kaulich, M., Richardson, A., Stender, J. D., Benner, C., Glass, C. K., Dowdy, S. F., Desai, A., Shiau, A. K., & Oegema, K. (2016). 53BP1 and USP28 mediate p53 activation and G1 arrest after centrosome loss or extended mitotic duration. Journal of Cell Biology, 214(2), 155–166.
121. Melino, G. (2003). Functional regulation of p73 and p63: development and cancer. Trends in Biochemical Sciences, 28(12), 663–670.
122. Mi, H., Muruganujan, A., Ebert, D., Huang, X., & Thomas, P. D. (2018). PANTHER version 14: more genomes, a new PANTHER GO-slim and improvements in enrichment analysis tools. Nucleic Acids Research, 47(D1), D419–D426.
123. Michl, J., Zimmer, J., & Tarsounas, M. (2016). Interplay between Fanconi anemia and homologous recombination pathways in genome integrity. The EMBO Journal, 35(9), 909–923.
124. Minten, E. V., & Yu, D. S. (2019). DNA Repair: Translation to the Clinic. Clinical Oncology, 31(5), 303–310.
125. Molina, J. R., Yang, P., Cassivi, S. D., Schild, S. E., & Adjei, A. A. (2008). Non-Small Cell Lung Cancer: Epidemiology, Risk Factors, Treatment, and Survivorship. Mayo Clinic Proceedings, 83(5), 584–594.
126. Mootha, V. K., Lindgren, C. M., Eriksson, K. F., Subramanian, A., Sihag, S., Lehar, J., Puigserver, P., Carlsson, E., Ridderstrale, M., Laurila, E., et al. (2003). PGC-1alpha-responsive genes involved in oxidative phosphorylation are coordinately downregulated in human diabetes. Nat Genet 34, 267-273.
127. Moses, M. A., George, A. L., Sakakibara, N., Mahmood, K., Ponnamperuma, R. M., King, K. E., & Weinberg, W. C. (2019). Molecular Mechanisms of p63-Mediated Squamous Cancer Pathogenesis. International Journal of Molecular Sciences, 20(14), 3590.
128. Mostafa MG, Fadil SH, Ahmed AN, Eltaher AM. CK-14 unequivocally distinguishes squamous cell carcinoma of the urinary bladder. AAMJ 2004; 2:1–12.
129. Mueller, S., Schittenhelm, M., Honecker, F., Malenke, E., Lauber, K., Wesselborg, S., Hartmann, J., Bokemeyer, C., & Mayer, F. (2006). Cell-cycle progression and response of germ cell tumors to cisplatin in vitro. International Journal of Oncology.
130. Mukhopadhyay, A., Berrett, K. C., Kc, U., Clair, P. M., Pop, S. M., Carr, S. R., Witt, B. L., & Oliver, T. G. (2014). Sox2 Cooperates with Lkb1 Loss in a Mouse Model of Squamous Cell Lung Cancer. Cell Reports, 8(1), 40–49.
131. Müller, I., Strozyk, E., Schindler, S., Beissert, S., Oo, H. Z., Sauter, T., Lucarelli, P., Raeth, S., Hausser, A., Al Nakouzi, N., Fazli, L., Gleave, M. E., Liu, H., Simon, H.-U., Walczak, H., Green, D. R., Bartek, J., Daugaard, M., & Kulms, D. (2020). Cancer Cells Employ Nuclear Caspase-8 to Overcome the p53-Dependent G2/M Checkpoint through Cleavage of USP28. Molecular Cell, 77(5), 970-984.e7.
132. Nagy, Á., Lánczky, A., Menyhárt, O., & Győrffy, B. (2018). Validation of miRNA prognostic power in hepatocellular carcinoma using expression data of independent datasets. Scientific Reports, 8(1).
133. Nalepa, G., & Clapp, D. W. (2018). Fanconi anaemia and cancer: an intricate relationship. Nature Reviews Cancer, 18(3), 168–185.

134. Nepal, M., Che, R., Zhang, J., Ma, C., & Fei, P. (2017). Fanconi Anemia Signaling and Cancer. Trends in Cancer, 3(12), 840–856.
135. Nicol, J. W., Helt, G. A., Blanchard, S. G., Raja, A., & Loraine, A. E. (2009). The Integrated Genome Browser: free software for distribution and exploration of genome-scale datasets. Bioinformatics, 25(20), 2730–2731.
136. Nikos, P. (2013). Subcellular Fractionation. Materials and Methods, 3.
137. Niraj, J., Färkkilä, A., & D'Andrea, A. D. (2019). The Fanconi Anemia Pathway in Cancer. Annual Review of Cancer Biology, 3(1), 457–478.
138. O'Grady, S., Finn, S. P., Cuffe, S., Richard, D. J., O'Byrne, K. J., & Barr, M. P. (2014). The role of DNA repair pathways in cisplatin resistant lung cancer. Cancer Treatment Reviews, 40(10), 1161–1170.
139. Parrales, A., & Iwakuma, T. (2015). Targeting Oncogenic Mutant p53 for Cancer Therapy. Frontiers in Oncology, 5.
140. Paull, T. T. (2015). Mechanisms of ATM Activation. Annual Review of Biochemistry, 84(1), 711–738.
141. Pendleton, K. P., & Grandis, J. R. (2013). Cisplatin-Based Chemotherapy Options for Recurrent and/or Metastatic Squamous Cell Cancer of the Head and Neck. Clinical Medicine Insights: Therapeutics, 5, CMT.S10409.
142. Perri, F., Pisconti, S., & Della Vittoria Scarpati, G. (2016). P53 mutations and cancer: a tight linkage. Annals of Translational Medicine, 4(24), 522–522.
143. Polyak, K., & Weinberg, R. A. (2009). Transitions between epithelial and mesenchymal states: acquisition of malignant and stem cell traits. Nature Reviews Cancer, 9(4), 265–273.
144. Poondla, N., Chandrasekaran, A. P., Kim, K.-S., & Ramakrishna, S. (2019). Deubiquitinating enzymes as cancer biomarkers: new therapeutic opportunities? BMB Reports, 52(3), 181–189.
145. Popov, N., Herold, S., Llamazares, M., Schülein, C., & Eilers, M. (2007). Fbw7 and Usp28 Regulate Myc Protein Stability in Response to DNA Damage. Cell Cycle, 6(19), 2327–2331.
146. Popov, N., Wanzel, M., Madiredjo, M., Zhang, D., Beijersbergen, R., Bernards, R., Moll, R., Elledge, S. J., & Eilers, M. (2007). The ubiquitin-specific protease USP28 is required for MYC stability. Nature Cell Biology, 9(7), 765–774.
147. Prieto-Garcia, C., Hartmann, O., Reissland, M., Braun, F., Fischer, T., Walz, S., Fischer, A., Calzado, M. A., Orian, A., Rosenfeldt, M., Eilers, M., & Diefenbacher, M. E. (2019). The USP28-ΔNp63 axis is a vulnerability of squamous tumours. Cold Spring Harbor Laboratory. BioXriv. **Preprint**: Officially published in peer-reviewed journal: Embo Molecular medicine (Prieto-Garcia et al. 2020).
148. Prieto-Garcia, C., Hartmann, O., Reissland, M., Fischer, T., Maier, C. R., Rosenfeldt, M., Schülein-Völk, C., Klann, K., Kalb, R., Dikic, I., Münch, C., & Diefenbacher, M. E. (2020). Inhibition of USP28 overcomes Cisplatin-Resistance of Squamous Tumors by Suppression of the Fanconi Anemia Pathway. Cold Spring Harbor Laboratory. BioXriv. **Preprint**: It has certified by peer review in Review Commons (https://www.reviewcommons.org/).
149. Prieto-Garcia, C., Hartmann, O., Reissland, M., Braun, F., Fischer, T., Walz, S., Schülein-Völk, C., Eilers, U., Ade, C. P., Calzado, M. A., Orian, A., Maric, H. M., Münch, C., Rosenfeldt, M., Eilers, M., & Diefenbacher, M. E. (2020). Maintaining protein stability of ΔNp63 via USP28 is required by squamous cancer cells. EMBO Molecular Medicine, 12(4).
150. Qiao, X., Liu, Y., Prada, M. L., Mohan, A. K., Gupta, A., Jaiswal, A., Sharma, M., Merisaari, J., Haikala, H. M., Talvinen, K., Yetukuri, L., Pylvänäinen, J. W., Klefström, J., Kronqvist, P., Meinander, A., Aittokallio, T.,

Hietakangas, V., Eilers, M., & Westermarck, J. (2020). UBR5 Is Coamplified with MYC in Breast Tumors and Encodes an Ubiquitin Ligase That Limits MYC-Dependent Apoptosis. Cancer Research, 80(7), 1414–1427.

151. R2: Genomics Analysis and Visualization Platform. http://r2.amc.nl.
152. Ramsey, M. R., Wilson, C., Ory, B., Rothenberg, S. M., Faquin, W., Mills, A. A., & Ellisen, L. W. (2013). FGFR2 signaling underlies p63 oncogenic function in squamous cell carcinoma. Journal of Clinical Investigation, 123(8), 3525–3538.
153. Ratovitski, E. A. (2014). Phospho-ΔNp63α/microRNA network modulates epigenetic regulatory enzymes in squamous cell carcinomas. Cell Cycle, 13(5), 749–761.
154. Reduced Lung-Cancer Mortality with Low-Dose Computed Tomographic Screening. (2011). New England Journal of Medicine, 365(5), 395–409.
155. Rezaee, M., Sanche, L., & Hunting, D. J. (2013). Cisplatin Enhances the Formation of DNA Single- and Double-Strand Breaks by Hydrated Electrons and Hydroxyl Radicals. Radiation Research, 179(3), 323–331.
156. Robinson, M. D., McCarthy, D. J., & Smyth, G. K. (2009). edgeR: a Bioconductor package for differential expression analysis of digital gene expression data. Bioinformatics, 26(1), 139–140.
157. Rocco, J. W., Leong, C.-O., Kuperwasser, N., DeYoung, M. P., & Ellisen, L. W. (2006). p63 mediates survival in squamous cell carcinoma by suppression of p73-dependent apoptosis. Cancer Cell, 9(1), 45–56.
158. Rocha, C., Silva, M., Quinet, A., Cabral-Neto, J., & Menck, C. (2018). DNA repair pathways and cisplatin resistance: an intimate relationship. Clinics, 73(Suppl 1).
159. Romano, R.-A., Smalley, K., Magraw, C., Serna, V. A., Kurita, T., Raghavan, S., & Sinha, S. (2012). Np63 knockout mice reveal its indispensable role as a master regulator of epithelial development and differentiation. Development, 139(4), 772–782.
160. Rottenberg, S., Disler, C., & Perego, P. (2020). The rediscovery of platinum-based cancer therapy. Nature Reviews Cancer, 21(1), 37–50.
161. Ruiz, E. J., Diefenbacher, M. E., Nelson, J. K., Sancho, R., Pucci, F., Chakraborty, A., Moreno, P., Annibaldi, A., Liccardi, G., Encheva, V., Mitter, R., Rosenfeldt, M., Snijders, A. P., Meier, P., Calzado, M. A., & Behrens, A. (2019).
162. LUBAC determines chemotherapy resistance in squamous cell lung cancer. Journal of Experimental Medicine, 216(2), 450–465.
163. Ruiz, E. J., Pinto-Fernandez, A., Turnbull, A. P., Lan, L., Charlton, T. M., Scott, H. C., Damianou, A., Vere, G., Riising, E. M., Da Costa, C., Krajewski, W. W., Guerin, D., Kearns, J., Ioannidis, S., Katz, M., McKinnon, C., O'Connell, J. C., Moncaut, N., Rosewell, I., …, Komander, D., Urbé, S., Clague, M.J., Kessler, B.M., Behrens, A. (2021). USP28 deletion and small molecule inhibition destabilises c-Myc and elicits regression of squamous cell lung carcinoma. Cold Spring Harbor Laboratory. BioXriv. **Preprint**: It has not been certified by peer review.
164. Sailo, B. L., Banik, K., Girisa, S., Bordoloi, D., Fan, L., Halim, C. E., Wang, H., Kumar, A. P., Zheng, D., Mao, X., Sethi, G., & Kunnumakkara, A. B. (2019). FBXW7 in Cancer: What Has Been Unraveled Thus Far? Cancers, 11(2), 246.
165. Saladi, S. V., Ross, K., Karaayvaz, M., Tata, P. R., Mou, H., Rajagopal, J., Ramaswamy, S., & Ellisen, L. W. (2017). ACTL6A Is Co-Amplified with p63 in Squamous Cell Carcinoma to Drive YAP Activation, Regenerative Proliferation, and Poor Prognosis. Cancer Cell, 31(1), 35–49.
166. Sánchez-Danés, A., & Blanpain, C. (2018). Deciphering the cells of origin of squamous cell carcinomas. Nature Reviews Cancer, 18(9), 549–561.

167. Sandulache, V. C., Chen, Y., Feng, L., William, W. N., Skinner, H. D., Myers, J. N., Meyn, R. E., Li, J., Mijiti, A., Bankson, J. A., Fuller, C. D., Konopleva, M. Y., & Lai, S. Y. (2017). Metabolic interrogation as a tool to optimize chemotherapeutic regimens. Oncotarget, 8(11), 18154–18165.

168. Sauer, F., Klemm, T., Kollampally, R. B., Tessmer, I., Nair, R. K., Popov, N., & Kisker, C. (2019). Differential Oligomerization of the Deubiquitinases USP25 and USP28 Regulates Their Activities. Molecular Cell, 74(3), 421-435.e10.

169. Schaefer, C. F., Anthony, K., Krupa, S., Buchoff, J., Day, M., Hannay, T., & Buetow, K. H. (2008). PID: the Pathway Interaction Database. Nucleic Acids Research, 37(suppl_1), D674–D679.

170. Schmidt, M. H. H., Furnari, F. B., Cavenee, W. K., & Bogler, O. (2003). Epidermal growth factor receptor signaling intensity determines intracellular protein interactions, ubiquitination, and internalization. Proceedings of the National Academy of Sciences, 100(11), 6505–6510.

171. Schukur, L., Zimmermann, T., Niewoehner, O., Kerr, G., Gleim, S., Bauer-Probst, B., Knapp, B., Galli, G. G., Liang, X., Mendiola, A., Reece-Hoyes, J., Rapti, M., Barbosa, I., Reschke, M., Radimerski, T., & Thoma, C. R. (2020). Identification of the HECT E3 ligase UBR5 as a regulator of MYC degradation using a CRISPR/Cas9 screen. Scientific Reports, 10(1).

172. Schülein-Völk, C., Wolf, E., Zhu, J., Xu, W., Taranets, L., Hellmann, A., Jänicke, L. A., Diefenbacher, M. E., Behrens, A., Eilers, M., & Popov, N. (2014). Dual Regulation of Fbw7 Function and Oncogenic Transformation by Usp28. Cell Reports, 9(3), 1099–1109.

173. Shearer, R. F., Iconomou, M., Watts, C. K. W., & Saunders, D. N. (2015). Functional Roles of the E3 Ubiquitin Ligase UBR5 in Cancer. Molecular Cancer Research, 13(12), 1523–1532.

174. Shimada, Y., Ishii, G., Nagai, K., Atsumi, N., Fujii, S., Yamada, A., Yamane, Y., Hishida, T., Nishimura, M., Yoshida, J., Ikeda, N., & Ochiai, A. (2009). Expression of podoplanin, CD44, and p63 in squamous cell carcinoma of the lung. Cancer Science, 100(11), 2054–2059.

175. Smardova, J., Liskova, K., Ravcukova, B., Malcikova, J., Hausnerova, j., Svitakova, M., Hrabalkova, R., Zlamalikova, I., Stano-Kozubik, K., Blahakova, I., Speldova, J., Jarkovsky, J., & Smarda, J. (2015). Complex analysis of the p53 tumor suppressor in lung carcinoma. Oncology Reports, 35(3), 1859–1867.

176. Soares, E., & Zhou, H. (2017). Master regulatory role of p63 in epidermal development and disease. Cellular and Molecular Life Sciences, 75(7), 1179–1190.

177. Somerville, T. D. D., Xu, Y., Miyabayashi, K., Tiriac, H., Cleary, C. R., Maia-Silva, D., Milazzo, J. P., Tuveson, D. A., & Vakoc, C. R. (2018). TP63-Mediated Enhancer Reprogramming Drives the Squamous Subtype of Pancreatic Ductal Adenocarcinoma. Cell Reports, 25(7), 1741-1755.e7.

178. Sos, M. L., & Thomas, R. K. (2012). Genetic insight and therapeutic targets in squamous-cell lung cancer. Oncogene, 31(46), 4811–4814.

179. Spruck, C.H., H. Strohmaier, O. Sangfelt, H.M. Muller, M. Hubalek, E. Muller-Holzner, C. Marth, M. Widschwendter, and S.I. Reed. (2002). hCDC4 gene mutations in endometrial cancer. Cancer Res. 62:4535–4539.

180. Subramanian, A., Tamayo, P., Mootha, V. K., Mukherjee, S., Ebert, B. L., Gillette, M. A., Paulovich, A., Pomeroy, S. L., Golub, T. R., Lander, E. S. & Mesirov, J. P. (2005) Gene set enrichment analysis: A knowledge-based approach for interpreting genome-wide expression profiles. Proc. Natl. Acad. Sci. USA 102, 15545-15550.

181. Summers, K. C., Shen, F., Sierra Potchanant, E. A., Phipps, E. A., Hickey, R. J., & Malkas, L. H. (2011). Phosphorylation: The Molecular Switch of Double-Strand Break Repair. International Journal of Proteomics, 2011, 1–8.

182. Tang, Z., Li, C., Kang, B., Gao, G., Li, C., & Zhang, Z. (2017). GEPIA: a web server for cancer and normal gene expression profiling and interactive analyses. Nucleic Acids Research, 45(W1), W98–W102.
183. Torgovnick, A., & Schumacher, B. (2015). DNA repair mechanisms in cancer development and therapy. Frontiers in Genetics, 6.
184. Valero, R., Bayés, M., Francisca Sánchez-Font, M., González-Angulo, O., Gonzàlez-Duarte, R., & Marfany, G. (2001). Genome Biology, 2(10), research0043.1.
185. van Wijk, S. J., Fulda, S., Dikic, I., & Heilemann, M. (2019). Visualizing ubiquitination in mammalian cells. EMBO Reports, 20(2).
186. Vanbokhoven, H., Melino, G., Candi, E., & Declercq, W. (2011). p63, a Story of Mice and Men. Journal of Investigative Dermatology, 131(6), 1196–1207.
187. Varca, A. C., Casalena, D., Chan, W. C., Hu, B., Magin, R. S., Roberts, R. M., Liu, X., Zhu, H., Seo, H.-S., Dhe-Paganon, S., Marto, J. A., Auld, D., & Buhrlage, S. J. (2021). Identification and validation of selective deubiquitinase inhibitors. Cell Chemical Biology.
188. Vigneswaran, N., & Williams, M. D. (2014). Epidemiologic Trends in Head and Neck Cancer and Aids in Diagnosis. Oral and Maxillofacial Surgery Clinics of North America, 26(2), 123–141.
189. Vita, M., & Henriksson, M. (2006). The Myc oncoprotein as a therapeutic target for human cancer. Seminars in Cancer Biology, 16(4), 318–330.
190. Walden, H., & Deans, A. J. (2014). The Fanconi Anemia DNA Repair Pathway: Structural and Functional Insights into a Complex Disorder. Annual Review of Biophysics, 43(1), 257–278.
191. Walsh, T., Casadei, S., Coats, K. H., Swisher, E., Stray, S. M., Higgins, J., Roach, K. C., Mandell, J., Lee, M. K., Ciernikova, S., Foretova, L., Soucek, P., & King, M.-C. (2006). Spectrum of Mutations in BRCA1, BRCA2, CHEK2, and TP53 in Families at High Risk of Breast Cancer. JAMA, 295(12), 1379.
192. Wang, F., Wang, L., Wu, J., Sokirniy, I., Nguyen, P., Bregnard, T., Weinstock, J., Mattern, M., Bezsonova, I., Hancock, W. W., & Kumar, S. (2017). Active site-targeted covalent irreversible inhibitors of USP7 impair the functions of Foxp3+ T-regulatory cells by promoting ubiquitination of Tip60. PLOS ONE, 12(12), e0189744.
193. Wang, H., Meng, Q., Ding, Y., Xiong, M., Zhu, M., Yang, Y., Su, H., Gu, L., Xu, Y., Shi, L., Zhou, H., & Zhang, N. (2020). USP28 and USP25 are downregulated by Vismodegib in vitro and in colorectal cancer cell lines. The FEBS Journal.
194. Wang, W. (2008) A major switch for the Fanconi anemia DNA damage–response pathway. Nat Struct Mol Biol 15, 1128–1130.
195. Wang, X.-M., Yang, C., Zhao, Y., Xu, Z.-G., Yang, W., Wang, P., Lin, D., Xiong, B., Fang, J.-Y., Dong, C., & Zhong, B. (2020). The deubiquitinase USP25 supports colonic inflammation and bacterial infection and promotes colorectal cancer. Nature Cancer, 1(8), 811–825.
196. Wang, X., Liu, Z., Zhang, L., Yang, Z., Chen, X., Luo, J., Zhou, Z., Mei, X., Yu, X., Shao, Z., Feng, Y., Fu, S., Zhang, Z., Wei, D., Jia, L., Ma, J., & Guo, X. (2018). Targeting deubiquitinase USP28 for cancer therapy. Cell Death & Disease, 9(2).
197. Wang, Z., Song, Q., Xue, J., Zhao, Y., & Qin, S. (2015). Ubiquitin-specific protease 28 is overexpressed in human glioblastomas and contributes to glioma tumorigenicity by regulating MYC expression. Experimental Biology and Medicine, 241(3), 255–264.
198. Warner, S. M. B., Hackett, T.-L., Shaheen, F., Hallstrand, T. S., Kicic, A., Stick, S. M., & Knight, D. A. (2013). Transcription Factor p63 Regulates Key Genes and Wound Repair in Human Airway Epithelial Basal Cells. American Journal of Respiratory Cell and Molecular Biology, 49(6), 978–988.

199. Weiss, J., Sos, M. L., Seidel, D., Peifer, M., Zander, T., Heuckmann, J. M., Ullrich, R. T., Menon, R., Maier, S., Soltermann, A., Moch, H., Wagener, P., Fischer, F., Heynck, S., Koker, M., Schottle, J., Leenders, F., Gabler, F., Dabow, I., … Thomas, R. K. (2010). Frequent and Focal FGFR1 Amplification Associates with Therapeutically Tractable FGFR1 Dependency in Squamous Cell Lung Cancer. Science Translational Medicine, 2(62), 62ra93-62ra93.

200. White, A. C., & Lowry, W. E. (2015). Refining the role for adult stem cells as cancer cells of origin. Trends in cell biology, 25(1), 11–20.

201. Wilkerson, M. D., Yin, X., Hoadley, K. A., Liu, Y., Hayward, M. C., Cabanski, C. R., Muldrew, K., Miller, C. R., Randell, S. H., Socinski, M. A., Parsons, A. M., Funkhouser, W. K., Lee, C. B., Roberts, P. J., Thorne, L., Bernard, P. S., Perou, C. M., & Hayes, D. N. (2010). Lung Squamous Cell Carcinoma mRNA Expression Subtypes Are Reproducible, Clinically Important, and Correspond to Normal Cell Types. Clinical Cancer Research, 16(19), 4864–4875.

202. Winters, I. P., Chiou, S.-H., Paulk, N. K., McFarland, C. D., Lalgudi, P. V., Ma, R. K., Lisowski, L., Connolly, A. J., Petrov, D. A., Kay, M. A., & Winslow, M. M. (2017). Multiplexed in vivo homology-directed repair and tumor barcoding enables parallel quantification of Kras variant oncogenicity. Nature Communications, 8(1).

203. Wu, Y., Wang, Y., Yang, X. H., Kang, T., Zhao, Y., Wang, C., Evers, B. M., & Zhou, B. P. (2013). The Deubiquitinase USP28 Stabilizes LSD1 and Confers Stem-Cell-like Traits to Breast Cancer Cells. Cell Reports, 5(1), 224–236.

204. Xiong, F., Ma, W., Hiscock, T. W., Mosaliganti, K. R., Tentner, A. R., Brakke, K. A., Rannou, N., Gelas, A., Souhait, L., Swinburne, I. A., Obholzer, N. D., & Megason, S. G. (2014). Interplay of Cell Shape and Division Orientation Promotes Robust Morphogenesis of Developing Epithelia. Cell, 159(2), 415–427.

205. Xu, C., Fillmore, C. M., Koyama, S., Wu, H., Zhao, Y., Chen, Z., Herter-Sprie, G. S., Akbay, E. A., Tchaicha, J. H., Altabef, A., Reibel, J. B., Walton, Z., Ji, H., Watanabe, H., Jänne, P. A., Castrillon, D. H., Rustgi, A. K., Bass, A. J., Freeman, G. J., … Wong, K.-K. (2014). Loss of Lkb1 and Pten Leads to Lung Squamous Cell Carcinoma with Elevated PD-L1 Expression. Cancer Cell, 25(5), 590–604.

206. Yeh, C.-H., Bellon, M., & Nicot, C. (2018). FBXW7: a critical tumor suppressor of human cancers. Molecular Cancer, 17(1).

207. Yi, M., Tan, Y., Wang, L., Cai, J., Li, X., Zeng, Z., Xiong, W., Li, G., Li, X., Tan, P., & Xiang, B. (2020). TP63 links chromatin remodeling and enhancer reprogramming to epidermal differentiation and squamous cell carcinoma development. Cellular and Molecular Life Sciences, 77(21), 4325–4346.

208. Yoh, K., & Prywes, R. (2015). Pathway Regulation of p63, a Director of Epithelial Cell Fate. Frontiers in Endocrinology, 6.

209. Yokobori T, Mimori K, Iwatsuki M, Ishii H, Tanaka F, Sato T, Toh H, Sudo T, Iwaya T, Tanaka Y, Onoyama I, Kuwano H, Nakayama KI, Mori, M. (2012). Copy number loss of FBXW7 is related to gene expression and poor prognosis in esophageal squamous cell carcinoma. International Journal of Oncology. Jul;41(1):253-9.

210. Zaorsky, N. G., Churilla, T. M., Egleston, B. L., Fisher, S. G., Ridge, J. A., Horwitz, E. M., & Meyer, J. E. (2017). Causes of death among cancer patients. Annals of Oncology, 28(2), 400–407.

211. Zhang, D., Zaugg, K., Mak, T. W., & Elledge, S. J. (2006). A Role for the Deubiquitinating Enzyme USP28 in Control of the DNA-Damage Response. Cell, 126(3), 529–542.

212. Zhang, L., & Shay, J. W. (2017). Multiple Roles of APC and its Therapeutic Implications in Colorectal Cancer. JNCI: Journal of the National Cancer Institute, 109(8).

213. Zhang, L., Xu, B., Qiang, Y., Huang, H., Wang, C., Li, D., & Qian, J. (2015). Overexpression of deubiquitinating enzyme USP28 promoted non-small cell lung cancer growth. Journal of Cellular and Molecular Medicine, 19(4), 799–805.
214. Zhang, P.-W., Chen, L., Huang, T., Zhang, N., Kong, X.-Y., & Cai, Y.-D. (2015). Classifying Ten Types of Major Cancers Based on Reverse Phase Protein Array Profiles. PLOS ONE, 10(3), e0123147
215. Zheng, S., Wang, X., Weng, Y.-H., Jin, X., Ji, J.-L., Guo, L., Hu, B., Liu, N., Cheng, Q., Zhang, J., Bai, H., Yang, T., Xia, X.-H., Zhang, H.-Y., Gao, S., & Huang, Y. (2018). siRNA Knockdown of RRM2 Effectively Suppressed Pancreatic Tumor Growth Alone or Synergistically with Doxorubicin. Molecular Therapy - Nucleic Acids, 12, 805–816.
216. Zhen, Y., Knobel, P. A., Stracker, T. H., & Reverter, D. (2014). Regulation of USP28 Deubiquitinating Activity by SUMO Conjugation. Journal of Biological Chemistry, 289(50), 34838–34850.
217. Zięba, S., Kowalik, A., Zalewski, K., Rusetska, N., Goryca, K., Piaścik, A., Misiek, M., Bakuła-Zalewska, E., Kopczyński, J., Kowalski, K., Radziszewski, J., Bidziński, M., Góźdź, S., & Kowalewska, M. (2018). Somatic mutation profiling of vulvar cancer: Exploring therapeutic targets. Gynecologic Oncology, 150(3), 552–561.
218. Zou, L., & Elledge, S. (2003). Sensing DNA Damage Through ATRIP Recognition of RPA-ssDNA Complexes. Science, 300(5625), 1542–1548.

7. Appendix

7.1 Abbreviations

Units

- Ampere (A)
- Dalton (Da)
- Degree celsius (°C)
- Gram (g)
- Hour (h)
- Liter (l)
- Meter (m)
- Minute (min)
- Mol / l (M)
- Parts per million (ppm)
- Rotations per minute (rpm)
- Second (s)
- Unit (u)
- Volt (V)
- Volume per volume (v/v)
- Weight per volume (w/v)

Prefixes

- (10^{-12}) Pico (p)
- (10^{-9}) Nano (n)
- (10^{-6}) Micro (µ)
- (10^{-3}) Milli (m)
- (10^{-2}) Centi (c)
- (10^{3}) Kilo (k)
- Murine (m)
- Human (h)
- Plasmid (p)

General abbreviations

- 4′,6 - diamidino - 2 - phenylindole (DAPI)
- 5 - Fluorouracil (5-FU)
- Acetonitrile (ACN)
- Adeno - associated virus (AAVs)
- Adenocarcinoma (ADC)
- Adenomatous polyposis coli (APC)
- Adenosine - triphosphate (ATP)

- Adenosintriphosphat (ATP)
- Adenosquamous (ADSCC)
- Adherent (adh.)
- Alanine (A or Ala)
- Alternative end joining (Alt-EJ)
- American Type Culture Collection (ATCC)
- Amino acid (aa)
- Ammonium bicarbonate (ABC)
- Ammoniumpersulfate (APS)
- Ampicillin (Amp)
- Antibody (AB)
- Aspartic Acid (D or Asp)
- Base 2 logarithm (Log2)
- Base 2 logarithm of fold change (Log2FC)
- Base excision repair (BER)
- Base pair (bp)
- Bovine serum albumine (BSA)
- Calf Intestinal.Phosphatase (CIP)
- Casp. (Caspase)
- Cervical squamous cell carcinoma (CESC)
- Cisplatin (CPPD)
- Clustered Regularly Interspaced Short Palindromic Repeats (CRISPR)
- Co - Immunoprecipitation (Co-IP)
- Complementary DNA (cDNA)
- Control (Ctrl)
- Correlation coefficient (R)
- CRISPR associated protein 9 (CAS9)
- Cullin (CUL)
- Cycloheximide (CHX)
- Cysteine (C or Cys)
- Cysteine protease domain (CPD)
- Cytomegalovirus (CMV)
- Chromatin immunoprecipitation (ChIP)
- Deoxynucleotidetriphosphates (dNTPs)
- Deoxyribonucleic acid (DNA)
- Deoxyribonucleoside-5'-triphosphate (dNTP)
- Deubiquitinating enzyme (DUB)
- Dimethyl sulfoxide (DMSO)
- Dithiothreitol (DTT)
- DNA binding domain (DBD)

- DNA damage response (DDR)
- Dulbeccos Modified Eagle-Medium (DMEM)
- Enhanced green fluorescent protein (eGFP)
- Enrichment score (ES)
- Epidermal growth factor (EGF)
- Escherichia coli (E. coli)
- Esophageal carcinoma (ESCA)
- Estrogen receptor (ER)
- Et alia (et al.)
- Etcetera (etc or …)
- Ethanol (Etoh)
- Ethylendiamintetraacetate (EDTA)
- European Collection of Authenticated Cell Cultures (ECACC).
- F - Box and WD Repeat Domain Containing 7 (FBXW7)
- False discovery rate (FDR)
- Fanconi Anemia (FA)
- Fetal bovine serum (FCS)
- Fetal calf serum (FCS)
- Floxed (Flox)
- Fluorescence activated cell sorting (FACS)
- Fold change (FC)
- Forward (FW)
- Gap1 phase (G1 phase)
- Gap2 phase (G2 phase)
- Gene ontology (GO)
- Gene set enrichment analysis (GSEA)
- Genetically engineered mouse models (GEMM)
- Glutathione S-transferase (GST)
- Glycine (G or Gly)
- Green fluorescent protein (GFP)
- Guide ribonucleic acid (gRNA)
- Half-maximal inhibition of cell growth (GI50)
- Half-maximal inhibitory concentration (IC50)
- Head and neck squamous carcinoma (HNSC)
- Hemagglutinin (HA)
- Hematoxylin and eosin (H&E)
- High performance liquid chromatography (HPLC)
- Histidine (His)
- Histone (H)
- Homologous recombination repair (HRR)

- Hydrogen peroxide (H2O2)
- Immunoblot (IB)
- Immunofluorescense (IF)
- Immunoglubulin (IgG)
- Immunohistochemistry (IHC)
- Immunoprecipitation (IP)
- Inhibitor (Inh.)
- Internal ribosome entry site (IRES)
- Interstrand crosslink (ICL)
- Ionizing radiation (IR)
- Kanamycin (Kan)
- Knock-out (KO)
- Kras G12 mutated to D; p53 and Lkb1 deleted (KPL)
- Kras G12 mutated to D; p53 deleted (KP)
- Kras G12 mutated to D; p53, Lkb1 and USP28 deleted (KPLU)
- Lentivirus (LV)
- Lox-Stop-Lox (LSL)
- Lung adenocarcinoma (LUAD)
- Lung squamous carcinoma (LUSC)
- Lysine (K or Lys)
- Machado Josephin Domain (MJD)
- Mass spectrometry (MS)
- Messenger RNA (mRNA)
- Methanol (MeOH)
- Micro RNA (miRNA)
- Mismatch repair (MMR)
- Mitotic phase (M phase)
- MIU - containing novel DUB family (MINDY)
- MOI (multiplicity of infection)
- Monocyte Chemotactic Protein-Induced Protein (MCPIP)
- N - ethylmaleimide (NEM)
- N,N - Dimethylformamid (DMF)
- N,N,N',N' - tetramethylenethylendiamine (TEMED)
- Natrium chloride (NaCl)
- Neomycin (Neo)
- Neutrally buffered formalin (NBF)
- Nitrilotriacetic acid (NTA)
- Non homologous end joining (NHEJ)
- Non transfected control (NTC)
- Non-Small Cell Lung Carcinoma (NSCLC)

- Nonidet P - 40 (NP-40)
- Normalized collision energy (NCE)
- Normalized enrichment score (NES)
- Not applicable (N/A)
- Nucleotide excision repair (NER)
- Nucleotides (nt)
- Number of biological replicate (n)
- Oligomerization domain (OD)
- Ovarian TUmour (OTU)
- Overnight (ON)
- Oxaliplatin (OXA)
- p - value (P)
- Pancreatic adenocarcinoma (PAAD)
- Paraformaldehyde (PFA)
- Phenylmethylsulfonyl fluoride (PMSF)
- Phosphate buffered saline (PBS)
- Phospho (p)
- Polyacrylamide-gel electrophoresis (PAGE)
- Polyethylenimin (PEI)
- Polymerase chain reaction (PCR)
- Polyvinylidene difluoride membranes (PVDF)
- Promoter (P)
- Propidium Iodide (PI)
- Puromycin (Puro)
- q-value (q)
- Quantitative polymerase chain reaction (qPCR)
- Radio frequency (RF)
- Radioimmunoprecipitation assay buffer (RIPA)
- Reactive oxygen species (ROS)
- Reads per kilobase per million mapped reads (RPKM)
- Real time - quantitative polymerase chain reaction (RT-qPCR)
- Recombinational repair (RR)
- Red fluorescent protein (RFP)
- Reverse (RV)
- Ribonuclease (RNase)
- Ribonucleic acid (RNA)
- Room temperature (RT)
- Roswell Park Memorial Institute (RPMI)
- Rotations per minute (rpm)
- RT-PCR (Real time - polymerase chain reaction)

- S - phase kinase-associated protein 1 (SKP1)
- Security level 1 (S1)
- Security level 2 (S2)
- Sequencing (Seq)
- Serine (S or Ser)
- Short hairpin RNA (shRNA)
- Short tandem repeat (STR)
- SKP1 - CUL1 - F-box complex (SCF)
- Slope (m)
- Small - Cell Lung Carcinoma (SCLC)
- Small ubiquitin-related modifier (SUMO)
- Sodium dodecyl sulfate (SDS)
- Squamous cell carcinoma (SCC)
- Standard deviation (SD)
- Standard error of the mean (SEM)
- Sterile alpha motif (SAM)
- Synchronous precursor selection (SPS)
- Synthesis phase (S phase)
- Tandem mass tag (TMT)
- Tandem ubiquitin binding entity (TUBE)
- The Federation of European Laboratory Animal Science Associations (FELASA)
- Threonine (T or Thr)
- Transactivation domain (TAD)
- Transactivation inhibitory domain (TID)
- Transcription factor (TF)
- Transfer RNA (tRNA)
- Translesion synthesis (TLS)
- Tris ethylendiamintetraacetate (TE)
- Tris (hydroxymethyl) aminomethan (TRIS)
- Tris acetate ethylendiamintetraacetate (TAE)
- Tris borate ethylendiamintetraacetate (TBE)
- Tris buffered saline - Tween-20 (TBS-T)
- Tris Buffered Saline (TBS)
- Tumor protein 53 (Tp53 or p53)
- Tumor protein 63 (Tp63 or p63)
- Tumor protein 73 (Tp73 or p73)
- Ubiquitin (Ub)
- Ubiquitin activating enzyme (E1)
- Ubiquitin associated domain (UBA)
- Ubiquitin binding domains (UBDs)

- Ubiquitin C-terminal Hydrolase (UCH)
- Ubiquitin conjugating enzyme (E2)
- Ubiquitin chain elongation factor (E4)
- Ubiquitin interacting motifs (UBI)
- Ubiquitin ligase (E3)
- Ubiquitin-proteasome system (UPS)
- Ubiquitin Specific Protease (USP)
- Ubiquitin suicide probes warheads (WH)
- Ultraviolet light (UV)
- Von Hippel-Lindau (VHL)
- Water (H2O)
- Western blot (WB)
- Wild type (WT)
- X - ray irradiation (IR)
- Zn - finger - UFSP domain protein (ZUFSP)

7.2 Acknowledgments

First of all, I would like to thank my supervisor and friend, Dr. Markus Diefenbacher, for the encouragement, support, advice, and guidance he provided me during my PhD in Wuerzburg. I can say that his supervision makes me a better scientist but also a better person. He inspired me constantly with such enthusiasm and everything I learned from him will help me a lot in my life and scientific career. I am really proud to be the first PhD student of Dr. Markus Diefenbacher and I really enjoyed all my time in his lab.

I would like to express my gratitude to Prof. Martin Eilers for the continuous support, honesty, guidance and motivation. I am particularly grateful to him because he gave me the opportunity to do my PhD in Wuerzburg and he always supported us with the multiple problems and issues we faced during my PhD time. I would also like to thank Prof. Ivan Dikic for the encouragement and continuous support. He inspired me constantly with his motivation and enthusiasm in regard to science. I would like to express my sincere gratitude to Prof. Ivan Dikic for all the trust he deposited on me and the opportunity to continue my scientific career in an excellent lab with a great collaborative environment. I also thank Prof. Gaubatz and Dr. Reinhard Kalb for their useful comments and suggestions during meetings and progress reports.

I wanted to thank my lab mates from Diefenbacher, Wolf, Gallant, Wiegering and Schulze groups who help me with technical help, scientific discussion but also they made my time in the lab unforgettable. Particularly, I would like to thank Oliver, Carina, Gabriel, Sarah, Michaela, Fabian, Thomas, Anna, Yiliam, Angela, Barbara, Dimi, Cathy, Markus, Niki, … for sharing so many good

moments together and make my life so easy in the lab! I really believe that the decision to do my PhD in Wuerzburg was great because of them.
Finally, I ineffably thank Maria for your continuous support, love, patience and great graphic designer skills. This would not have been possible without sharing my life with you! I would like also to thank my parents who always believed in me and my daughter Gala, who makes incredible special my last months in Wuerzburg.

7.3 Publications

Prieto-Garcia, C., Hartmann, O., Reissland, M., Braun, F., Fischer, T., Walz, S., Schülein-Völk, C., Eilers, U., Ade, C. P., Calzado, M. A., Orian, A., Maric, H. M., Münch, C., Rosenfeldt, M., Eilers, M., & Diefenbacher, M. E. (2020). Maintaining protein stability of ΔNp63 via USP28 is required by squamous cancer cells. EMBO Molecular Medicine, 12(4).

Hartmann, O., Reissland, M., Maier, C. R., Fischer, T., **Prieto-Garcia, C.**, Baluapuri, A., Schwarz, J., Schmitz, W., Garrido-Rodriguez, M., Pahor, N., Davies, C. C., Bassermann, F., Orian, A., Wolf, E., Schulze, A., Calzado, M. A., Rosenfeldt, M. T., & Diefenbacher, M. E. (2021). Implementation of CRISPR/Cas9 Genome Editing to Generate Murine Lung Cancer Models That Depict the Mutational Landscape of Human Disease. Frontiers in Cell and Developmental Biology, 9.

Diehl, V., Wegner, M., Grumati, P., Husnjak, K., Schaubeck, S., Gubas, A., Shah, V. J., Polat, I. H., Langschied, F., **Prieto-Garcia, C.**, Müller, K., Kalousi, A., Ebersberger, I., Brandts, C. H., Dikic, I., & Kaulich, M. (2021). Minimized combinatorial CRISPR screens identify genetic interactions in autophagy. Nucleic Acids Research, 49(10), 5684–5704.

7.4 Conferences

2015 47th Meeting of European Pancreatic Club. Toledo (Spain).
2018 Frankfurt Cancer Conference. Frankfurt (Deutschland).
2018 Eureka internationale Symposium. Wuerzburg (Deutschland).
2019 Deubiquitylases: from mechanism to physiology. Edinburgh (Scotland).

7.5 Curriculum Vitae

7.5 Affidavit

I hereby confirm that my thesis entitled "USP28 regulates Squamous cell oncogenesis and DNA repair via ΔNp63 deubiquitination" is the result of my own work. I did not receive any help or support from commercial consultants. All sources and / or materials applied are listed and specified in the thesis.

Furthermore, I confirm that this thesis has not yet been submitted as part of another examination process neither in identical nor in similar form.

Place, Date Signature

Eidesstattliche Erklärung

Hiermit erkläre ich an Eides statt, die Dissertation "USP28 reguliert die Plattenepithel Onkogenese und DNA-Reparatur über die Deubiquitinierung von ΔNp63" eigenständig, d.h.insbesondere selbständig und ohne Hilfe eines kommerziellen Promotionsberaters, angefertigt und keine anderen als die von mir angegebenen Quellen und Hilfsmittel verwendet zu haben.

Ich erkläre außerdem, dass die Dissertation weder in gleicher noch in ähnlicher Form bereits in einem anderen Prüfungsverfahren vorgelegen hat.

Ort, Datum Unterschrift